ESTIMATION OF THE FATIGUE CRACK INITIATION LIFE IN WELDS USING LOW CYCLE FATIGUE CONCEPTS

By

R. J. Mattos

F. V. Lawrence

Department of Metallurgical Engineering

ABSTRACT

An analytical model for calculating the fatigue crack initiation life of welds has been developed. In order to use the model, the stresses and strains at the critical location (toe of the weld) and a mechanics analysis to relate these local stresses and strains to the remotely applied stresses and strains are needed. Computation of the local stresses and strains was performed using Neuber's equation, and the fatigue behavior of the material at the critical location was computer simulated using a rheological model. Verification of the model was accomplished by comparing fatigue crack initiation life predictions with data obtained by testing simulated weld specimens and by utilizing data from the literature for several notch geometries, materials and fatigue loading conditions. The results of these comparisons indicate that a very good estimate of the fatigue crack initiation life can be obtained if the material properties at the critical location are well known.

Based on the analytical model developed, an analysis of the factors influencing the fatigue crack initiation life of welds was made. The results of this analysis indicate that the fatigue crack initiation life of welds is influenced by the micro- and macrogeometry of the weld reinforcement, the residual stresses, and very markedly by the material properties. It also indicates that the fraction of the fatigue life spent in fatigue crack initiation is dependent on the material and on the fatigue regime under consideration.

A Report of the

FRACTURE CONTROL PROGRAM

College of Engineering, University of Illinois
Urbana, Illinois 61801

October, 1975

ACKNOWLEDGMENTS

The authors wish to thank the sponsors of the University of Illinois Fracture Control Program and the Department of Metallurgy and Mining Engineering, Professor C. A. Wert, Head, for providing financial support. Particular thanks are extended to Caterpillar Tractor Company for their help in the residual stress measurements and to Deere and Company and General Motors, Electro-Motive Division for providing specimens and data.

Special thanks are owed to Professor JoDean Morrow (Theoretical and Applied Mechanics) for his helpful suggestions, encouragement and for providing access to his equipment.

Very special acknowledgments are made to: Mr. James Burk for his helpful discussions, Mr. James Sterner for his assistance in the mechanical testing, and Mrs. Laura Hickman for her careful typing of the manuscript.

TABLE OF CONTENTS

LIST OF TABLES

LIST OF FIGURES

LIST OF SYMBOLS

α	Geometric factor
a	Material constant
b	Fatigue strength exponent
c	Fatigue ductility exponent; also, crack length
C	Crack propagation material constant
E	Elastic modulus
E_i	Stiffness of the i^{th} element
E_i^*	Stiffness for the i^{th} segment of the stress-strain curve
e,Δe	Nominal strain, range
ε,$\Delta\varepsilon$	True strain, range
ε_e,$\Delta\varepsilon_e$	True elastic strain, range
ε_f'	Fatigue ductility coefficient
ε_m	Mean strain
ε_p,$\Delta\varepsilon_p$	True plastic strain, range
h	Height of the weld reinforcement
k	Material parameter function of the strain amplitude
K	Monotonic strength coefficient; also, stress intensity factor; also, stress factor
ΔK	Stress intensity factor range
K'	Cyclic strength coefficient
K_f	Fatigue notch factor
K_ε	Strain concentration factor
K_σ	Stress concentration factor
K_t	Elastic stress concentration factor

m	Crack propagation material constant
n	Monotonic strain hardening exponent
n'	Cyclic strain hardening exponent
$2N_f$	Number of reversals to failure
N_I	Fatigue crack initiation life
N_p	Fatigue crack propagation life
N_T	Total fatigue life
$2N_t$	Transition fatigue life
ν	Poisson's ratio
ψ	Angle of rotation
ϕ	Edge preparation angle
r	Notch radius
R	Stress ratio
$R\ C$	Relaxation constant
$S,\Delta S$	Nominal stress, range
S_{off}	Stress offset
S_u	Ultimate tensile strength
$\sigma,\Delta\sigma$	True stress, range
σ_a	Stress amplitude
σ_f	True fracture strength
σ'_f	Fatigue strength coefficient
σ_o	Mean stress
$\sigma_{o,i}$	Initial mean stress
$\sigma_{o,2N}$	Mean stress at reversal 2N
σ_r	Residual stress

$\sigma_{r,i}$	Initial residual stress
σ_{xx}	Stress in x-direction
σ_{ll}	Principal stress
t	Plate thickness
θ	Flank angle of the weld; also, Bragg angle
w	Width of the weld reinforcement

I. INTRODUCTION

The fatigue strength of a welded joint can be as little as 20 percent of the unwelded plate (1)*. Several factors contribute to this marked reduction in fatigue strength: the notches provided by various discontinuities in geometry, residual stresses, deleterious microstructures in the heat affected zone (HAZ), internal weld defects such as porosity, lack of fusion, etc.

Phenomenologically, the fatigue process consists of three stages (2): (a) crack nucleation, (b) stage I or crystallographically oriented crack growth, and (c) stage II or stable, crack growth perpendicular to the maximum tensile stress. However, from an engineering point of view, it is more convenient to consider the fatigue life to be composed of the number of cycles needed to initiate a "crack", N_I (fatigue crack initiation period) and of the number of cycles required for the propagation of the "active" fatigue crack to final failure, N_p (fatigue crack propagation period). Although arbitrary, these definitions of the crack initiation and propagation stages prove to be more convenient for predictions and analysis than the phenomenological definitions previously mentioned.

The traditional approach to the fatigue analysis of notched structural components has been based on the classical S-N curve. The empiricism of this approach has led to the exploration of recently developed disciplines; fracture mechanics and low cycle fatigue, to develop methods for more rational and accurate analyses. Unfortunately, no unified approach has as yet been developed

---

* Number in parentheses refer to the list of references.

and, at the present time, independent estimations of the fatigue crack initiation and propagation lives are made based on low cycle fatigue and fracture mechanics concepts, respectively.

A. Fatigue Crack Propagation Estimates

The most accepted approach to the analysis of fatigue crack propagation by linear-elastic fracture mechanics has been to use a semi-empirical power law expression which relates the cyclic rate of crack growth, dc/dN to the stress intensity factor range, ΔK ($\Delta K = K_{max} - K_{min}$), i.e.,

$$\frac{dc}{dN} = C\,(\Delta K)^m \tag{1}$$

where C and m are material constants (3). This equation provides a satisfactory description of behavior only for the mid-range of growth rates (typically 10^{-6} - 10^{-3} in./cycles). The complete variation of dc/dN with ΔK is more complicated, being roughly sigmoidal in form and bounded at the extremes by ΔK_{th} and K_c, the threshold range of the stress intensity and critical stress intensity factor.

The number of cycles required to propagate a crack from an initial crack size c_o, to a final crack, c_f, can be calculated from:

$$N_p = \int_0^{N_p} dN = \int_{c_o}^{c_f} \frac{dc}{dc/dN} \tag{2}$$

and using Eq. 1 for the cyclic rate of crack growth, Eq. 2 becomes,

$$N_p = \int_{c_o}^{c_f} \frac{dc}{C(\Delta K)^m} \tag{3}$$

The final crack size can be approximated by:

$$c_f \approx \frac{1}{\pi\alpha^2} \left(\frac{K_c}{S} \right)^2 \qquad (4)$$

The value of the integral (Eq. 3) is not too sensitive to c_f. The initial crack size, c_o, must be carefully defined. The value of the integral (Eq. 3) is very sensitive to c_o. In no case c_o can be smaller than

$$c_o \approx \frac{1}{\pi\alpha^2} \left(\frac{\Delta K_{th}}{S} \right)^2 \qquad (5)$$

An equation of the form, $\Delta K = S \alpha \sqrt{\pi c}$ is usually assumed to relate the stress intensity factor range, ΔK, with the nominal stress, S, and with the crack length, c; α is a factor related to the specific geometry in question.

Fatigue crack propagation estimates in the low ΔK region using fracture mechanics arguments to relate the cyclic rate of crack growth to the range of stress intensity factor have not been fully developed. Preliminary work in this area suggests that a relationship similar to Paris' power law (Eq. 1) might be used for modeling the rate of crack growth with the range of stress intensity factor (4,5). However, uncertainties as to the initial crack size, (c_o), and the sensitivity of this region to mean stress, microstructure and environment (6-8) provide complications which at the present make the extension of fatigue crack propagation predictions into this region impractical.

B. Fatigue Crack Initiation Estimates

Fatigue crack initiation models have been developed mainly within the framework of low cycle fatigue. In a notched member, fatigue cracks

initiate at the region of maximum strain concentration as a result of repeated plastic strains. Assuming that the most highly strained region can be represented by a filament of material whose mechanical response is similar to that of a smooth fatigue specimen, Topper, et al., (9) proposed that: (a) the fatigue crack initiation of a notched member can be considered to occur by the rupture of the filament of material; (b) under an appropriate control, the smooth specimen can be used to reproduce the stress-strain history of the filament; and (c) for identical stress-strain history of the filament and the smooth specimen, the fatigue life of the smooth specimen can be taken as the fatigue life of the filament (crack initiation life). The use of this model assumes the availability of information concerning the material properties, the stress-strain history of the most highly strained region, and a cumulative fatigue damage analysis. Extensive and successful use of this model has been made by the aircraft industry.

C. Estimations of the Fatigue Life in Weldments

Estimates of the fatigue crack propagation life in weldments have been made based on fracture mechanics models and empirical expressions relating the cyclic rate of crack growth with the range of the stress intensity factor as previously explained. Work in this field has been carried out by Maddox (10-13) and Lawrence (14-16) among others.

In contrast with the situation which prevails for the case of crack propagation, there presently exist no sound analytical models for estimating the fatigue crack initiation life in weldments. It is often alledged that the fatigue crack initiation portion in welds is eliminated by the existence

of crack-like defects in the form of slag or other non-metallic inclusions present at the toe of the weld (17). These assumptions however, seem unjustified, mainly because it is very unlikely that all welds are defective and because even for sharp notches, a period of crack initiation is required before a fatigue crack starts to propagate (4,5). There are other factors which the present fatigue crack propagation models are unable to explain: residual stresses and their relaxation, improvement of the fatigue life by slight alterations of the weld reinforcement (TIG dressing), and more importantly, the disagreement between the estimated fatigue crack propagation life and the total fatigue life mainly in the long life regime.

It seems, therefore, that a model for estimating the fatigue crack initiation life in welds is needed. Although fatigue crack propagation estimates can provide a lower bound to the total fatigue life, omission of the crack initiation life can lead to serious underestimations of the total life. This is especially true in the high cycle fatigue life regime where the crack initiation portion occupies the greatest proportion of the total life.

D. Scope

This investigation was concerned with the development of an analytical procedure to estimate the fatigue crack initiation life of weldments, with the analysis of some of the factors influencing this life and with the development of a model to study the cyclic relaxation of the welding residual stresses.

Fatigue crack initiation was assumed to occur by the rupture of a hypothetical uniaxial fatigue specimen located at the most highly strained region (toe of the weld). To compute the local stresses and strains at the

toe of the weld, a mechanics analysis based on the Neuber's equation was performed. Peterson's equation which relates the fatigue notch factor to the stress concentration factor was assumed to be valid. The elastic stress concentration factors associated with the geometry of the weld reinforcement were determined by finite element methods. The cyclic stress-strain and fatigue properties of the material at the toe of the weld were assumed to be identical to those of the base metal. The cyclic hystory of the critical location was computer simulated by rheological models, and a cumulative fatigue analysis was performed on a reversal by reversal basis. Figure 1 schematically illustrates the fatigue analysis for the calculation of the fatigue crack initiation life. Comparisons of the fatigue crack initiation life predictions with actual data were made by testing simulated weld specimens and by utilizing data from the literature.

An extension of the model to the analysis of the factors which influence the fatigue behavior of welds was made. With the model, the effects of the micro-and macrogeometry of the weld reinforcement, material properties and welding residual stresses were considered. Based on the behavior of the cyclic relaxation of the mean stress from strain controlled experiments, a model was also proposed to estimate the cyclic relaxation of the welding residual stresses. The model takes into account the material properties of the critical location, the severity of the notch, the initial residual stress and the remotely applied stress range.

II. MODEL TO CALCULATE THE FATIGUE CRACK INITIATION LIFE IN WELDS

A. General

Fatigue failures invariably initiate at the most highly strained regions of a structure, and the stresses and strains at these locations cause and govern the fatigue failure process. In welded structures, the potential sites for nucleation of a crack; the toe and defects such as pores, inclusions, etc., (18) are more numerous than in unwelded structures. Due to the high concentration of stress at these notches, localized yielding occurs even when the remainder of the structure behaves elastically. Elastic analysis of the notch-root stresses and strains is therefore inapplicable. To estimate the fatigue crack initiation life of a welded structure, then, a knowledge of the stress-strain history and an ability to predict the response of the material to that history at these critical locations are mandatory.

B. The Critical Location Approach

Numerous analyses are available which predict the fatigue crack initiation life in notched members (9, 19-24). In all of these analyses, it is assumed that a smooth specimen under appropriate control, can simulate the stress-strain behavior of the metal at the notch root; and consequently, the smooth specimen and the notch member will have the same crack initiation life. Topper and Morrow (24) have summarized the necessary requirements for such an analysis:

1. A mechanics analysis for the determination of the stress-strain behavior at the critical location (notch).
2. Knowledge of the cyclic stress-strain properties of the metal to determine the response of the material at the notch to remotely applied stresses.
3. Knowledge of the fatigue properties of the metal for use in an appropriate cumulative damage procedure.
4. A cumulative fatigue damage summation method to accurately predict life for any arbitrary stress-strain sequence.
5. A method of combining 1-4 such that fatigue crack initiation life of a notched member subjected to any arbitrary loading sequence can be calculated on a reversal by reversal basis using computer simulation methods.

1. Mechanics Analysis

In notched members which have yielding at the notch root, there exists no simple stress-strain relationship like Hooke's law. To address the problem of relating nominal stress/strain to local stress/strain, the expressions derived by Neuber (25) and by Stowell (26) have been widely used. Although both relationships give the same degree of accuracy (27), Neuber's formulation has gained more popularity because of its simplicity.

For any linear or nonlinear elastic material, Neuber (25) states that the theoretical elastic stress concentration factor is equal to the geometric mean of the actual stress- and strain-concentration factors, i.e.,

$$K_t = (K_\sigma \cdot K_\varepsilon)^{1/2} \qquad (6)$$

where

K_t = Theoretical elastic stress concentration factor

K_σ = Stress concentration factor

K_ε = Strain concentration factor

Expressing K_σ and K_ε in terms of its definitions, Eq. 6 becomes,

$$K_t = \left(\frac{\sigma}{S} \cdot \frac{\varepsilon}{e}\right)^{1/2} \tag{7}$$

where

σ and ε = Local stress and strain at the notch root

S and e = Nominal remotely applied stress and strain

Topper et al. (9) have shown that Eq. 6 can be applied to the notch fatigue problem if K_f is substituted for K_t, and K_σ and K_ε are written in terms of the ranges of stress and strain,

$$K_f = \left(\frac{\Delta\sigma}{\Delta S} \cdot \frac{\Delta\varepsilon}{\Delta e}\right)^{1/2} \tag{8}$$

where

K_f = Fatigue notch factor (usually less than K_t)

$\Delta\sigma$ and $\Delta\varepsilon$ = Local stress and strain ranges at the notch root

ΔS and Δe = Remotely applied stress and strain ranges

Rearranging Eq. 8 and multiplying both sides by $\sqrt{E}$,

$$K_f\,(\Delta S \Delta e E)^{1/2} = (\Delta\sigma\Delta\varepsilon E)^{1/2} \tag{9}$$

where

E = Elastic modulus

In most engineering problems, the nominal stresses and strains are elastic, so that Hooke's law may be used. Therefore, $\Delta S = \Delta e E$; and Eq. 9 becomes,

$$\Delta\sigma\Delta\varepsilon = \frac{(K_f \Delta S)^2}{E} \tag{10}$$

Equation 10 relates the remotely applied stress-strain behavior of a notched member to the stress-strain behavior at the notch root. Using Eq. 10, Wetzel (28) showed that a smooth specimen forced to undergo a stress-strain history given by the left side of Eq. 10, may be used to simulate the stress-strain history of the metal at the notch root and, furthermore, that the fatigue life of that smooth specimen may be used to estimate the fatigue crack initiation life of the notched specimen being simulated.

Equation 10 assumes that the stress state at the notch is uniaxial as in the smooth specimen. The state of stress at the root of a notch is biaxial. Preliminary results of Miller (29) show that the fatigue crack initiation lives of uniaxial tests are the same as those measured for a biaxial stress field. It is also assumed that the stress gradient in the notched region is small so that the plastic zone is large relative to the diameter of the smooth specimen. For smaller plastic zones or higher gradients, Coffin (30) suggests the use of either proportionally smaller fatigue specimens or an earlier indication of failure than obtained in standard size specimens (approximately 0.25 in. diameter).

2. Cyclic Stress-Strain Behavior

a. Monotonic Stress-Strain Behavior

If a smooth specimen is pulled in tension, its total strain may be decomposed into its elastic and plastic components.

$$\varepsilon = \varepsilon_e + \varepsilon_p \tag{11}$$

where

ε = Total true strain

ε_e = True elastic strain

ε_p = True plastic strain

The true elastic strain is given by Hooke's law and the true plastic strain by a power function (31,32)

$$\varepsilon_p = \left(\frac{\sigma}{K}\right)^{1/n} \tag{12}$$

where

σ = True stress

K = Monotonic strength coefficient

n = Monotonic strain hardening exponent

Equation 11 can be expressed as

$$\varepsilon = \frac{\sigma}{E} + \left(\frac{\sigma}{K}\right)^{1/n} \tag{13}$$

E, K and n are experimentally determinable constants for a specific metal which characterize its monotonic behavior.

b. Cyclic Stress-Strain Behavior

As with the monotonic properties, the cyclic stress-strain properties are determined by testing a smooth specimen under axial, cyclic-strain control. Landgraf et al. (33) define the cyclic stress-strain curve as the locus of tips of the stable hysteresis loops from several companion tests at different, completely-reversed, constant-strain amplitudes. Landgraf et al. (33) and Endo and Morrow (34) pointed out that this curve could be considered as a measure of the steady state cyclic deformation resistance of a material.

A typical stable hysteresis loop is illustrated in Fig. 2 and a set of stable loops with a cyclic stress-strain curve drawn through the loop tips is illustrated in Fig. 3. Halford and Morrow (35) and Morrow (31) observed that for many metals the cyclic stress-strain curve, when magnified by two, approximately describes the stable hysteresis loop shape. This observation is consistent with Massing's postulate (36) which assumes that the hysteresis curve is geometrically similar to the cyclic stress-strain curve magnified by a factor of two. If Massing's postulate is obeyed, then one can generate the hysteresis loop shape from the cyclic stress-strain curve with no modification other than doubling the ordinates. As will be subsequently discussed, the material studied in this work did not obey Massing's postulate so that a more difficult method of generating hysteresis loops from the cyclic stress-strain data had to be used.

The equation describing the cyclic stress-strain curve is given by (31)

$$\frac{\Delta\varepsilon}{2} = \frac{\Delta\sigma/2}{E} + \left(\frac{\Delta\sigma/2}{K'}\right)^{1/n'} \tag{14}$$

where

$\Delta\varepsilon$ = Total true strain range

$\Delta\sigma$ = Total true stress range

K' = Cyclic strength coefficient

n' = Cyclic strain hardening exponent

The definition of the cyclic stress-strain curve implies that this curve can be obtained by connecting the tips of the stable hysteresis loops from several companion specimens tested at different, completely-reversed, strain ranges. Since this method requires a number of identical specimens and considerable testing time, alternative methods have been devised for obtaining the information required using only one specimen. These methods are based on the fact that most metals will stabilize rather quickly after changes in the cyclic strain amplitude. Landgraf et al. (33) suggest methods that can be used for the determination of the cyclic stress-strain curve.

The cyclic stress-strain behavior of metals usually exhibit several general attributes. Krempl (37) considered that the most significant attributes are: memory, cyclic dependent hardening and softening, and cyclic dependent stress relaxation. A short explanation of these terms is given below.

By memory one recognizes that the cyclic stress-strain curve at any time is dependent on deformations which occurred at previous times. The material remembers its previous strain history.

In a completely reversed, strain-controlled test, cyclic hardening

produces an increase in the stress range during cycling, while cyclic softening produces a decrease in the stress range. If the cyclic stress-strain curve lies above the monotonic curve, the material has cyclically hardened; if the cyclic stress-strain curve is below the monotonic curve, the material has cyclically softened.

Cyclic dependent stress relaxation is defined as a decrease in the absolute value of the mean stress under constant strain amplitude cycling.

3. Fatigue Behavior

Morrow (31) has shown that four empirically determined quantities are needed to characterize the fatigue behavior of a metal. The expressions defining these properties involve relations between elastic strain-fatigue life and plastic strain-fatigue life. Landgraf (38) divides these properties into stress and plastic strain resistance.

a. Stress Resistance

The stress amplitude and reversals* to failure are related through the relation called Basquin's law:

$$\sigma_a = \sigma_f' (2N_f)^b \qquad (15)$$

where

σ_a = Stress amplitude

*A reversal is defined as a branch of a stress-strain curve over which the total strain is either monotonically increasing or monotonically decreasing. In constant amplitude testing, one cycle is equal to two reversals.

σ_f' = Fatigue strength coefficient, which is the stress intercept of the $\Delta\varepsilon_e/2 - 2N_f$ diagram at one reversal ($2N_f = 1$)

b = Fatigue strength exponent or Basquin's exponent, which is the slope of the logarithmic stress amplitude-life plot

σ_f' and b are considered to be the fatigue strength properties of a metal.

Since the elastic strain amplitude is given by σ_a/E, the relationship between elastic strain and life is,

$$\frac{\Delta\varepsilon_e}{2} = \frac{\sigma_a}{E} = \frac{\sigma_f'}{E} (2N_f)^b \tag{16}$$

where

$\frac{\Delta\varepsilon_e}{2}$ = Elastic strain amplitude

The influence of the mean stress on the stress resistance of a metal is taken into account by modifying Eq. 15 to the form (39),

$$\sigma_a = (\sigma_f' - \sigma_o) (2N_f)^b \tag{17}$$

where

σ_o = Mean stress

b. Plastic Strain Resistance

The equation relating the plastic strain amplitude and reversals to failure is,

$$\frac{\Delta\varepsilon_p}{2} = \varepsilon_f' (2N_f)^c \tag{18}$$

where

$\frac{\Delta\varepsilon_p}{2}$ = Plastic strain amplitude

ε_f' = Fatigue ductility coefficient, which is the plastic strain intercept of the $\Delta\varepsilon_p/2 - 2N_f$ diagram at one reversal

c = Fatigue ductility exponent, which is the slope of the logarithmic plastic strain amplitude-life plot.

ε_f' and c are considered to be the fatigue ductility properties of a metal. Equation 18 is of the same form as the Coffin (40) and Manson (41) low cycle fatigue law.

c. Total Strain Resistance

The total strain resistance of a metal is considered to be the summation of its elastic and plastic strain resistance (42)

$$\frac{\Delta\varepsilon}{2} = \frac{\Delta\varepsilon_e}{2} + \frac{\Delta\varepsilon_p}{2} \tag{19}$$

Thus, adding Eqs. 16 and 18, an expression relating the total strain amplitude and fatigue life is obtained:

$$\frac{\Delta\varepsilon}{2} = \frac{\sigma_f'}{E}(2N_f)^b + \varepsilon_f'(2N_f)^c \tag{20}$$

4. Cumulative Fatigue Damage Analysis

Although several cumulative fatigue damage procedures have been developed to calculate the crack initiation life under constant stress or strain amplitude or under random stress-strain history (43-48),a more efficient

and accurate technique, appropriate for use in high speed digital computers, are those which compute the fatigue damage associated with each reversal. To perform these reversal by reversal cumulative damage calculations, a knowledge of the elastic and plastic strain and mean stress for each reversal is necessary. For a given reversal, damage is imparted by the value of the elastic strain, plastic strain and level of the mean stress.

The damage in terms of the elastic strain amplitude of a particular reversal is obtained from Eq. 15,

$$\left(\frac{1}{2N_f}\right)_e = \left(\frac{\Delta\sigma/2}{\sigma_f'}\right)^{-1/b} \tag{21}$$

The damage in terms of the plastic strain amplitude is obtained from Eq. 18,

$$\left(\frac{1}{2N_f}\right)_p = \left(\frac{\Delta\varepsilon_p/2}{\varepsilon_f'}\right)^{-1/c} \tag{22}$$

To calculate the damage due to the mean stress alone, Martin (49) developed the following expression from Eqs. 17, 22 and 12 in terms of ranges of plastic strain and stress,

$$\left(\frac{1}{2N_f}\right)_o = (\varepsilon_f')^{1/c}\left[\left(\frac{\Delta\sigma/2}{K'}\right)^{-1/n'c}\right]\left[\left(1 - \frac{\sigma_o}{\sigma_f'}\right)^{1/n'c} - 1\right] \tag{23}$$

The damage is obtained either from Eq. 21 or 22 and modified according to Eq. 23 as follows,

$$\frac{1}{2N_f} = \left[\left(\frac{1}{2N_f}\right)_e \text{ or } \left(\frac{1}{2N_f}\right)_p\right] + \left(\frac{1}{2N_f}\right)_o \tag{24}$$

The crack initiation period is assumed to end when the Palmgren (50)-Miner (51) rule (linear cumulative damage rule) is satisfied, i.e.,

$$\sum_{i} \left(\frac{1}{2N_f}\right) (2N_i) = 1 \qquad (25)$$

where

2N = Number of reversals necessary to initiate a crack

5. Model of Cyclic Stress-Strain Behavior

As stated in the beginning of this section, the last requirement for a successful analysis of fatigue at a notch is the development of a mathematical model able to reproduce the material response previously discussed. As was discussed, the model not only needs to reproduce the hysteresis loop shape and have memory to take into account the history dependence of the material, but also must simulate hardening and softening and relaxation of the mean stress. Of the models proposed (52,53) to execute this computer simulation, the highly developed rheological model developed by Martin (49,52) and extended by Jhansale and Topper (54) and by Plummer (55) was adopted.

The basic rheological model consists of spring and frictional slider elements as shown in Fig. 4. The elastic modulus of an element, E_i, is linear. The slider locks the element until the yield stress of the element, $\bar{\sigma}_i$, is exceeded in tension or compression. Each spring-slider element is capable of storing residual stresses which in turn, produce the memory capabilities of the model.

The following example illustrates some of the characteristics of a multielement model. Consider the system of elements shown in Fig. 4. Let the slider yield stresses of the second and third elements be $\bar{\sigma}_2 = 40$ and $\bar{\sigma}_3 = 50$ respectively and let a stress $\sigma^* = \pm 60$ be applied (the first

element models elastic response and has no slider, i.e., $\bar{\sigma}_1 = 0$). The response of the model is shown in Fig. 5. Along the initial loading path O-A-B-C, the second element yields at 40 and the third element yields at 50. The slope, E_i^*, for the ith segment of the curve is obtained from

$$\frac{1}{E_i^*} = \frac{1}{E_1} + \left(\frac{1}{E_2} + \frac{1}{E_3} + \ldots + \frac{1}{E_i}\right) \tag{26}$$

where i is summed over the spring-slider elements which have been yielded. Residual stresses stored in the second and third elements are 20 and 10 respectively. At C, $\sigma^* = 60$, the loading direction is reversed. On unloading, the path C-D-E-F is obtained. The slope of each linear segment is the same as for the corresponding increment on the curve OC, however, the residual stresses double the stress increment and strain increment over each linear segment.

The usefulness of this type of model can be appreciated by the following:

1. Memory, as previously discussed, is inherent to the model's response.
2. Hardening and softening can be accomplished if the parameters $\bar{\sigma}_i$ and E_i of each element are varied for each reversal of loading in an appropriate manner.
3. Cyclic relaxation of the mean stress is achieved by multiplying the stiffness of each spring by a relaxation function, $f|\sigma|$. This function should be of such a form that it reduces the value of the element moduli with increasing $|\sigma|$.

4. The Massing's postulate, i.e., that the hysteresis curve is geometrically similar to the cyclic stress-strain curve when magnified by a factor of two, is satisfied.
5. Due to the relative simplicity of the model, it can be programmed for the digital computer; and hence, a cumulative fatigue damage analysis can be performed on a reversal by reversal basis since the elastic and plastic strains and the mean stress can be calculated for each reversal.

III. DETERMINATION OF THE FATIGUE NOTCH FACTOR FOR BUTT WELDS

Numerous empirical equations, among them that of Peterson, relate the observed fatigue notch factor, K_f, to the elastic stress concentration factor, K_t (56-60). Raske (61) reviewed the ability of these equations to accurately predict K_f and concluded that none of them consistently produces superior results. Raske (62) devised a method to predict K_f using the features of existent theories and obtained good results. His method, however, requires an elasto-plastic analysis of the notched region which is difficult to perform for even the simplest geometries.

A. Peterson's Formulation

All the methods proposed to estimate the fatigue notch factor, K_f, involve relationships between K_f and K_t and some material parameter; the simplest of these is the one proposed by Peterson (57),

$$K_f = 1 + \frac{K_t - 1}{1 + \frac{a}{r}} \tag{27}$$

where

r = Radius at the notch root

a = Experimentally determined material parameter.

B. Determination of K_t

The theoretical stress concentration factor, K_t, is generally available for simple geometries--holes, ellipses, grooves, etc. (63)

Unfortunately, few attempts (64) have been made to determine the stress concentration factor for the weld geometries, partly because these geometries are very complicated in shape and partly because of the many variables involved.

In order to describe the geometry of a butt weld specimen, Lawrence (14) approximates the weld reinforcement by a segment of a circle, as shown in Fig. 6. If the flank angle and the edge preparation angle can be used to specify the geometry, then the relationship between these parameters and the ratios h/w and w/t are (14),

$$\frac{h}{w} = \frac{1}{2} \tan \frac{\theta}{2} \tag{28}$$

$$\frac{w}{t} = \tan \frac{\phi}{2} \tag{29}$$

where

h = Height of the reinforcement

w = Width of the reinforcement

t = Thickness of the Plate

θ = Flank angle

ϕ = Edge preparation angle.

Although θ and ϕ completely describe the external or macrogeometry, the stress concentration factor is also a function of the microgeometry at the toe of the weld. A variable radius at the toe of the weld was chosen to represent this microgeometry.

Determinations of the elastic stress concentration factor, K_t, for selected butt weld geometries were carried out using an elastic finite

element computer program (FEM). Details of this program are given in Appendix A. Figures 7 and 8 present the result of the analysis. The ratio r/t is plotted against K_t for several values of θ keeping ϕ constant (Fig. 7) or varying ϕ but maintaining θ constant (Fig. 8). For ratios r/t greater than 0.10, K_t values are close to the results of Derecho and Munse, (64) however, for lower values of r/t, the results of the Derecho and Munse are conservative. This discrepancy is believed to be the result of the coarse mesh used in their finite-difference solution.

C. Determination of K_f

The fatigue notch factor of butt weld specimens was determined using the Peterson's equation and the stress concentration factor determined by FEM for each ratio r/t. Figures 9 and 10 present the plot of K_f vs r/t for butt welds made of A-36 steel. A value of a = 0.010 in. was used to calculate K_f (Eq. 27) as suggested by Peterson (65). This value of "a" corresponds to the base plate material (A-36 steel), no attempt was made to ascertain the exact value for the material of the heat affected zone.

The salient feature of these plots is that K_f goes through a maximum at a "critical value" of the ratio r/t. In a welded specimen, the radius at the toe of the weld is not known and is certainly not constant along the weld bead; and since fatigue cracking will start from the most critical region, i.e., the location of highest K_f, it is felt that the maximum value of K_f corresponding to this critical value of r/t is the one which should be used. (For a typical butt weld, $\theta = 30°$, $\phi = 90°$ and t = 1 in., $(K_f)_{max}$ is 2.10 according to Fig. 9). This maximum value

of K_f would result in conservative estimates of the fatigue crack initiation life. Unless otherwise indicated, this maximum value was used in all calculations of the fatigue crack initiation life in butt welds.

IV. DETERMINATION OF THE CYCLIC STRESS-STRAIN AND FATIGUE PROPERTIES OF A-36 STEEL

A. Material and Specimen

Hot rolled ASTM A-36 steel was selected because of its wide range in the structural and ground vehical industry. Smooth specimens were cut and carefully machined from 5/8-in. flat plate. After machining, the specimens were mechanically polished with three successively finer grades of emery paper to the dimensions and geometry shown in Fig. 11.

B. Apparatus and Testing Procedure

Testing was conducted on a ±20 kips MTS close-loop servo-controlled hydraulic test system similar to that described by Feltner and Mitchell (66). Wood's metal grips were used to insure proper axial alignment of the specimen (34). Strains were measured by an Instron clip-on extensometer with a 1/2-in. gage length. Amplified signals from the clip-on extensometer and load cell were continuously recorded with two-pen strip chart recorder and monitored on an oscilloscope. Tests were conducted at frequencies from 0.1 to 10 Hz at room temperature. A sine wave function generator was used to control strain amplitude. In order to maintain isothermal conditions during the high frequency tests, cold water was allowed to flow thru the Wood's metal grip on one end of the specimen.

C. Test Program

A total of 11 specimens were tested to characterize the monotonic,

cyclic stress-strain and fatigue properties of A-36 steel. A monotonic tension test was performed on one specimen. Nine companion specimens were cycled to fracture at essentially a constant strain range, and one specimen was tested at several strain ranges to study the cyclic relaxation of the mean stress. A continuous record of the hysteresis loops was taken during the first few cycles and periodically thereafter using an X-Y recorder. All fatigue tests were started in compression.

D. Experimental Results

1. Monotonic Stress-Strain Behavior

The monotonic behavior of A-36 steel is illustrated in Fig. 12. Like other mild steels, A-36 steel exhibits pronounced upper and lower yield points in both tension and compression. A Lüders strain region follows the initiation of yielding and strain hardening develops only after about 2 percent strain. True plastic strain, ε_p, versus true stress, σ, data are plotted in Fig. 13. The strength coefficient, K, and the strain hardening exponent, n, were determined by least-squares fit of the data shown in Fig. 13. A single fit for those data would not be appropriate; therefore, the stress-strain curve was divided into two segments. One line fits the relatively flat-topped, Lüders portion of the stress-strain curve and the other line fits the rapid hardening segment.

Table 1 lists the properties obtained from the monotonic tension test.

2. Cyclic Stress-Strain Behavior

Figure 12 shows the cyclic stress-strain curve determined by companion specimens; also included in this figure is the monotonic curve. The constants K' and n' for Eq. 14 were determined by plotting the true plastic strain amplitude, $\Delta\varepsilon_p/2$, versus the true stress amplitude, $\Delta\sigma/2$, each of these was obtained from stabilized hysteresis loops. Figure 14 shows the behavior of the data. A straight line on the log-log coordinates through the data points was made by the least-squares method. Table 2 lists the cyclic stress-strain properties of A-36 steel.

Ideally, Eq. 14 should be able to describe an outer trace of a stable hysteresis loop at any strain range if Massing's postulate is obeyed. A check of this assumption was obtained by plotting a set of fully reversed stabilized hysteresis loops with their lower loop tips superimposed at a common origin (see Fig. 15). In this case, the cyclic stress-strain curve magnified by a factor of two does not accurately describe the stable hysteresis loop shape, and an alternative but more tedious method of obtaining the hysteresis loops from the cyclic stress-strain curve was used and will be described in Chapter V.

a. Cyclic Hardening and Softening

Cyclic hardening and softening were studied from data obtained at constant strain amplitude as shown in Fig. 16. From this figure and from Fig. 12, it can be seen that A-36 steel may cyclically harden, cyclically soften or remains relatively stable. As a rule of thumb, cyclic hardening

occurs when the fully reversed strains exceed the value of strain at which the cyclic and monotonic stress-strain curves intersect. For smaller fully reversed strains, cyclic softening occurs.

b. Cyclic Relaxation of Mean Stress

From the data generated in constant amplitude, strain-controlled tests, it was considered that for the steel under investigation a 0.004 strain amplitude will produce a negligible change in the stress amplitude in the range from 100 to 10,000 reversals (negligible hardening or softening). A single smooth specimen was fatigue cycled at a strain amplitude of 0.004 for 1000 cycles to ensure stabilization of the hysteresis loop before inducing a mean stress to study the material's relaxation behavior. By this means, the mean stress relaxation behavior obtained was not affected by the transient effect of hardening or softening. If the mean stress relaxed completely or became nearly stable before failure, new strain limits were chosen so as to produce a different value of the mean stress. The complete test then, consisted of several blocks at 0.004 strain amplitude which provided stabilization of the hysteresis loop and zero mean stress for the subsequent block, alternating between blocks in which mean stress was induced and from which the mean stress relaxation data were obtained. Figure 17 illustrates the strain block sequence. As can be seen from the preceding figure, two different tests were run:

1. Tests at constant strain amplitude but variable mean strain, and

2. Tests at constant mean strain but at variable strain amplitude.

Mean stress was measured as the average of two stress peaks.

Figure 18 shows the results of the tests conducted at constant mean strains but variable strain amplitudes and Fig. 19 presents the results of the tests conducted at constant strain amplitude but at variable mean strains. Although only tensile mean stresses were induced, the same rate of relaxation has been observed for corresponding compressive stresses (49).

From these experiments the following conclusions can be drawn:

1. The rate of relaxation of the mean stress is a function of the strain amplitude, mean strain and number of cycles.
2. Higher rates of relaxation are obtained for greater strain amplitudes or for greater mean strains.
3. At high strain amplitudes or mean strains, mean stresses relaxed toward zero or to a practically stable value for lower strain amplitudes. It seems that for strain amplitudes which do not produce large plastic strains, there will not be any relaxation.

3. Fatigue Behavior

Results of the completely reversed strain-controlled tests are presented in Table 3. Data for determining the stress and strain amplitude for each test were taken from a hysteresis loop at approximately half of the fatigue life. Elastic strain was computed by extrapolating the elastic

line of the hysteresis loop on the strain axis. Plastic strain was computed by subtracting the elastic strain from the total strain. The fatigue strength coefficient, σ_f', and the fatigue strength exponent, b, were obtained by fitting a straight line to the elastic strain-reversals to failure data by the least-squares method. Similarly, the fatigue ductility coefficient, ε_f', and the fatigue ductility exponent, c, were estimated by a straight line, least-squares fit, to the plastic strain-reversals to failure data. Figure 20 shows the results of these tests in terms of strain and reversals to failure. Table 4 gives the fatigue properties of A-36 steel.

E. Discussion of Experimental Results

A-36 steel shows much the same characteristics as other mild steels, i.e.,

1. Its monotonic behavior is far different from its cyclic behavior.
2. Cyclic hardening and softening is a function of the strain range. Furthermore, cyclic softening is possible even if it is fatigue cycled at stresses below the upper or lower yield point.
3. Cyclic relaxation of the mean stress is very rapid in the first 1000 cycles.
4. Massing's postulate is not obeyed for this steel.

V. ADAPTATION OF THE RHEOLOGICAL MODEL TO A-36 STEEL

A. Stable Cyclic Stress-Strain Curve

In the last chapter, it was shown that for A-36 steel, the Massing's postulate was not obeyed: The cyclic stress-strain curve when magnified by a factor of two, did not represent the stable hysteresis loop shape. This behavior of A-36 steel is not consistent with the inherent characteristics of the rheological model as proposed by Martin (52).

Based on observations of the same phenomena in several materials, Jhansale (54,68) has shown that the upper branches of the stabilized hysteresis loops could be accurately matched by suitable translation of these branches along the initial elastic slopes. He postulated (for the materials studied) that all transient or steady state hysteresis branches of a given metal subjected to constant amplitude (stress or strain) cycling are identical in shape after deletion in each case of an appropriate initial elastic portion. For those materials which do not obey Massing's postulate, the linear portion of the steady state of the hysteresis curves is a function of the hysteresis loop size. The "skeleton curve" is defined as the portions of the hysteresis branches which are identical in shape and are independent of cyclic history at constant amplitude.

An extension of the above postulates to A-36 steel was made by translating the stable hysteresis loops (shown in Fig. 15) along the elastic line until the upper branches were nearly coincident, as illustrated in Fig. 21. The origin of coordinates shown was chosen based on the fact

that A-36 steel should be stable at about 0.004 strain amplitude according to Figs. 12 and 16. A doubled skeleton curve was defined with respect to the origin O. Stress offsets determined from Fig. 21 are plotted in Fig. 22 as a function of the total strain range for stable A-36 steel. The complete description of an outer trace of a given hysteresis branch is performed by adding the stress offset to the corresponding hysteresis curve. The stress offsets are positive for strain ranges in which the material hardens and negative for those in which the material softens.

B. Cyclic Hardening and Softening

Attempts to model the cyclic hardening and softening of A-36 steel according to Martin's procedure (52) were unsuccessful because the variation of the parameters K' and n' which are used to simulate hardening and softening (by changes in their values during cycling) behave in an irrational way throughout the cyclic history of the material.

Successful modeling of hardening and softening for this material was accomplished following the approach suggested by Jhansale (54,68) and extended by Plummer (55). The analysis involved consists of fitting the various branches of the hysteresis plots to the doubled skeleton curve for the stable material. This fitting was carried out by superposition of the individual branches of the hysteresis loops on the doubled skeleton curve and translation of the loops along the common elastic slope until the upper loop tips were approximately tangent to the doubled skeleton curve. Figures 23 through 25 show the individual branches of the hysteresis loops fitted to the doubled skeleton curve obtained in Fig. 21. Stress offsets

determined from these plots are then function of the number of reversals and the total strain range. Figure 26 shows that a family of straight lines could represent the behavior of the data.

C. Cyclic Relaxation of the Mean Stress

Simulation of cyclic relaxation of mean stress was performed using Martin's relaxation function (49)

$$f(|\sigma|) = 1 - \frac{|\sigma|}{R\,C} \tag{30}$$

where

R C = Relaxation constant.

The relaxation constant was determined by comparing actual relaxation test data with that produced by the model. Figure 27 shows the simulation results for four values of the relaxation constant. A final value of the relaxation constant equal to 2×10^7 psi was chosen based on the several mean stress relaxation tests. Although the form of the relaxation function is different from that of the test results, it produces the same change in the mean stress in the same number of reversals, i.e., they go to zero mean stress in the same number of reversals. Moreover, the use of Eq. 30 would tend to yield conservative results in the damage analysis.

D. Results

Constant amplitude, strain-control simulations were made using a digital computer and were compared with those obtained experimentally.

The predicted and actual stress-strain response of the model are compared in Figs. 28 and 29. It can be seen from these figures that the model accurately predicts the response of A-36 steel for both the virgin material (at high strain amplitude including the phenomenon of cyclic hardening) and for the stable material (at lower strain amplitude).

The model used in conjunction with a damage summation procedure, as explained previously, produces an accurate life prediction as illustrated in Table 5.

E. Summary

The main purpose of the strain controlled simulation of A-36 steel as presented in this section was to gain an understanding and confidence in the development of similar simulation under Neuber control. Since every event (hardening, softening, relaxation of the mean stress) which happens to the material under strain control limits will also happen under Neuber control, the simulation technique should also work using Neuber control. A detailed description, together with a computer program, of Neuber control for A-36 steel is presented in Appendix B. The basic model follows that developed by Martin (49) and Plummer (55) and incorporates all the characteristic features inherent in A-36 steel including cyclic hardening and softening and relaxation of the mean stress. A damage procedure based on a reversal by reversal basis is incorporated into the model. Although the computer program has been designed for constant amplitude loadings, its modification for random loadings can be easily performed.

VI. FATIGUE CRACK INITIATION PREDICTIONS

A. Introduction

The main purpose of this study was to estimate the fatigue crack initiation life in welded specimens using the previously explained low cycle fatigue concepts.

Welds are difficult to analyze because of the many factors which can influence their fatigue resistance: misalignment of the welded pieces (bending stresses), residual stresses, variability in weld geometry, etc. In predicting the crack initiation life in welds, another factor--the actual fatigue properties of the material at the critical notches--also should be known. No information concerning the fatigue properties of such locations (heat affected zone, weld metal, etc.), is given in the literature. With the above points in mind then, fatigue crack initiation predictions were performed for simple and reproducible geometries where the above problems were minimized (simulated welds) and progressed to more complicated situations (real welds) where all the mentioned factors were present.

B. Fatigue Crack Initiation Predictions for Simulated Butt Weld Specimens

1. Material and Specimens

Idealized weld specimens were produced to test the ability and accuracy of the low cycle fatigue rheological model to predict the crack initiation life of welds. For present purposes, it was considered that a simulated weld specimen should: (a) have a very well defined and reproducible geometry so that the stress concentration factor (K_t) and the fatigue

notch factor (K_f) should be the same for all specimens, (b) have a minimal variability in material properties throughout the specimen so that the material properties of the base plate could be assumed for the notch root, (c) have no residual stresses at the notch root so that the fatigue crack initiation life would not be affected by this factor, and (d) have no bending stresses so that the stress concentration factor (K_t) and the fatigue notch factor (K_f) could be easily determined.

Simulated weld specimens were fabricated from a 7/8-in. thick, hot-rolled, ASTM A-36 steel plate. Specimen blanks were flame cut so that the direction of rolling would be parallel to the applied stress. A milling tool having a semicircular profile (r = 1/2 in.) was used to produce a single, 1/4-in. high, simulated "butt-weld" reinforcement. The thickness of the specimen was then reduced to 5/8-in. by machining the side having the "weld bead".

After machining, the specimens were stress relieved at 1200°F for two hours. After annealing, the specimens were polished with a 120 disc grinder and with successively finer emery paper (up to 4/0). The scratches produced by the polishing operation were removed by chemical polishing with a solution of 85 ml H_2O_2, 15 ml H_2O and 5 ml HF; in this way, a smooth, reproducible surface was created which permitted the easy detection of the cracks and at the same time, minimized potential crack initiation sites other than the "toe" of the simulated weld. Lastly, the radii of the "toes of the weld" were measured from microphotographs of the specimen profile. Radii between 0.012 in. to 0.045 in. were measured. Figure 30 shows the geometry and the dimensions of the specimens used.

2. Apparatus and Testing Procedure

The simulated welds were fatigue tested in a MTS ±50 kips closed-loop servo-controlled testing machine using a completely reversed stress cycle (R = -1). Figure 31 shows the fatigue test set-up. The tests were conducted at frequencies from 3 to 20 Hz depending on the stress amplitude. A sine wave function generator was used to control the load amplitude. To avoid errors associated with drift in the load signal, an oscilloscope was used to monitor the load cell during the high frequency tests.

3. Determination of the Crack Initiation Life

The crack initiation life was measured by means of microminiature strain gages of 0.015 in. gage length (Micro Measurements EA-06-015CK-120) mounted as close as 0.020 in. to the toe of the simulated weld: see Fig. 32. The strain at the "weld toe" was recorded on magnetic tape and/or plotted versus load using an X-Y plotter. Periodic observations of the "toe of the weld" were made with a low power magnifying glass (X10).

When a crack developed at the "toe of the weld", the strain gage closest to the crack sensed its presence by an increase in the strain gage reading. Further extension of the crack resulted in a further increase of the strain reading until the crack extended beneath the strain gage; at which point the strain gage reading began to decrease because the material below the strain gage was no longer strained. If the crack happened to initiate directly beneath the strain gage, then a sharp decrease in the strain gage reading was noticed immediately. Figure 33 shows schematically the changes

in the strain gage readings as the crack initiates and grows, and Fig. 34 shows positive maximum strain values versus number of cycles. Crack initiation was defined as the number of cycles needed to produce a small change in the strain gage reading (± 5 percent).

In order to determine the size of the crack sensed by the arbitrary ± 5 percent change in strain gage reading, one test was stopped when the strain gages indicated a +5 percent change. The maximum tensile load was applied to the specimen to open the crack, and the crack surfaces were heat-tinted by torch. The specimen was allowed to cool and then, fatigued at a R ratio of + 0.1. After failure, the fracture surface was examined with a microscope to determine the size of the crack which had been sensed. The fractograph of Fig. 35 shows that the heat tinted crack depth was 0.032 in. The strain gages located on the opposite "toe" shown in Fig. 35 also indicated about the same change in strain reading before heat tinting. Microscopic observations were made on sections cut from these areas. Figure 36 shows that a 0.011 in. crack had developed in this area. It was concluded that a ± 5 percent change in strain reading corresponded to the presence of an approximately 0.01 in. crack depth.

4. Results of Fatigue Testing and Fatigue Crack Initiation Predictions

The test results for the simulated butt weld specimens are presented in Table 6. Also included in this table is the ratio N_I/N_T. For the range of stresses investigated, it seems that the fatigue crack initiation life could be as much as 40% and as little as 20% of the total fatigue life.

The stress concentration factor (K_t) was determined as a function of the radius of the "toe of the weld" using finite element methods. Details

of these calculations are given in Appendix A. Peterson's equation (Eq. 27) with a = 0.010 in. was used to calculate the fatigue notch factor (K_f) as a function of the radius of the "toe of the weld". Results of these calculations are given in Fig. 37. The maximum value of K_f (2.20), corresponding to a radius of 0.023 in., was used in the fatigue crack initiation life predictions.

A comparison of the predicted K_f value with that given by its definition (fatigue strength of unnotched specimen/fatigue strength of notched specimen) can be obtained using reported values for the fatigue strength of 1015-1020 steel (69-70). Fatigue strengths (at 10^7 cycles) from 25 to 30 ksi are typical so that the range of K_f experimentally determined would be about 1.7 to 2.0; these values are close to that predicted using $(K_f)_{max}$ using Peterson's equation with a=0.01 in. (i.e., K_f=2.20).

Fatigue crack initiation life predictions were made using the cyclic stress-strain and fatigue properties previously determined for this steel and K_f equal to 2.20 as discussed. The computer program used for these predictions is given in Appendix B. Results of the fatigue crack initiation life are presented in Fig. 38. A very good agreement between the predicted and measured values of the fatigue crack initiation life was obtained. These results show that reliable predictions of the fatigue crack initiation life can be made if the fatigue notch factor and the cyclic stress-strain and fatigue properties are accurately known.

Fatigue crack initiation life predictions were performed for various notch geometries other than the simulated welds utilizing data reported in the literature. Unless otherwise indicated, in all of these estimations it was assumed that the cyclic stress-strain and fatigue properties of the material at the notch root were those of A-36 steel.

C. Fatigue Crack Initiation Predictions For A Hole In A Plate

Stallmeyer (71) determined the fatigue crack initiation life for an ASTM-A7 steel plate with a central, circular hole. Fatigue tests were conducted using a tension-compression stress cycle (R=1). The stress concentration factor for the geometry is given in Peterson's book (63) (K_t = 2.37). Peterson's equation (Eq. 27) was used to compute K_f (K_f=2.34). The cyclic stress-strain and fatigue properties of ASTM-A7 steel were assumed to be the same as those of ASTM-A36 steel. Results of the predicted crack initiation life as well as the data of Stallmeyer are shown in Fig. 39. As can be seen from Fig. 39, the predicted and measured fatigue crack initiation lives are almost coincident for the entire range of fatigue life reported. The range of the experimentally determined K_f is from 1.70 to 2.00. The lack of agreement between this range of K_f and that calculated using Eq. 27 is believed due to the relatively short fatigue lives (2×10^5 cycles) used for its determination.

Stallmeyer (71) also determined the fatigue crack initiation life for the same steel and notch geometry but for a zero to tension stress cycle (R = 0). Figure 40 shows the data points generated by Stallmeyer and the fatigue crack initiation life predictions. Again, very good agreement between the predicted and actual test data was obtained.

Crack propagation life estimates were made using the Paris' power law (3). The values of the coefficient C, and of the exponent m, were taken from Barsom (72) for A-36 steel. The Bowie (73) solution for a double cracked hole corrected for finite plate width was used for the stress intensity factor.

Results of these predictions are given in Fig. 41 from which it can be seen that the test results and predictions do not agree well at longer lives.

The predicted and actual total fatigue life ($N_T = N_I + N_p$) is presented in Fig. 42. The best fit curve to the data point and the predicted curve are nearly coincident throughout the entire life range considered. Figure 43 presents the percentage of the total fatigue life spent in initiation and its variation with the total life (N_T). The predicted line is above the experimentally determined ratios of N_I/N_T by 20 percent. This fact is a consequence of the difference between the predicted and measured fatigue crack propagation portion of the total fatigue life. However, this figure shows that for the life range investigated, the contribution of the fatigue crack initiation life is approximately 65 percent of the total fatigue life.

Raske (62) measured the fatigue crack initiation life for a central circular hole in a 7075-T6 Aluminum plate. A fully reversed stress cycle was employed (R =-1). The fatigue notch factors (K_f) used in the present estimations of the fatigue crack initiation life were those predicted and reported by Raske (62) and were calculated by Raske, using his method. The cyclic stress-strain and fatigue properties for this alloy were determined by Martin (49) and have been used for the fatigue crack initiation life estimates. Table 7 and Fig. 44 present the predicted crack initiation life together with the experimental results determined by Raske (62). Very good agreement between the reported data and the estimated fatigue crack initiation life is noticed throughout the life range investigated.

The partitioning of the fatigue crack initiation and propagation

lives is presented in Fig. 45. The ratios N_I/N_T reported in this figure are based on (N_I) predicted/(N_T) experimental. From this figure, it can be seen that at long life, most of the fatigue life is spent in crack initiation, whereas at short life, most of the life is spent in crack propagation.

The very good agreement between the calculated and measured fatigue crack initiation lives presented in the previous examples suggests that reliable results can be obtained using the low cycle fatigue rheological model. However, knowledge of the fatigue notch factor and of the cyclic stress-strain and fatigue properties of the material of the notch root is required.

Fatigue crack initiation life predictions were performed for actual welds using data from the literature and will be discussed next. No attempts were made to determine the cyclic stress-strain and the fatigue properties of the heat affected zone or weld metal in the location of the critical notches; the properties of these locations were assumed to be the same as those of A-36 steel.

D. Fatigue Crack Initiation Predictions For Welds

Burk (74) measured the crack initiation life in butt welds made of a 3/8-in. thick, SAE 1020 steel plate by means of strain gages mounted at the surface of the plates. By artificially inducing cracks of known size at the toe of the weld and measuring the corresponding changes in the strain gages readings after application of the load, Burk (74) showed that the strain gages were able to sense an initial crack size of the order of 0.01 in.

Figure 46 shows the predicted and actual values of the fatigue crack initiation lives for these specimens. Since the specimens used by Burk

were subjected to small bending stresses when fatigue cycled (due to weld joint distortions), the nominal stress for each data point in this figure was taken as the sum of the remote applied stress and the induced bending stresses. The fatigue crack initiation life estimate is based on a single K_f value which has not been corrected for the effects of bending. Good agreement is observed between the predicted and reported crack initiation life.

Using the power law proposed by Paris (3) and the procedure developed by Lawrence (14), Burk (74) also calculated the fatigue crack propagation life for these specimens. Results of these calculations are shown in Fig. 47.

Figure 48 shows the total fatigue life calculated using the two separate procedures. A least-squares fit to the data points is nearly coincident with the line representing the predicted values. Figure 49 presents the partitioning of the initiation and propagation lives as a function of the total life. As can be seen from this figure, the fatigue crack initiation life accounts for more than 80 percent of the total fatigue life in the long life regime (> 10^6 cycles).

Burk (74) also measured the fatigue crack initiation life and the total fatigue life in butt welds made of a 5/8-in. thick, SAE 1020 steel plate. Figure 50 shows the predicted fatigue crack initiation life and the data points as obtained by Burk (74). Good agreement between Burk's results and the fatigue crack initiation life estimates is observed. Fatigue crack propagation estimates (determined as previously mentioned) were taken from Burk's results and reported in Fig. 51. The estimates of the total fatigue life using the present approach to calculate the initiation portion and Lawrence's (14) procedure to estimate the propagation portion are presented in Fig. 52,

also included in this figure are the test results determined by Burk (74). Good agreement between the predicted and actual test results is observed. The partitioning of the crack initiation and the crack propagation lives as a function of the total fatigue life is shown in Fig. 53. The data points and the predicted partitioning show that the fatigue crack initiation life is the dominant process at long lives and accounts for as much as 80 percent of the total fatigue life.

Testin (75) determined the fatigue crack initiation life in a series of SAE 1015-1020 steel, fillet welds using a tension-compression stress cycle. The specimen geometry and dimensions are shown in Fig. 54. Before fatigue testing, the specimens were stress relieved at 1200°F for one hour. The tests were controlled using strain gages mounted on the surfaces of the plate.

The elastic stress concentration factors (K_t) for the welds were calculated and are plotted as a function of the ratio r/t in Fig. 55. The fatigue notch factor (K_f) was calculated using Eq. 27 and is also plotted in Fig. 55 as a function of the ratio r/t. The actual, measured r/t ratio for the specimens was 0.04 which corresponds to K_t = 2.56, the corresponding K_f value for this r/t ratio was 2.20. The maximum value of K_f derived from the plot of K_f versus r/t (Fig. 55) was 2.40.

Figure 56 shows the results of the predicted fatigue crack initiation life using K_f values of 2.40 and 2.20; also included in this figure are the test results. A difference of one order of magnitude between the observed and predicted crack initiation life exists at low stress levels ($N_I > 10^6$ cycles); whereas, this difference is a factor of two in life for higher stress levels. Possible causes of this disagreement may be differences

in cyclic stress-strain and fatigue properties of the heat affected zone and those of the base plate; in fact, hardness determinations made in the heat affected zone and in the material used to generate the cyclic stress-strain and fatigue properties (A-36 steel) indicated a difference of about 50 Brinell hardness points. This difference is equivalent to a rise of the ultimate tensile strength of the heat affected zone (HAZ) up to 85 ksi, and consequently the fatigue strength coefficient (σ_f') and the fatigue strength exponent (b) of the heat affected zone should be different from the values for A-36 steel (σ_f' and $|b|$ will be higher). The uncertainty in the calculated K_f value may provide another source of error; first, the "a" value used in Peterson's equation could be influenced by the microstructure and mechanical properties of the material at the toe of the weld; and second, it is known that with the correct value of "a", Peterson's equation could be in error by as much as ± 20 percent which could cause roughly a factor of two or three in life.

E. Summary and Conclusions

Fatigue crack initiation predictions were performed for a variety of materials, notch geometries and loading conditions. For all the cases studied, it was assumed that the cyclic stress-strain and fatigue properties of the material at the critical notches were identical to those of the parent material.

The results of the comparison of the model's predictions and experimental data can be summarized as follows:

1. An excellent agreement between the estimated fatigue crack initiation life and test results was obtained for those materials and notch geometries (simulated welds in an A-36 steel plate and a circular hole in a 7075-T6 aluminum plate) which were very well characterized in terms of their geometry and their cyclic stress-strain and fatigue properties at the critical notch (these experiments did not test the relaxation of mean stress part of the computer program).
2. A surprisingly good agreement between the estimated fatigue crack initiation life and test results was obtained for materials and notch geometries (a hole in an A-7 steel plate and butt welds in 1020 steel) which were not very well defined in terms of the cyclic stress-strain and fatigue properties of the material at the critical notch. Although no direct verification is available of the influence of the mean stresses on the fatigue crack initiation life, the results of the low cycle fatigue rheological model suggest that their effects on the fatigue crack initiation life should be minor since the mean stresses will relax very rapidly for cyclic stresses above the fatigue limit.
3. A poor agreement between the estimated fatigue crack initiation life and test results was obtained for the

fillet welds in 1020 steel for which the cyclic stress-strain and fatigue properties of the material at the critical notch apparently differed significantly from those of an A-36 steel.

4. The fatigue crack initiation life is dependent on the material, notch geometry and type of loading (R ratio). At long lives, the fatigue crack initiation life may account for most of the total life, whereas at short lives, it is a small fraction of the total fatigue life.
5. A good estimate of the total fatigue life can be made using the present procedure to calculate the fatigue crack initiation portion and fracture mechanics concepts to estimate the fatigue crack propagation portion of the total life.

VII. DISCUSSION

The results presented in the preceding section have shown that the low cycle fatigue rheological model accurately estimates the fatigue crack initiation life of welds if the fatigue notch factor, K_f, and the material properties at the toe of the welds are known. Assuming the validity of this model, an analysis of the factors which influence the fatigue crack initiation life of welds will be presented.

A. Effect of the Weld Reinforcement Geometry on N_I

For a given material, the fatigue crack initiation life of a weld depends very strongly on the fatigue notch factor, K_f, which, according to Peterson's equation, is in turn a function of the stress concentration factor, K_t. The stress concentration factor is a function of the microgeometry (radius at the toe of the weld) and of the macrogeometry (flank and edge preparation angles) of the weld reinforcement as shown in Figs. 7 and 8.

1. Effect of Microgeometry

For a given material and for a fixed macrogeometry of the weld reinforcement, the fatigue notch factor is sensitive to small changes of the microgeometry (r/t) as shown in Figs. 9 and 10. Increasing the radius at the toe of the weld or decreasing the thickness of the plate, greatly decreases the fatigue notch factor.

The predicted influence of the increase of the radius at the toe of the weld on the fatigue crack initiation life in butt welds is shown in

Fig. 57 for A-36 and HY-130 steels. Estimations of N_I for HY-130 were performed using the cyclic stress-strain and fatigue properties reported by Majumdar (76); also Eq. 27 was assumed valid with a=0.003 in. (65). Increasing the radius at the toe of the weld from 0.02 in. to 0.05 in. lengthens the fatigue crack initiation life by as much as a factor of two for the A-36 steel or for one order of magnitude for HY-130 steel.

The marked effect of increasing the fatigue life by increasing the radius at the toe of the weld has been demonstrated by Sanders, et al., (77) in simulated weld specimens and by Millington (78) in TIG-dressed non-load-carrying fillet welds; an increase in life by as much as an order of magnitude was obtained by Millington (78). Although Millington (78) argues that the improvement of the fatigue life was caused by the removal of slag intrusions at the toe of the weld by the TIG dressing technique, it is also equally possible that the main cause of this improvement was the decrease of K_f by increasing the radius at the toe of the weld. This conclusion is also supported by the series of macrophotographs published by Millington.

2. Effect of Macrogeometry

The circle segment idealization of the macrogeometry of the weld reinforcement which is characterized by the flank angle, θ, and by the edge preparation angle, ϕ, was previously mentioned. The influence of the flank angle, θ, on the fatigue notch factor, K_f, is shown in Fig. 58 for A-36 and HY-130 steels for a constant $\phi = 90°$ and $r = 0.05$ in. Increasing the flank angle of the weld reinforcement, i.e., increasing the height of the weld crown, rapidly increases the fatigue notch factor. In the range,

$0° < \theta < 40°$, the fatigue notch factor is much more sensitive to changes in the flank angle than for $\theta > 40°$. Also, for the same geometry, K_f for HY-130 steel is higher than that of A-36 steel.

The calculated influence of varying the flank angle on the fatigue crack initiation life in A-36 and HY-130 steel is shown in Fig. 59 for $\phi = 90°$ and $r = 0.05$ in. Decreasing the flank angle, θ, from 60° to 30°, lengthens the fatigue crack initiation life by a factor of two in A-36 steel and by one order of magnitude for HY-130 steel.

The influence of the flank angle on the fatigue life of welded and simulated welded specimens has been confirmed by Yamaguchi, et al. (79) and by Sanders, et al. (77). These investigators have found that the fatigue life of welded and simulated weld specimens is markedly reduced by increasing the flank angle and that the relationship between the fatigue notch factor, K_f, and the flank angle, θ, is of the same form as that presented in Fig. 58. The influence of the edge preparation angle, ϕ, on the fatigue notch factor, K_f, is shown in Fig. 60 for A-36 and HY-130 steels for $\theta = 60°$ and $r = 0.05$ in. Decreasing the edge preparation angle, ϕ, i.e., decreasing the width and weld height but keeping the same shape of weld crown, decreases the fatigue notch factor.

The predicted effect of varying the flank angle from 60° to 90° is shown in Fig. 61 for A-36 and HY-130 steels. A variation in the fatigue crack initiation life as much as a factor of two or one order of magnitude could be obtained for the respective steels. Although the experimental confirmation of the influence of the edge preparation angle upon the fatigue life has not

been carried out yet, the present analysis suggests that the fatigue crack initiation life could be lengthened by using narrow gap weldments.

B. Effect of the Material Properties on N_I

The calculated effect of different material properties ("a" values in Eq. 27 and cyclic stress-strain and fatigue properties) on the fatigue crack initiation life of butt welds is shown in Fig. 62 in which 7075-T6 Aluminum, HY-130, HY-80 and A-36 steels are compared for the same geometry ($\theta = 60°$, $\phi = 90°$ and $r = 0.05$ in.). Cyclic stress-strain and fatigue properties and "a" values used to calculate N_I are summarized in Table 8.

The fatigue crack initiation life estimations as presented in Fig. 62 show that high strength steels, like HY-130 and HY-80, exhibit much longer fatigue crack initiation lives than A-36 steel and 7075-T6 Aluminum. Examination of the material properties of these alloys, listed in Table 8, suggests that the fatigue crack initiation resistance is markedly dependent on their cyclic strength coefficient, K', and on their fatigue strength exponent, b. The higher the values of these properties the more resistance to fatigue crack initiation the alloy becomes.

Fatigue crack propagation life estimates for the alloys and geometry under study were performed using the procedure developed by Lawrence (14). In carrying out these estimates, it was assumed that the fatigue crack propagation period begins with a 0.01 in. crack size and ends at 0.3t final crack size (for all cases, t = 1 in. was assumed). Since at the present time, no method has been developed to treat crack propagation estimates under a tension-compression stress cycle, the present estimates

were made assuming that the crack propagates only under the tension portion of the stress cycle. Representative values of C and m for the steels and the aluminum alloy were taken from Barsom (72) and Jaske, et al. (80), respectively. Figure 63 shows the fatigue crack propagation life estimates for the alloys under study. This figure shows that the high strength steels, HY-130 and HY-80, exhibit much shorter fatigue crack propagation lives than A-36 steel but much larger fatigue crack propagation lives than 7075-T6 Aluminum. The results presented in Figs. 62 and 63 show that A-36 steel is less resistant to crack initiation but more resistant to crack propagation than HY-130 and HY-80 steels. 7075-T6 Aluminum exhibits poor resistance to both crack initiation and crack propagation.

Estimations of the total fatigue life, N_T, ($N_T = N_p + N_I$) were performed assuming the additivity of the present procedure to calculate N_I and the Lawrence's procedure (14) to calculate N_p. The results of these estimations are shown in Fig. 64. From this figure the following can be drawn:

1. In the long life regime, HY-130 steel exhibits much longer total fatigue life than HY-80 and A-36 steels and 7075-T6 Aluminum. At intermediate lives however, (3×10^4 cycles) HY-130 and HY-80 steels exhibit about the same total fatigue life.
2. In the life regime from 4×10^4 to 4×10^5 cycles, HY-80 and A-36 steels have about the same total fatigue life resistance. At long lives ($> 4 \times 10^5$ cycles), HY-80 steel exhibits longer total fatigue life than A-36 steel.

3. 7075-T6 Aluminum exhibits poor fatigue resistance as compared with HY-130, HY-80 and A-36 steels.

Figure 65 compares the alloys under investigation in terms of the partition of the fatigue crack initiation and propagation lives as a function of the total fatigue life. This figure clearly shows that the percentage of the total fatigue life spent in fatigue crack initiation depends on the material and on the range of the total fatigue life being considered. The following conclusions can be drawn from this figure:

1. For materials like A-36 steel and for life up to 10^6 cycles, the percentage of the fatigue life spent as initiation is at most 20 percent; at longer lives, the contribution of the crack initiation life could account for as much as 60 percent.
2. For materials like 7075-T6 Aluminum and for lives in excess to 10^4 cycles, the contribution of crack initiation life to the total fatigue life could account at least for 80 percent of the total life.
3. For high strength materials, like HY-130 and HY-80 steels, the contribution of the crack initiation life to the total fatigue life is midway that of 7075-T6 Aluminum and A-36 steel; however, at long lives ($> 2 \times 10^5$ cycles), the fatigue crack initiation life is the dominant one.

The analysis of the effect of different material properties on the crack initiation life of butt welds under completely reversed nominal stresses

has shown that for some alloys, like 7075-T6 Al, and for lives in excess to 4×10^4 cycles, fatigue crack initiation estimates can be used as a lower bound to the total fatigue life; on the other hand, for alloys like A-36 steel, and for lives less than 4×10^6 cycles, fatigue crack propagation estimates can be used as a lower bound of the total fatigue life. For other alloys, like HY-130 and HY-80 steels, and for the life regime from 2×10^4 to 2×10^5 cycles, fatigue crack initiation or crack propagation estimates do not represent lower bound to the total fatigue life; for these alloys however, fatigue crack initiation life estimates can be used as lower bounds for lives in excess of 3×10^5 cycles. With the above considerations in mind, it was considered that an index denoting the predominant portion of the total fatigue life should be looked for if fatigue crack initiation or propagation estimates have to be used as lower bounds of the total fatigue life. From comparisons of the transition fatigue life, N_t^*, of the alloys under study (see Table 8) and the results presented in Fig. 65 the following can be concluded: the fraction of the total life spent in fatigue crack initiation is related to the transition fatigue life; the lower the transition fatigue life, N_t, the greater is the proportion of the total fatigue life spent in fatigue crack initiation.

---

* The transition fatigue life, N_t, is the life at which $\Delta\varepsilon_p/2 = \Delta\varepsilon_e/2$; i.e.,

$$N_t = \frac{1}{2} \left(\frac{\varepsilon_f' E}{\sigma_f'} \right)^{\frac{1}{b-c}}$$

C. Effect of the Residual Stresses on N_I

The damage due to the mean stress and the relaxation of it throughout the fatigue life can be estimated by the low cycle fatigue rheological model if the relaxation constant for the material is known (Eq. 30). Since this datum is not available for steels other than the A-36 steel investigated, the influence of residual stresses on the fatigue crack initiation life will be discussed for this material only.

To assess the effect of the welding residual stresses on the fatigue crack initiation life of welds, the hypothetical fatigue specimen simulated by the low cycle fatigue rheological model was precompressed or prestressed (thereby inducing tensile or compressive residual stresses, respectively) until, upon unloading, the magnitude of the residual stresses was of the order of the yield strength (35 ksi). Fatigue cycling of the specimen being simulated was continued until the mean stress had relaxed completely or until the model indicated that no relaxation of the mean stress would occur. Figure 66 shows the calculated influence of the residual stresses on the fatigue crack initiation life for A-36 steel. Although not shown in this figure (see Appendix C), the residual stresses relax very quickly for lives less than 10^6 cycles so that their influence on the fatigue crack initiation life is negligible as shown in Fig. 66; for lives in excess of 10^6 cycles, the residual stresses will not relax and their effect on the fatigue crack initiation life could amount to a factor of two or three (at lives greater than 10^6 cycles).

The analysis of the relaxation of the mean stress, discussed in Appendix C, suggests that no relaxation of the mean stress will occur for

local stresses below the cyclic yield stress and that rapid relaxation of the mean stress will occur for higher local stresses. These facts indicate that for completely reversed applied stresses lower than σ_y/K_f, the fatigue crack initiation life can be computed directly from the Basquin's formula (modified with the corresponding mean stress, Eq. 17). For high stress levels, the mean stress can be ignored and the fatigue crack initiation life can be computed from the strain amplitude-reversals to failure plot. In the regime where the mean stress takes considerable number of cycles to relax, a model which takes into account both the mean stress and its relaxation is needed.

D. Summary

Based on the validity of the low cycle fatigue rheological model, an analysis of the factors which could influence the fatigue crack initiation life of welds was performed. The effects of the micro- and macrogeometry of the weld reinforcement, material properties and residual stresses were considered. The results of this analysis can be summarized as follows:

1. The fatigue crack initiation life of welds could be improved by increasing the radius of the toe of the weld and/or decreasing the flank angle and/or the edge preparation angle. For steels like A-36 steel , modification of one of these parameters could account for as much as a factor of two in initiation life, whereas for steels like HY-130 steel, the same modification could account for one order of magnitude.

2. For alloys whose cyclic yield stress is low (like A-36 steel), residual welding stresses will relax quickly during their fatigue life if they are fatigue cycled at stresses above the cyclic yield stress; consequently welding residual stresses will only affect the fatigue crack initiation life in their long life regime (10^6 cycles and greater for A-36 steel).
3. By far the most influential variable affecting the fatigue crack initiation life in welds is material properties. For alloys like A-36 steel, whose transition fatigue life is large, the fatigue crack initiation life is relatively short as compared with the total fatigue life; for these alloys, fatigue crack propagation estimates can provide a lower bound for the total fatigue life. For alloys like 7075-T6 Aluminum, whose transition fatigue life is short, the fatigue crack propagation life is short as compared with the total fatigue life; for these alloys fatigue crack initiation estimates provide a lower bound for the total fatigue life. For alloys like HY-130 and HY-180 steels, whose transition fatigue life is not too large, both fatigue crack initiation and propagation lives estimates need to be made for the determination of their total fatigue life since their proportion depends on the life regime being

considered. For all the alloys investigated, the fatigue crack initiation life is the dominant portion of the total fatigue life at long lives.

VIII. SUMMARY, CONCLUSIONS AND RECOMMENDATIONS

A. Summary and Conclusions

The objective of this investigation were as follows: First, to develop an analytical procedure to calculate the fatigue crack initiation life of welded structures. Second, to verify this analytical procedure with experimentally determined fatigue crack initiation data. Third, to perform an assessment of the factors which influence the fatigue crack initiation life of welds.

To accomplish the first objective, the stresses and strains at the critical location (toe of the weld) had to be obtained. These stresses and strains were computed using Neuber's equation (9,25). The uniaxial behavior at the critical location was computer simulated using a rheological model which was shown to accurately reproduce the stress and strain history and to accurately predict the failure of smooth specimens. By these methods, the fatigue crack initiation lives were calculated using a cumulative fatigue damage analysis.

To accomplish the second objective, fatigue crack initiation life predictions were performed and compared with actual fatigue crack initiation life data obtained by testing simulated weld specimens and by utilizing data from the literature for a circular hole in a plate. These materials and notch geometries were very well defined in terms of their geometry and their cyclic stress-strain and fatigue properties at the critical location. An excellent agreement was obtained between the model's predictions and the experimental data. Fatigue crack initiation life predictions were also

made and compared with fatigue crack initiation life data reported in the literature. For these cases, the agreement between the model's predictions and the reported data was agreed best when the assumed material properties were closest to those of the material at the critical location.

To accomplish the third objective, it was assumed that the material properties at the critical location were identical to those of the parent material. The results of this analysis suggest the following conclusions:

1. The fatigue crack initiation life of welds is influenced by the microgeometry (radius at the toe of the weld) of the weld reinforcement. The increase of the crack initiation life by modification of the radius at the toe of the weld was found to be greater for high strength steels than for low strength steels.
2. The fatigue crack initiation life of welds is affected by the flank and edge preparation angles. The increase of the fatigue crack initiation life by modification of the mentioned parameters was found to be greater for high strength steels than for low strength steels.
3. The fraction of the total fatigue life spent in crack initiation is most dependent of the material properties (cyclic stress-strain and fatigue properties and "a" values) of the weld as well as on the fatigue life regime under consideration. For the high strength steels studied, the fatigue crack initiation life occupied most of the total fatigue life in the intermediate and long life regimes. For the

low strength steel studied, the fatigue crack initiation life occupied only a small fraction of the fatigue life in the intermediate life regime; for this material however, the fatigue crack initiation life occupied most of the fatigue life at long lives (lives greater than 5×10^6 cycles).

4. For the mild steel studied, the welding residual stresses affect the fatigue crack initiation life in the long life regime where they do not relax. At low and intermediate lives (less than 10^6 cycles), relaxation of the residual stresses occurs so quickly that their influence on the fatigue crack initiation life can be ignored.

B. Recommendations for Future Study

The proposed model to estimate the fatigue crack initiation life was based on the rupture of hypothetical filamentary specimens located at the most highly strained region. Because of their thinness, the fatigue crack propagation life of these filaments can be considered to be nil. However, the calculations of the fatigue crack initiation life were based on data generated on smooth specimens having finite thickness; and, consequently, the data obtained from these specimens contain some fatigue crack propagation. Although low cycle fatigue testing and fatigue crack propagation estimates performed on these specimens indicate that the fraction of their fatigue life spent as fatigue crack propagation is small, a more direct way of determining or minimizing this fraction should be investigated.

Cyclic relaxation of the mean stress using the rheological model was performed by multiplying the stiffness of each spring by a relaxation function, $f(|\sigma|)$. Although for the steel investigated, this approach gave a reasonable representation of the relaxation of the mean stress, an alternative and probably more accurate approach will be the use of the model developed (Appendix C) for the cyclic relaxation of the mean stress.

The lack of agreement between the predicted and actual fatigue crack initiation life in the fillet welds suggests that the cyclic stress-strain and fatigue properties of the heat affected zone and weld metal should be better known; determination of these properties will undoubtedly improve the accuracy of the fatigue crack initiation estimates.

Perhaps the most useful application of the analytical procedure developed is for the estimation of the fatigue crack initiation life of welded structures under complicated fatigue histories; this was not undertaken since fatigue crack initiation life predictions for this type of loading were beyond the scope of the present investigation.

REFERENCES

1. Mann, J. Y., Fatigue of Materials, Melbourne University Press, Australia, 1967.

2. Forsyth, P. J. E., The Physical Basis of Metal Fatigue, American Elsevier, New York, 1969.

3. Paris, P. C., and Erdogan, F., " A Critical Analysis of Crack Propagation Laws," Journal of Basic Engineering, ASME Transactions, Vol. 85, Series D, No. 4, pp. 528, 1963.

4. Jack, A. R., and Price, A. T., " The Initiation of Fatigue Cracks from Notches in Mild Steel Plates," International Journal of Fracture Mechanics, Vol. 6, No. 4, pp. 401, 1970.

5. Jack, A. R., and Price, A. T., "Effect of Thickness on Fatigue Crack Initiation and Growth in Notched Mild Steel Specimens," Acta Metallurgica, Vol. 20, pp. 857, July 1972.

6. Cooke, R. J., and Beevers, C. J., "The Effect of Load Ratio on the Threshold Stresses for Fatigue Crack Growth in Medium Carbon Steels," Engineering Fracture Mechanics, Vol. 5, No. 4, pp. 1061, 1973.

7. Klesnil, M., and Lukas, P., "Effect of Stress Cycle Asymmetry on Fatigue Crack Growth," Materials Science and Engineering, Vol. 9, No. 4, pp. 231, 1972.

8. Beevers, C. J., Cooke, R. J., Knott, J. F., and Ritchie, R. O., "Some Considerations of the Influence of Sub-Critical Cleavage Growth During Fatigue-Crack Propagation in Steels," Metal Science, Vol. 9, pp. 119, 1975.

9. Topper, T. H., Wetzel, R. M., and Morrow, JoDean, "Neuber's Rule Applied to Fatigue of Notched Specimens," Journal of Materials, Vol. 4, pp. 200, 1969.

10. Maddox, S. J., "Calculating the Fatigue Strength of a Weld Joint Using Fracture Mechanics," Metal Construction, Vol. 2, No. 8, pp. 327, 1970.

11. Maddox, S. J., "A Fracture Mechanics Analysis of The Fatigue Behavior of a Fillet Welded Joint," The Welding Institute, Report No. E/50/72, January 1973.

12. Maddox, S. J., "An analysis of Fatigue Cracks in Fillet Welded Joints," The Welding Institute, Report No. E/49/72, January 1973.

13. Maddox, S. J., "Assessing the Significance of Flaws in Welds Subject to Fatigue," Welding Research Supplement, Vol. 53, No. 9, pp. 401S, 1974.

14. Lawrence, F. V., "Estimation of Fatigue-Crack Propagation Life in Butt Welds," Welding Research Supplement, Vol. 52, No. 5, pp. 212S, 1973.

15. Lawrence, F. V., and Mainali, P. C., "Fatigue Crack Propagation Life Predictions for Butt and Fillet Welds," Fracture Control Program Report No. 11, College of Engineering, University of Illinois, Urbana, Illinois, March 1974.

16. Lawrence, F. V., and Munse, W. H., "Fatigue Crack Propagation in Butt Welds Containing Joint Penetration Defects," Welding Research Supplement, Vol. 52, No. 5, pp. 221S, 1973.

17. Signes, E. G., Baker, R. G., Harrison, J. D., and Burdekin, F. M., "Factors Affecting the Fatigue Strength of Welded High Strength Steels," British Welding Journal, Vol. 14, pp. 108, 1967.

18. Gurney, T. R., Fatigue of Welded Structures, Cambridge University Press, Cambridge, U.K., 1968.

19. Manson, S. S., and Hirschberg, M. H., "Low Cycle Fatigue of Notched Specimens by Consideration of Crack Initiation and Propagation," National Aeronautics and Space Administration, NASA TN D-3146, 1965.

20. Peterson, R. E., "Fatigue of Metals III - Engineering and Design Aspects," Materials Research and Standards, Vol. 3, pp. 122, February 1963.

21. Crews, J. H., Jr. and Hardrath, H. F., "A Study of Cyclic Plastic Stresses at a Notch Root," Experimental Mechanics, Vol. 6, No. 6, pp. 313, June 1966.

22. Crews, J. H., "Crack Initiation at Stress Concentrations as Influenced by Prior Local Plasticity," Achievements of High Fatigue Resistance in Metals and Alloys, ASTM STP 467. American Society for Testing and Materials, pp. 37, 1970.

23. Impellizeri, L. F., "Cumulative Damage Analysis in Structural Fatigue," Effect of Environment and Complex Load History on Fatigue Life, ASTM STP 462, American Society for Testing and Materials, pp. 40, 1970.

24. Topper, T. H., and Morrow, JoDean, Editors, "Simulation of the Fatigue Behavior at the Notch Root in Spectrum Loaded Notched Members (U)," TAM Report No. 333, Department of Theoretical and Applied Mechanics, University of Illinois, Urbana, Illinois, January 1970.

25. Neuber, H., "Theory of Stress Concentration for Shear Strained Prismatical Bodies with Arbitrary Non Linear Stress-Strain Law," Journal of Applied Mechanics, pp. 544, December 1961.

26. Stowell, E. Z., "Stress and Strain Concentration at a Circular Hole in an Infinite Plate," National Advisory Committee for Aeronautics, Technical Note 2073, April 1950.

27. Morrow, JoDean, Welzel, R. M., and Topper, T. H., "Laboratory Simulation of Structural Fatigue Behavior, "Effect of Environment and Complex Load History on Fatigue Life," ASTM STP 462, American Society for Testing and Material, pp. 74, 1970.

28. Wetzel, R. M., "Smooth Specimen Simulation of Fatigue Behavior of Notches," Journal of Materials, JMLSA, Vol. 3, No. 3, pp. 646, September 1968.

29. Miller, J., "Low Cycle Fatigue Under Biaxial Strain Controlled Conditions," Journal of Materials, JMLSA, Vol. 7, No. 3, pp. 307, September 1972.

30. Coffin, L. F., "Fatigue at High Temperature," General Electric, Metallurgy and Ceramics Laboratory, Technical Information Series, Report No. 72CRD 135, April 1972.

31. Morrow, JoDean, "Cyclic Plastic Strain Energy and Fatigue of Metals," Internal Friction, Damping, and Cyclic Plasticity, ASTM STP 378, American Society for Testing and Materials, pp. 45, 1965.

32. Raske, D. T., and Morrow, JoDean, "Mechanics of Materials in Low Cycle Fatigue Testing," Manual of Low Cycle Fatigue Testing, ASTM STP 465, American Society for Testing and Materials, pp. 1, 1969.

33. Landgraf, R. W., Morrow, JoDean, and Endo, T., "Determination of the Cyclic Stress-Strain Curve," Journal of Materials, JMLSA, Vol. 4, No. 1, pp. 176, March 1969.

34. Endo, T., and Morrow, JoDean, "Cyclic Stress-Strain and Fatigue Behavior of Representative Aircraft Metals," Journal of Materials, JMLSA, Vol. 4, No. 1, pp. 159, March 1969.

35. Halford, G. R., and Morrow, JoDean, "Low Cycle Fatigue in Torsion," Proceedings of the ASTM, Vol. 62, pp. 697, 1962.

36. Massing, G., "Eigenspannungen und Verfestigung beim Messing," Proceedings of the 2nd International Congress of Applied Mechanics, pp. 332, Zurich, 1926.

37. Krempl, E., "Some Properties of Hysteresis Curves of Structural Metals at Room Temperature," American Society of Mechanical Engineers, Paper No. 69-WA/Met-4, 1969.

38. Landgraf, R. W., "The Resistance of Metals to Cyclic Deformation," Achievement of High Fatigue Resistance in Metals and Alloys, ASTM STP 467, American Society for Testing and Materials, pp. 3, 1970.

39. Morrow, JoDean, Section 3.2 of Fatigue Design Handbook, Society of Automotive Engineers, New York, 1968.

40. Coffin, L. F., Jr, "A Study of the Effects of Cyclic Thermal Stresses on a Ductile Metal," Transactions, American Society of Mechanical Engineers, Vol. 76, pp. 931, 1954.

41. Manson, S. S., "Behavior of Materials Under Conditions of Thermal Stress," NACA TN 2933, 1954.

42. Manson, S. S., and Hirschberg, M. J., in Fatigue An Interdisciplinary Approach, Syracuse University Press, Syracuse, New York, pp. 133, 1964.

43. Dowling, N. E., "Fatigue Failure Predictions for Complicated Stress-Strain Histories," Journal of Materials, JMLSA, Vol. 7, No. 1, pp. 71, March 1972.

44. Manson, S. S., "Interpretative Report on Cumulative Fatigue Damage in the Low Cycle Range," Welding Research Supplement, pp. 344S, August 1964.

45. Manson, S. S., Freche, J. C., and Ensign, C. R., "Application of a Double Linear Damage Rule to Cumulative Fatigue," Fatigue Crack Propagation, ASTM STP 415, American Society for Testing and Materials, pp. 384, 1967.

46. Ichikawa, M., "Fatigue Under Variable Stress Amplitude as Successive Stochastic Processes," Report Research Institute, Strength and Fracture of Materials, Tohoku University, Vol. 7, pp. 63, 1971.

47. Yokobori, T., Ichikawa, M., and Kawamoto, H., "Fatigue Reliability Under Random Loadings, "Report Research Institue, Strength and Fracture of Materials, Tohoku University, Vol. 8, pp. 55, 1972.

48. Thang, B. Q., Dubuc, J., Bazergui, A., and Biron, A., "Cumulative Fatigue Damage Under Strain Controlled Conditions," Journal of Materials, JMLSA, Vol. 6, No. 3, pp. 718, September 1971.

49. Martin, J. F., "Fatigue Damage Analysis For Irregular Shaped Structures Subjected to Representative Loads," Fracture Control Program Report No. 10, College of Engineering, University of Illinois, Urbana, Illinois, December 1973.

50. Palmgren, A., "Die Lebensdauer von Kvgellagern," Verein Deutscher Ingenieure Zeitschrift, Vol. 68, pp. 339, 1924.

51. Miner, M. A., "Cumulative Damage in Fatigue," Journal of Applied Mechanics, Vol. 12, pp. A159, 1945.

52. Martin, J. F., Topper, T. H., and Sinclair, G. M., "Computer Based Simulation of Cyclic Stress-Strain Behavior With Applications to Fatigue," Materials Research and Standards, MTRSA, Vol. 11, No. 2, pp. 23.

53. Wetzel, R. M., "A Method of Fatigue Damage Analysis," Metallurgy Department, Technical Report No. SR71-107, Scientific Research Staff, Ford Motor Co., September 1974.

54. Jhansale, H. R., and Topper, T. H., "Engineering Analysis of the Inelastic Stress Response of a Structural Metal Under Variable Cyclic Strains," Cyclic Stress-Strain Behavior--Analysis, Experimentation, and Fatigue Prediction, ASTM STP 519, American Society for Testing and Materials, pp. 246, 1973.

55. Plummer, F. B., Jr, "Cyclic Plasticity and Structural Energy Dissipation," Ph.D. Thesis, Theoretical and Applied Mechanics, University of Illinois, Urbana, Illinois, 1973.

56. Neuber, H., Theory of Notch Stress: Principles for Exact Stress Calculations, J. W. Edwards, Ann Arbor, Michigan, 1946.

57. Peterson, R. E., "Notch Sensitivity," Metal Fatigue, Chapter 13, Sines and Waisman, Editors, McGraw-Hill Book Co., Inc. 1959.

58. Harris, H. J., Metal Fatigue, Pergamon Press, New York, 1961.

59. Heywood, R. B., Designing by Photoelasticity, Chapman and Hall Ltd., London, 1952.

60. Kuguel, R., "The Highly Stressed Volume of Materials as a Fundamental Parameter in the Fatigue Strength of Metal Members," TAM Report No. 169, Department of Theoretical and Applied Mechanics, University of Illinois, Urbana, Illinois, June 1960.

61. Raske, D. T., "The Variation of the Fatigue Notch Factor With Life," M.Sc. Thesis, Theoretical and Applied Mechanics, University of Illinois, Urbana, Illinois, 1971.

62. Raske, D. T., "Section and Notch Size Effects in Fatigue," TAM Report No. 360, Department of Theoretical and Applied Mechanics, University of Illinois, Urbana, Illinois, August 1972.

63. Peterson, R. E., Stress Concentration Factors, Wiley and Sons, Inc. New York, 1974.

64. Derecho, A. T., and Munse, W. H., "Stress Concentration Factors at External Notches in Members Subjected to Axial Loadings," Engineering Experiment Station, Bulletin 494, University of Illinois, Urbana, Illinois, 1967.

65. Peterson, R. E., "Analytical Approach to Stress Concentration Effect in Fatigue of Aircraft Structures," WADS Symposium, Wright Air Development Center, August, 1959.

66. Feltner, C. E., and Mitchell, M. R., "Basic Research on the Cyclic Deformation and Fracture Behavior of Materials," Manual on Low Cycle Fatigue Testing, ASTM STP 465, American Society for Testing and Materials, pp. 27, 1969.

67. Dieter, G. E., Jr., Mechanical Metallurgy, McGraw-Hill Book Co, Inc., New York, pp. 251. 1961.

68. Jhansale, H. R., "A New Parameter for the Hysteretic Stress-Strain Behavior of Metals," Transactions of the ASME, pp. 33, January 1975.

69. Heywood, R. B., Designing Against Fatigue of Metals, Reinhold Publishing Corp., New York, pp. 29, 1962.

70. Radziminski, J. B., Srinvasan, R., Moore, D., Thrasher, C., and Munse, W. H., "Fatigue Data Bank and Data Analysis Investigation," Civil Engineering Studies, Structural Research Series No. 405, University of Illinois, Urbana, Illinois, June 1973.

71. Stallmeyer, J. E., "The Effect of Stress History on Cumulative Damage in Fatigue," Ph.D. Thesis, Civil Engineering, University of Illinois, Urbana, Illinois, 1953.

72. Barsom, J. M., "Fatigue Crack Propagation in Steels of Various Yield Strength," Transactions of the ASME, Journal of Engineering for Industry, Vol. 93, pp. 1190, November 1971.

73. Bowie, O. L., "Analysis of an Infinite Plate Containing Radial Cracks Originating from the Boundary of an Internal Circular Hole," Journal of Mathematics and Physics, Vol. 35, pp. 60, 1956.

74. Burk, J. D., "Predictions of the Fatigue Crack Propagation Lives of Butt Weldments Subjected to Axial and Bending Stresses," M.Sc. Thesis, University of Illinois, Urbana, Illinois, 1974.

75. Testin, R. A., Private Communication, Electro-Motive Division, General Electric, Lagrange, Illinois, 1975.

76. Majumdar, S., "Low Cycle Fatigue Behavior and Crack Propagation in Some Steels," TAM Report No. 387, Department of Theoretical and Applied Mechanics, University of Illinois, Urbana, Illinois, April 1974.

77. Sanders, W. W., Derecho, A. T., and Munse, W. H., "Effect of External Geometry on Fatigue Behavior of Welded Joints," Welding Research Supplement, Vol. 30, No. 297, 1965.

78. Millington, D., "TIG Dressing to Improve Fatigue Properties in Welded High-Strength Steel," Metal Construction and British Welding Journal, pp. 40, October 1973.

79. Yamaguchi, I., Tereda, Y., and Nitta, A., "On the Fatigue Strength of Steels for Ship Structures," International Institute of Welding Documentation, No. XIII, pp. 425, 1966.

80. Jaske, C. E., Feddersen, C. E., Davies, K. B., and Rice, R. C., "Analysis of Fatigue, Fatigue-Crack Propagation, and Fracture Data," National Aeronautics and Space Administration, NASA CR-132332, Langley Research Center, Battelle, Columbus Laboratories, November 1973.

81. Gurney, T. R., "Influence of Residual Stresses on Fatigue Strength of Plates with Fillet Welded Attachments," British Welding Journal, pp. 415, June 1960.

82. Dugdale, D. S., "Effect of Residual Stress on Fatigue Strength," Welding Research Supplement, pp. 45S, January 1959.

83. Masubuchi, K., "Analytical Investigation of Residual Stresses and Distortions Due to Welding," Welding Research Supplement, pp. 525S, December 1960.

84. Gurney, T. R., "Influence of Residual Stresses and of Mean Stress on the Fatigue Strength of Specimens with Longitudinal Non-Load-Carrying Fillet Welds," Journal Mechanical Engineering Science, Vol. 12, No. 6, pp. 381, 1970.

85. Nagaraja, N. R., Estuar, I. R., and Tall, L., "Residual Stresses in Welded Shapes," Welding Research Supplement, pp. 295S, July 1964.

86. Nelson, D. V., Ricklefs, R. E., and Evans, W. P., "The Role of Residual Stresses in Increasing Long-Life Fatigue Strength of Notched Machine Members," Achievements of High Fatigue Resistance in Metals and Alloys, ASTM STP 467, American Society for Testing and Materials, pp. 228, 1970.

87. Taira, S., Honda, K., and Abe, T., "X-Ray Investigation on Fatigue Damage of Metals Under Mean Stress," Bulletin JSME, Vol. 9, No. 33, pp. 40, 1966.

88. Taira, S., "X-Ray Diffraction Approach for Studies on Fatigue and Creep," Presented at Third SESA International Congress on Experimental Mechanics, Los Angeles, May 1973.

89. Taira, S., "X-Ray Approach for the Study on Mechanical Behavior of Metals," Mechanical Behavior of Materials, Proceedings of the International Conference on Mechanical Behavior of Materials, The Society of Materials Science, Japan, Special Vol., 1972.

90. Taira, S., and Honda, K., "X-Ray Investigation on Fatigue of Metals," Proceedings of the First International Conference on Fracture, Sandai, Japan, Vol. 3, 1965.

91. Morrow, JoDean, Ross, A. S., and Sinclair, G. M., "Relaxation of Residual Stresses Due to Fatigue Loadings," T.A.M. Report No. 568, University of Illinois, Urbana, Illinois, January 1959.

92. SAE Handbook, Supplement TR-198, "Influence of Residual Stress on Fatigue of Steels," SAE J 783, JoDean Morrow and J. F. Millan, Editors, July 1961.

93. Mitchell, M. M., and Wetzel, R. M., "Cumulative Fatigue Damage Analysis of a Light Truck Frame," Scientific Research Staff, Ford Motor Co.

94. Ricklefs, R. E., and Evans, W. P., "X-Ray Stress Measurements Apparatus Using Curved Back Reflection Cameras," Journal of the Society of Materials Science, Japan, Vol. 17, No. 183, pp. 13, December 1968.

95. Residual Stress Measurements by X-Ray Diffraction, SAE J 784a, Society of Automotive Engineers, Inc., 1971.

96. Barrett, C. S., and Massalski, T. B., Structure of Metals, McGraw-Hill, pp. 473, 1966.

97. Koistinen, D. P., and Marburger, R. E., "Simplified Procedure for Calculating Peak Position in X-Ray Residual Stress Measurements on Hardened Steels," Transactions American Society for Metals, Vol. 51, pp. 537, 1959.

TABLE 1

Monotonic Tensile Properties of A-36 Steel

Upper tensile yield points, ksi.	42.0
Lower tensile yield point, ksi.	32.0
0.2% offset yield strength, ksi.	32.5
Ultimate tensile strength, S_u, ksi.	60.0
Modulus of elasticity, E, x 10^3 ksi.	27.5
True fracture strength, σ_f, ksi.*	138.0/116.0
True fracture ductility, ε_f	1.19
Percent reduction in area, % RA	69.7
Strength coefficient, K, ksi.	113.0
Strain hardening exponent, n**	0.0146/0.258

* The first value is the load just before it suddenly decreased prior to fracture divided by the final area of the fracture specimen. The second value is corrected for triaxial stress due to necking as proposed by Bridgman (67).

**The first value represents the initial portion of the plastic strain-stress curve, i.e., for plastic strain ranging from 0.0001 to 0.01. The second value is for plastic strains from 0.01 to 0.20.

TABLE 2

Stable Cyclic Stress-Strain Properties of A-36 Steel*

Cyclic strength coefficient, K', ksi.	158.75
Cyclic strain hardening exponent, n'	0.249
Cyclic yield strength, 0.2% offset, ksi.	33.6

* The values reported are those obtained from companion specimen.

TABLE 3

Completely Reversed Strain Controlled Test Results for A-36 Steels

Total strain amplitude $\Delta\varepsilon/2$	Total stress amplitude $\Delta\sigma/2$ (ksi.)	Plastic strain $\Delta\varepsilon_p/2$	Elastic strain $\Delta\varepsilon_e/2$	Reversals to failure $2N_f$
0.02070	56.5	0.01850	0.00220	400
0.01535	51.0	0.01315	0.00220	1,100
0.01020	49.0	0.00825	0.00195	2,000
0.00722	43.0	0.00550	0.00172	4,800
0.00520	40.5	0.00355	0.00165	20,000
0.00312	36.0	0.00180	0.00132	44,000
0.00205	28.5	0.00100	0.00105	230,000
0.00156	25.0	0.00066	0.00090	760,000
0.00125	23.0	0.00047	0.00078	1,400,000

TABLE 4

Fatigue Properties of A-36 Steel

Fatigue strength coefficient, σ_f' ksi.	147.4
Fatigue ductility coefficient, ε_f'	0.271
Fatigue strength exponent, b	-0.132
Fatigue ductility exponent, c	-0.451
Transition fatigue life, reversals, $2N_t$	200,000

TABLE 5

Results of Computer Simulation of Smooth Specimens Under Completely Reversed Strain (Strain Control)

Strain Amplitude $\Delta\varepsilon/2$	Actual stress Amplitude $\Delta\sigma/2$ (ksi.)	Predicted stress Amplitude $\Delta\sigma/2$ (ksi.)	Actual life* $2N_f$ (Reversals)	Predicted life $2N_f$ (Reversals)
0.01540	51.0	52.0	8.00×10^2	7.80×10^2
0.01020	49.0	47.0	2.30×10^3	2.20×10^3
0.00722	43.0	43.2	5.80×10^3	5.30×10^3
0.00520	40.5	40.5	1.40×10^4	1.32×10^4
0.00312	36.0	36.0	6.40×10^4	6.60×10^4
0.00205	28.5	28.0	2.30×10^5	2.25×10^5
0.00156	25.0	24.3	6.40×10^5	5.95×10^5
0.00125	23.0	22.0	1.40×10^6	1.50×10^6
0.00100	----	20.0	4.00×10^6	4.42×10^6

* From Fig. 20

TABLE 6

Results for Simulated Butt Weld Specimens

Specimen No.	S (ksi.)	N_I (Cycles)	N_T (Cycles)	N_I/N_T(%)
1	±26.0	30,000	77,500	38.7
2	±22.0	57,000	---	--
3	±20.0	88,000	333,000	26.4
4	±17.0	225,000	1,020,000	22.0
5	±15.0	900,000	2,170,000	41.5

TABLE 7

Fatigue Crack Initiation Predictions for 7075-T6 Aluminum Plate With K_t = 2.37

Nominal stress S, ksi.	Cycles to N_f	Observed K_f	Predicted (1) K_f	Observed N_I, Cycles	Predicted (2) N_I, Cycles
± 40.0	1,340	1.82	1.81	300	400
± 30.0	5,090	2.06	2.07	2,050	2,500
± 25.0	13,280	2.08	2.10	6,900	6,600
± 20.0	35,700	2.10	2.08	30,000	25,200
± 15.0	158,600	2.17	2.07	---	138,000

(1) Predicted according to Raske's method. (62)

(2) Predicted by computer simulation using K_f values predicted by Raske. (62)

TABLE 8

Material Properties for HY-130, HY-80, A-36 Steels and 7075-T6 Al

Material	n'	K' (ksi.)	σ'_f (ksi.)	b	ε'_f	c	N^*_t (Cycles)	a (65) (in.)
HY-130 (76)	0.100	220.	216.	-0.060	0.90	-0.64	1800	0.003
HY-80 (76)	0.146	190.	196.	-0.096	0.89	-0.62	5200	0.005
A-36	0.249	158.	147.	-0.132	0.27	-0.45	110,000	0.010
7075-T6 (49)	0.049	106.	268.	-0.172	1.65	-1.29	20	0.025

* The transition fatigue life, N_t, is the life at which $\frac{\Delta\varepsilon_p}{2} = \frac{\Delta\varepsilon_e}{2}$; i.e., $N_t = \frac{1}{2}\left(\frac{\varepsilon'_f E}{\sigma'_f}\right)^{\frac{1}{b-c}}$

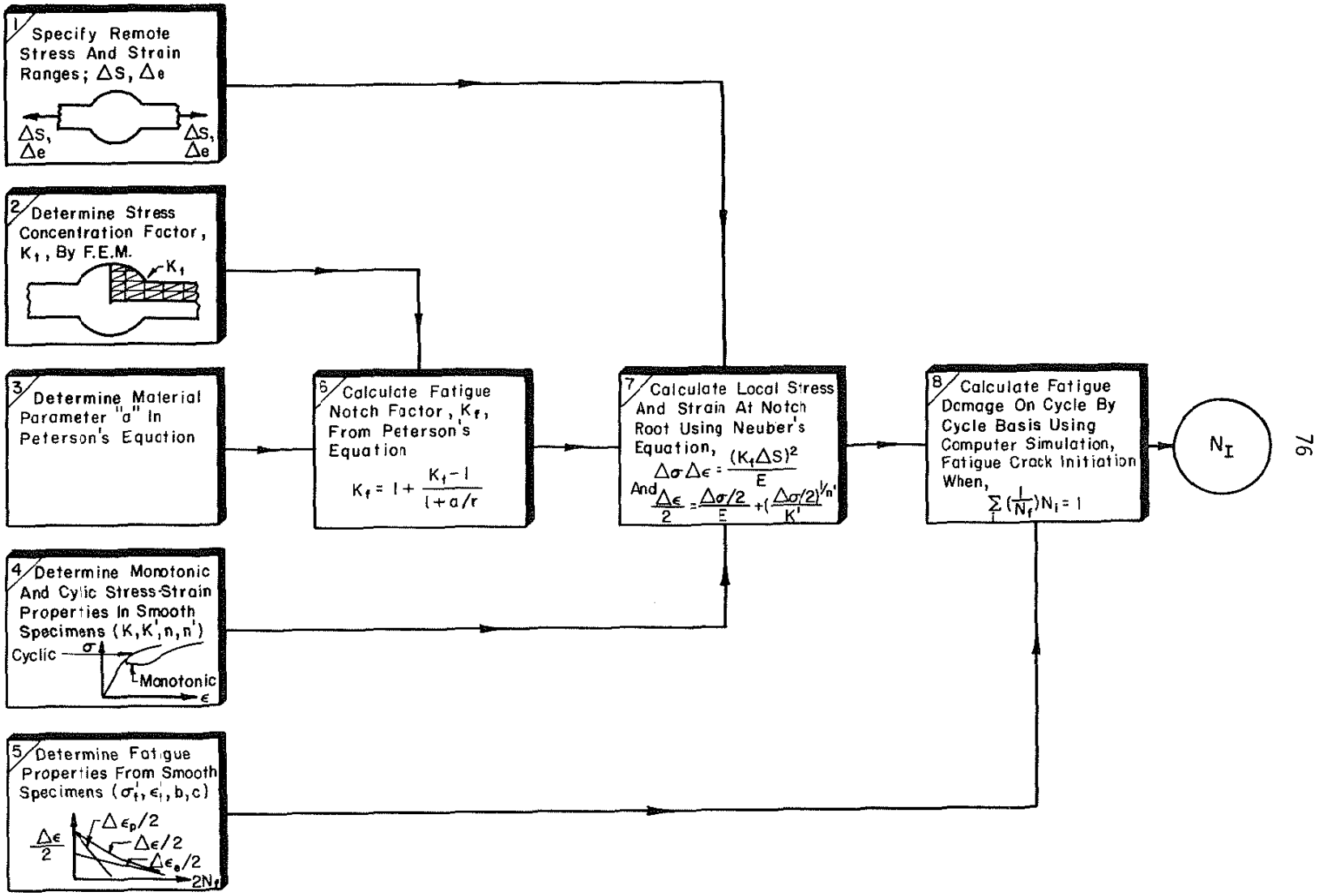

Fig. 1 Determination of the Fatigue Crack Initiation Life, N_I. Steps 1 and 2 Require Stress Analysis Results; Steps 3 through 5 Require the Determination of Material Properties; Steps 7 and 8 Constitute the Computer Calculation of Damage

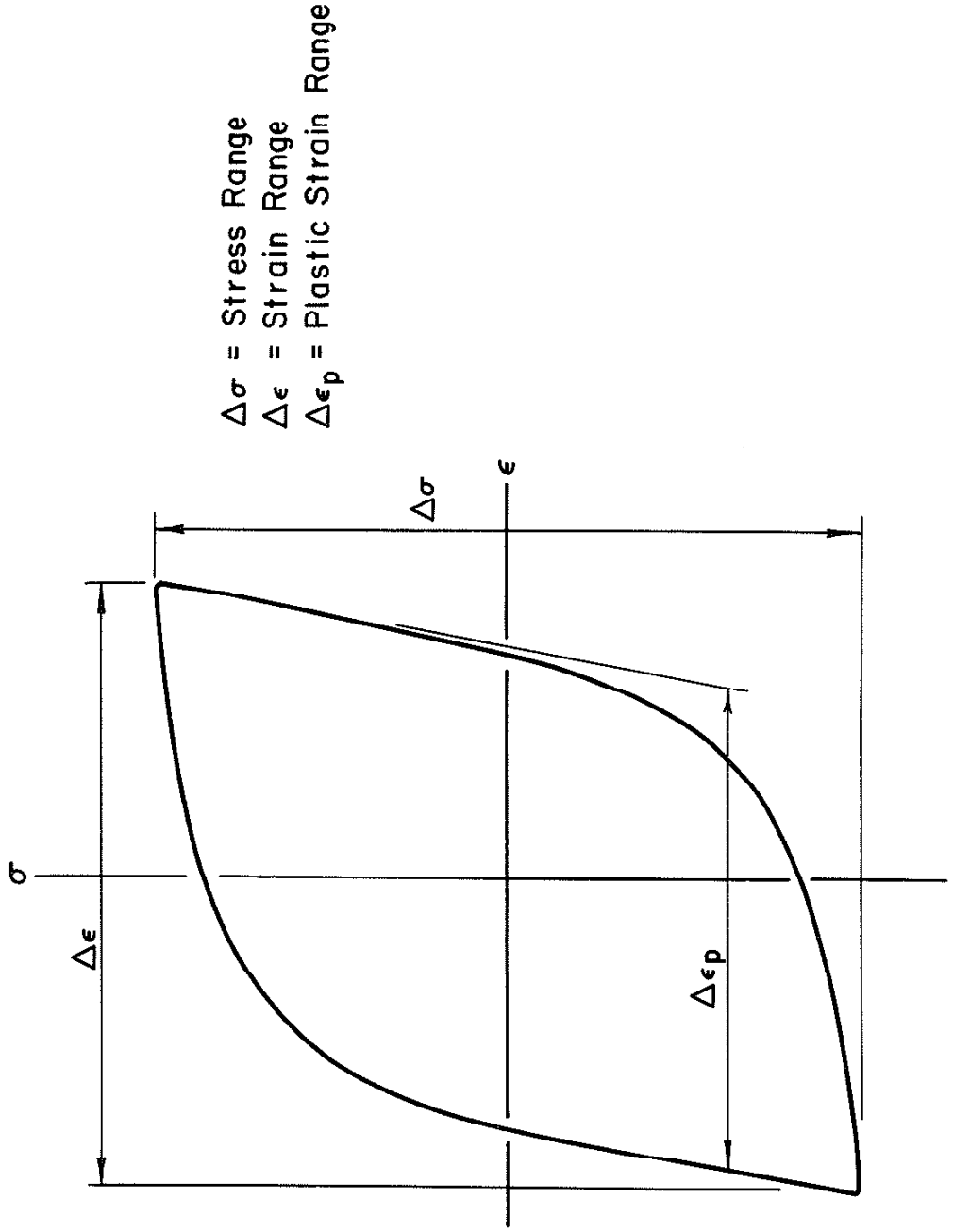

Fig. 2 Stable Stress-Strain Hysteresis Loop Parameters

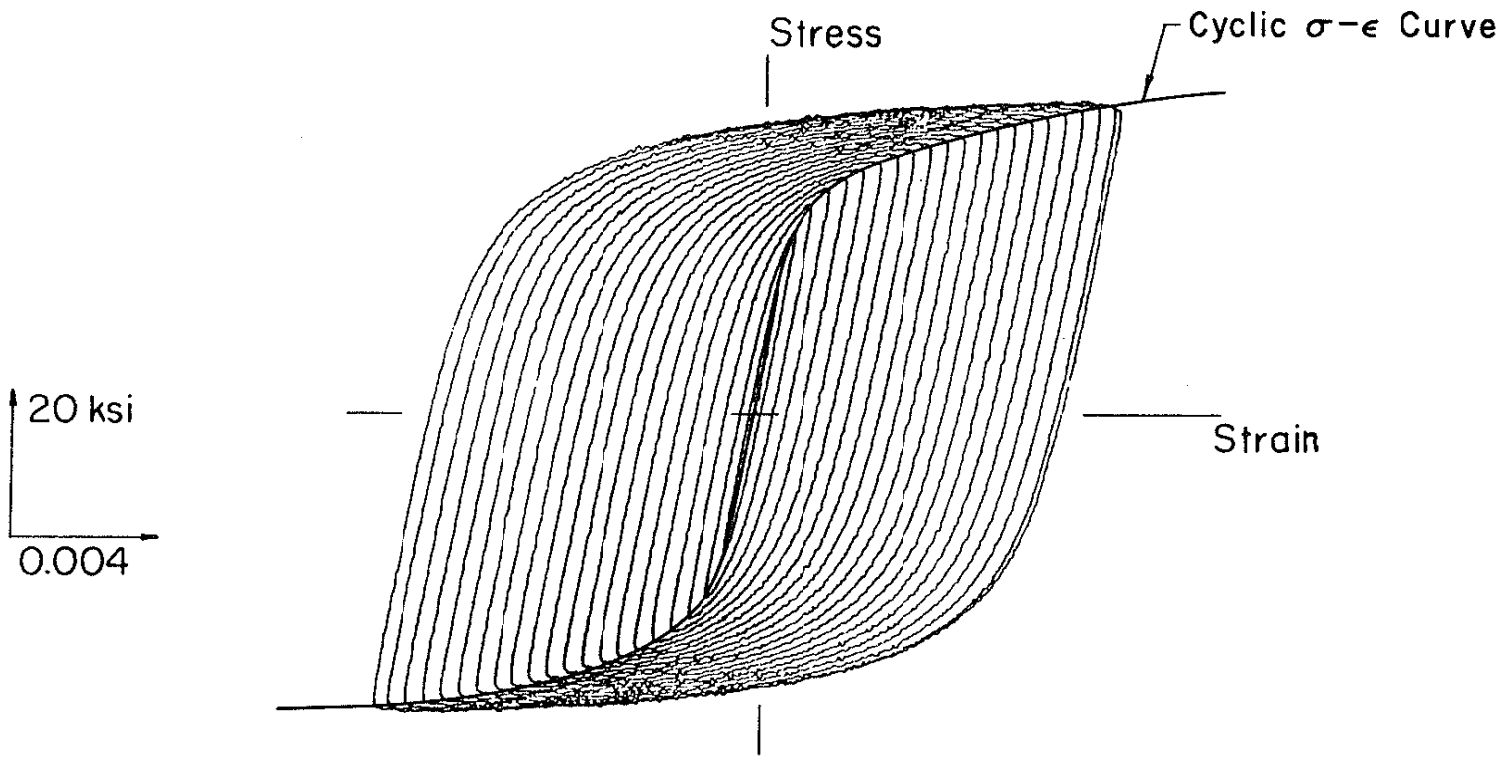

Fig. 3 Cyclic Stress-Strain Curve Drawn through Stable Loop Tips

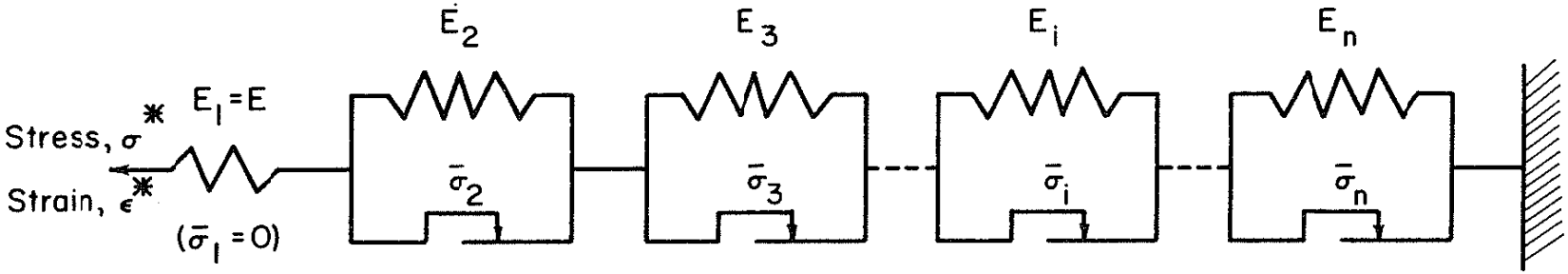

a. Schematic Of Rheological Model

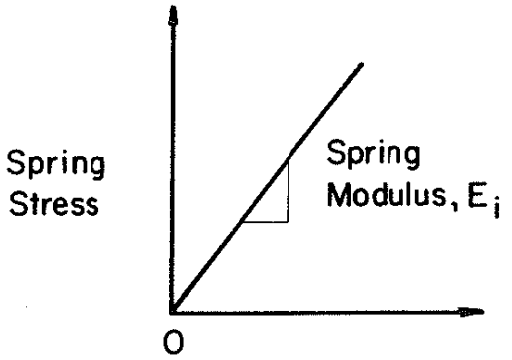

b. Spring Response

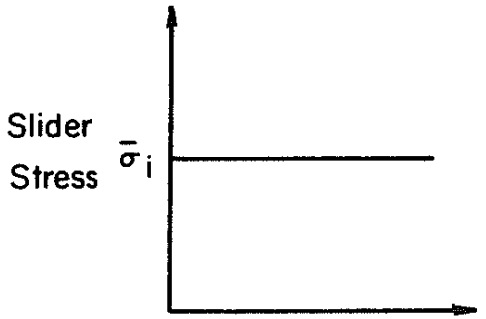

c. Frictional Slider Response

Fig. 4 Mechanical Analog for Cyclic Stress-Strain Simulation

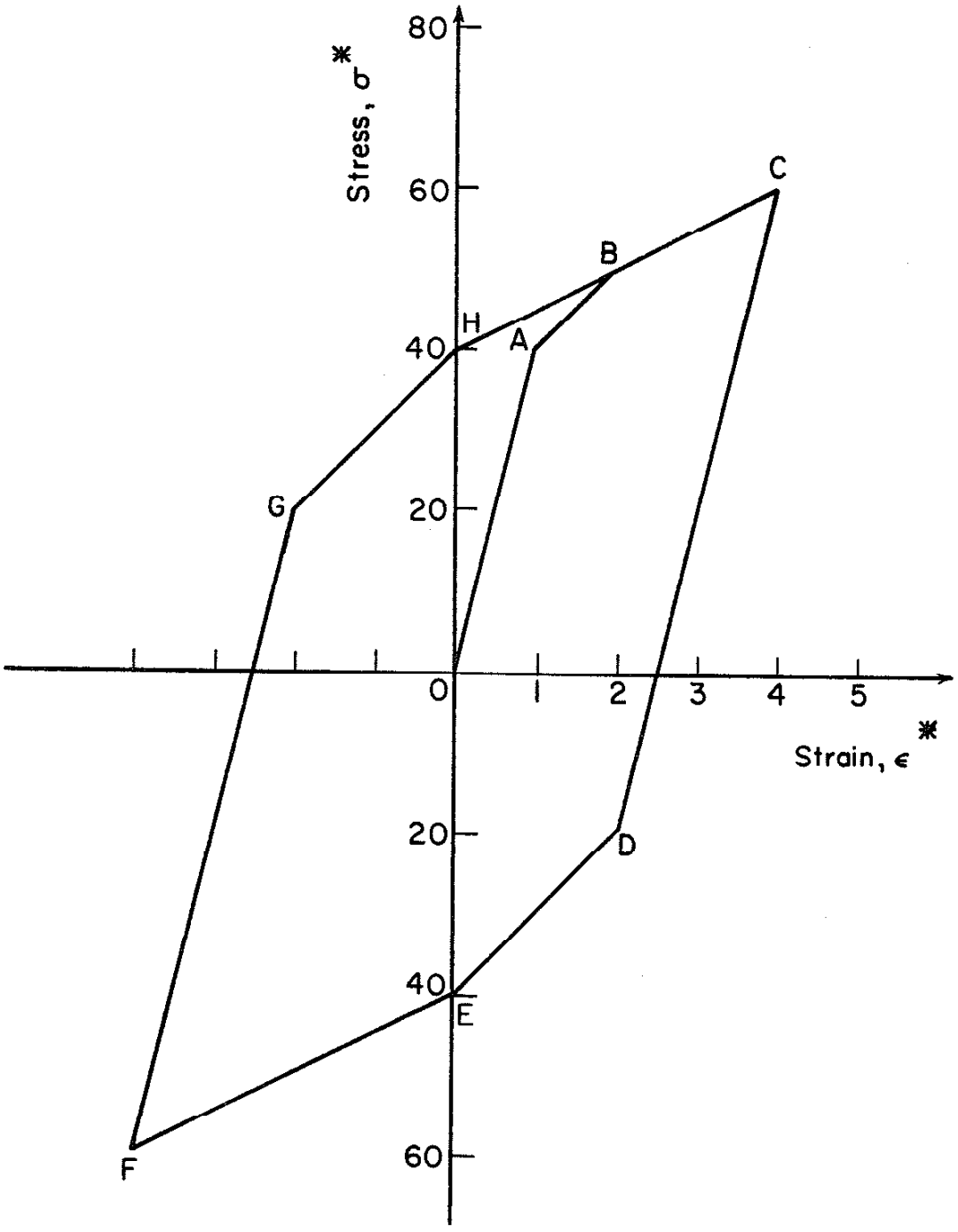

Fig. 5 Stress-Strain Response of a Three-Element Rheological Model

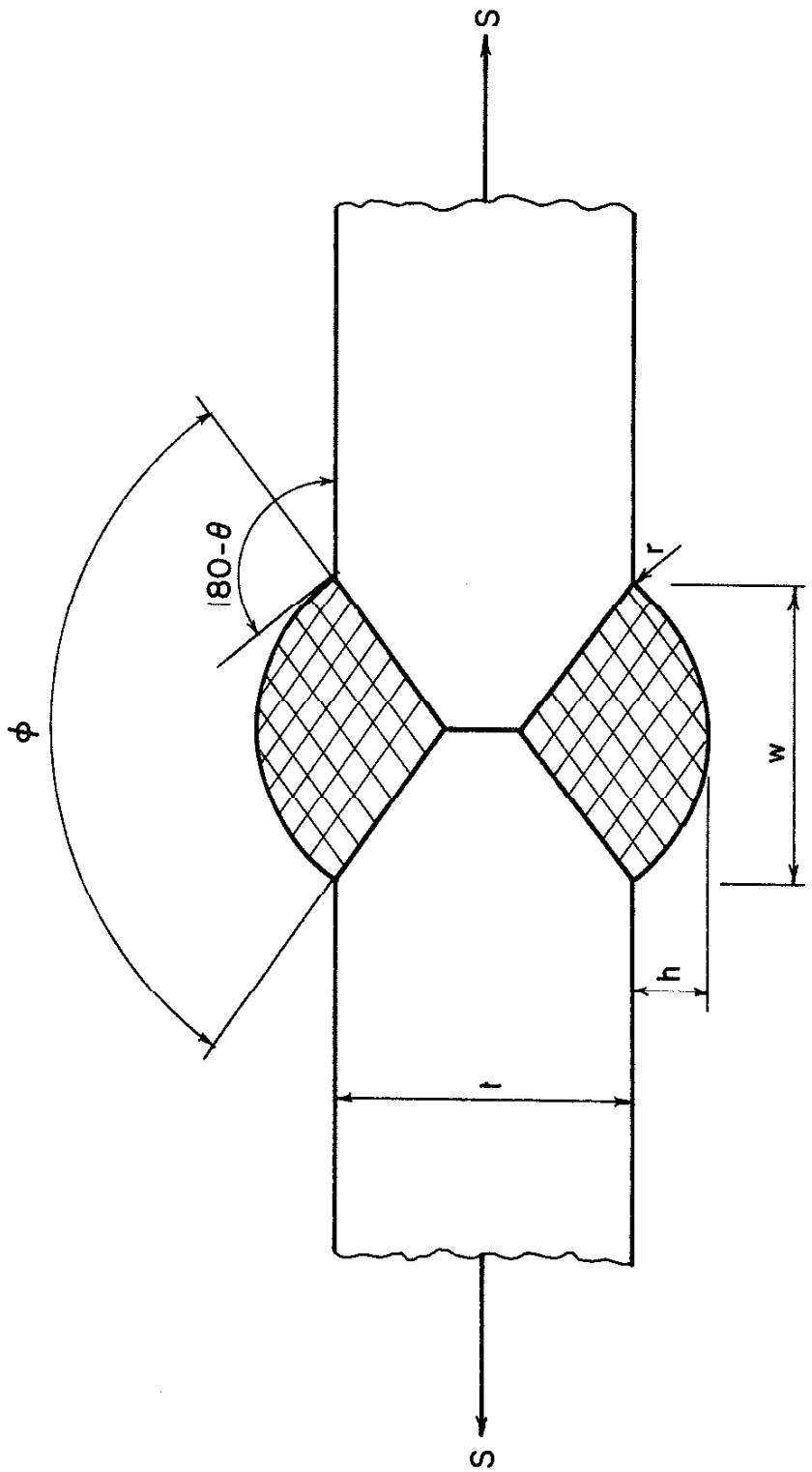

Fig. 6 Circle Segment Approximation of a Double-Vee Butt Weldment Geometry (14)

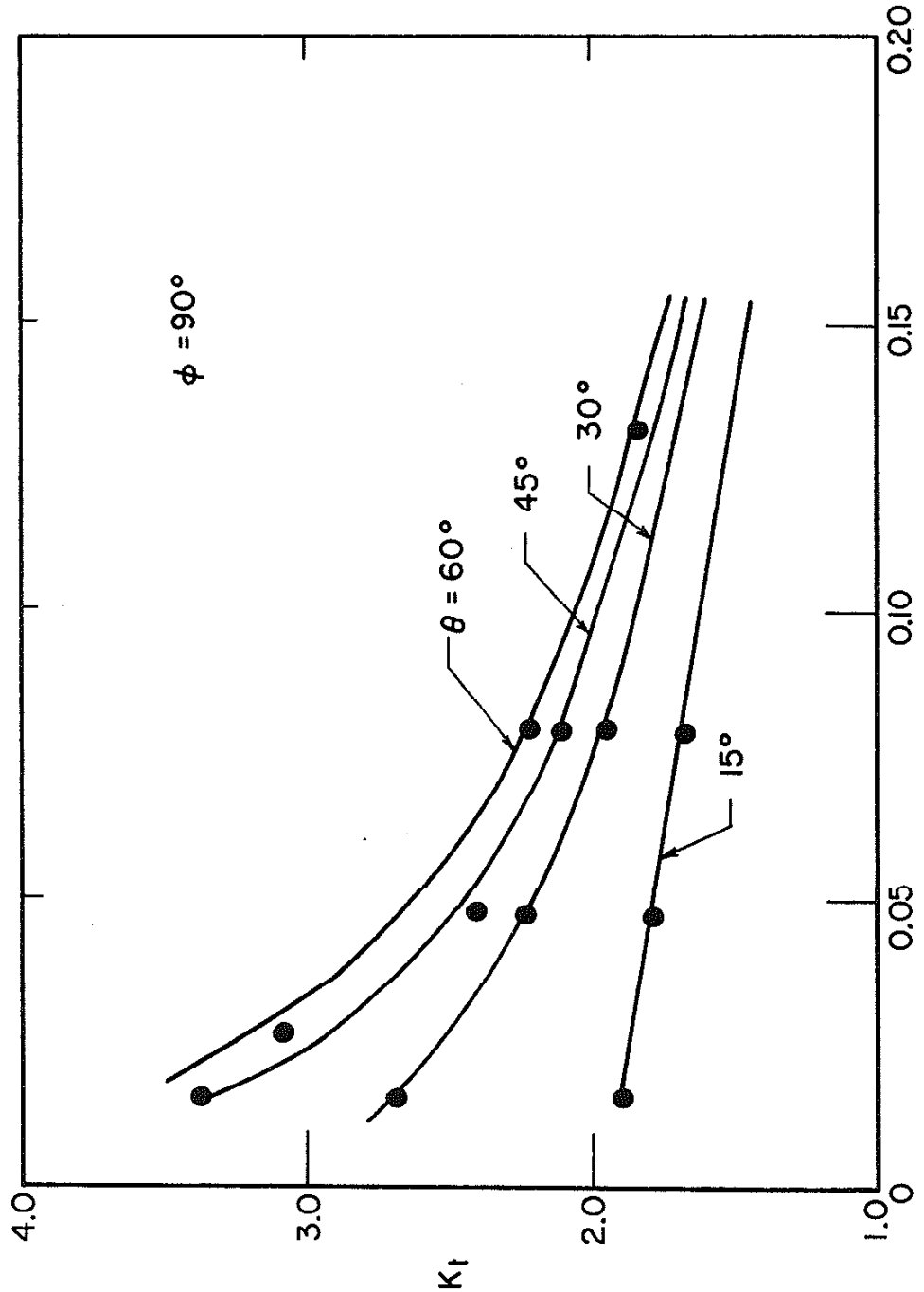

Fig. 7 Stress Concentration Factor, K_t, as a Function of r/t for Various θ Angles ($\phi = 90°$). Butt Welds

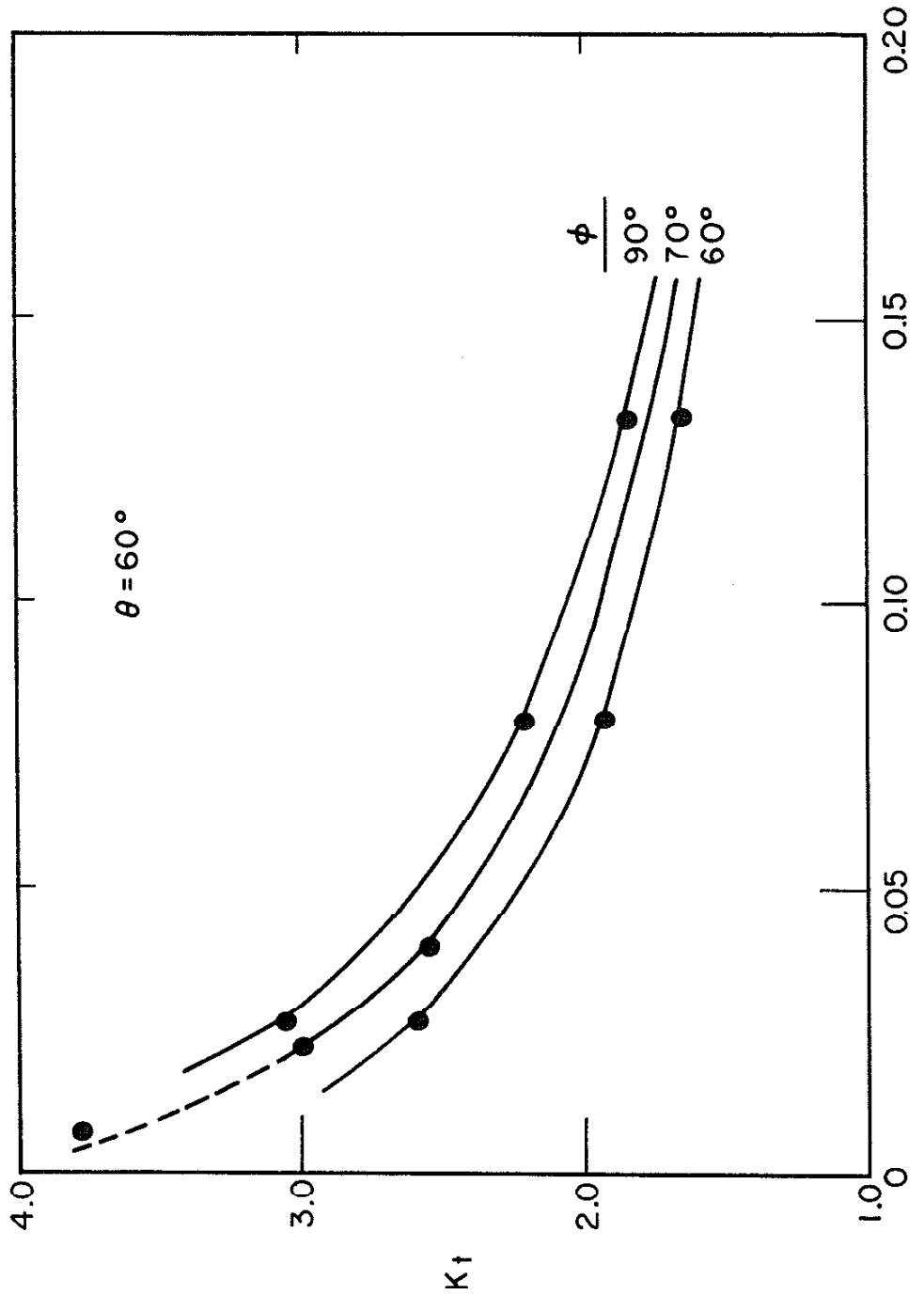

Fig. 8 Stress Concentration Factor, K_t, as a Function of r/t for Various ϕ Angles (θ = 60°). Butt Welds

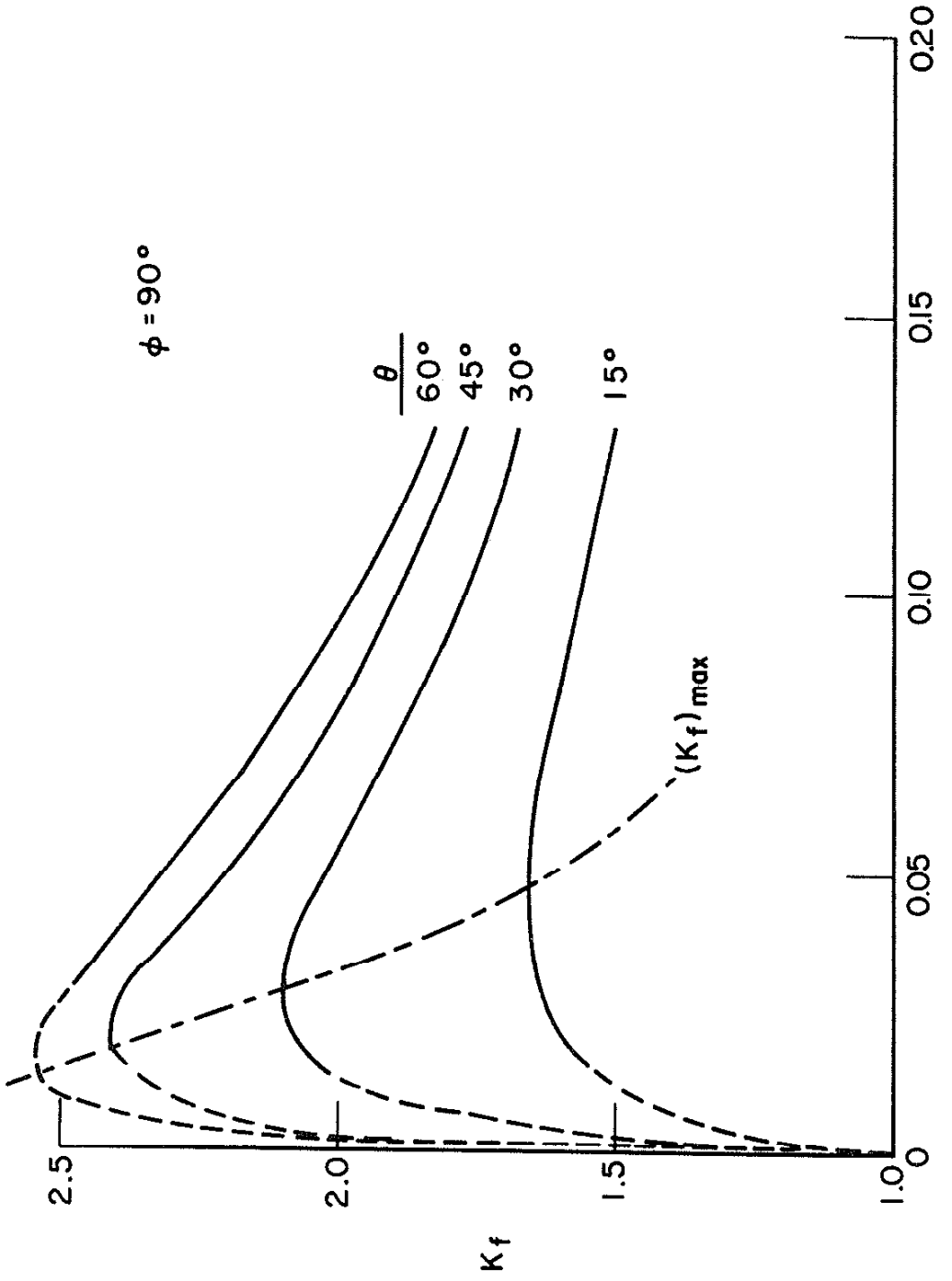

Fig. 9 Fatigue Notch Factor, K_f, as a Function of r/t for Various θ Angles (φ = 90°). Butt Welds (A-36 Steel, a=0.01 in.). $(K_f)_{max}$ Varies with θ. The Ratio r/t Corresponding to $(K_f)_{max}$ Is not Constant for Various θ.

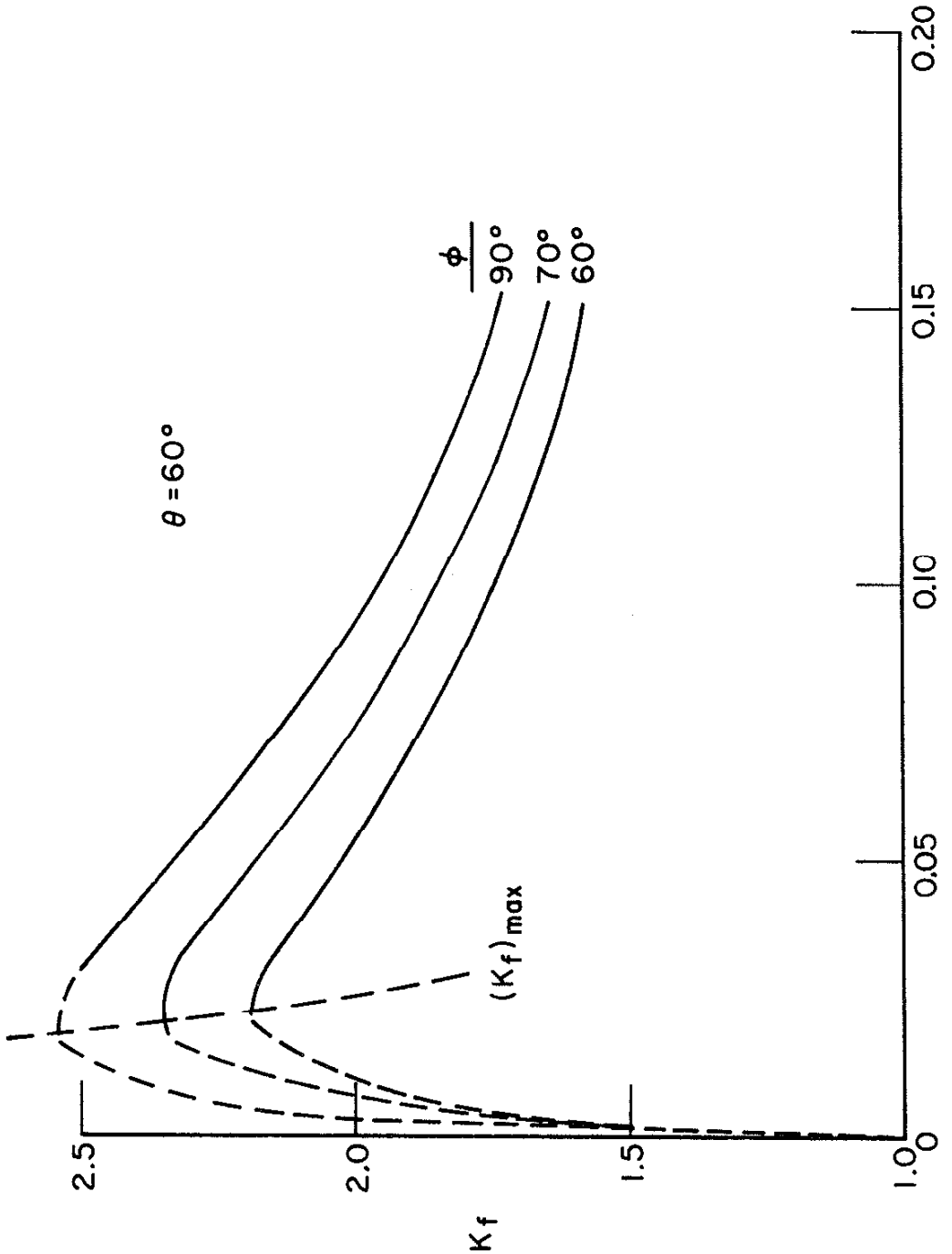

Fig. 10 Fatigue Notch Factor, K_f, as a Function of r/t for Various ϕ Angles (θ = 60°). Butt Welds (A-36 Steel, a=0.01 in.)

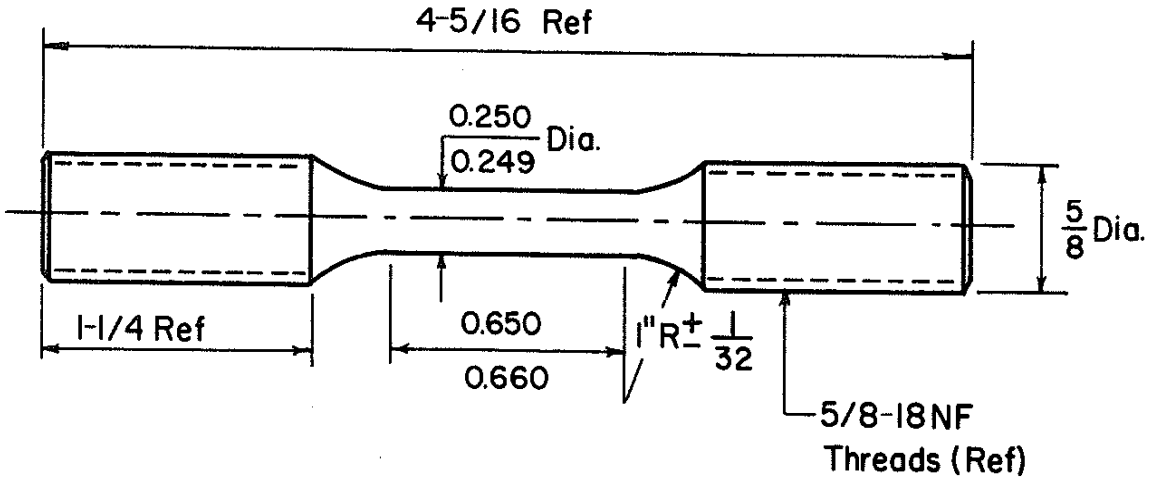

Fig. 11 Smooth Specimen Geometry (Dimensions in inches)

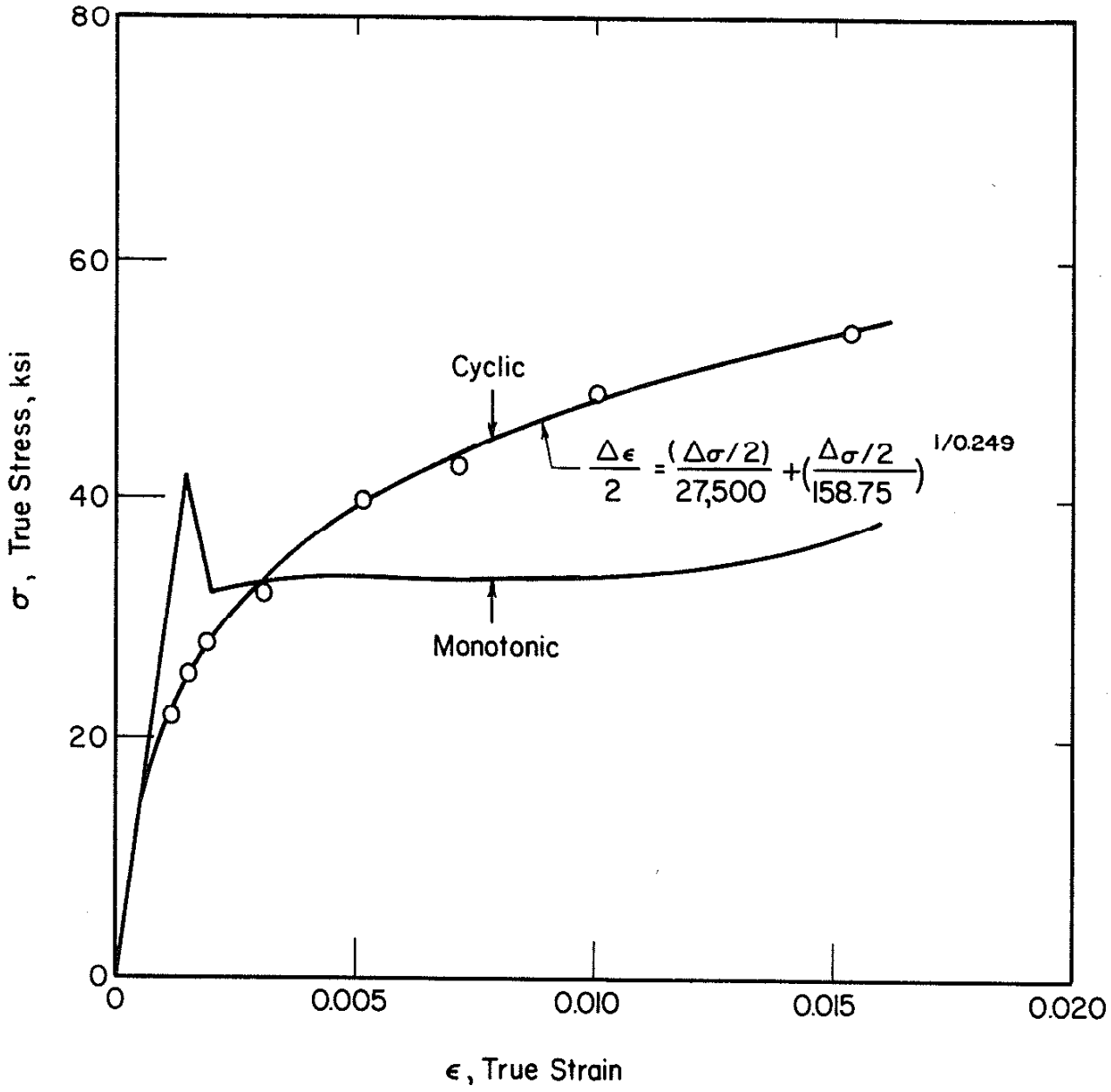

Fig. 12 Initial Portions of the Monotonic and the Cyclic Stress-Strain Curves for A-36 Steel

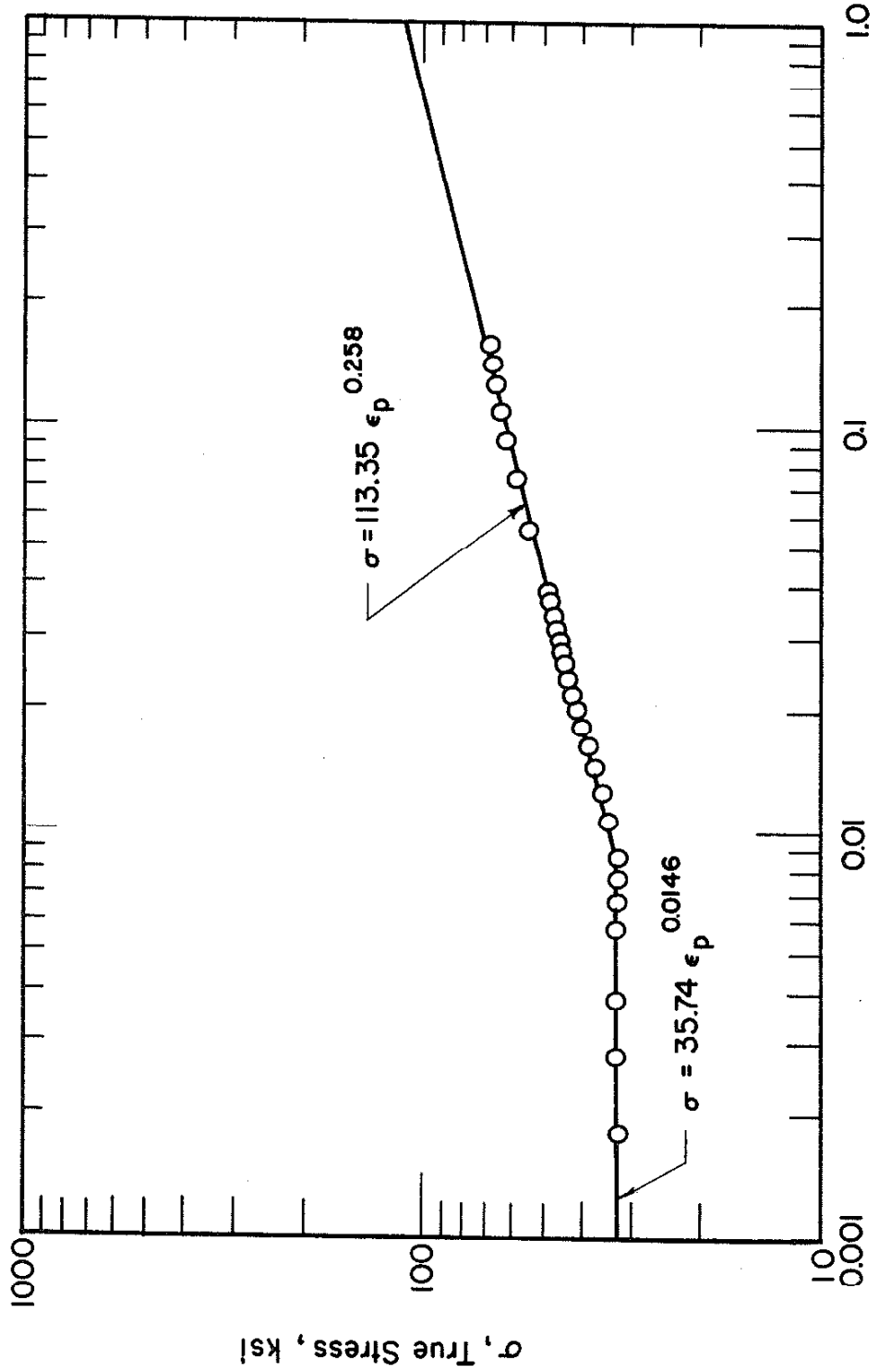

Fig. 13 Monotonic Stress-Plastic Strain Data for A-36 Steel

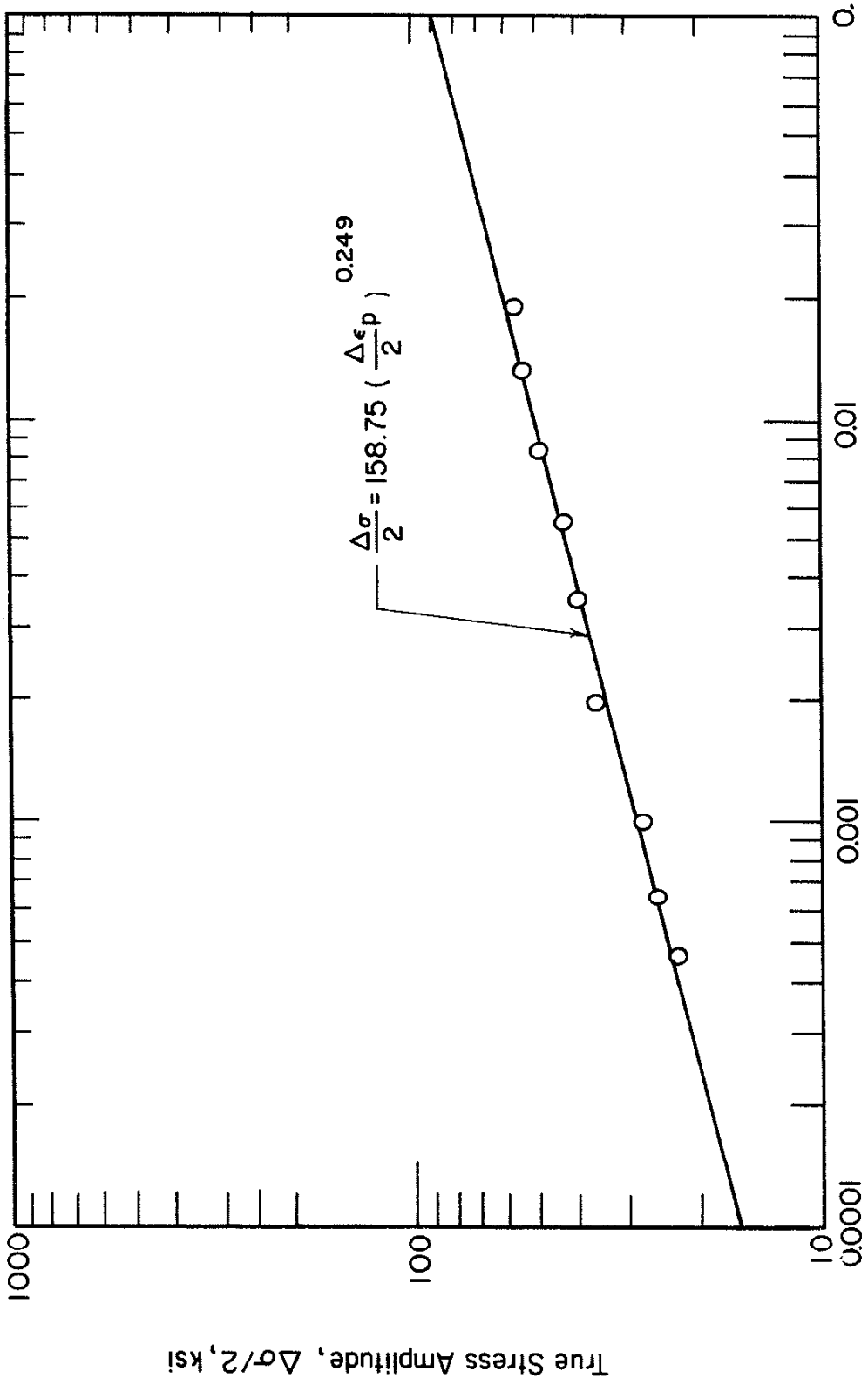

Fig. 14 Cyclic Stress-Plastic Strain Data for A-36 Steel

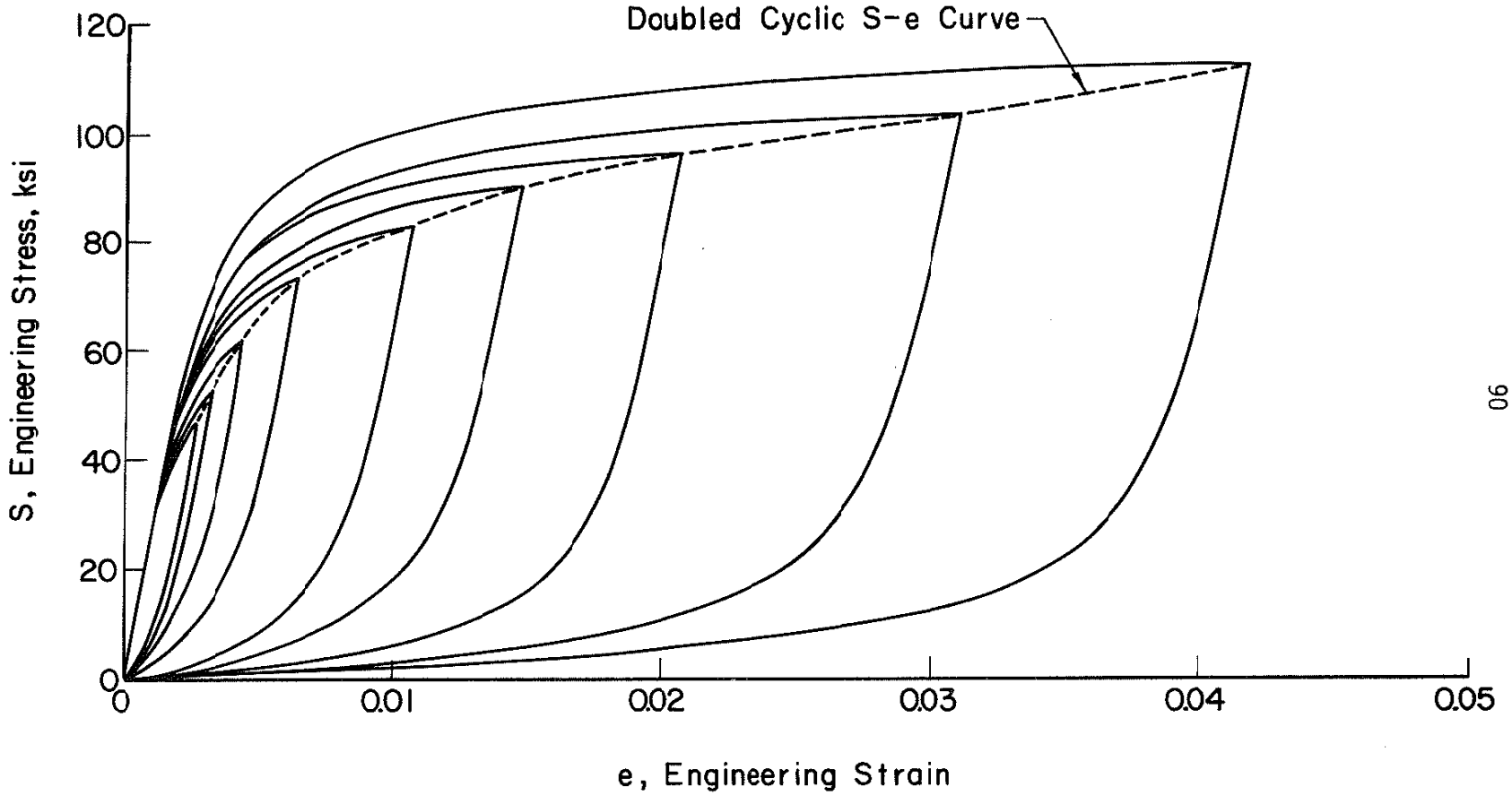

Fig. 15 Stabilized Hysteresis Loops for A-36 Steel with a Common Origin

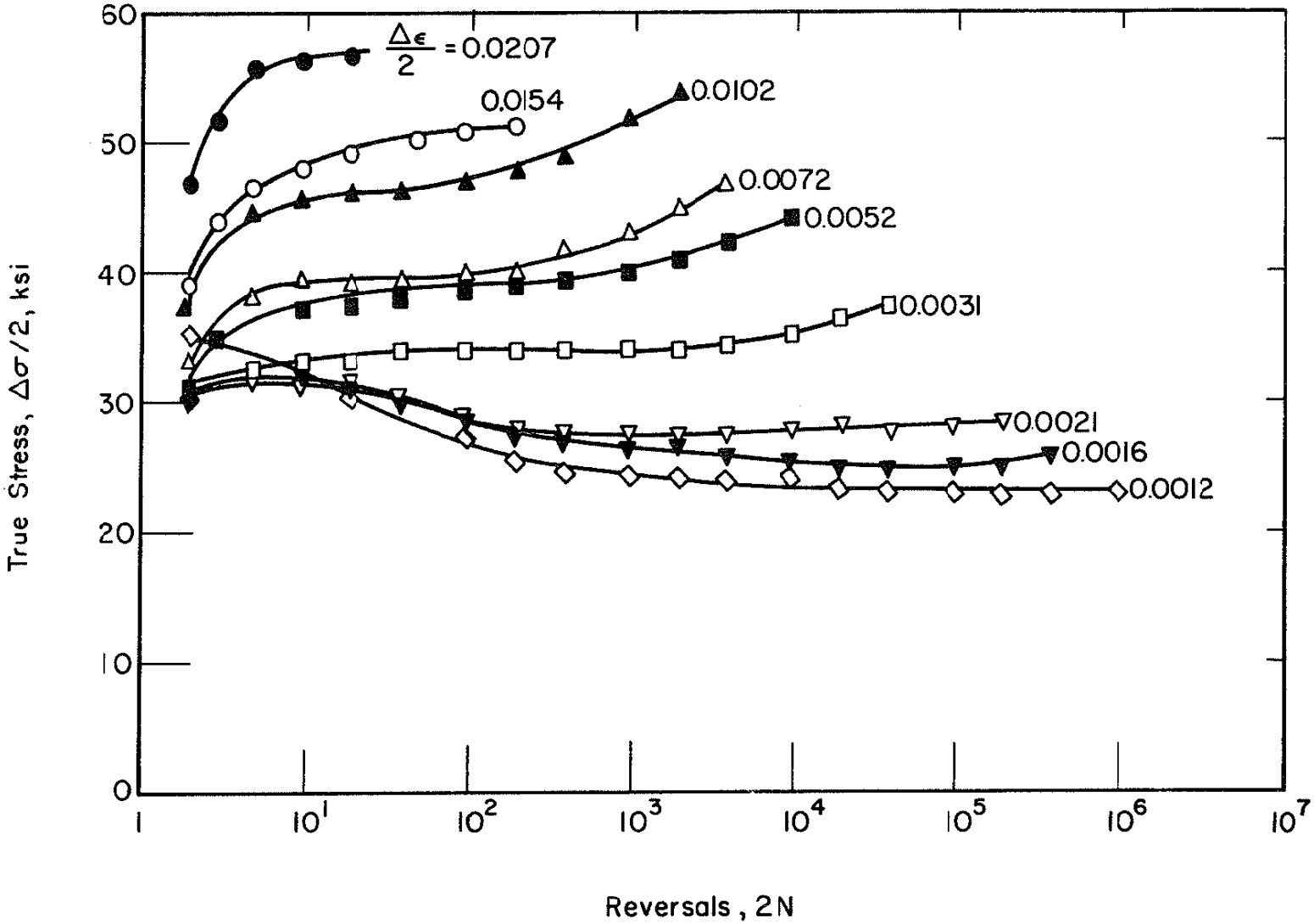

Fig. 16 Cyclic Hardening and Softening Behavior for Constant Amplitude Strain Controlled Tests on A-36 Steel

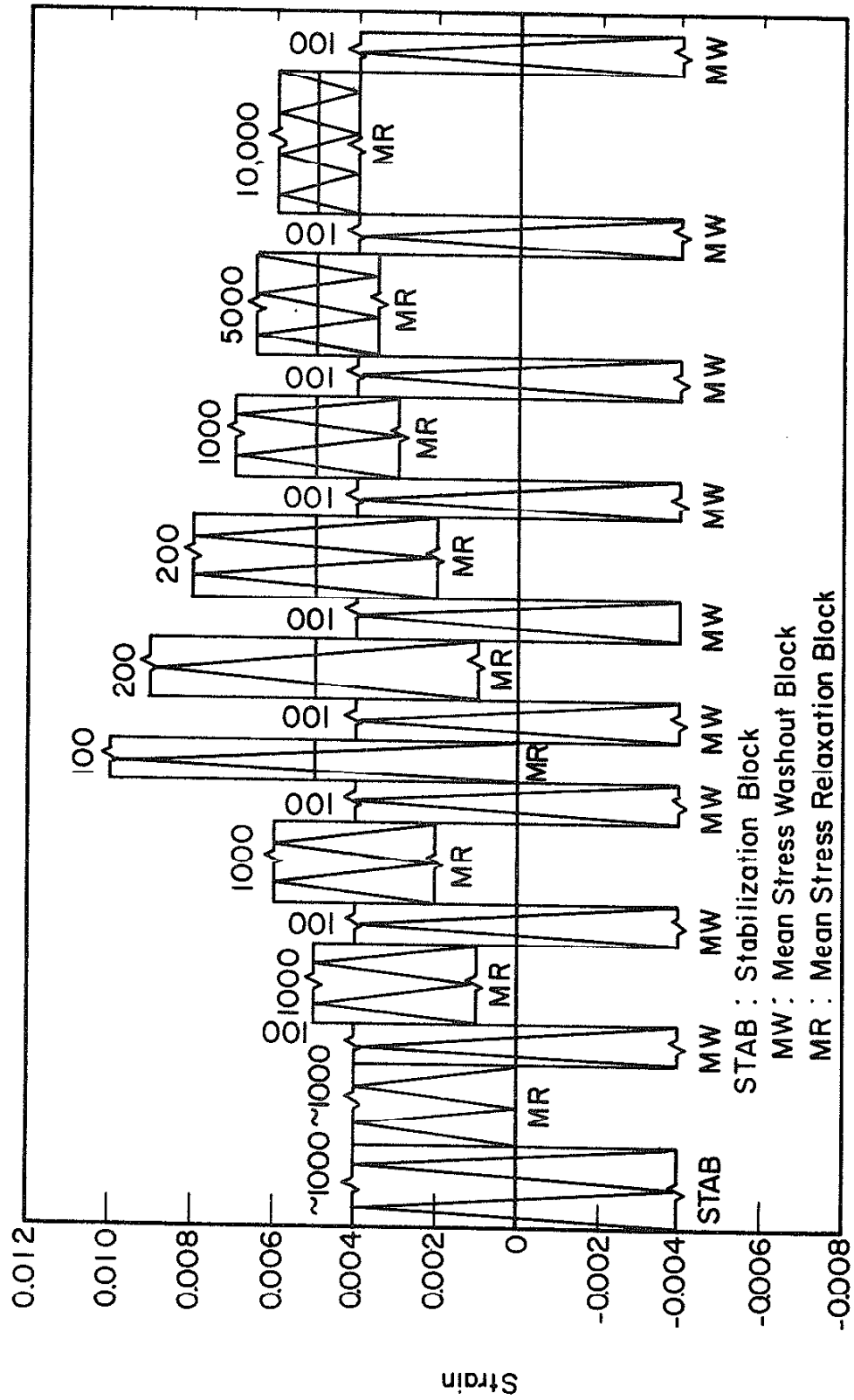

Fig. 17 Block Sequence for Mean Stress Relaxation Tests on A-36 Steel

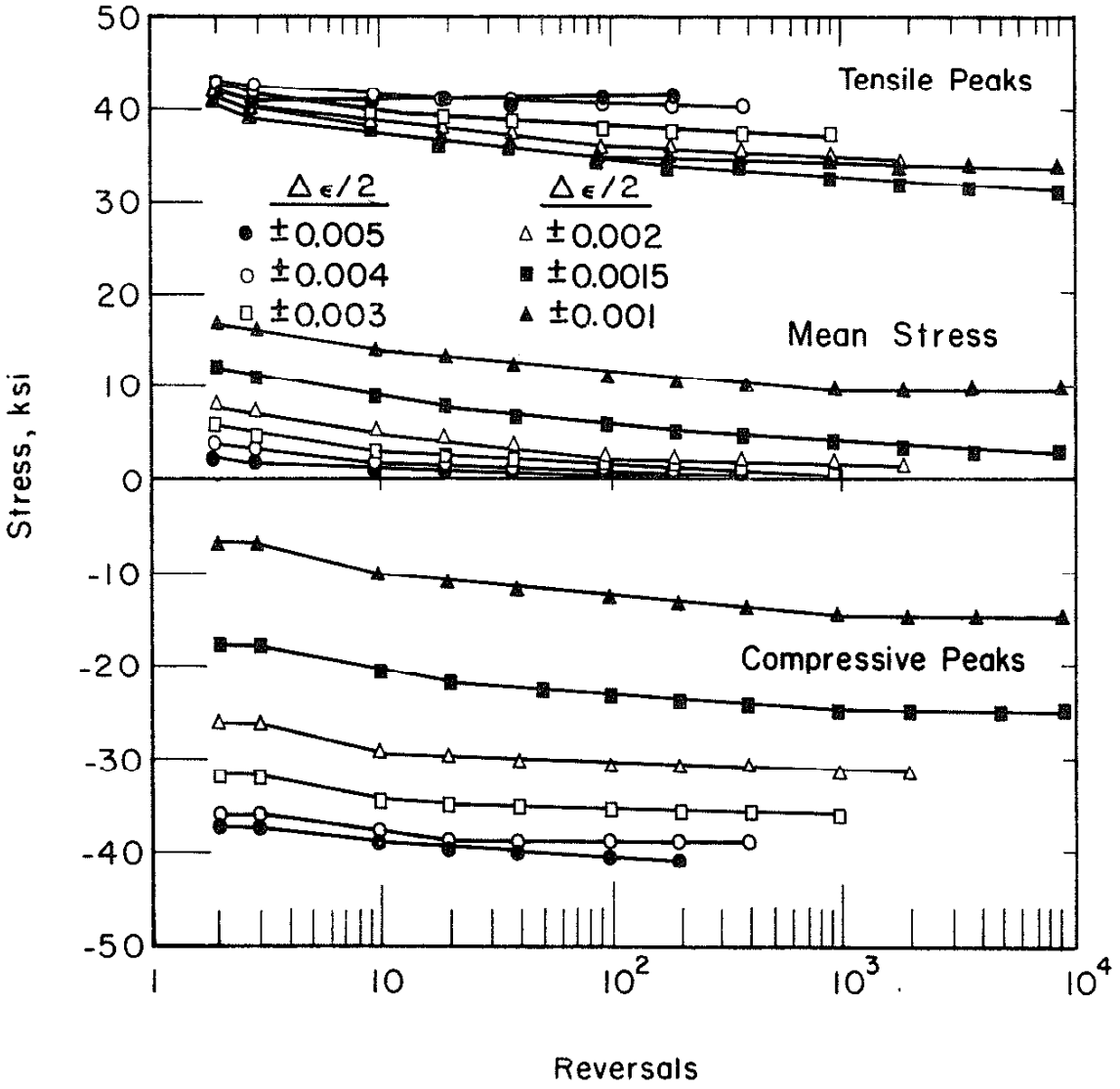

Fig. 18 Cyclic Mean Stress Relaxation Data for Five Strain Amplitudes at a Constant Mean Strain (+0.005)

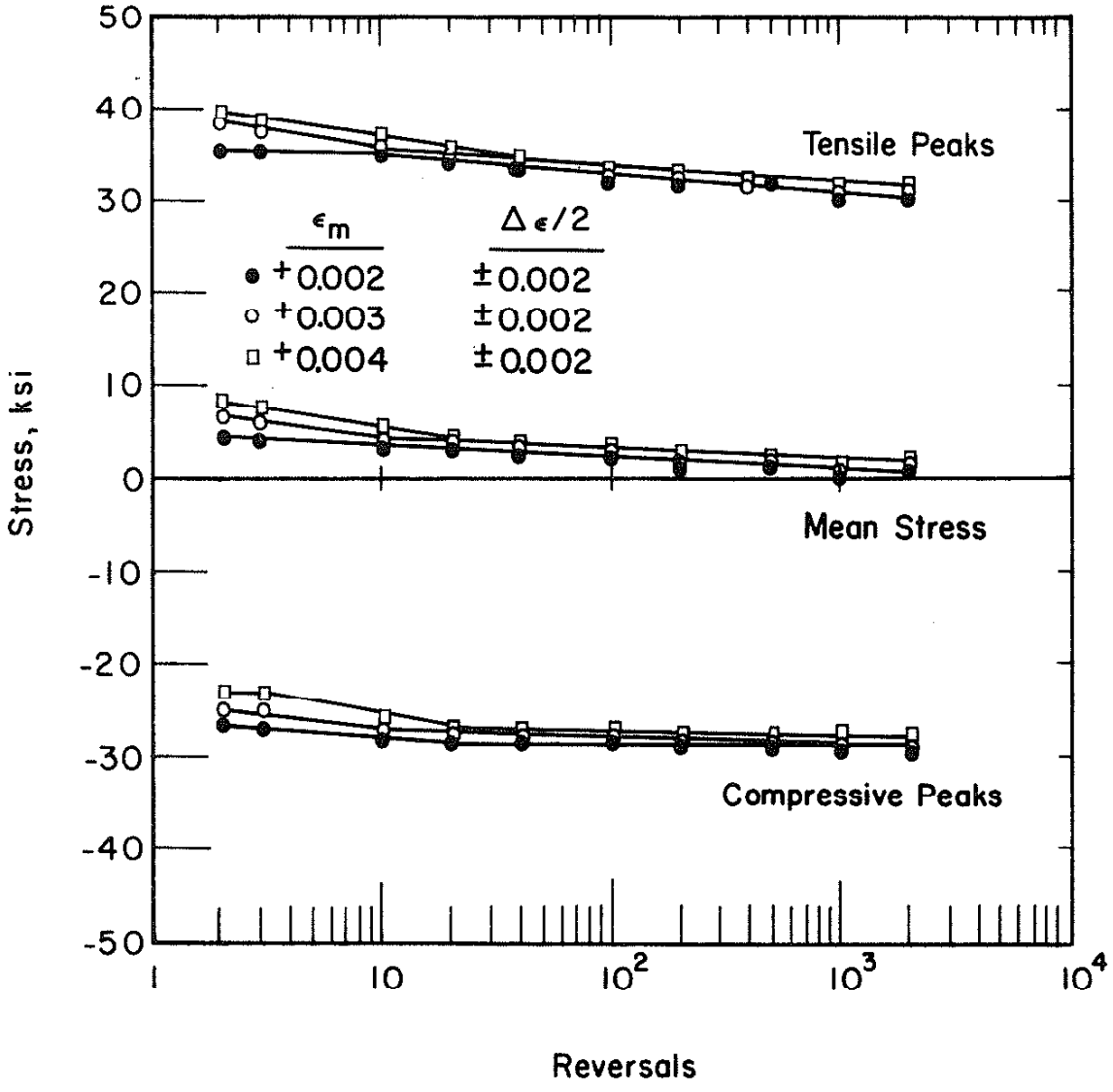

Fig. 19 Cyclic Mean Stress Relaxation Data for Three Mean Strains at a Constant Strain Amplitude (±0.002)

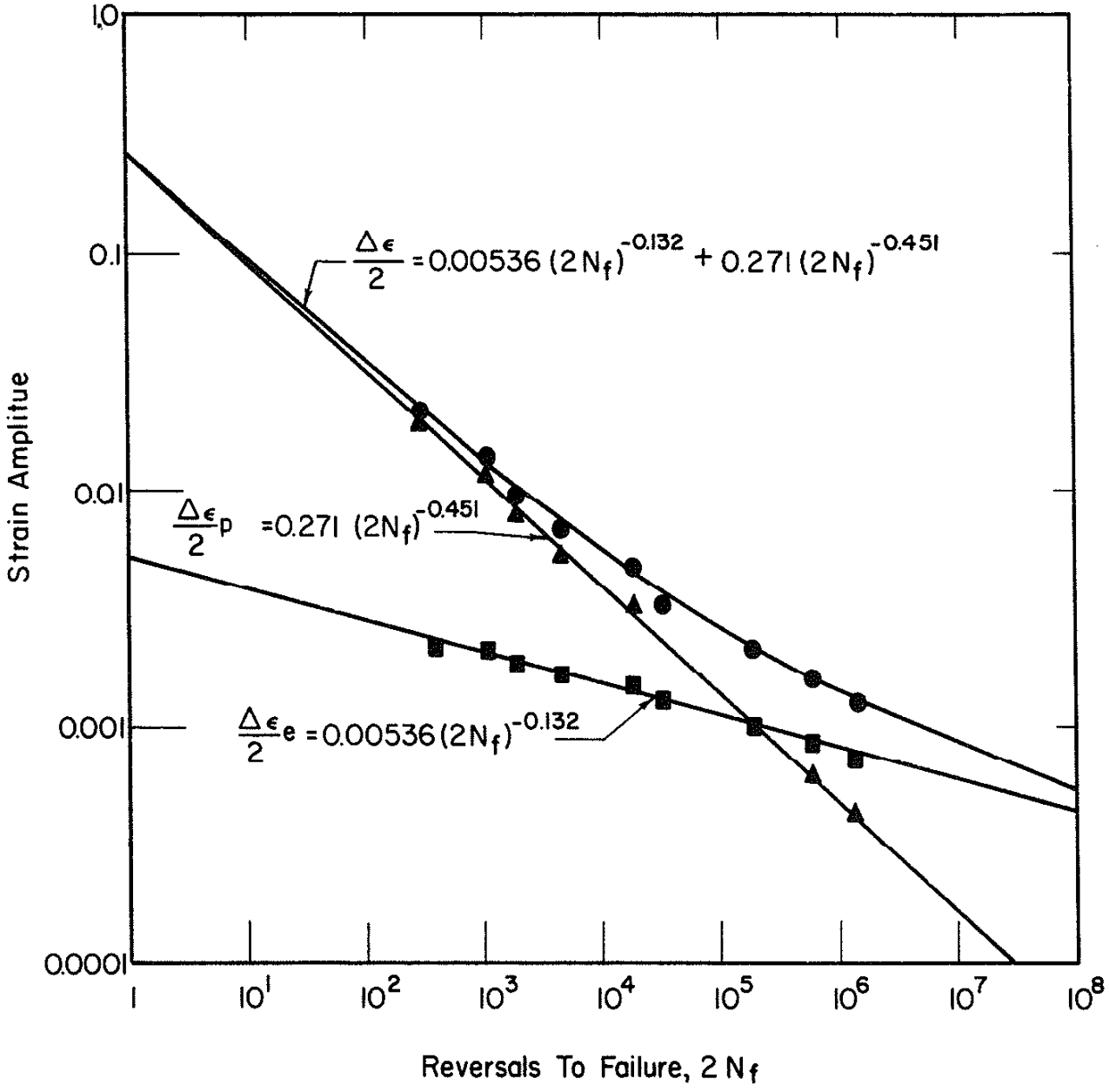

Fig. 20 Strain-Reversals to Failure Data for A-36 Steel

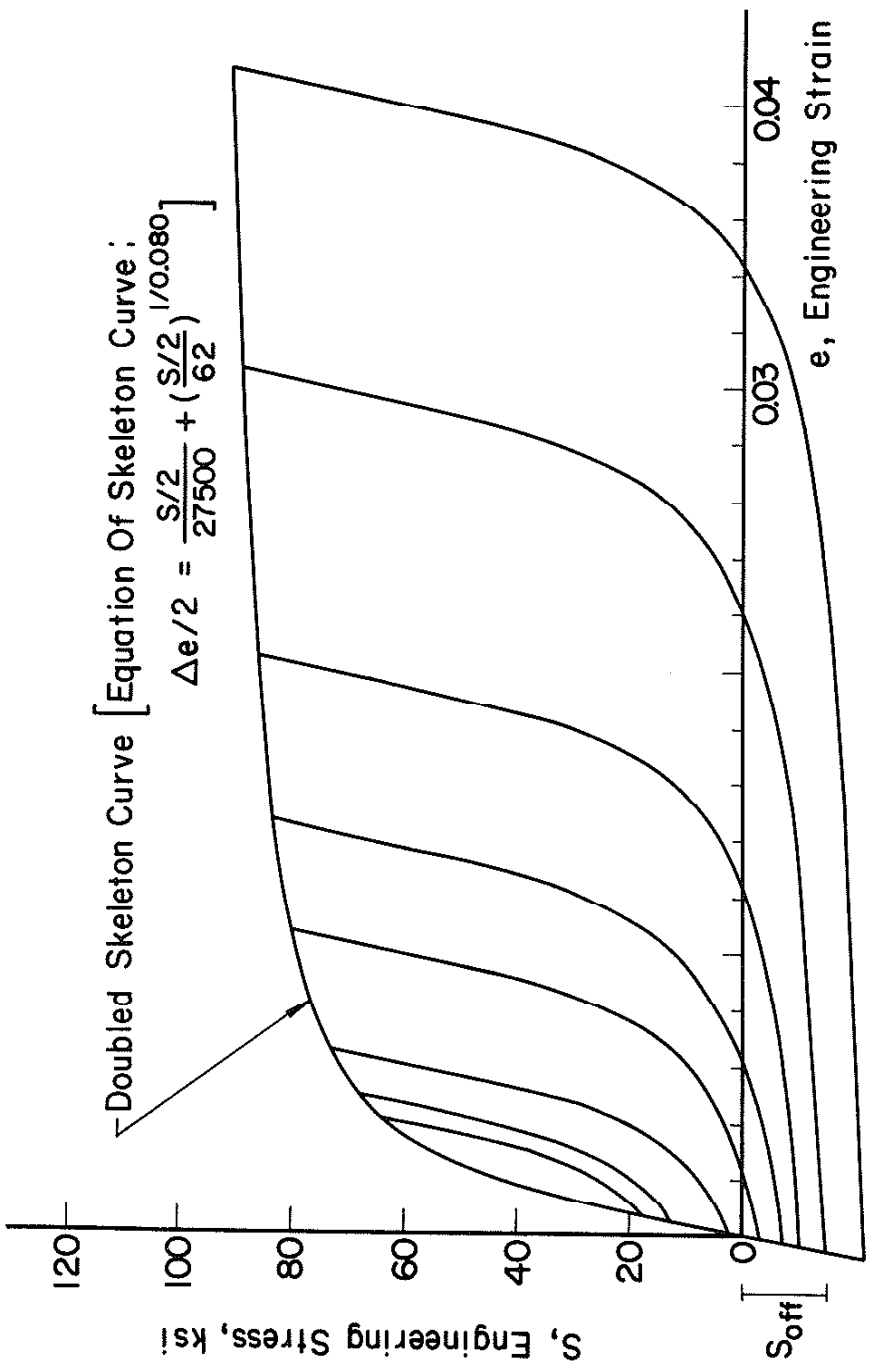

Fig. 21 Stable Hysteresis Loops for A-36 Steel Translated along the Elastic Line. S_{off} Is Stress Offset

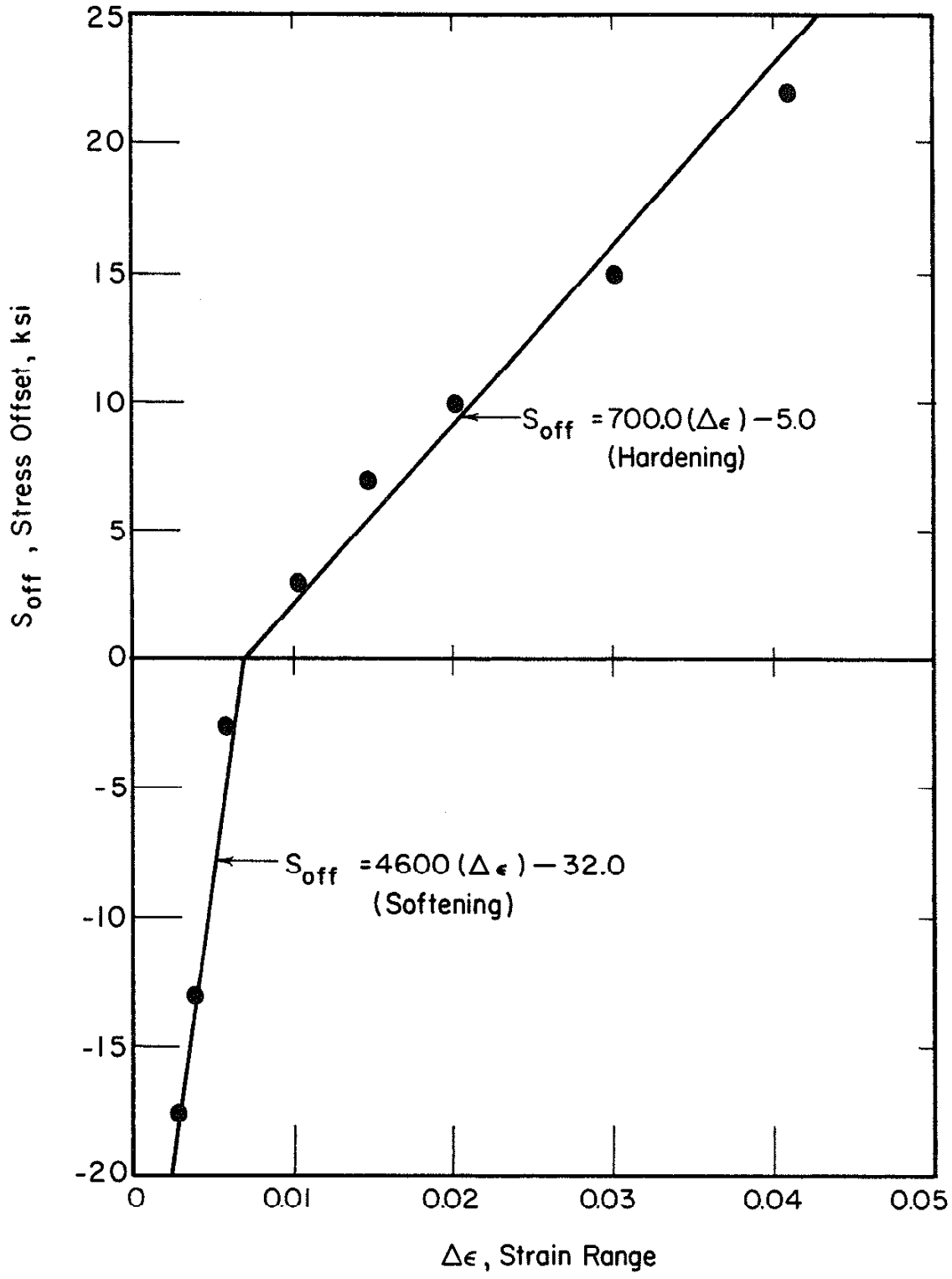

Fig. 22 Stress Offset, S_{off}, vs. Strain Range, $\Delta\varepsilon$, for "Stable" A-36 Steel

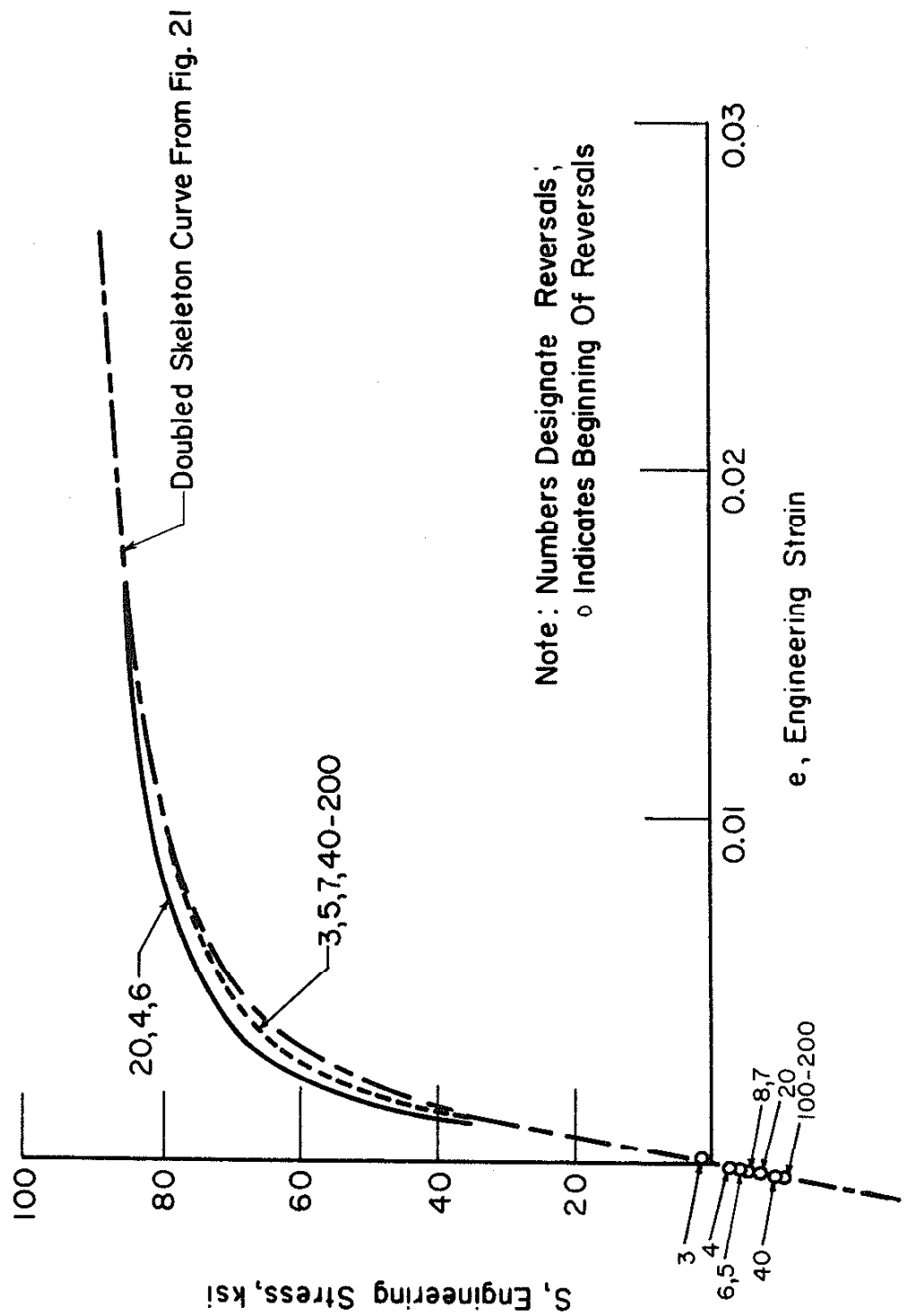

Fig. 23 Hysteresis Loop Branches for Constant Amplitude Strain Controlled Test (±0.0102) Fitted to the Doubled Skeleton Curve for A-36 Steel

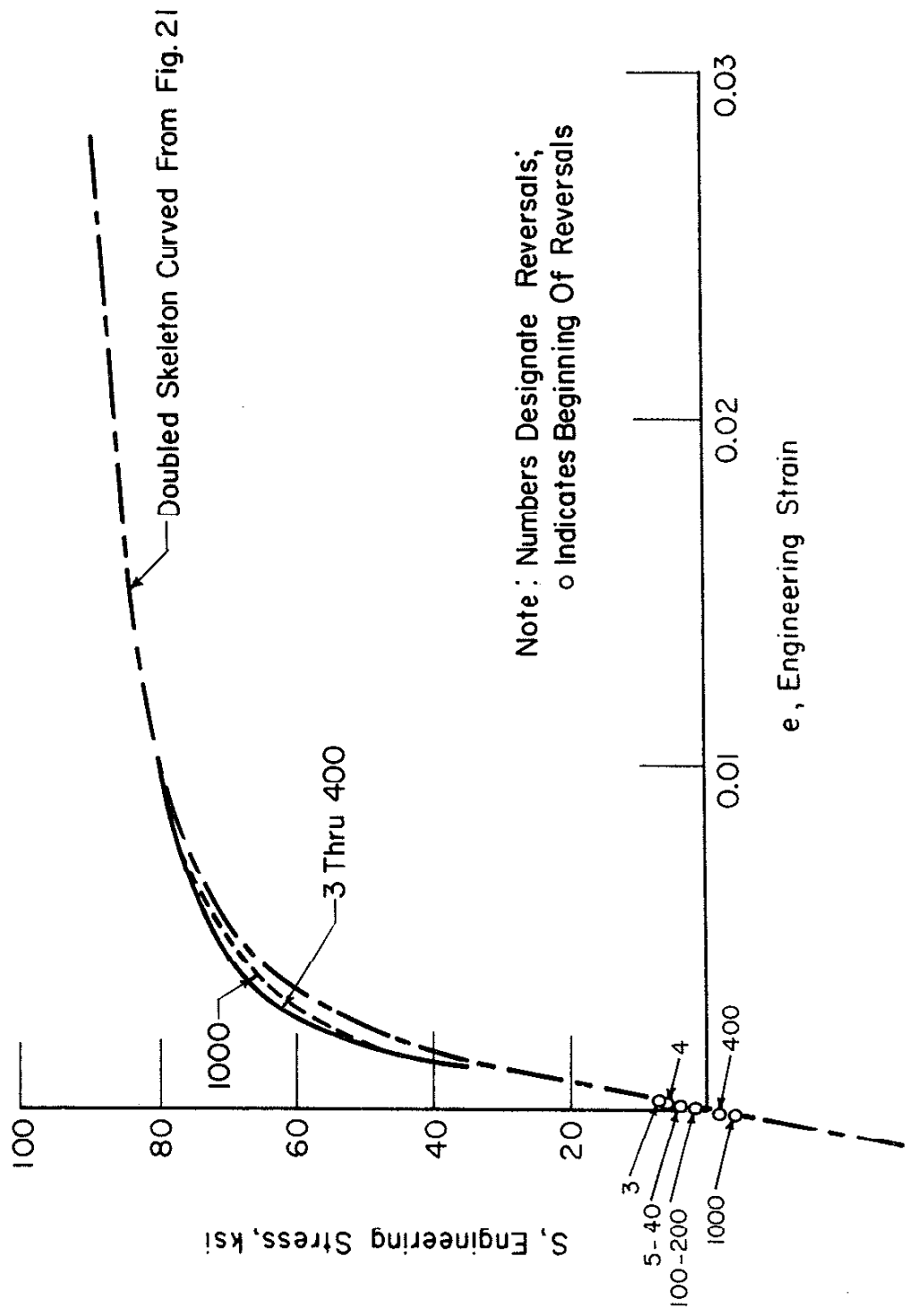

Fig. 24 Hysteresis Loop Branches for Constant Amplitude Strain Controlled Test (±0.0072) Fitted to the Doubled Skeleton Curve for A-36 Steel

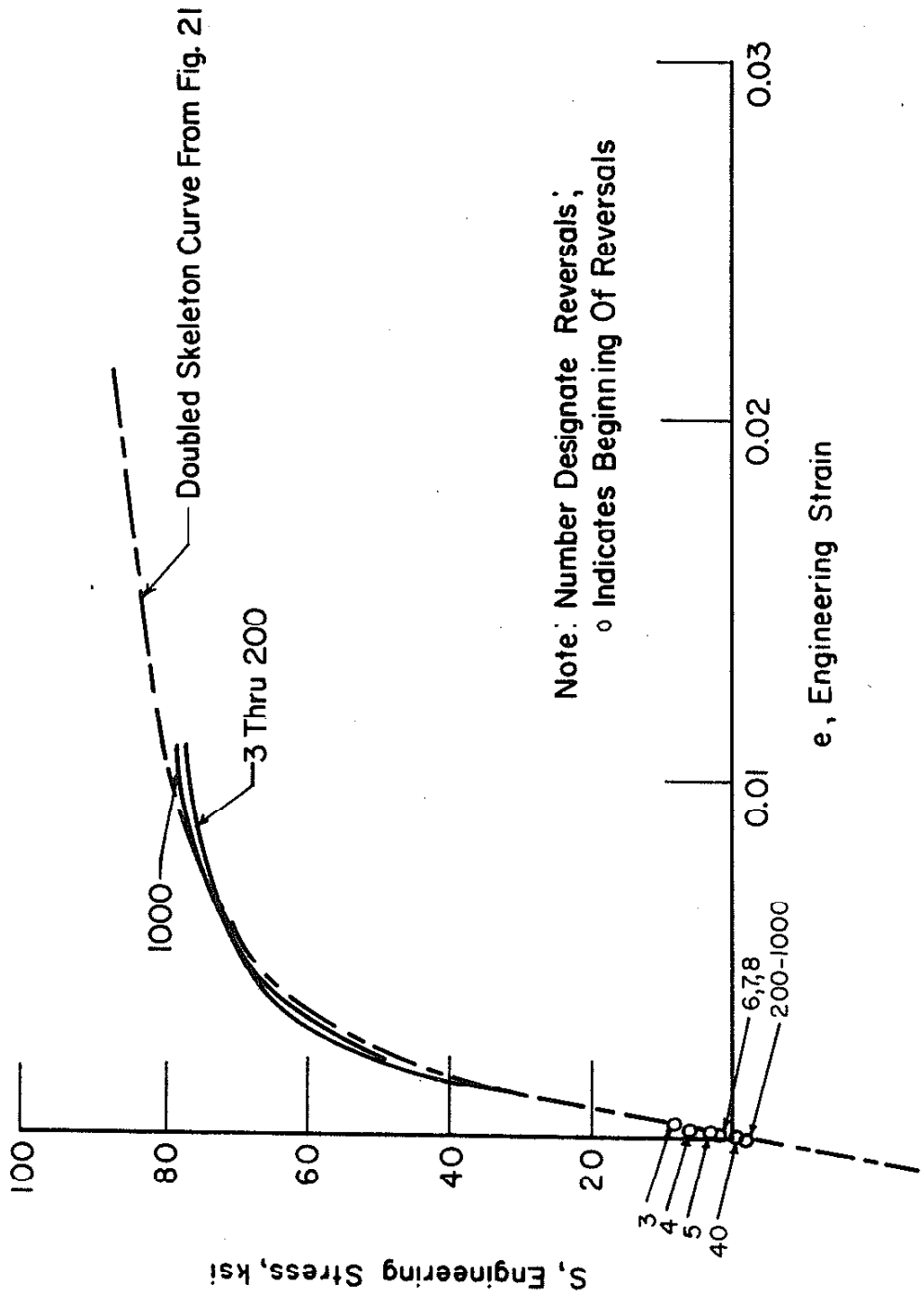

Fig. 25 Hysteresis Loop Branches for Constant Amplitude Strain Controlled Test (±0.0052) Fitted to the Doubled Skeleton Curve for A-36 Steel

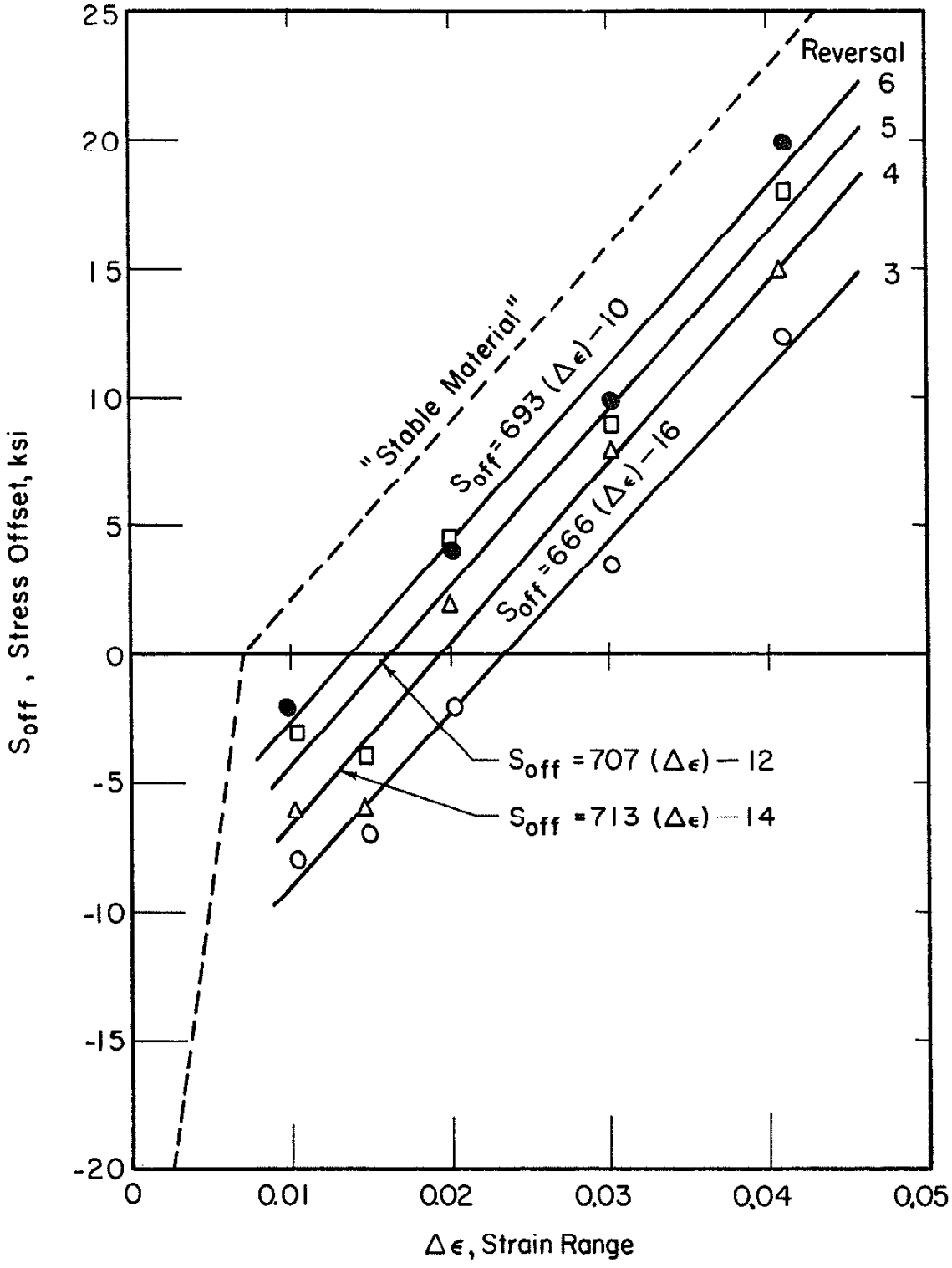

Fig. 26 Stress Offset, S_{off}, vs. Strain Range, $\Delta\varepsilon$, for Hardening Behavior of A-36 Steel

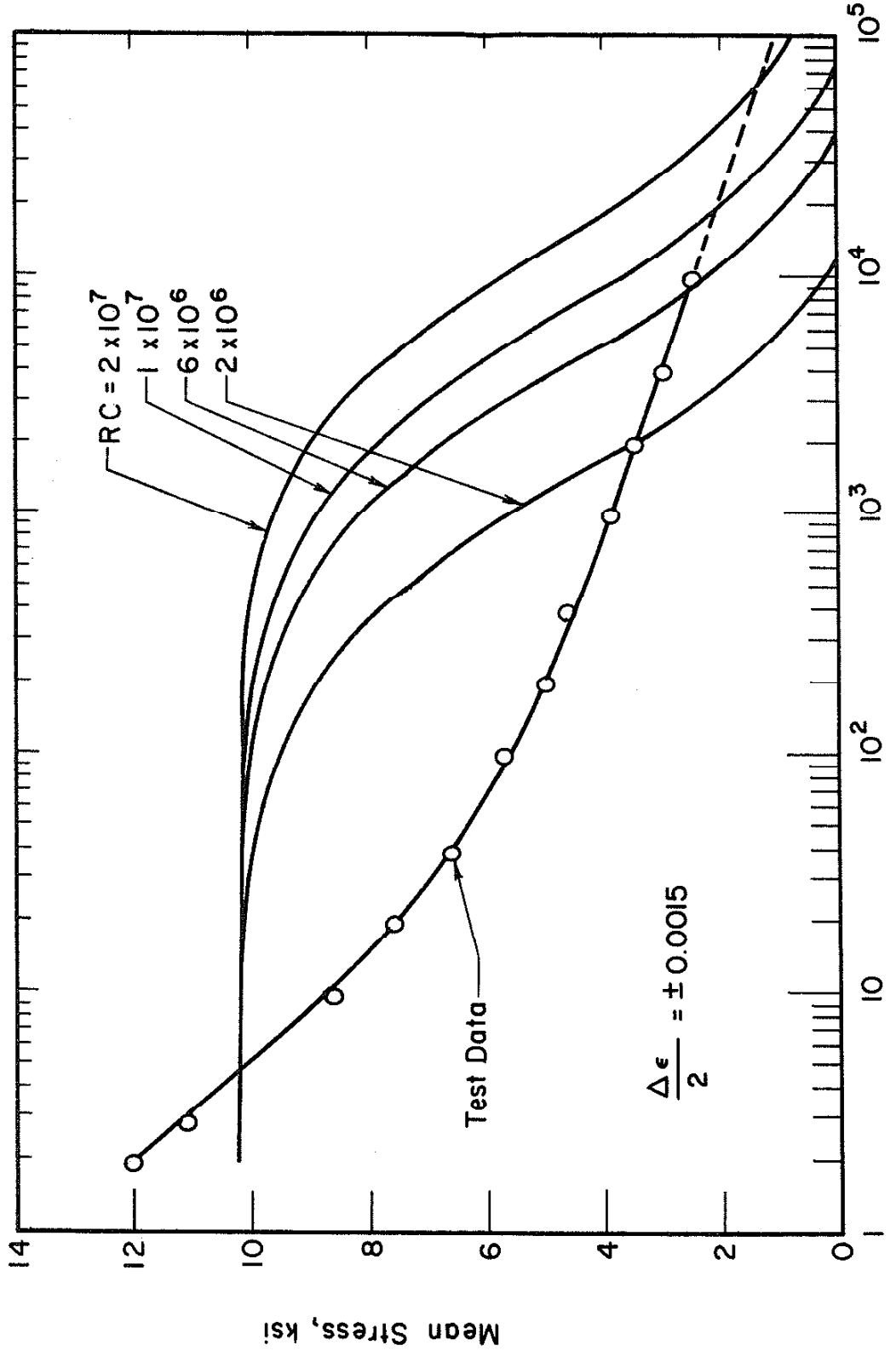

Fig. 27 Computer Simulation and Cyclic Relaxation Data for A-36 Steel. Solid Lines Indicate Behavior of Model for Various Relaxation Constant, RC

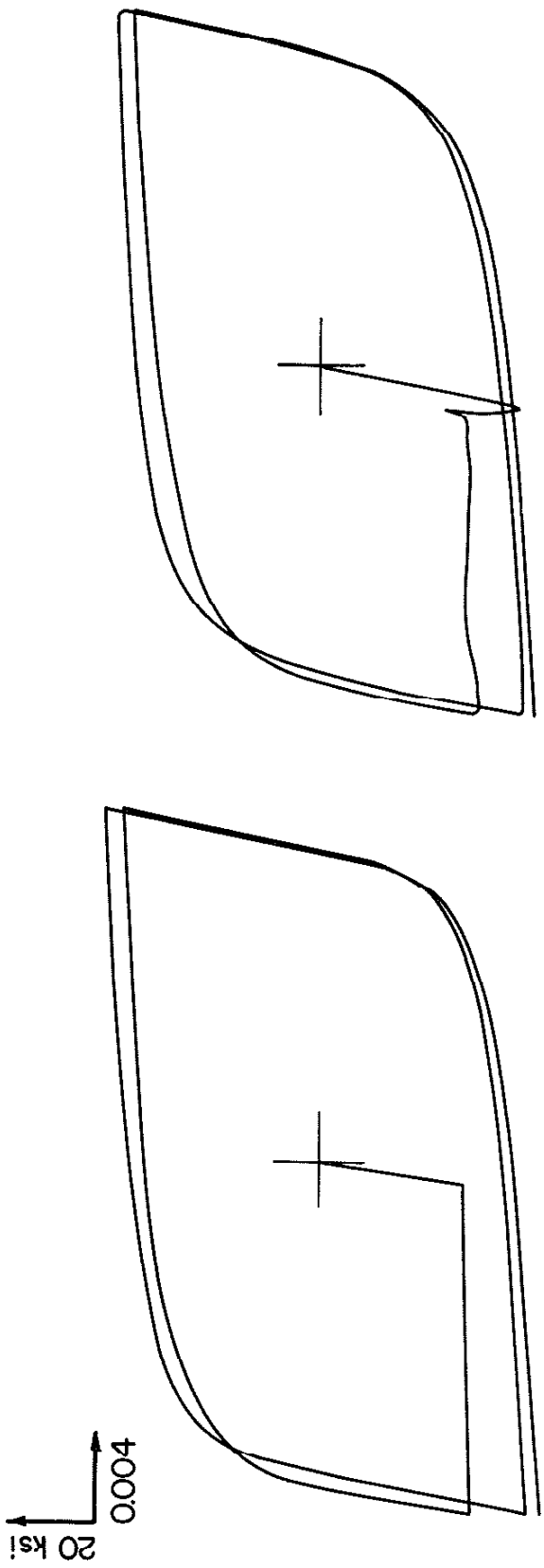

(a) Computer Simulation

(b) Test Results

Fig. 28 Predicted and Actual Stress-Strain Response for Virgin A-36 Steel ($\frac{\Delta\varepsilon}{2} = \pm 0.015$)

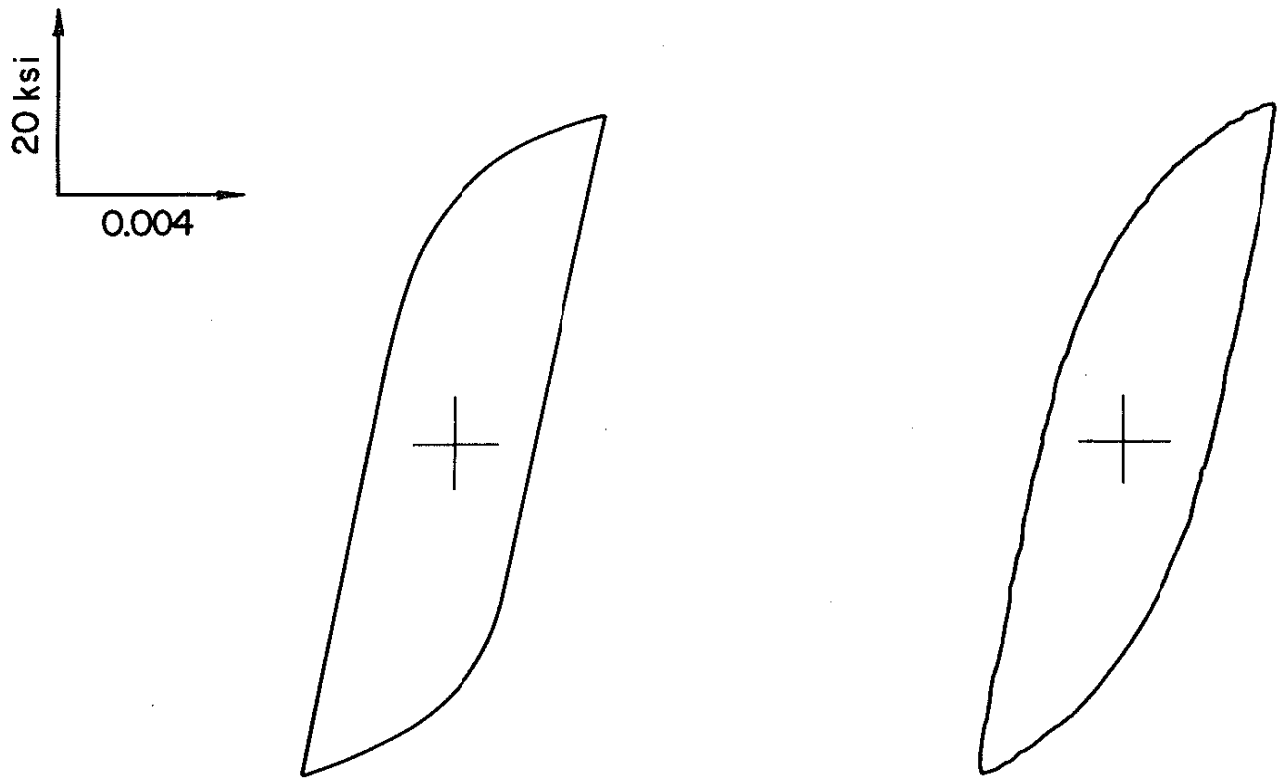

(a) Computer Simulation

(b) Test Results

Fig. 29 Predicted and Actual Stress-Strain Response for Stable A-36 Steel ($\frac{\Delta\epsilon}{2} = \pm 0.0031$)

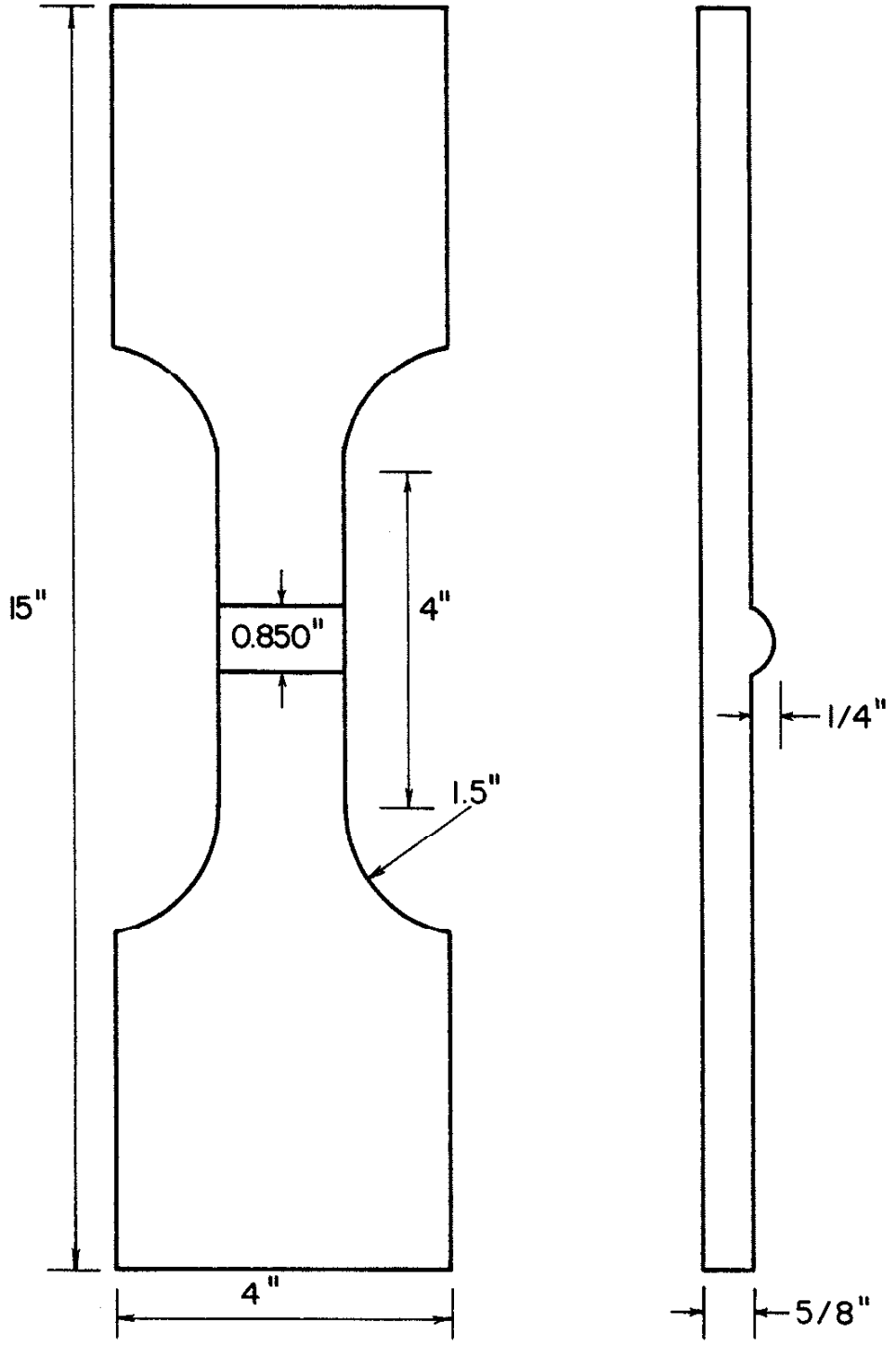

Fig. 30 Geometry of Simulated Weld Specimens

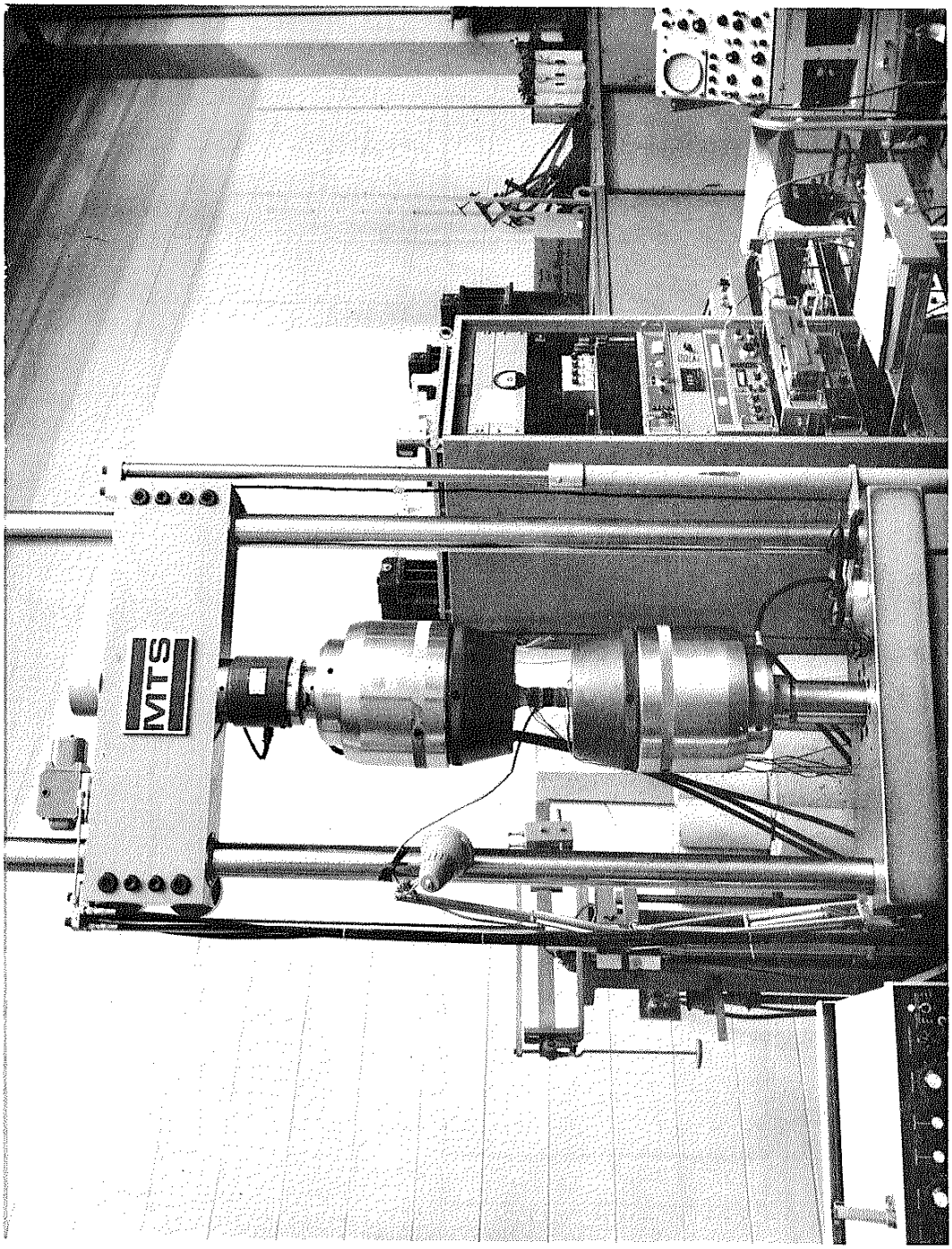

Fig. 31 Fatigue Test Set-up

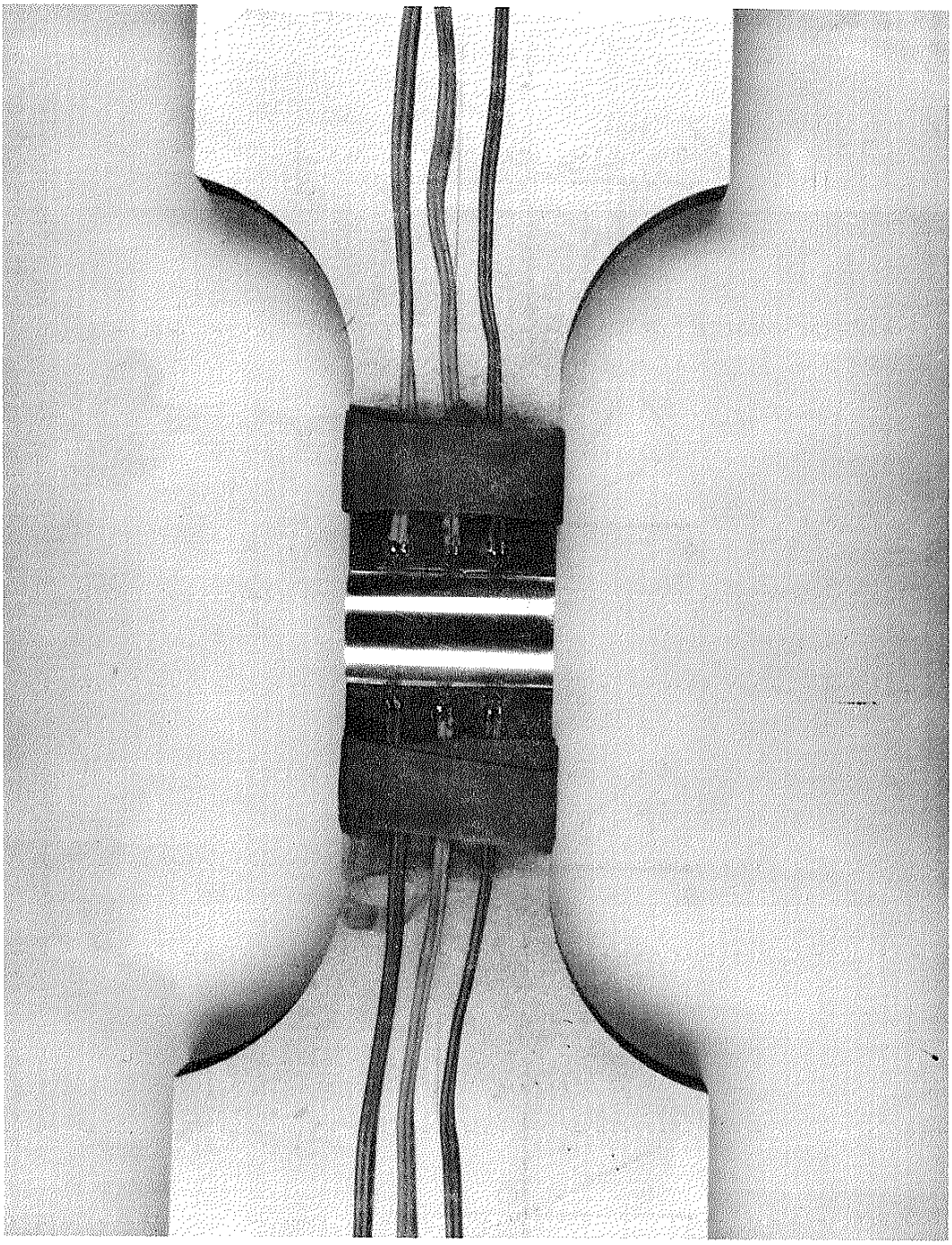

Fig. 32 Simulated Weld Specimen with Six Miniature Strain Gages

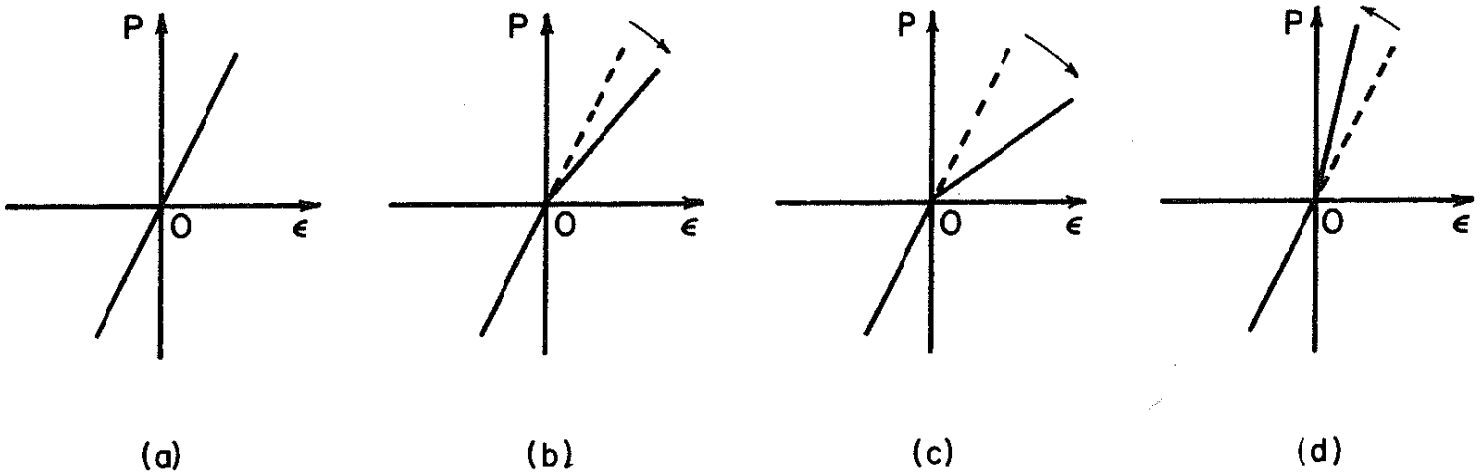

Fig. 33 Schematic Representation of the Changes in Strain Gage Readings as a Crack Develops and Grows: (a) No Crack, (b) Crack Formed, (c) Further Crack Growth, and (d) Crack Extended Beneath Strain Gage

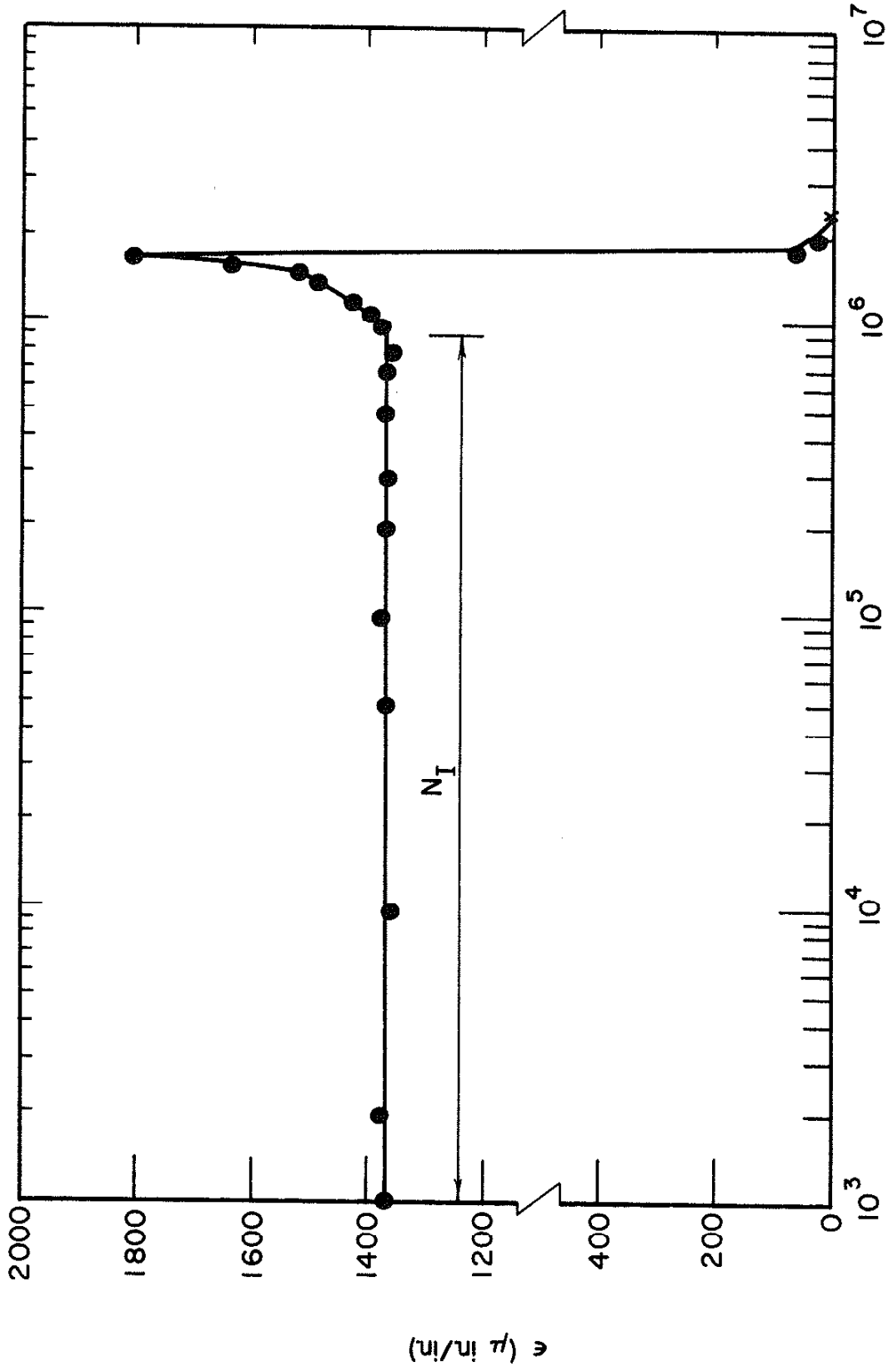

Fig. 34 Actual Record of Changes in Strain Gage Readings as a Crack Initiates and Grows

Fig. 35 Macrophotograph Showing the Crack Size Sensed by the Strain Gage. Arrow Indicates Depth of Crack Indicated by Heat Tinting

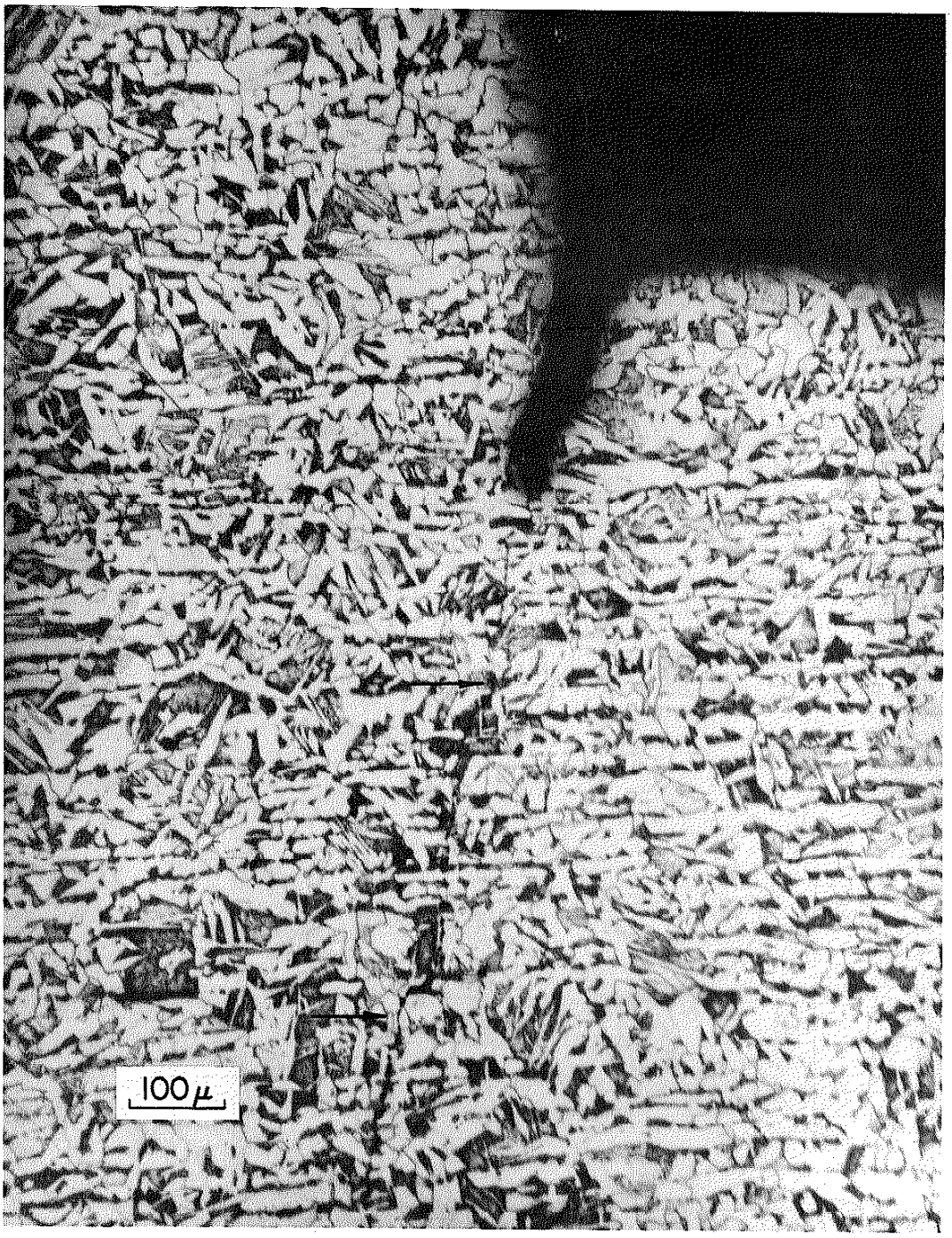

Fig. 36 Microphotograph Showing the Crack Sensed by the Strain Gage. Further Extension of the Crack Due to Higher Tensile Fatigue Load Indicated by Arrows

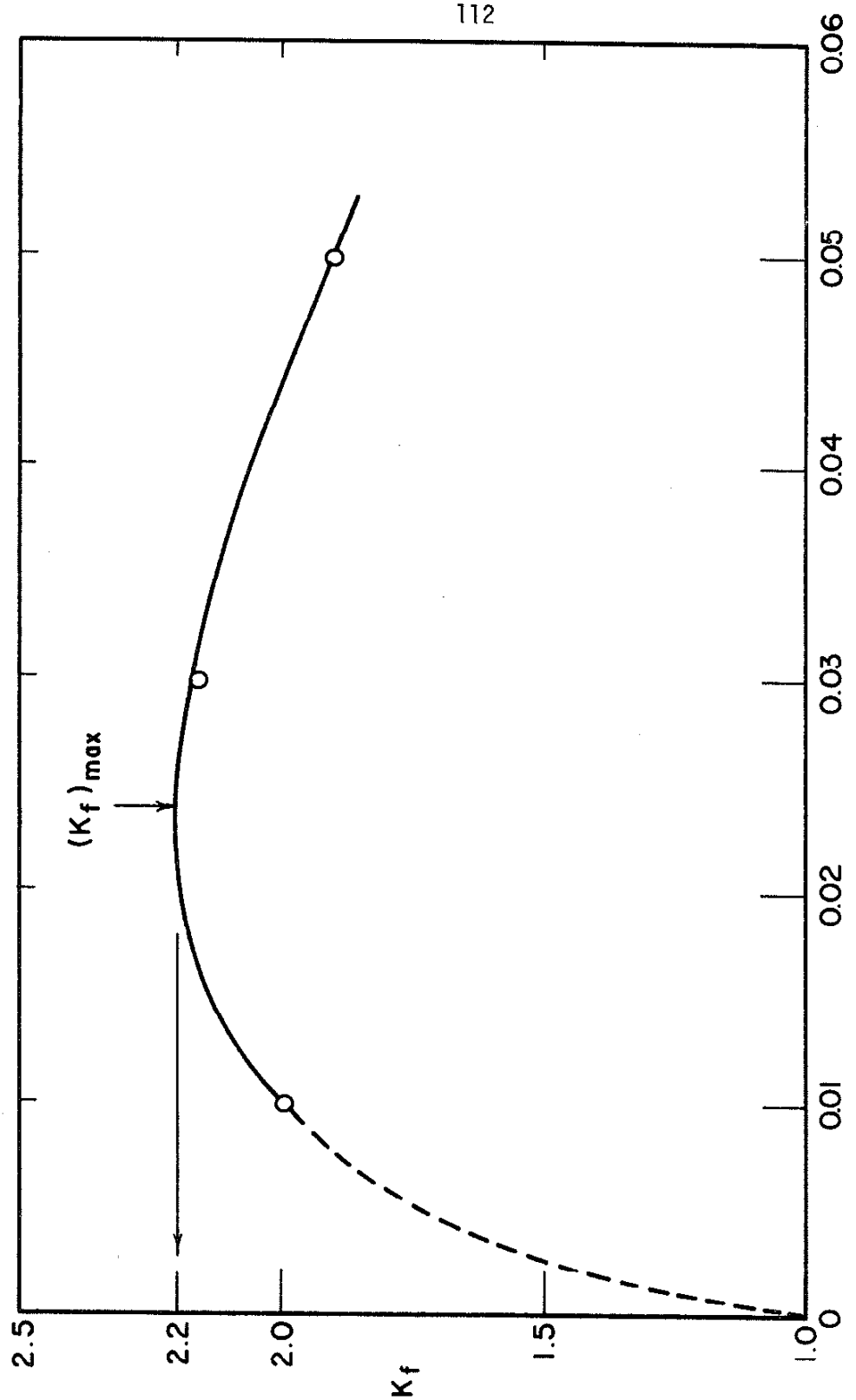

Fig. 37 Fatigue Notch Factor, K_f, as a Function of the Radius at the "Toe of the Weld" for Simulated Butt Weld Specimens

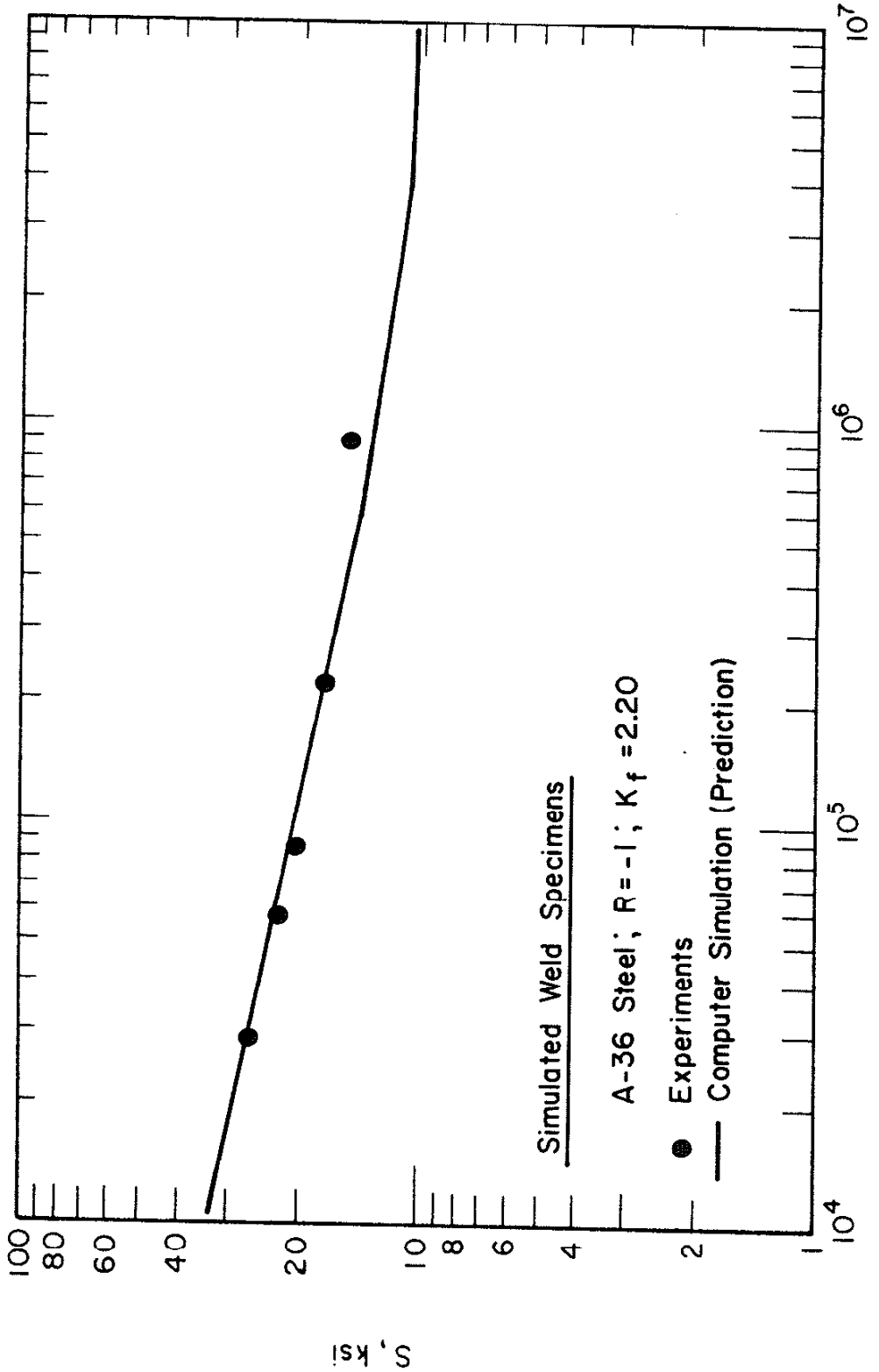

Fig. 38 Predicted and Actual Fatigue Crack Initiation Life for Simulated Butt Welds (R=-1)

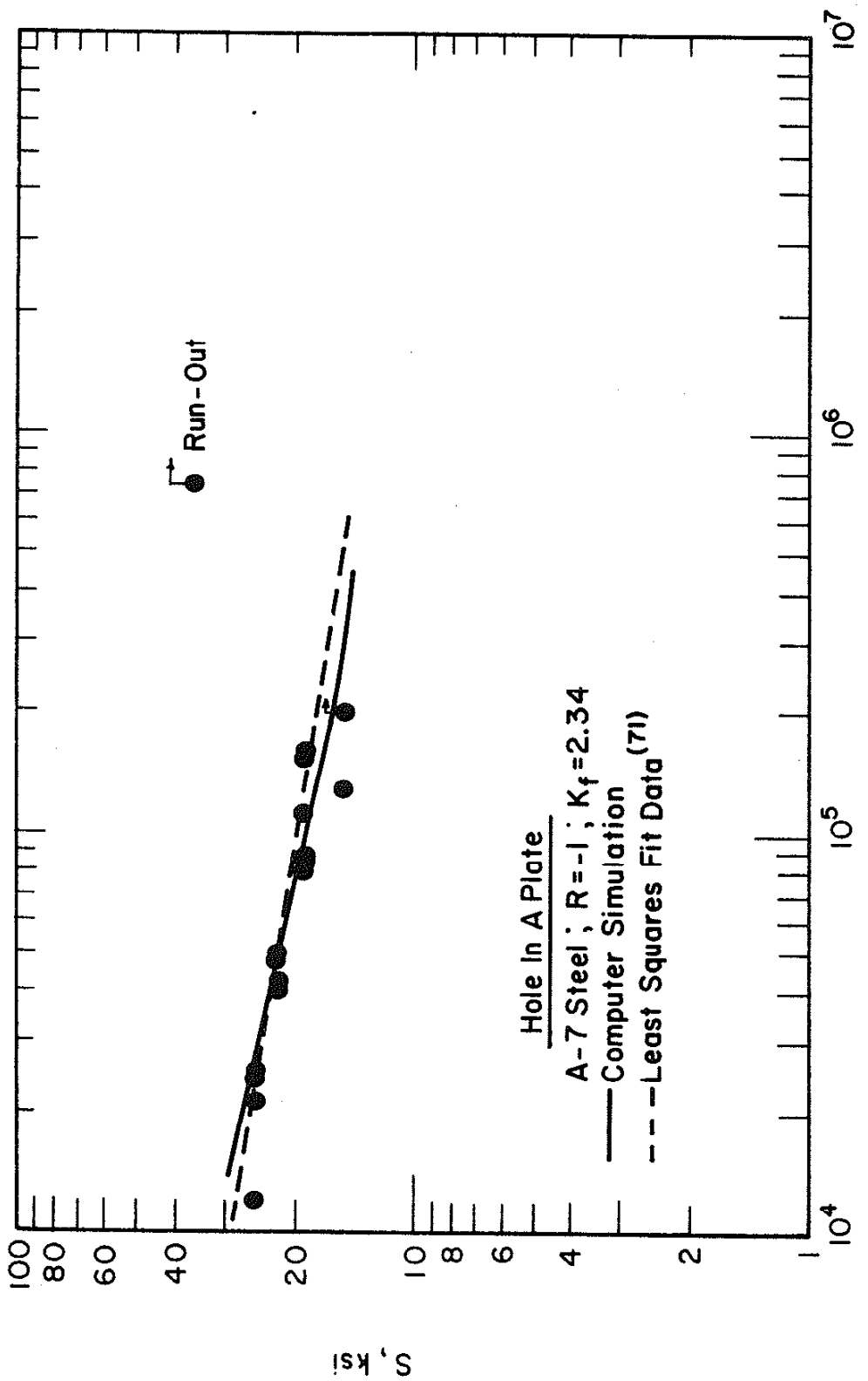

Fig. 39 Predicted and Actual Fatigue Crack Initiation Life for a Circular Hole in an A-7 Steel Plate (R=-1)

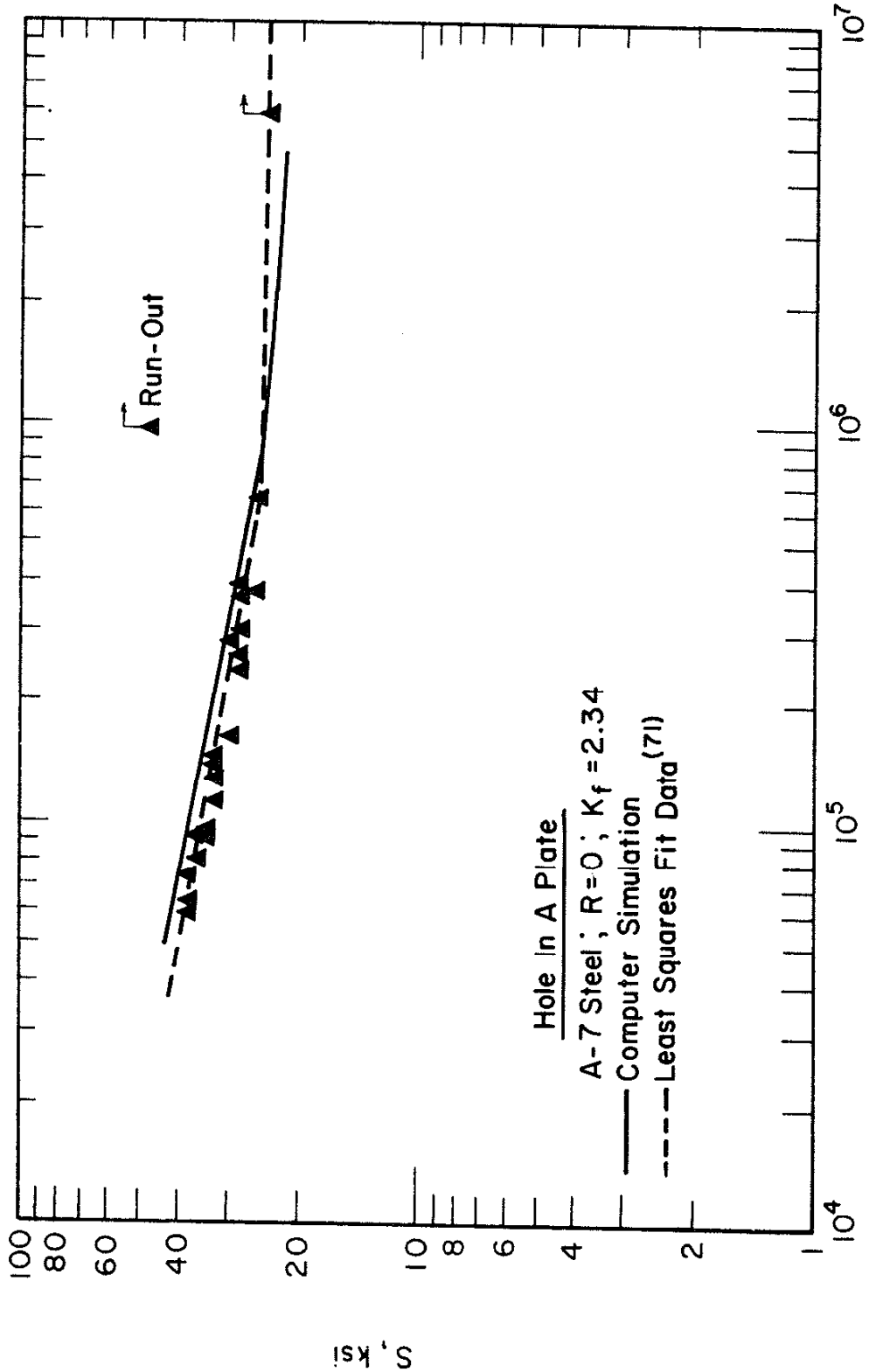

Fig. 40 Predicted and Actual Fatigue Crack Initiation Life for a Circular Hole in an A-7 Steel Plate (R=0)

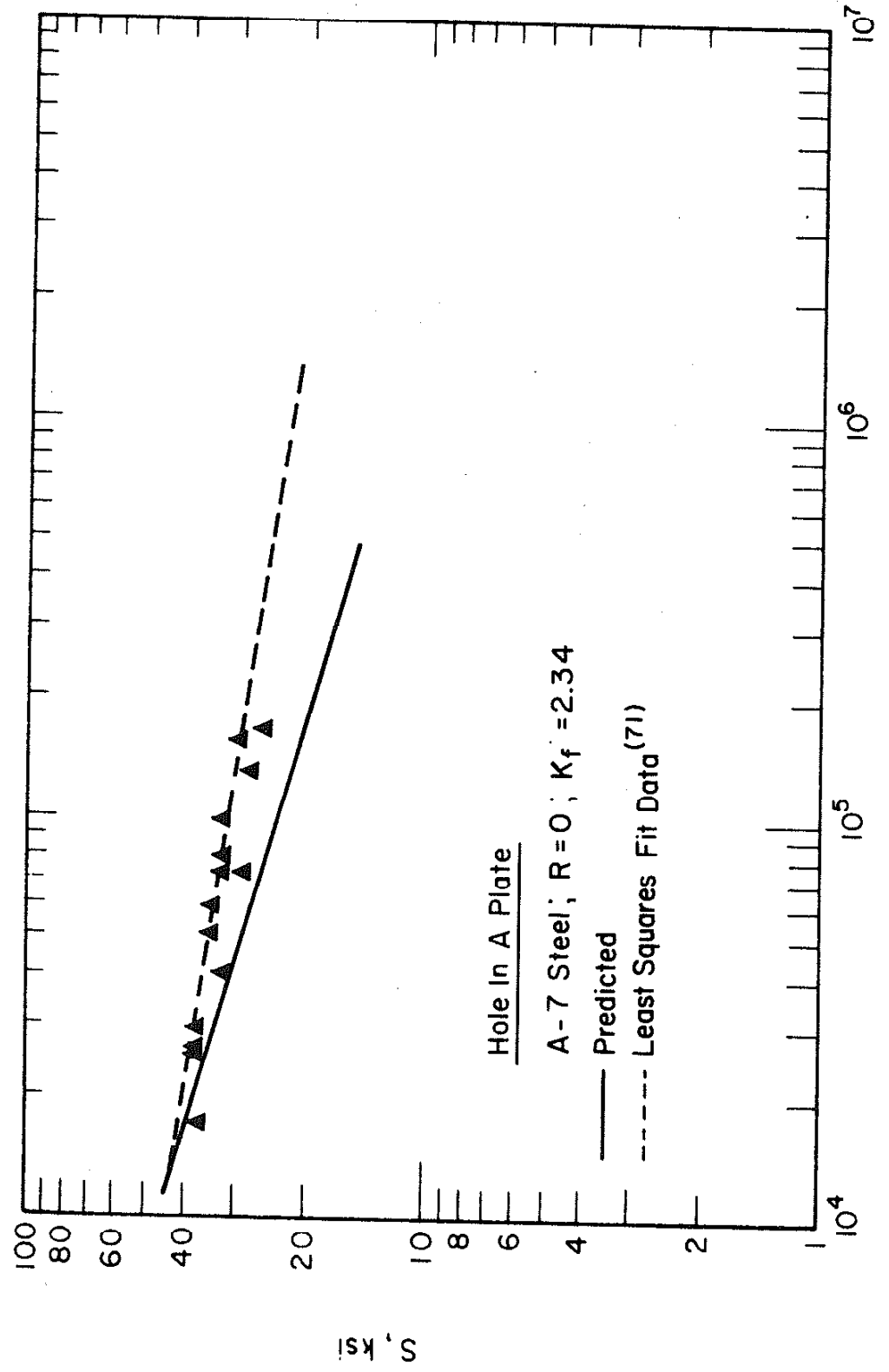

Fig. 41 Predicted and Actual Fatigue Crack Propagation Life for a Circular Hole in an A-7 Steel Plate (R=0)

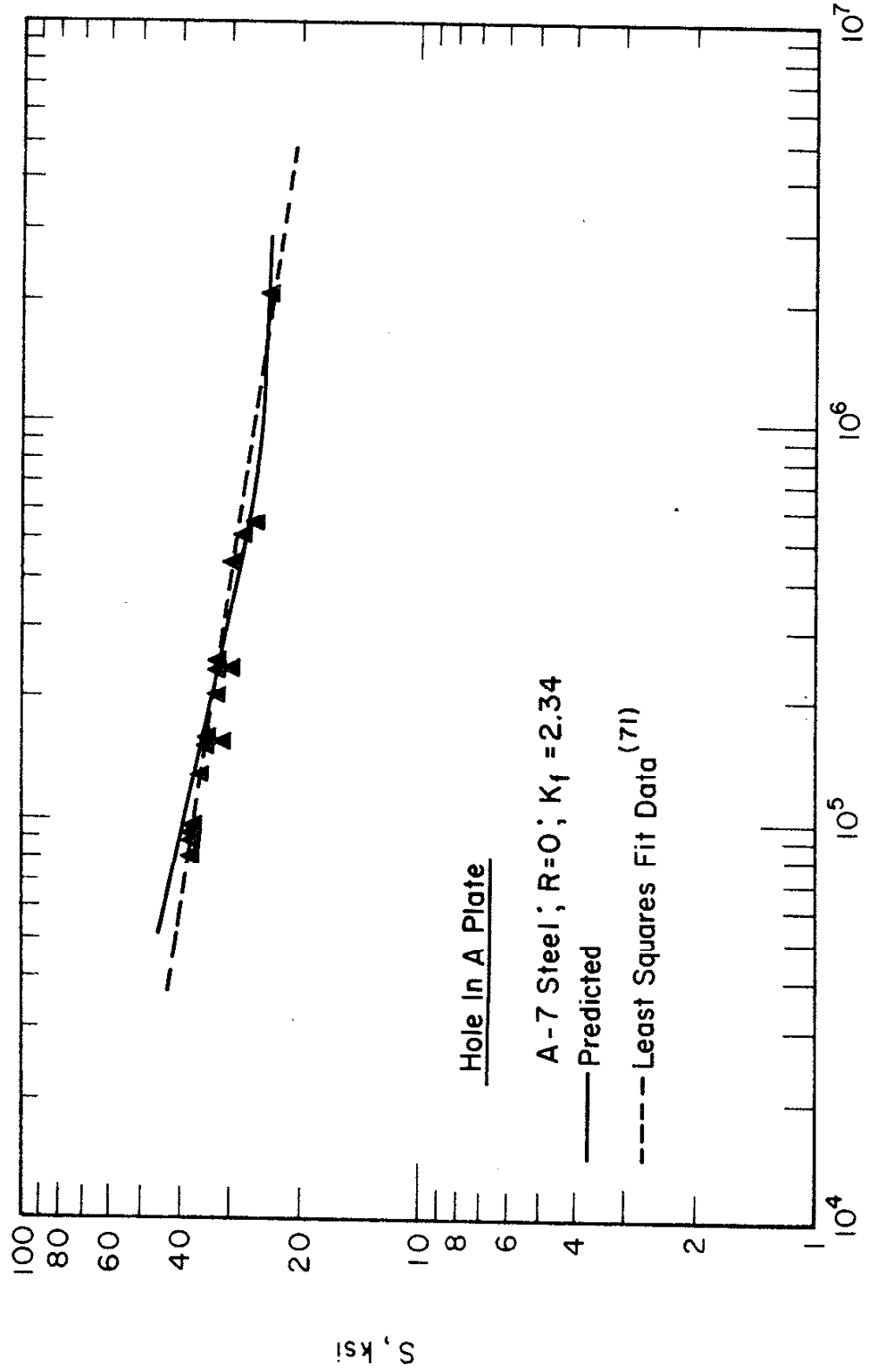

Fig. 42 Predicted and Actual Total Fatigue Life for a Circular Hole in an A-7 Steel Plate (R=0)

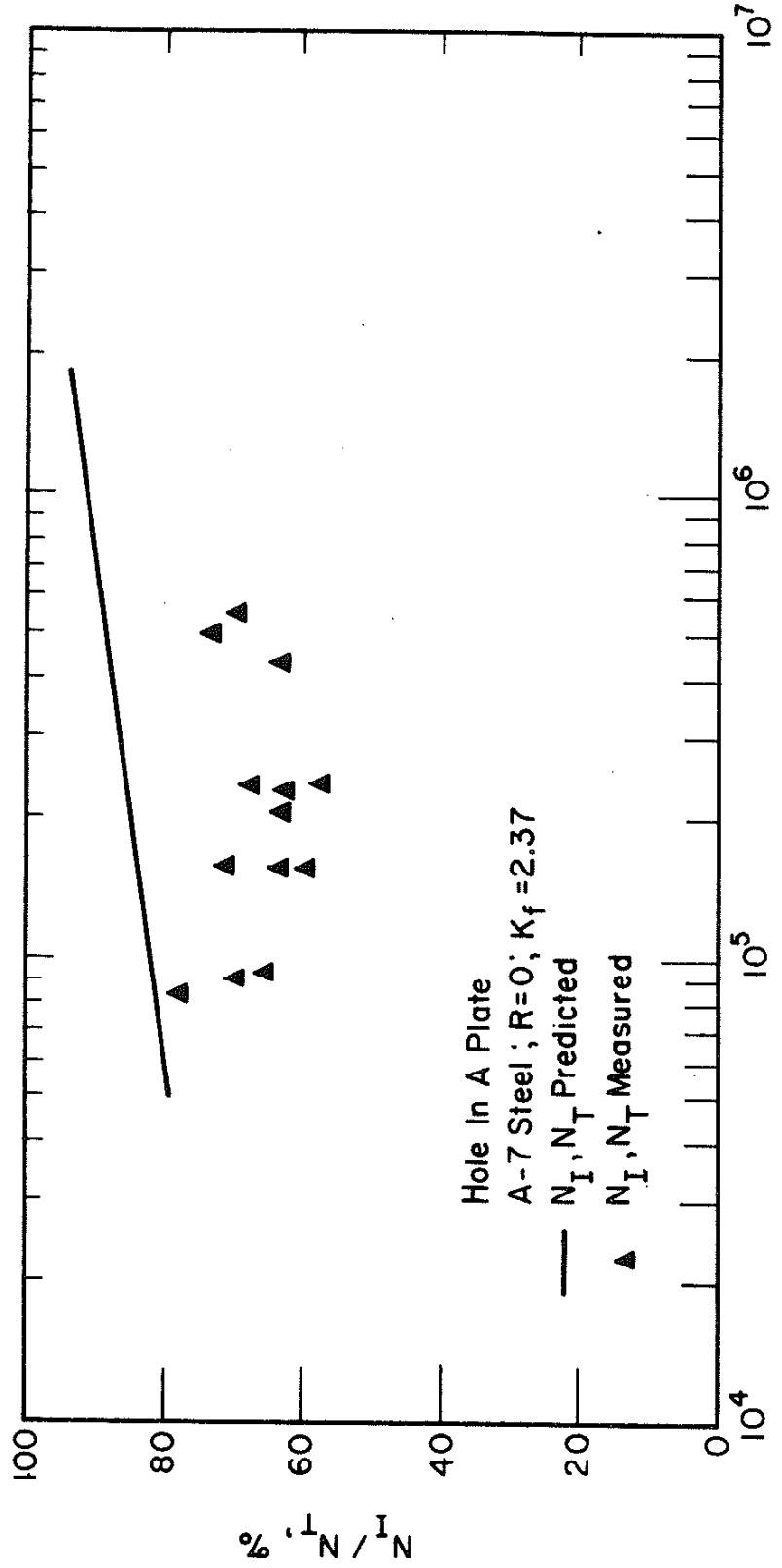

Fig. 43 Partitioning of the Crack Initiation Life as a Function of the Total Fatigue Life for a Circular Hole in an A-7 Steel Plate (R=0)

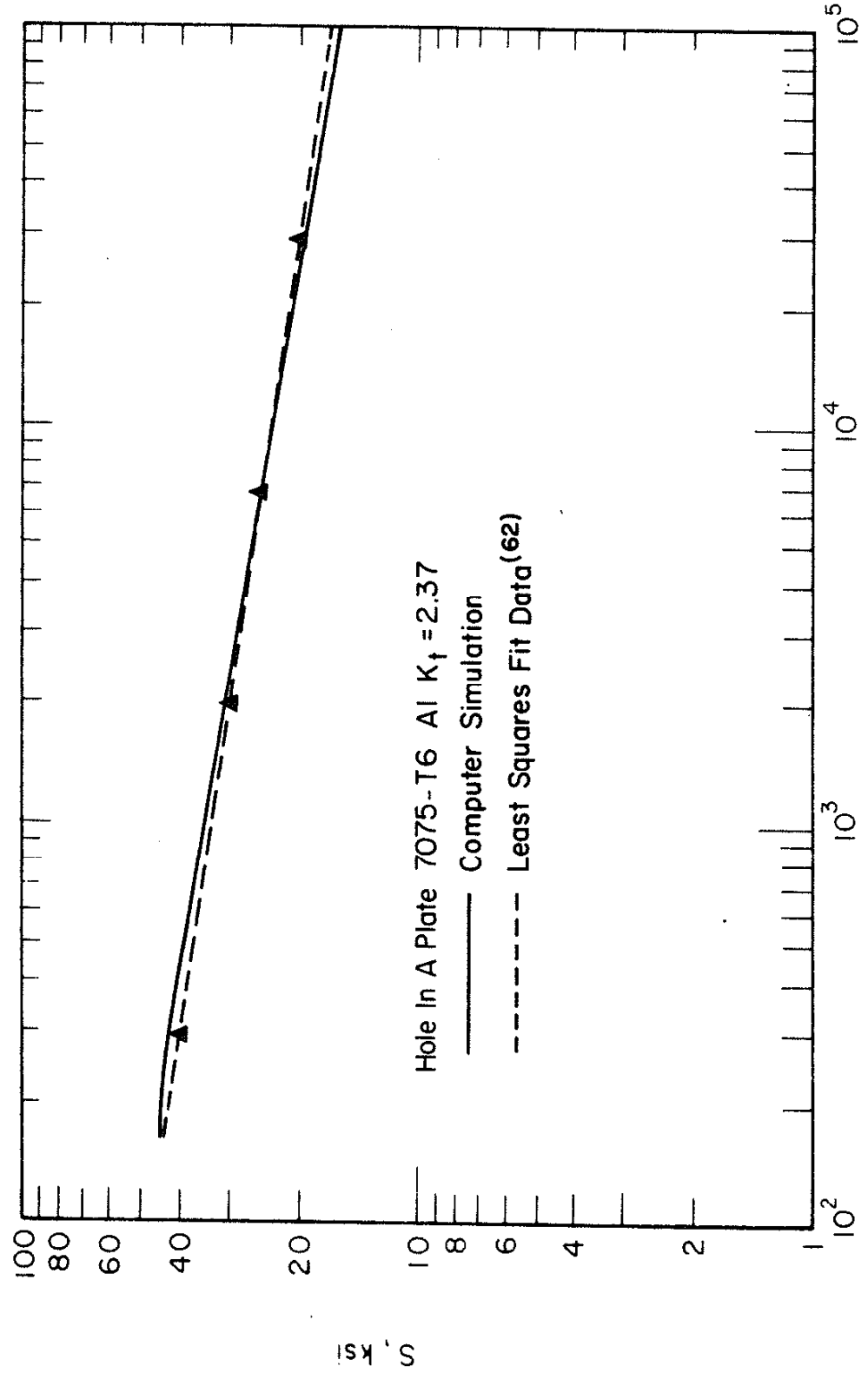

Fig. 44 Predicted and Actual Fatigue Crack Initiation Life for a Circular Hole in a 7075-T6 Al Plate (R=-1)

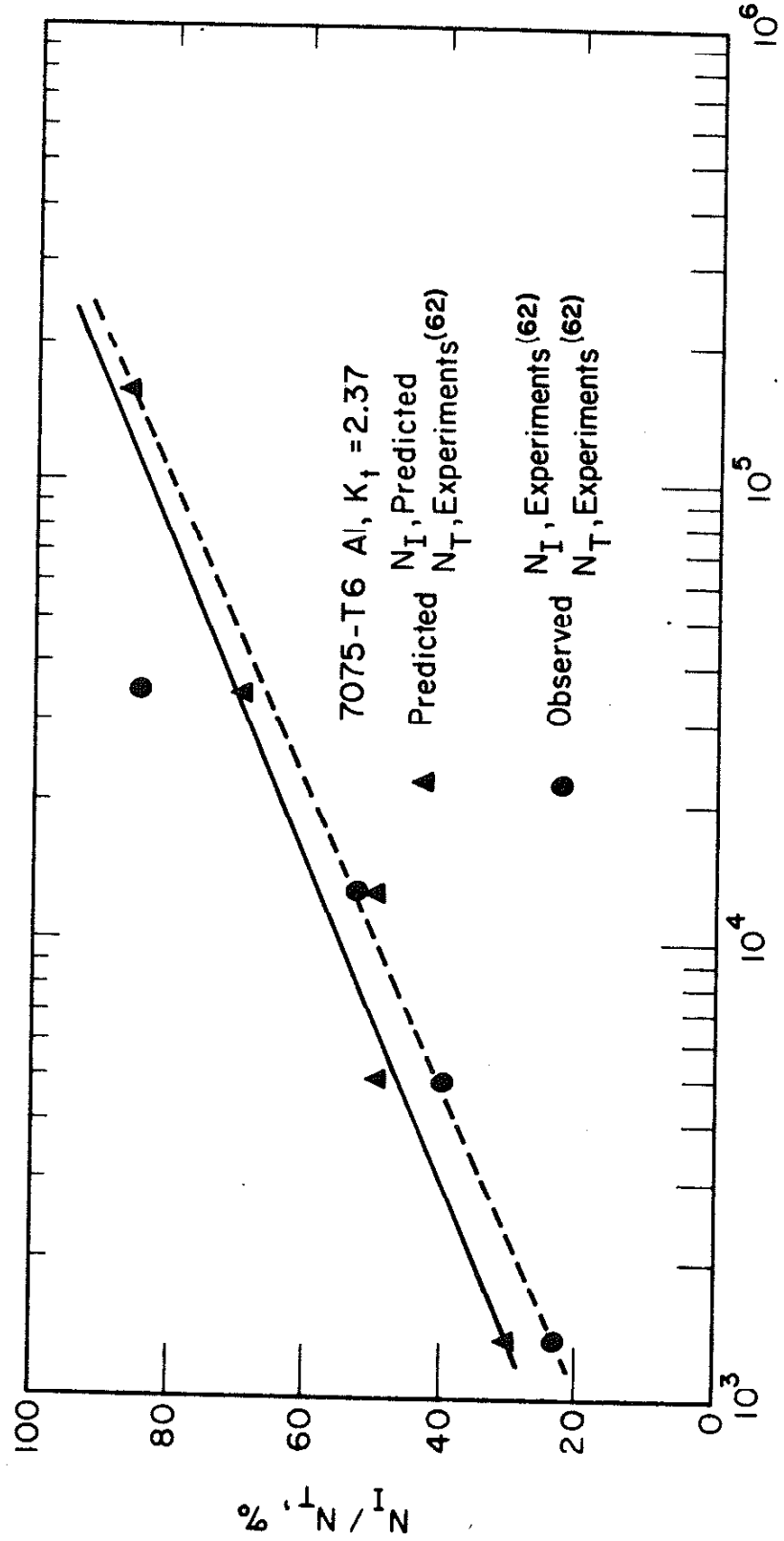

Fig. 45 Partitioning of the Crack Initiation Life as a Function of the Total Fatigue Life for a Circular Hole in a 7075-T6 Al Plate. The Solid Line Represents the Predicted Partitioning and the Dashed Line Represents the Actual Partitioning

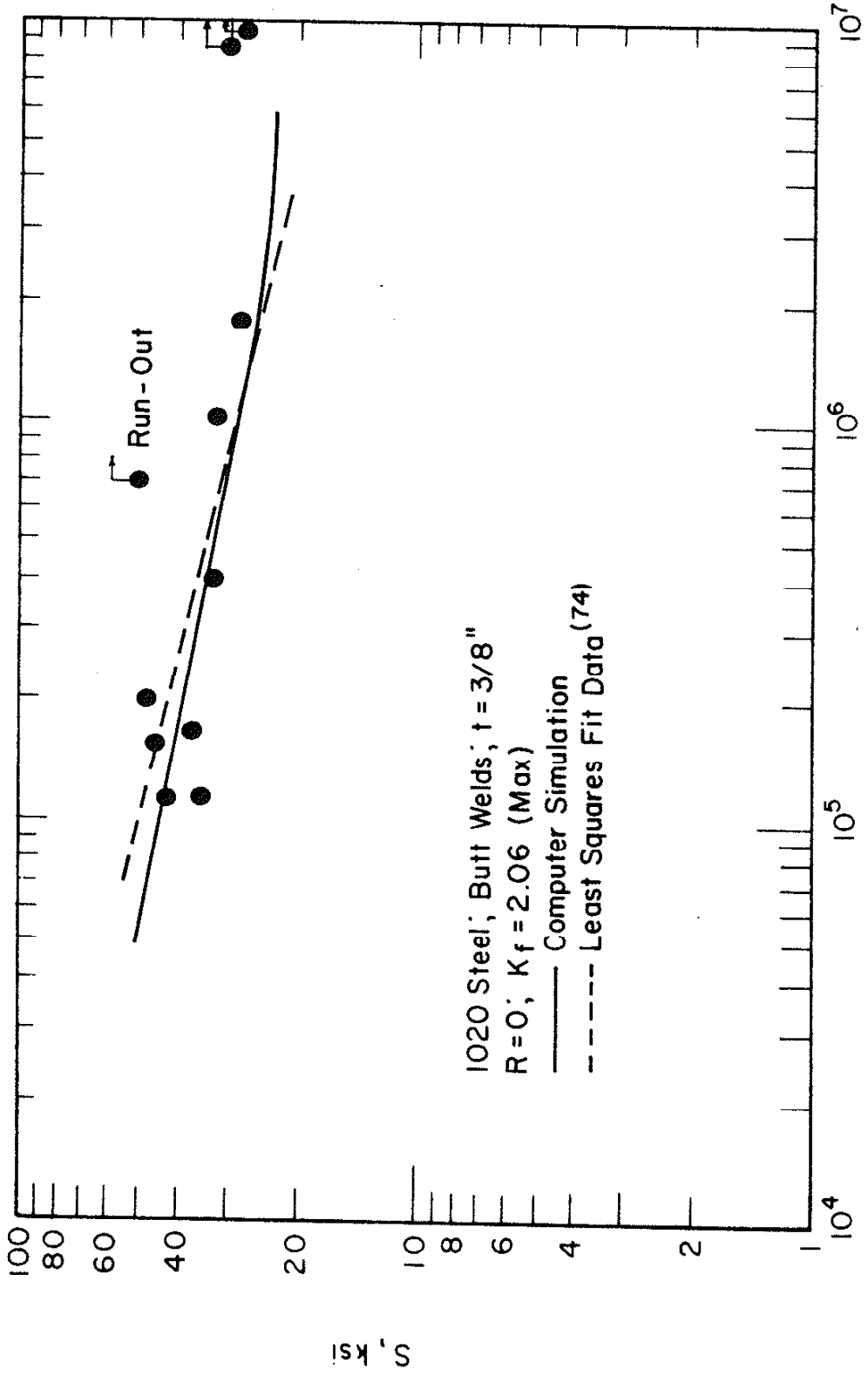

Fig. 46 Predicted and Actual Fatigue Crack Initiation Life for Butt Welds in 102C Steel Plate (t=3/8 in., R=0)

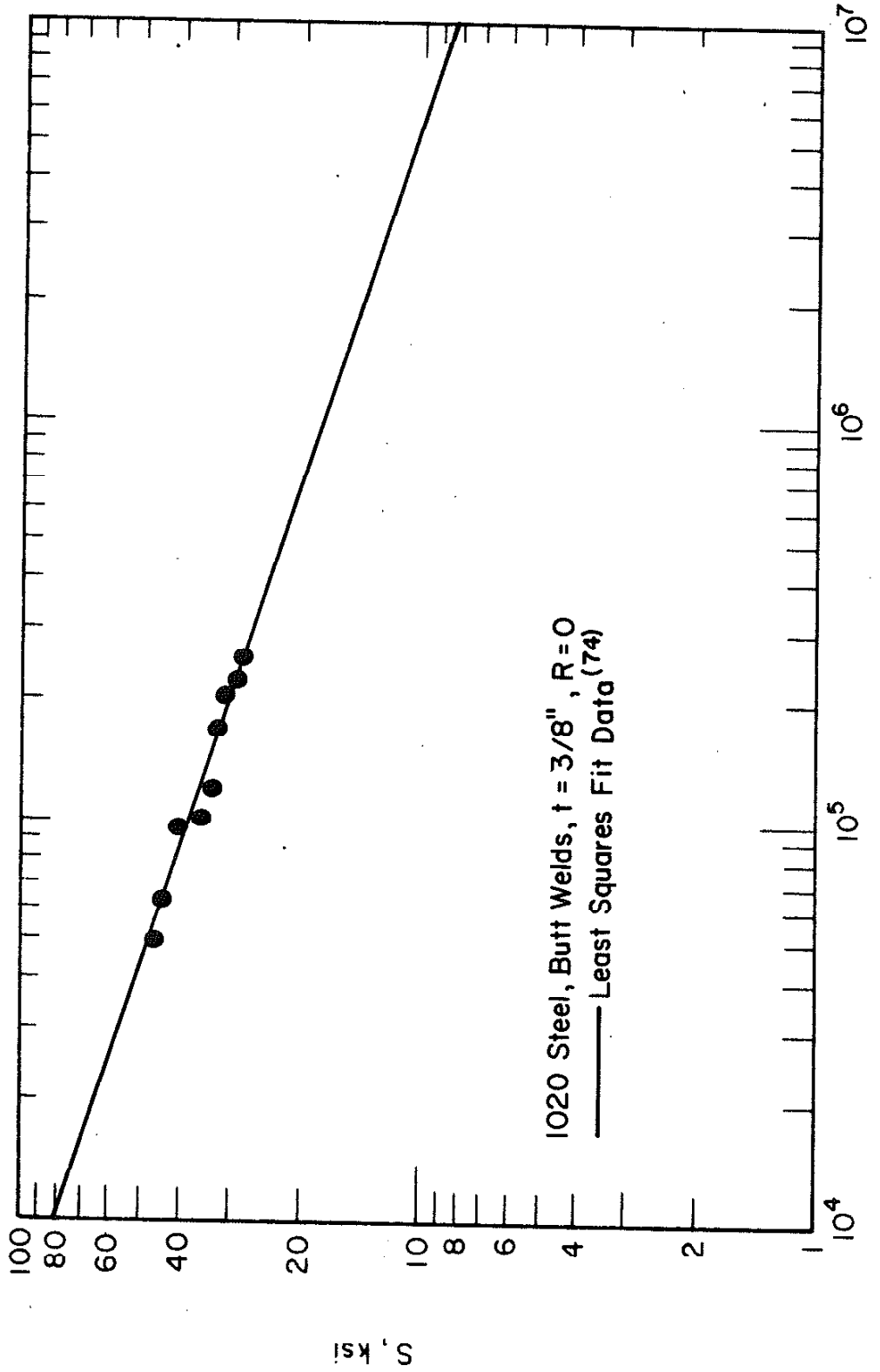

Fig. 47 Predicted and Actual Fatigue Crack Propagation Life for Butt Welds in 1020 Steel Plate (74) (t=3/8 in., R=0)

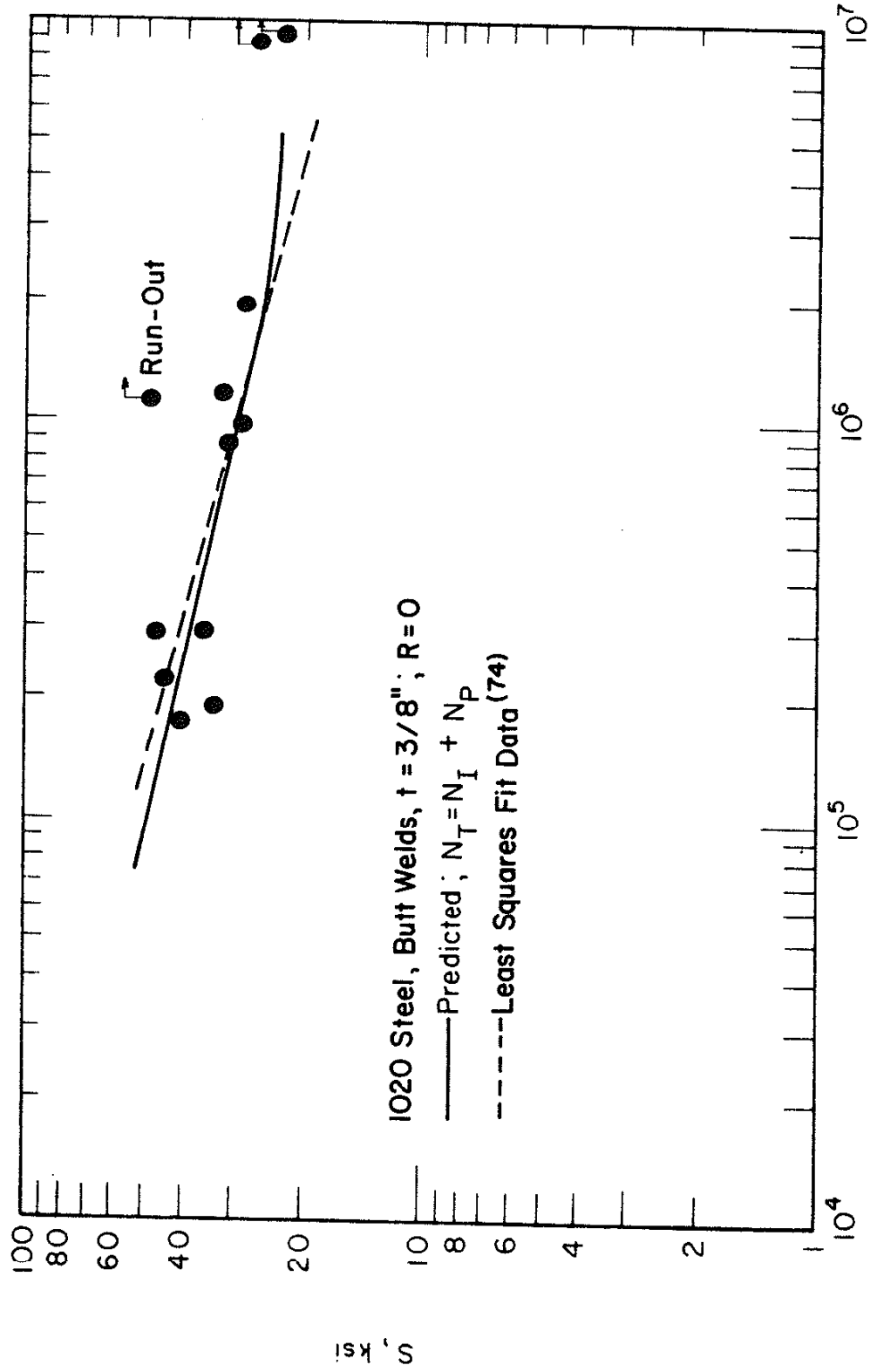

Fig. 48 Predicted and Actual Total Fatigue Life for Butt Welds in 1020 Steel Plate (t=3/8 in., R=0)

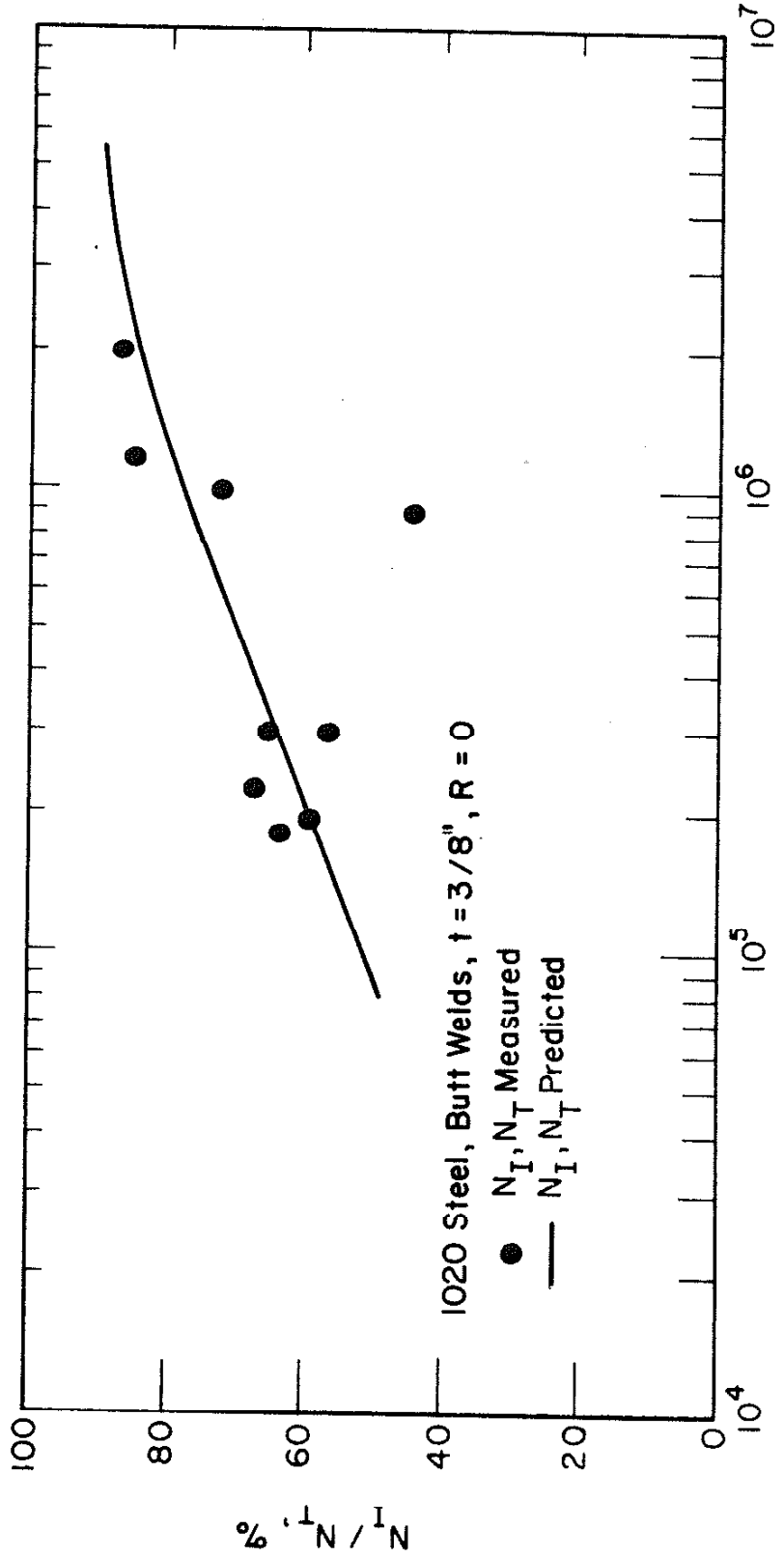

Fig. 49 Partitioning of the Fatigue Crack Initiation Life as a Function of the Total Fatigue Life for Butt Welds in 1020 Steel Plate (t=3/8 in., R=0)

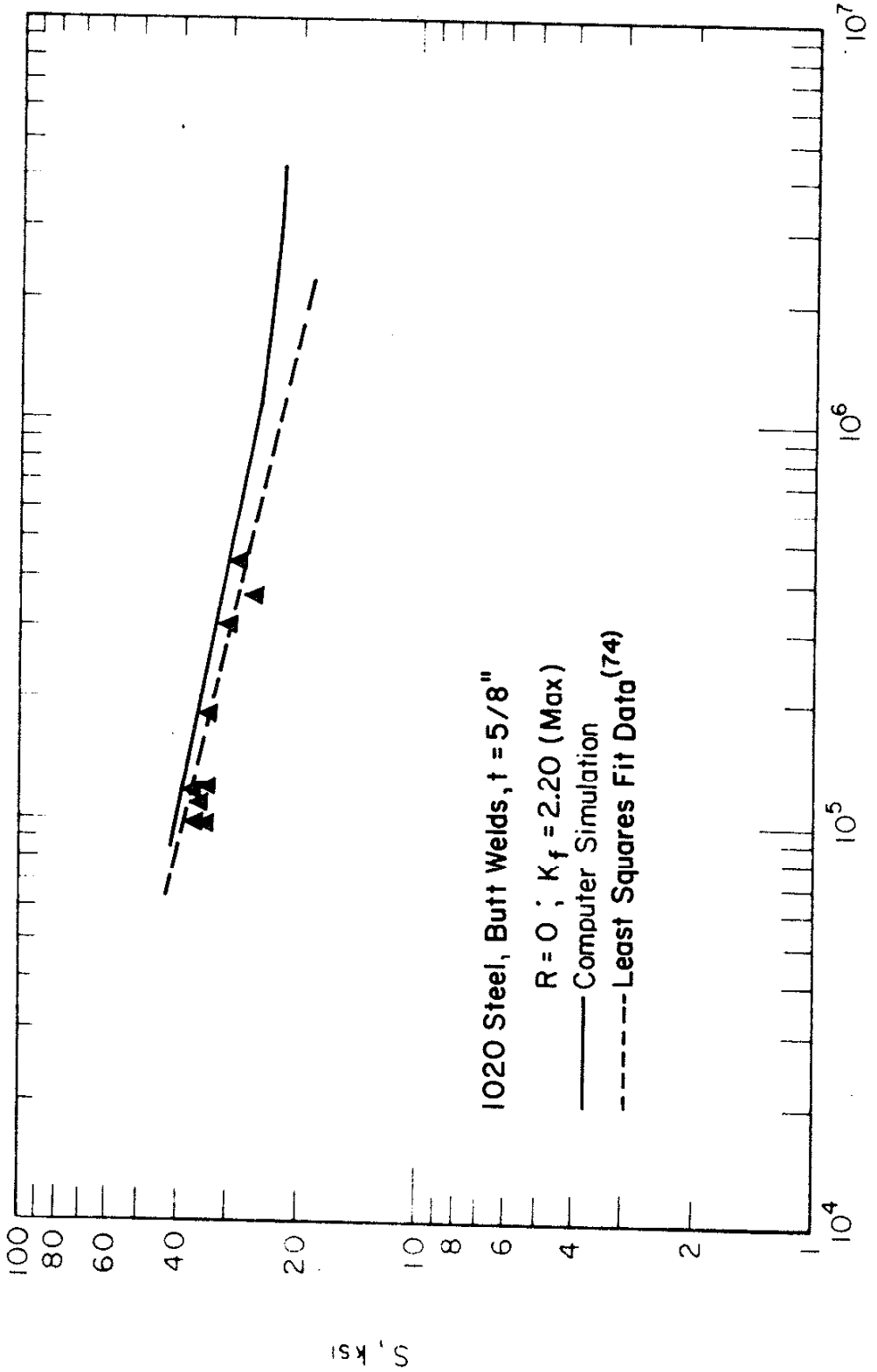

Fig. 50 Predicted and Actual Fatigue Crack Initiation Life for Butt Welds in 1020 Steel Plate (t=5/8 in., R=0)

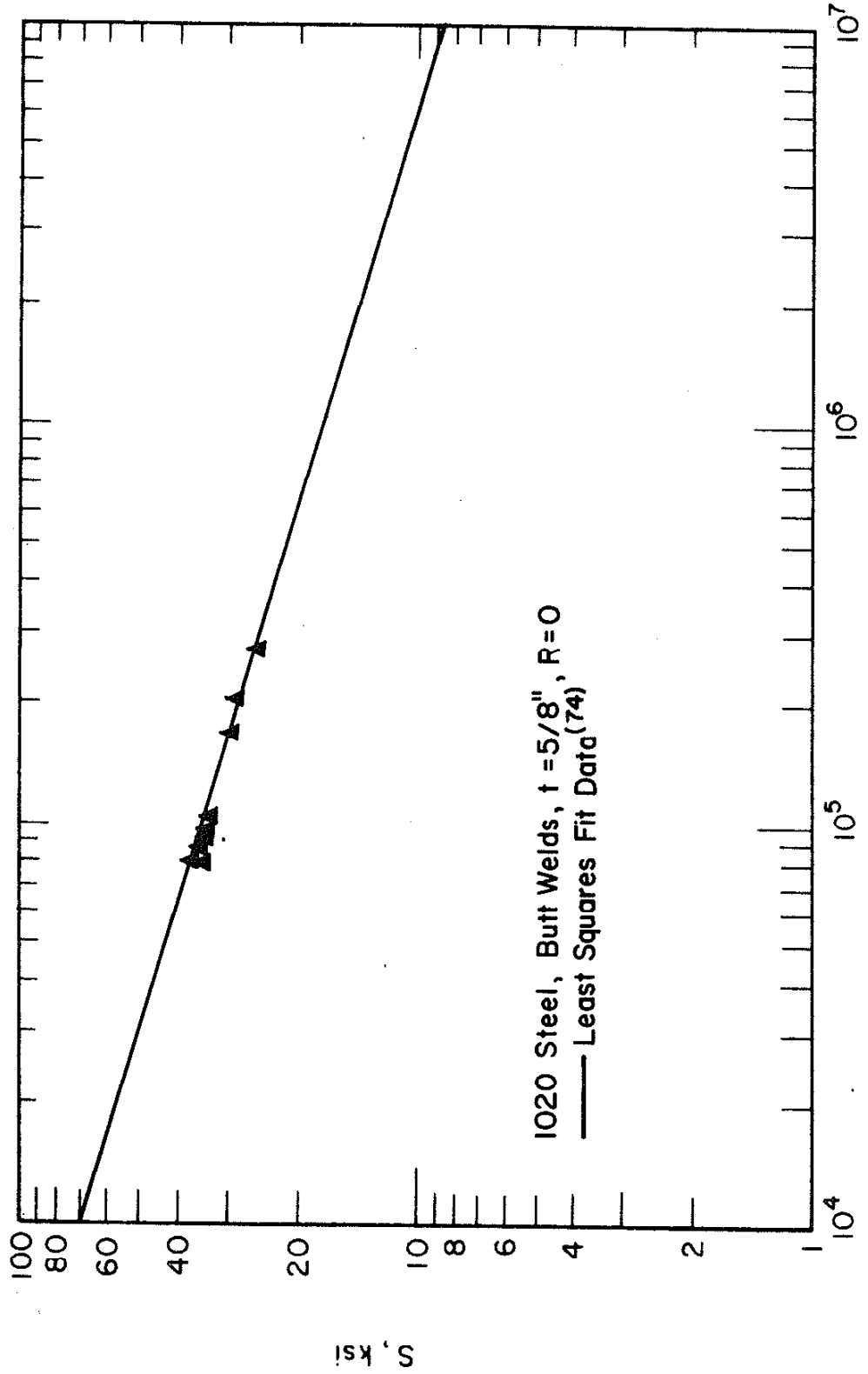

Fig. 51 Predicted and Actual Fatigue Crack Propagation Life for Butt Welds in 1020 Steel Plate (74) (t=5/8 in., R=0)

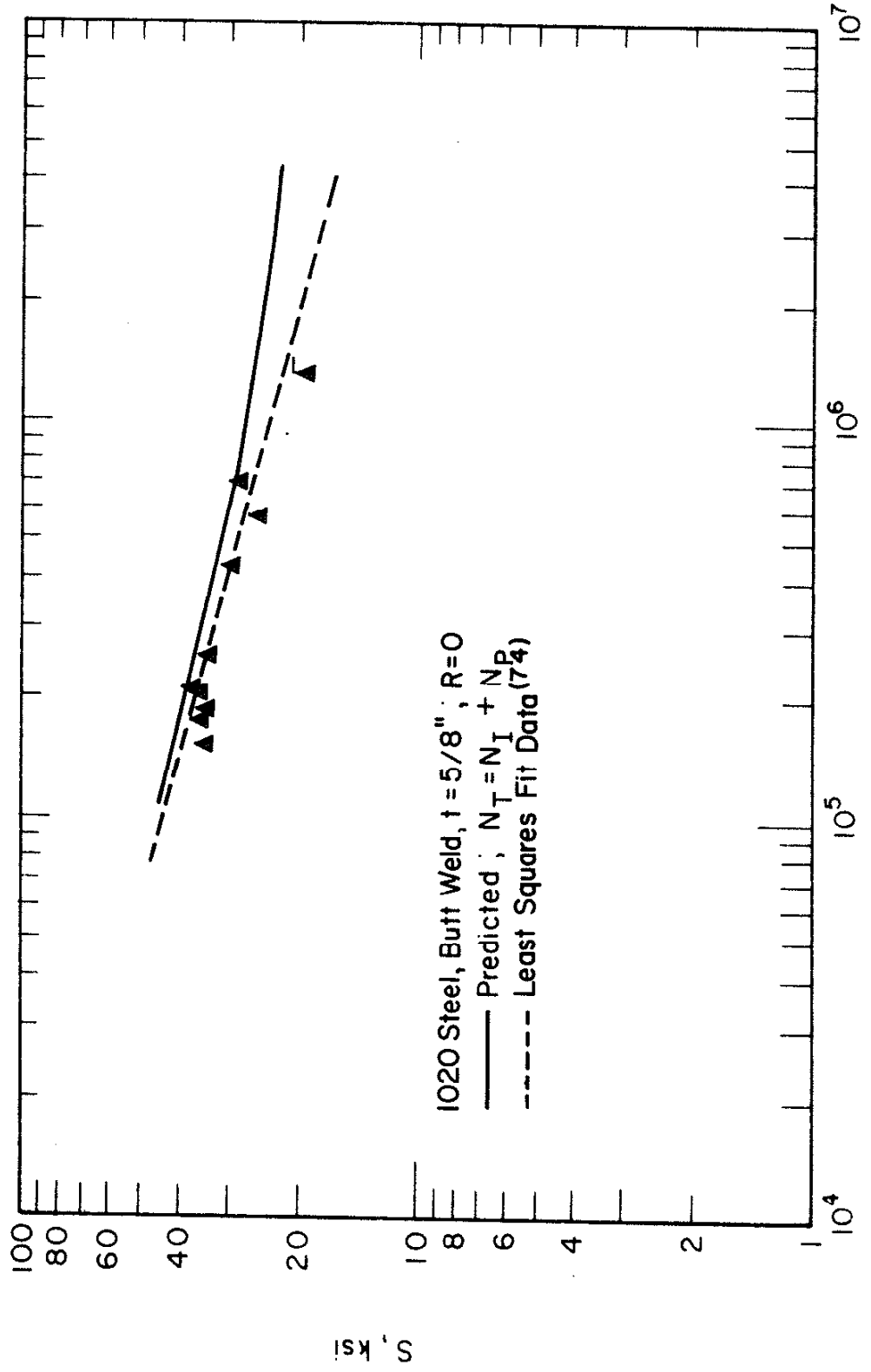

Fig. 52 Predicted ard Actual Total Fatigue Life for Butt Welds in 1020 Steel Plate (t=5/8 in., R=0)

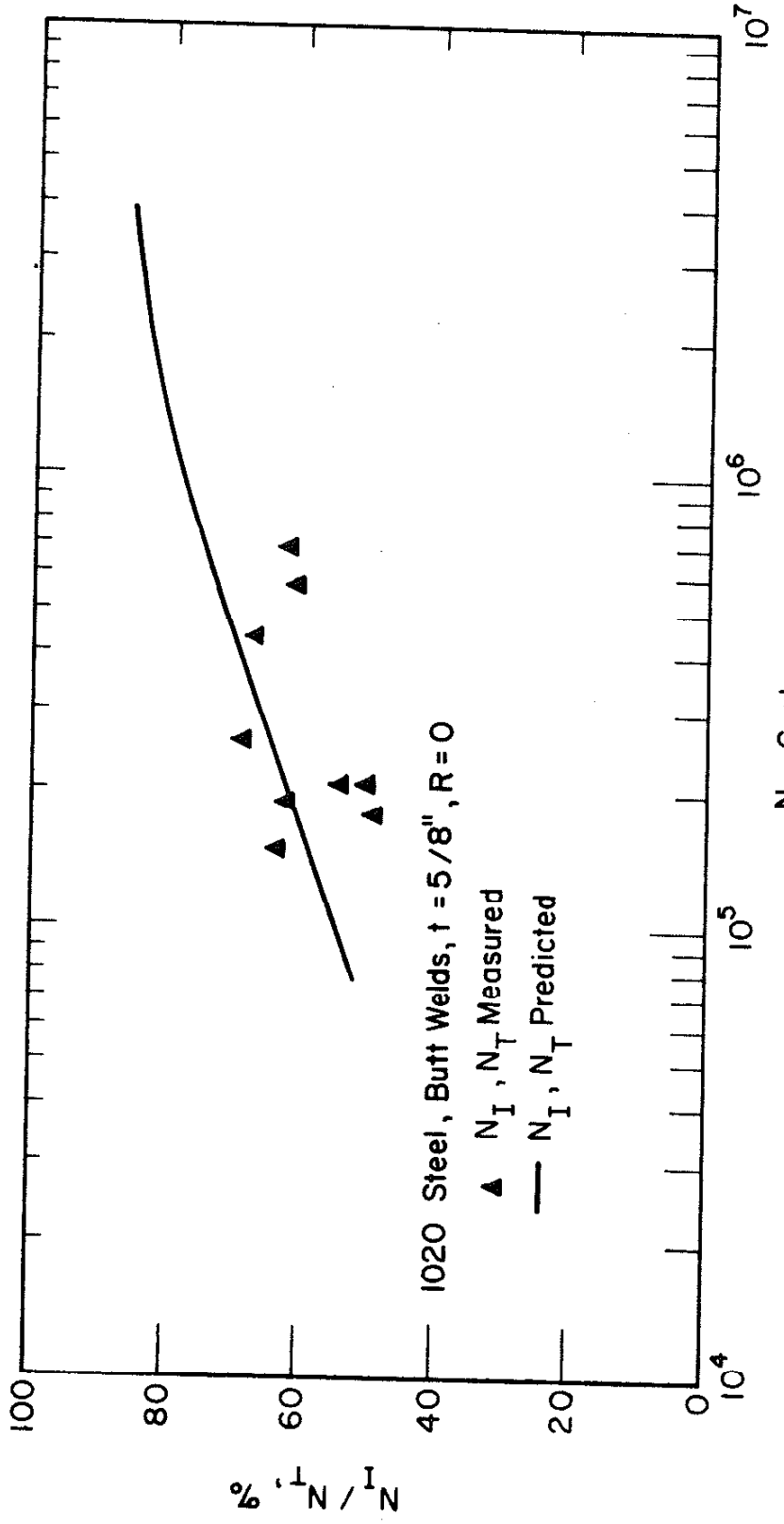

Fig. 53 Partitioning of the Fatigue Crack Initiation Life as a Function of the Total Fatigue Life for Butt Welds in 1020 Steel Plate (t=5/8 in., R=0)

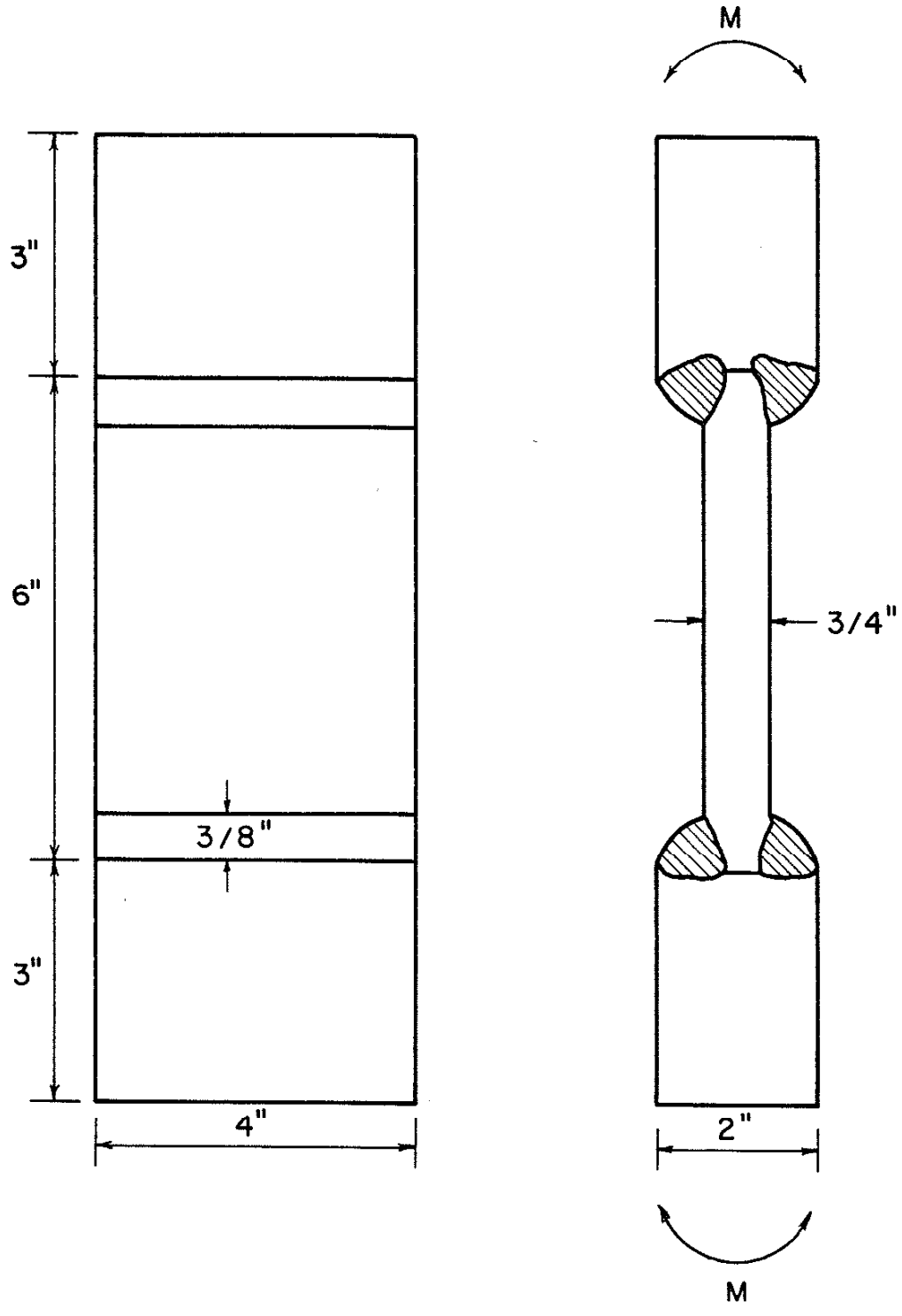

Fig. 54 Specimen Geometry of Fillet Welds. Specimen Was Loaded in Reverse Pure Bending

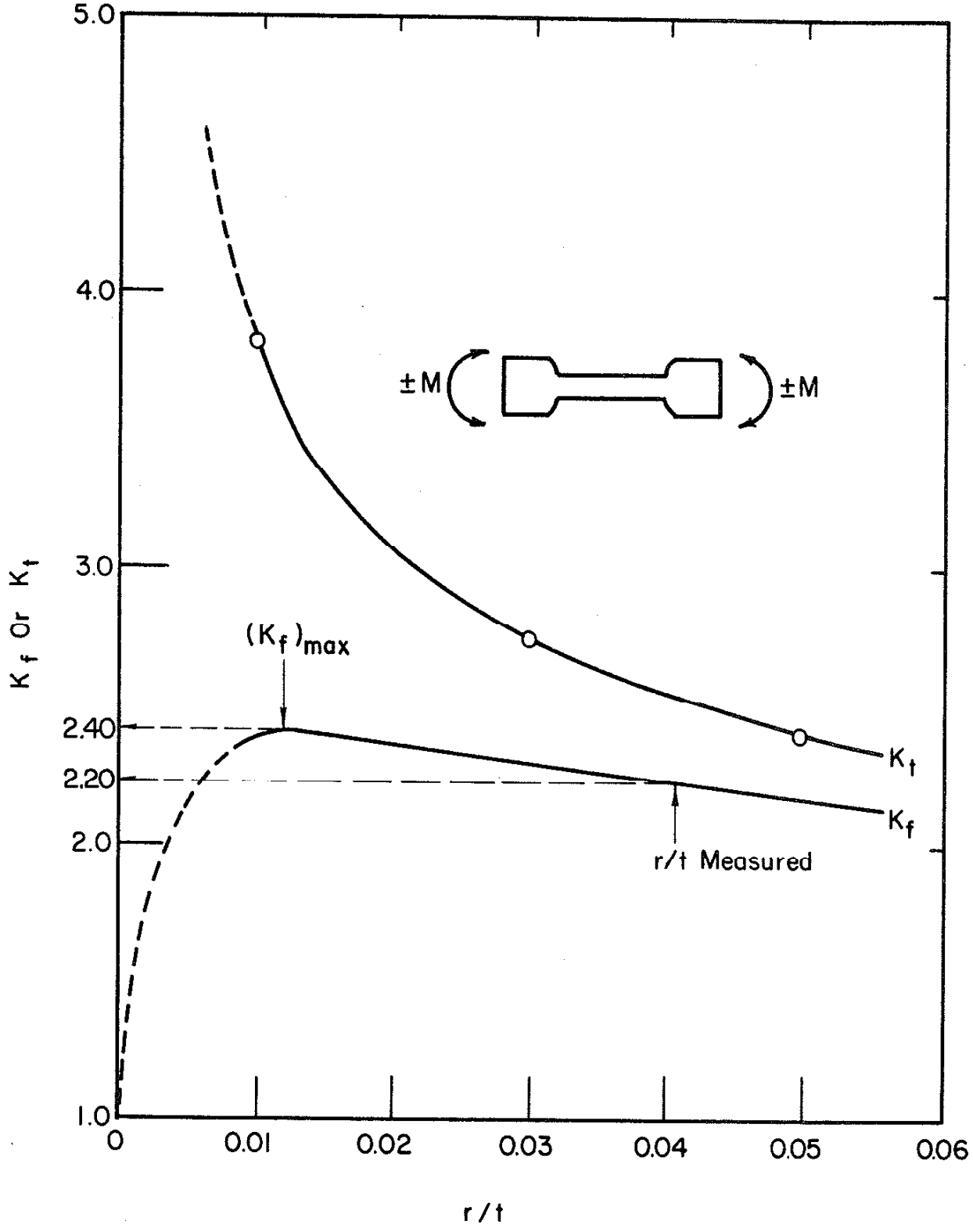

Fig. 55 Stress Concentration Factor, K_t, and Fatigue Notch Factor, K_f, as a Function of r/t for Fillet Weld Specimens. K_f Corresponding to r/t Measured Is 2.20 and $(K_f)_{max}$ Is 2.40

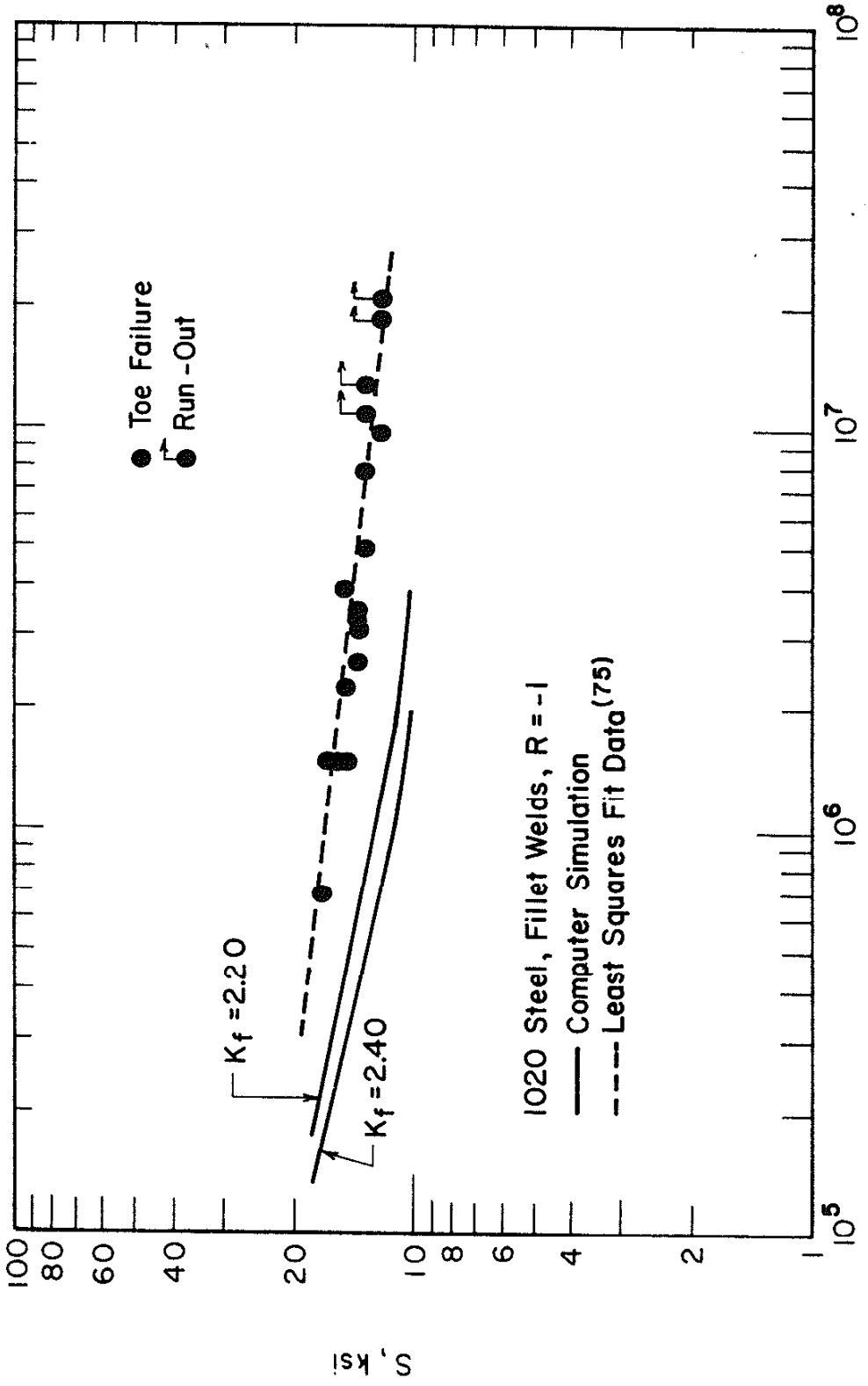

Fig. 56 Predicted and Actual Fatigue Crack Initiation Life for Fillet Welds in 1020 Steel Plate (R=-1)

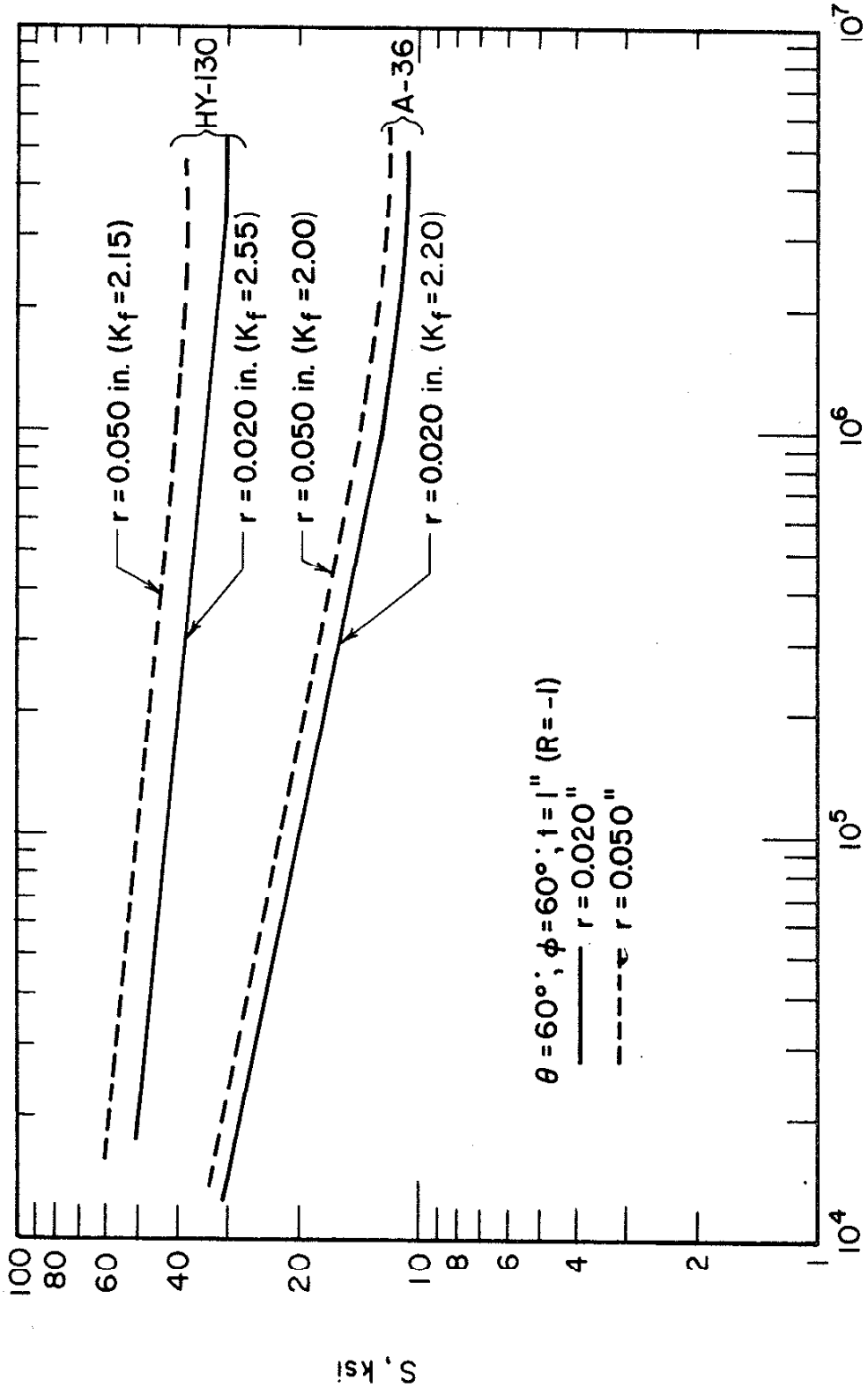

Fig. 57 Predicted Effect of the Radius of the Toe of the Weld, r, on the Fatigue Crack Initiation Life for A-36 and HY-130 Steel Butt Weldments of Identical Geometries

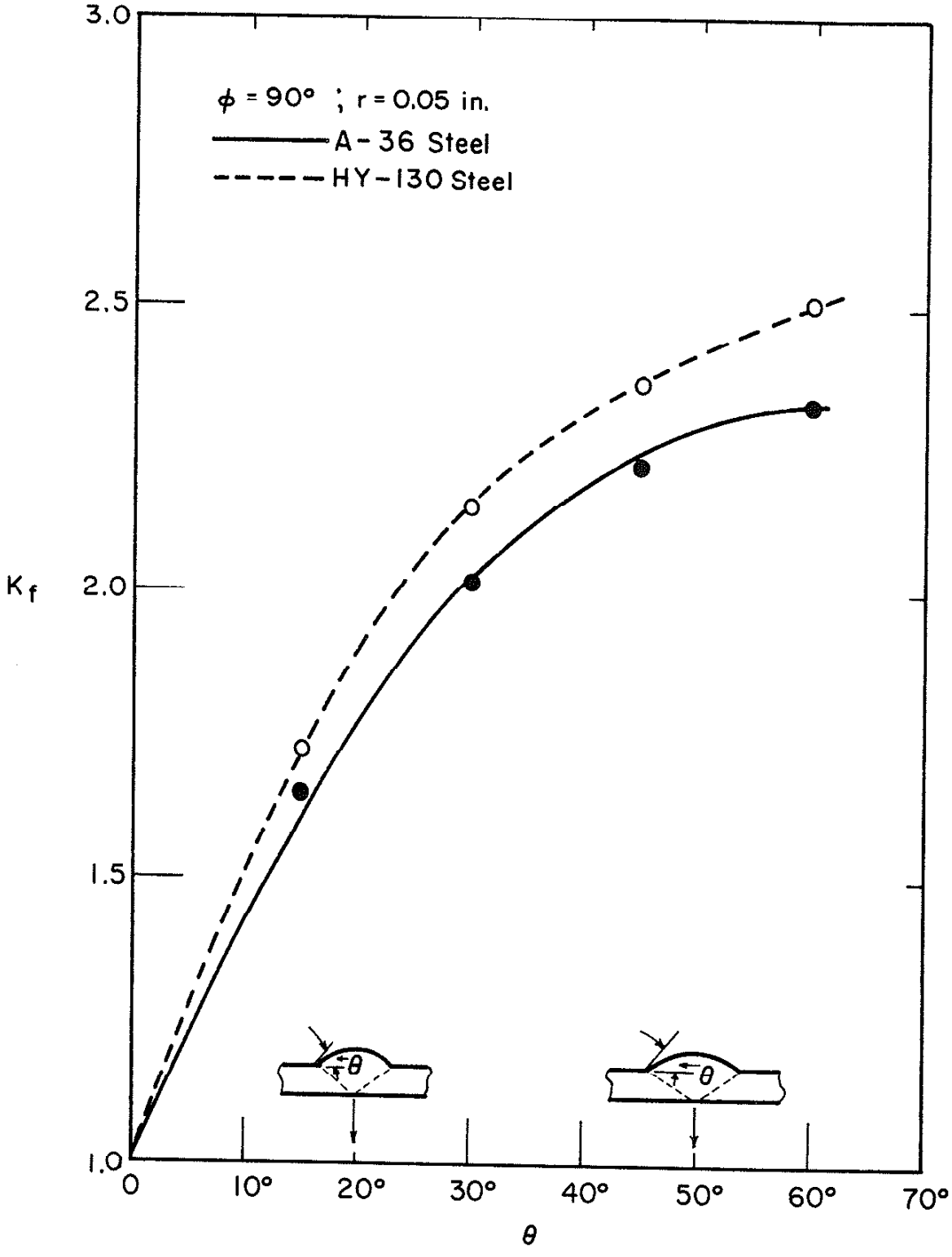

Fig. 58 Effect of Flank Angle, θ, on the Fatigue Notch Factor, K_f, for A-36 and HY-130 Steel Butt Weldments (Differences in K_f Are Due to Different "a" Values)

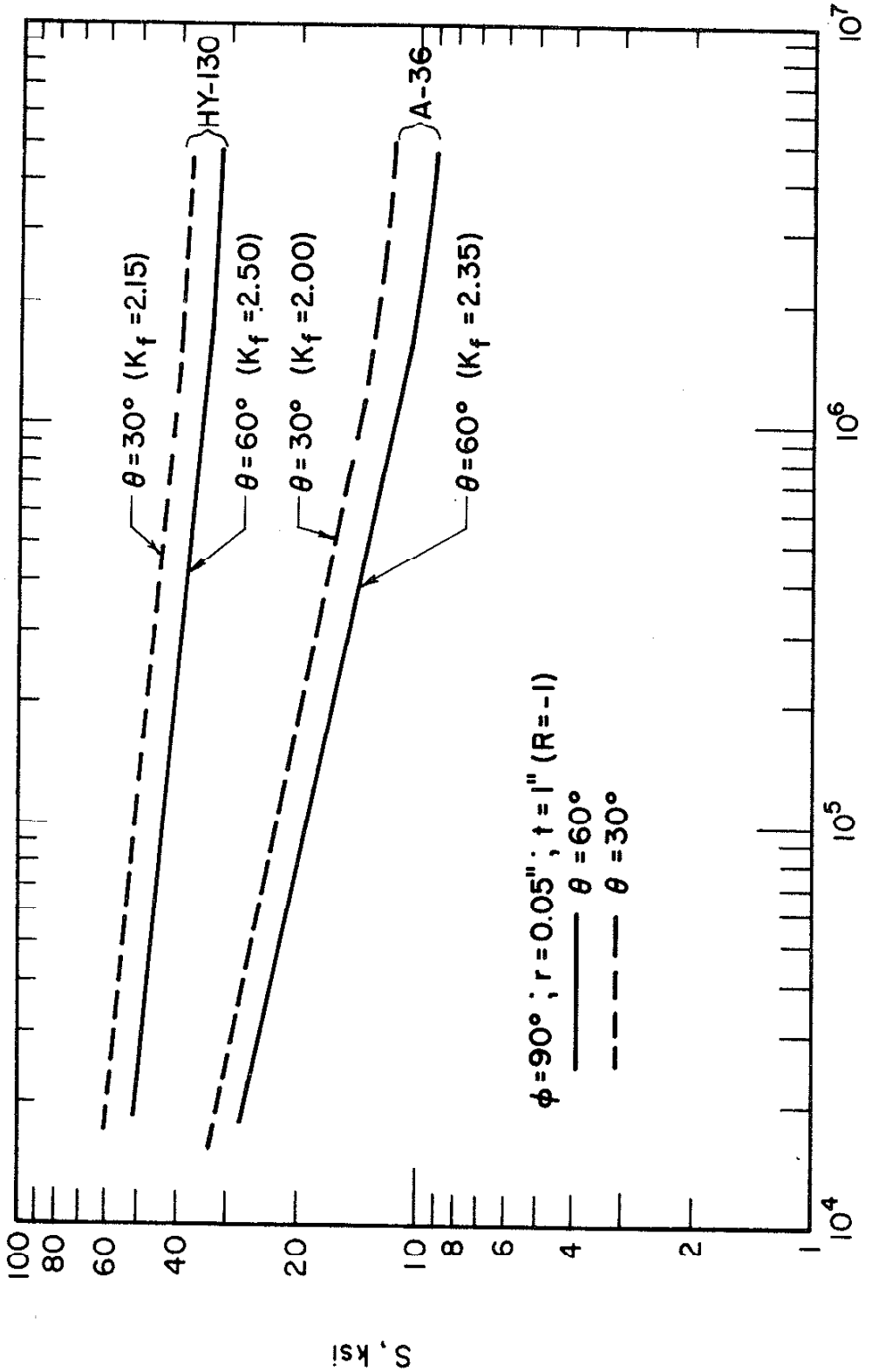

Fig. 59 Predicted Effect of the Flank Angle, θ, on the Fatigue Crack Initiation Life for A-36 and HY-130 Steel Butt Weldments of Identical Geometries

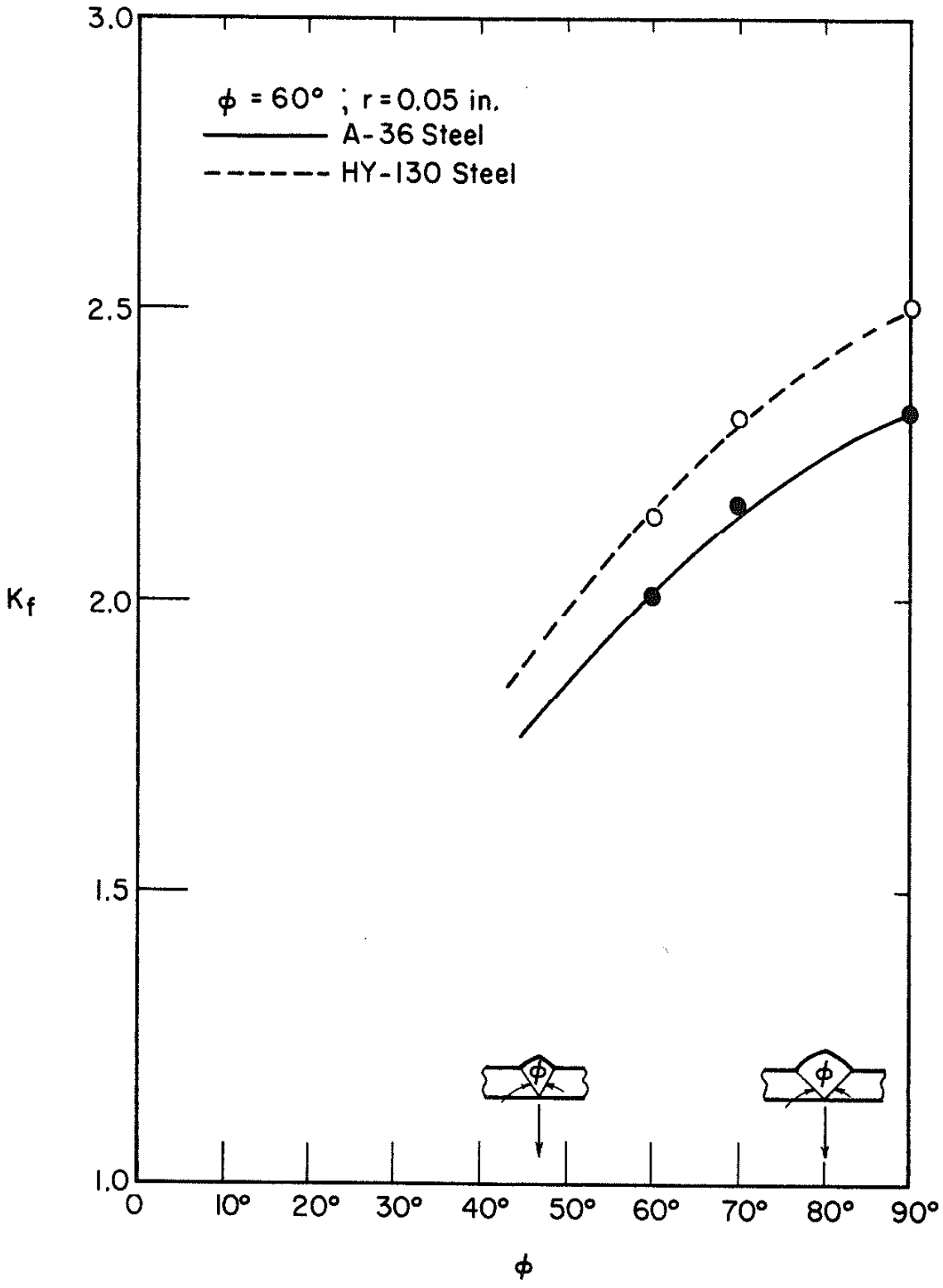

Fig. 60 Effect of the Edge Preparation Angle, ϕ, on the Fatigue Notch Factor, K_f, for A-36 and HY-130 Steel Butt Weldments (Differences in K_f Are Due to Different "a" Values)

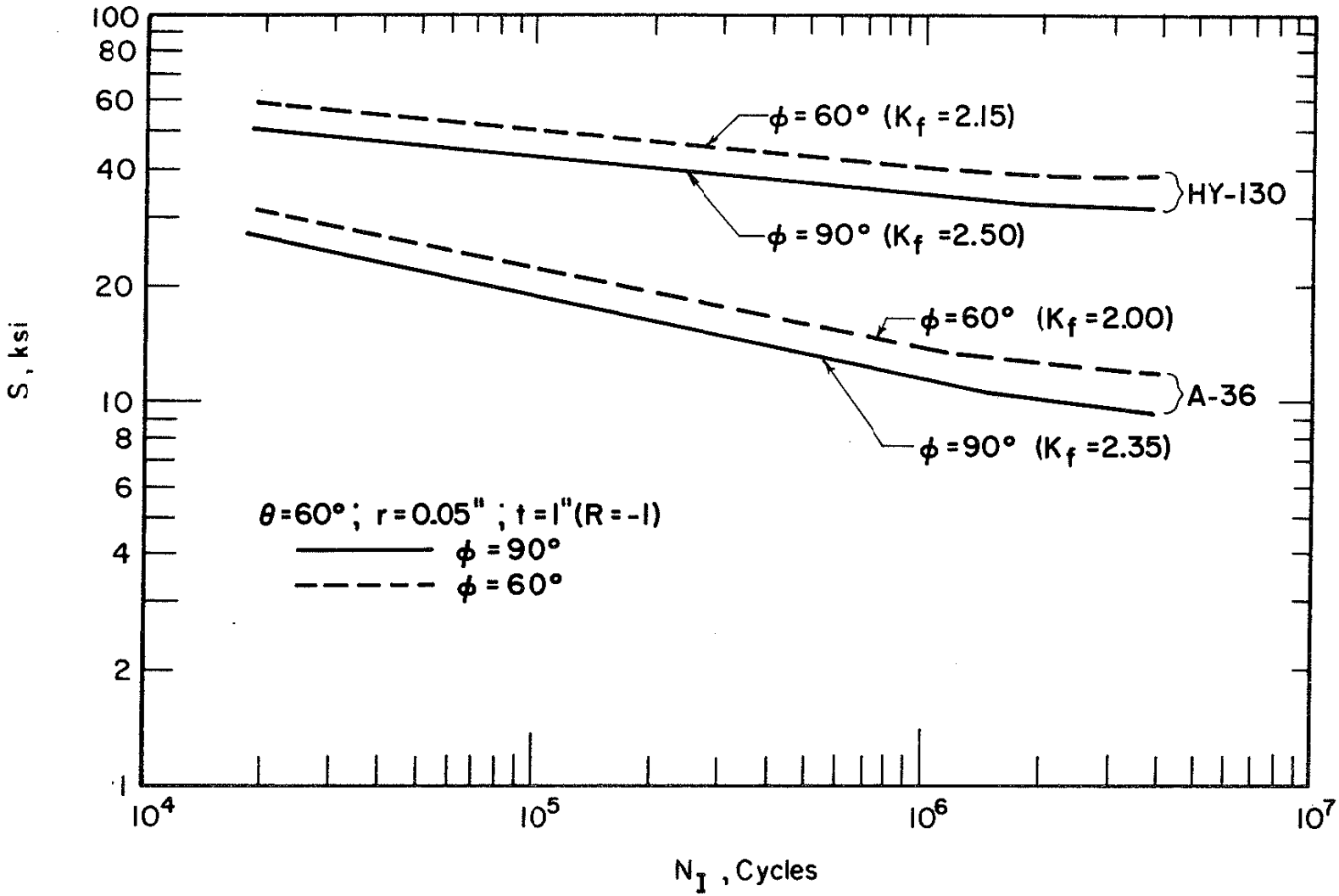

Fig. 61 Predicted Effect of the Edge Preparation Angle, ϕ, on the Fatigue Crack Initiation Life for A-36 and HY-130 Steel Butt Weldments of Identical Geometries

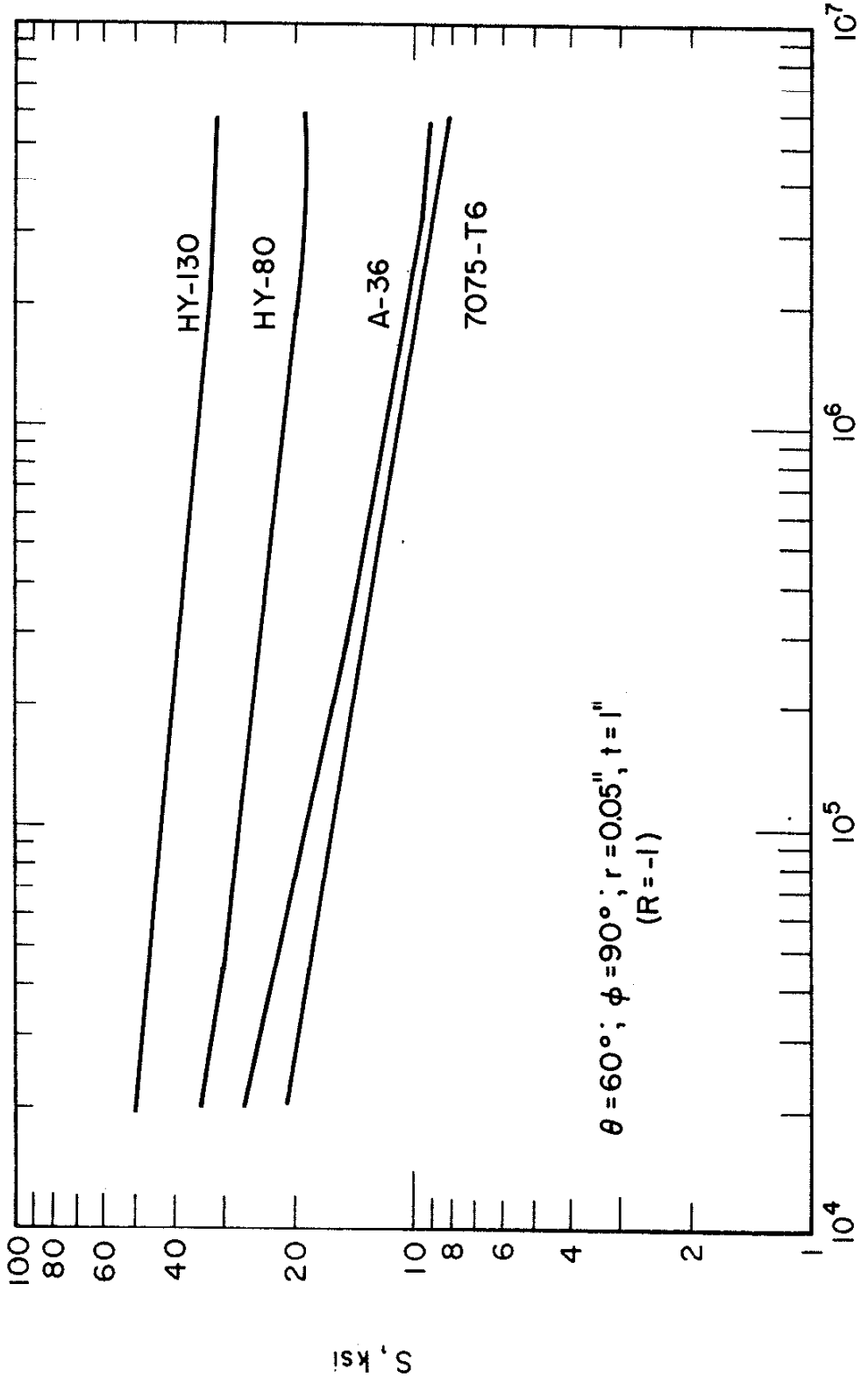

Fig. 62 Predicted Effect of Material Properties on the Crack Initiation Life for 7075-T6 Al, A-36, HY-80, and HY-130 Steel Butt Weldments of Identical Geometries

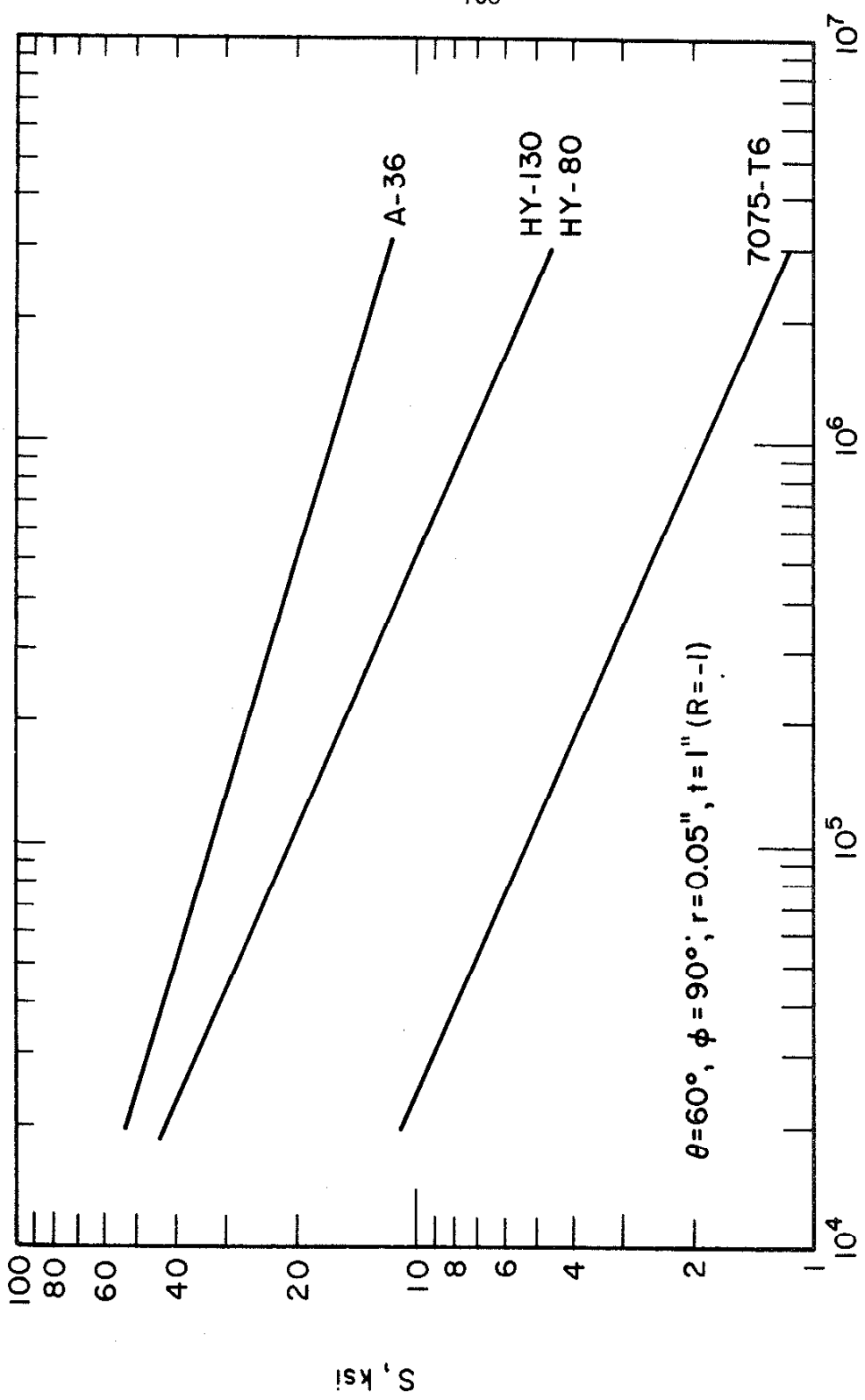

Fig. 63 Predicted Effect of Material Properties on the Crack Propagation Life for 7075-T6 Al, A-36, HY-80, and HY-130 Steel Butt Weldments of Identical Geometries

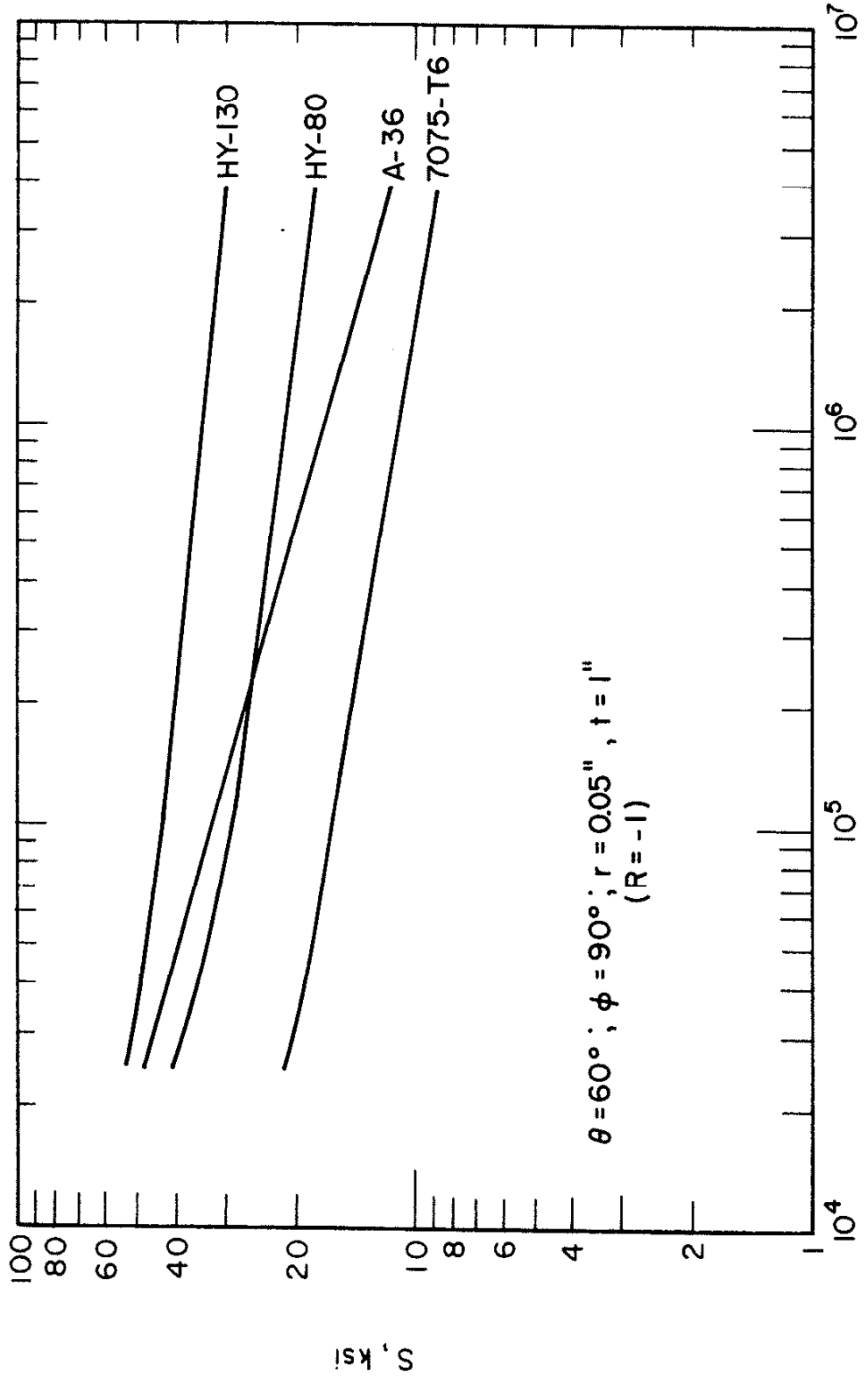

Fig. 64 Predicted Effect of Material Properties on the Total Fatigue Life for 7075-T6 Al, A-36, HY-80, and HY-130 Steel Butt Weldments of Identical Geometries

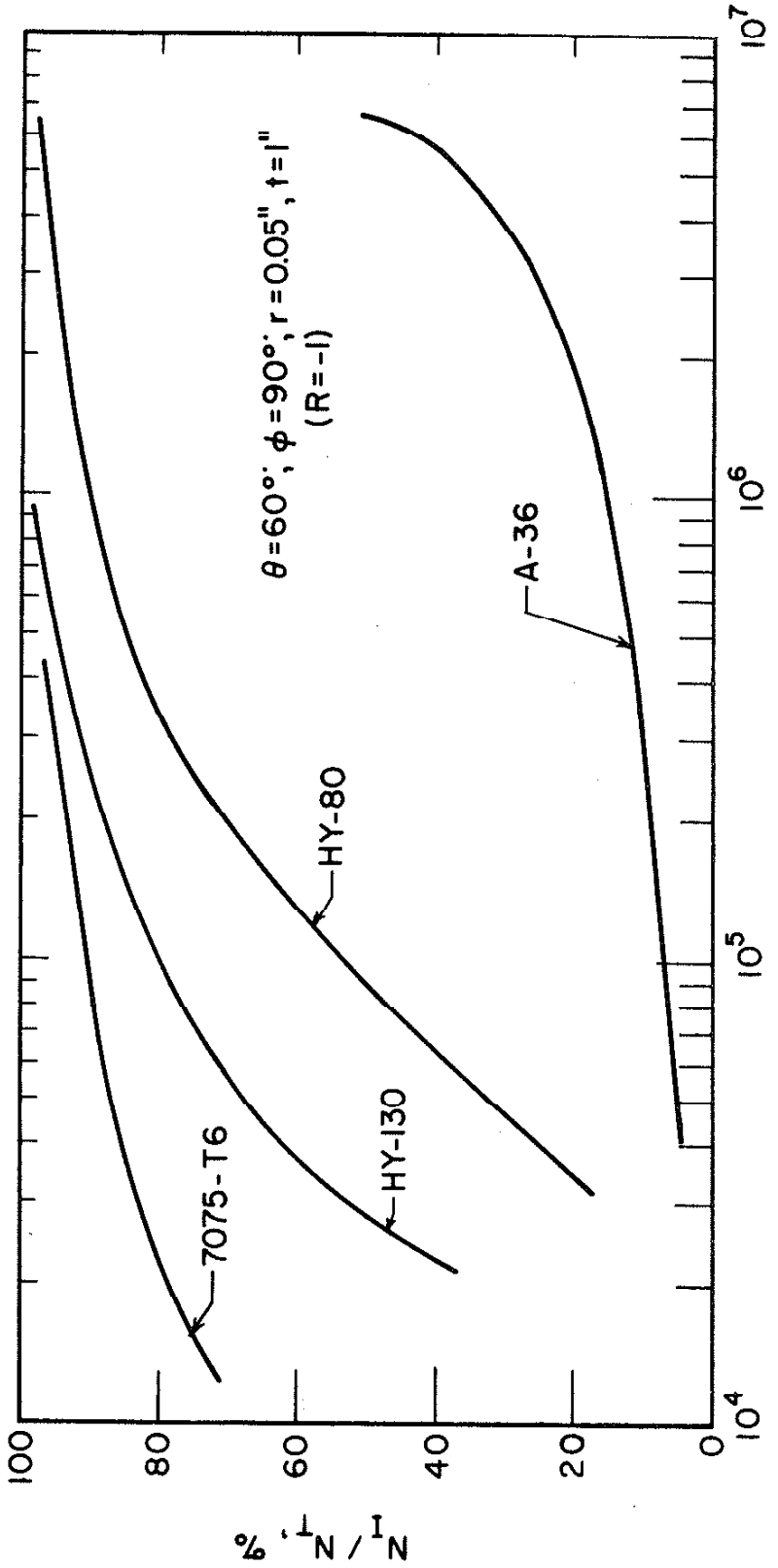

Fig. 65 Predicted Partitioning of the Fatigue Crack Initiation Life as a Function of the Total Fatigue Life for 7075-T6 Al, A-36, HY-80, and HY-130 Steel Butt Weldments of Identical Geometries

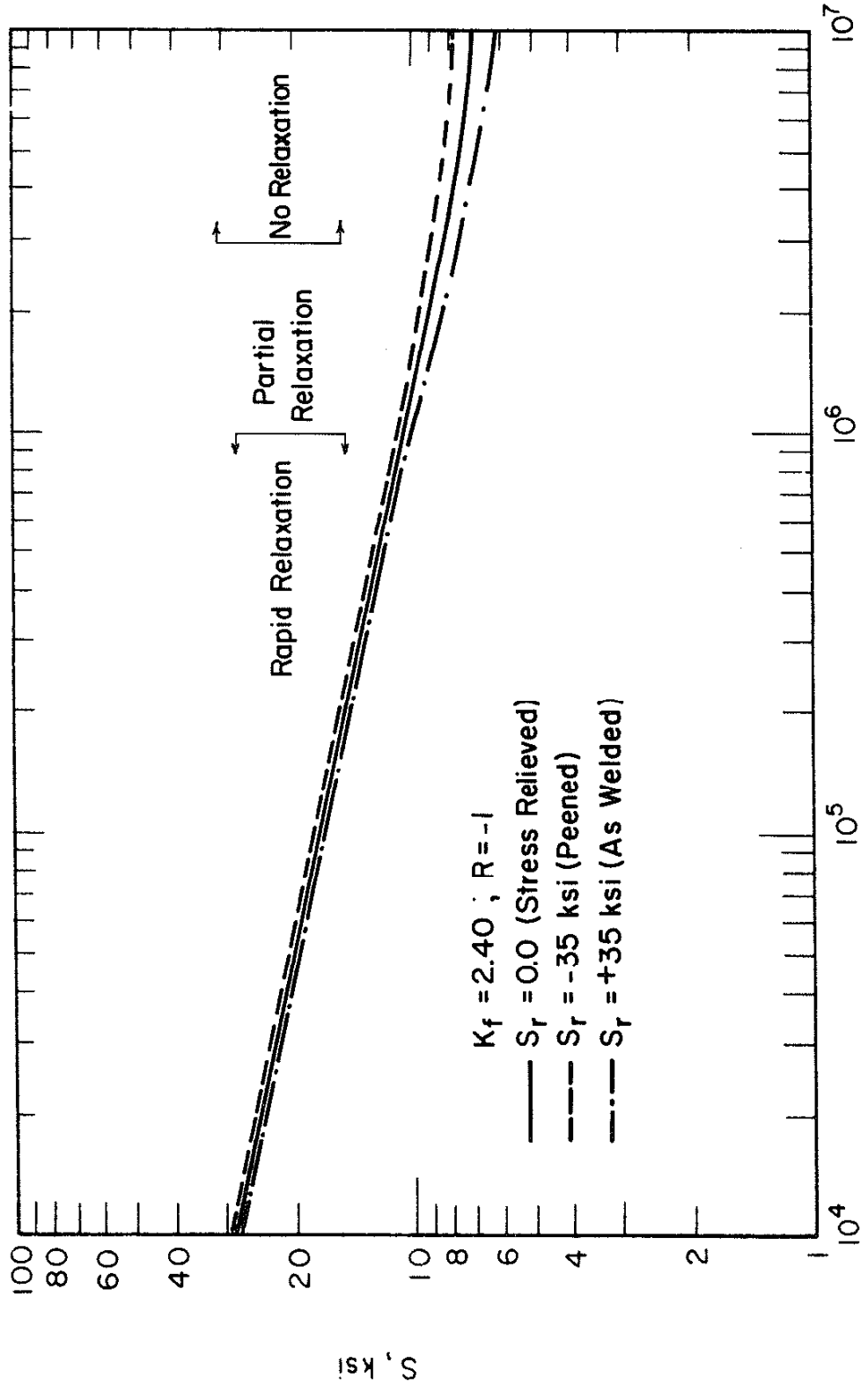

Fig. 66 Predicted Effect of the Residual Stresses on the Fatigue Crack Initiation Life for A-36 Steel Butt Weldments

APPENDIX A

FINITE ELEMENT ANALYSIS

The determination of the elastic stress concentration factor as a function of the radius of the toe of the weld was carried out using an elastic, finite-element computer program. The analysis presented in this section refers only to the simulated welded specimens; a similar analysis was performed with the welded specimens but with appropriately modified boundary conditions.

The geometry of the simulated weld specimens was modeled by subdividing it into a mesh of interconnected triangles. Accurate determination of the stress distribution in areas close to the toe of the weld was determined by using a very fine mesh in areas close to these regions. Figures A-1a, A-1b and A-1c show the finite element representation for this particular geometry. Figures A-1b and A-1c are the enlarged sections abcd of Fig. A-1a and efgh of Fig. A-1b respectively. In view of the symmetry of the problem, it was sufficient to consider only one half of the specimen. The program employs linear strain triangular elements. The ratio of the height to the width of a particular element was always less than 3 and plane strain conditions were assumed. The applied stresses were replaced by equivalent nodal forces. With reference to Fig. A-1a, boundary conditions were specified as follows:

Nodes along AB; $P_x = 0$; $P_y = 0$

Nodes along BC: U_x = Uniform; $\Sigma P_x = (0.620)(S)$

Nodes along CDE: $P_x = 0$; $P_y = 0$

Nodes along AE: $U_x = 0$; $P_y = 0$

Input parameters include the elastic modulus and Poisson's ratio. The output of this program consists of stresses and strains at each node which were obtained by averaging the stresses and the strains among triangles adjacent to the node. Figure A-2 shows the local variation of σ_{xx}/S with the ratio x/r for three different radii. The location of maximum values of σ_{xx}/S is close to the tangency point of the circle defined by r. The variation of σ_{xx}/S inward from the point of maximum σ_{xx}/S at the toe of the weld is shown in Fig. A-3. As this figure shows, this variation is very steep and it is also dependent of the radius of the toe of the weld. The spatial distribution of σ_{xx}/S is presented in Fig. A-4. All of the three previous figures show that the highly stressed region is very localized with pronounced stress gradients. Consequently, it is very likely that a residual stress would be "washed out" during the fatigue process and furthermore that their measurement would require a very small x-ray beam aimed precisely at this location.

Figure A-5 shows the functional dependence of the stress concentration factor with the radius at the toe of the weld for the particular geometry shown in Fig. A-1a. Decreasing the radius at the toe of the weld from 0.01 in. to 0.05 in. causes the stress concentration factor to decrease from 3.00 to 2.08.

Figure A-6 shows the principal stress trajectories at nodal points. If it is assumed that fatigue cracking will proceed in a direction normal to the maximum principal stress, initial fatigue crack will then make an angle of 76° with the axis of the specimen; this indeed was noticed in the simulated weld specimens and is shown in Fig. 36. In this figure the crack makes an angle of 75° with the axis of the specimen.

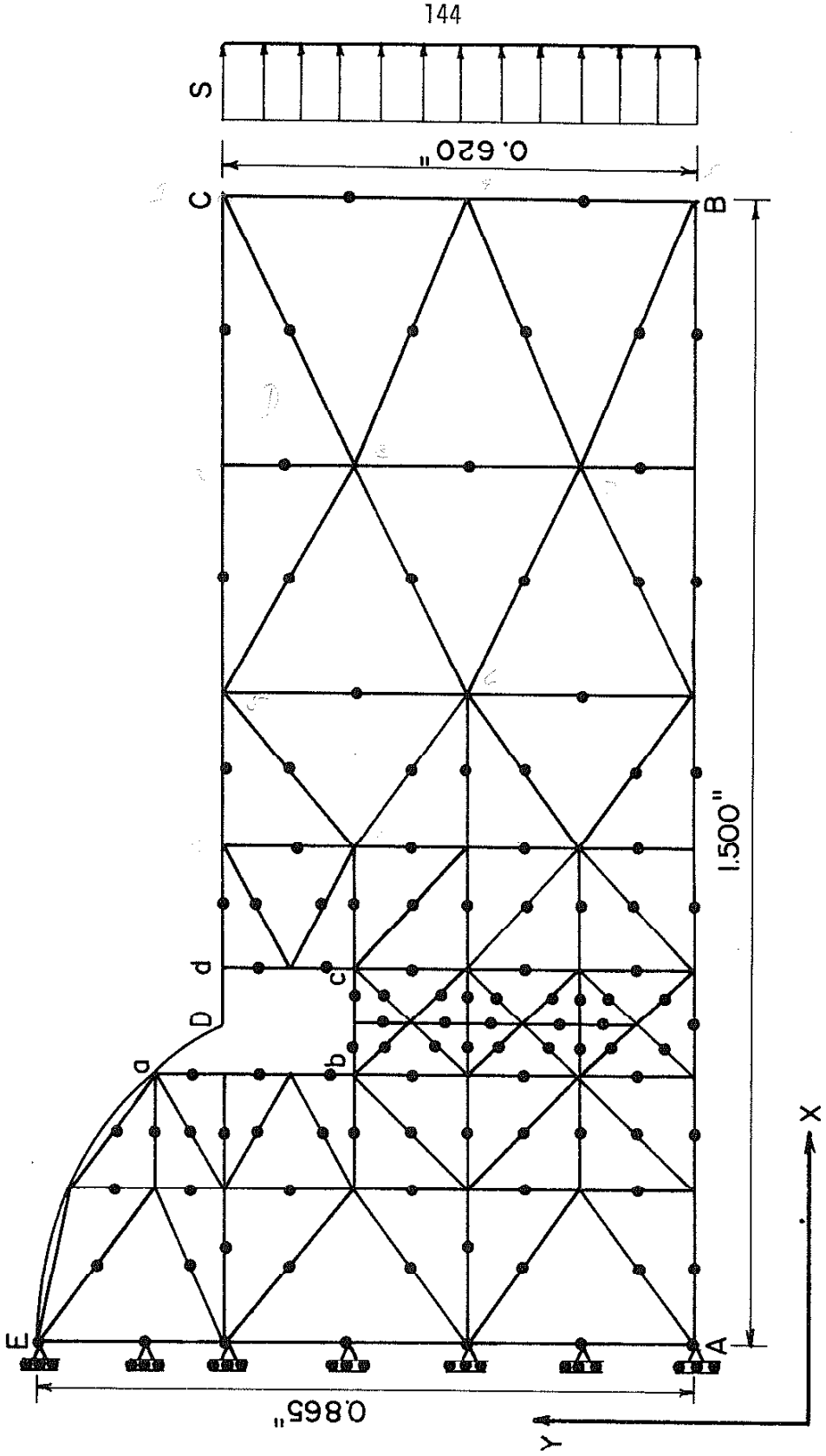

Fig. A-1a Finite Element Network for Determining Stress Distribution Near the Toe of Simulated Butt Weld Specimens

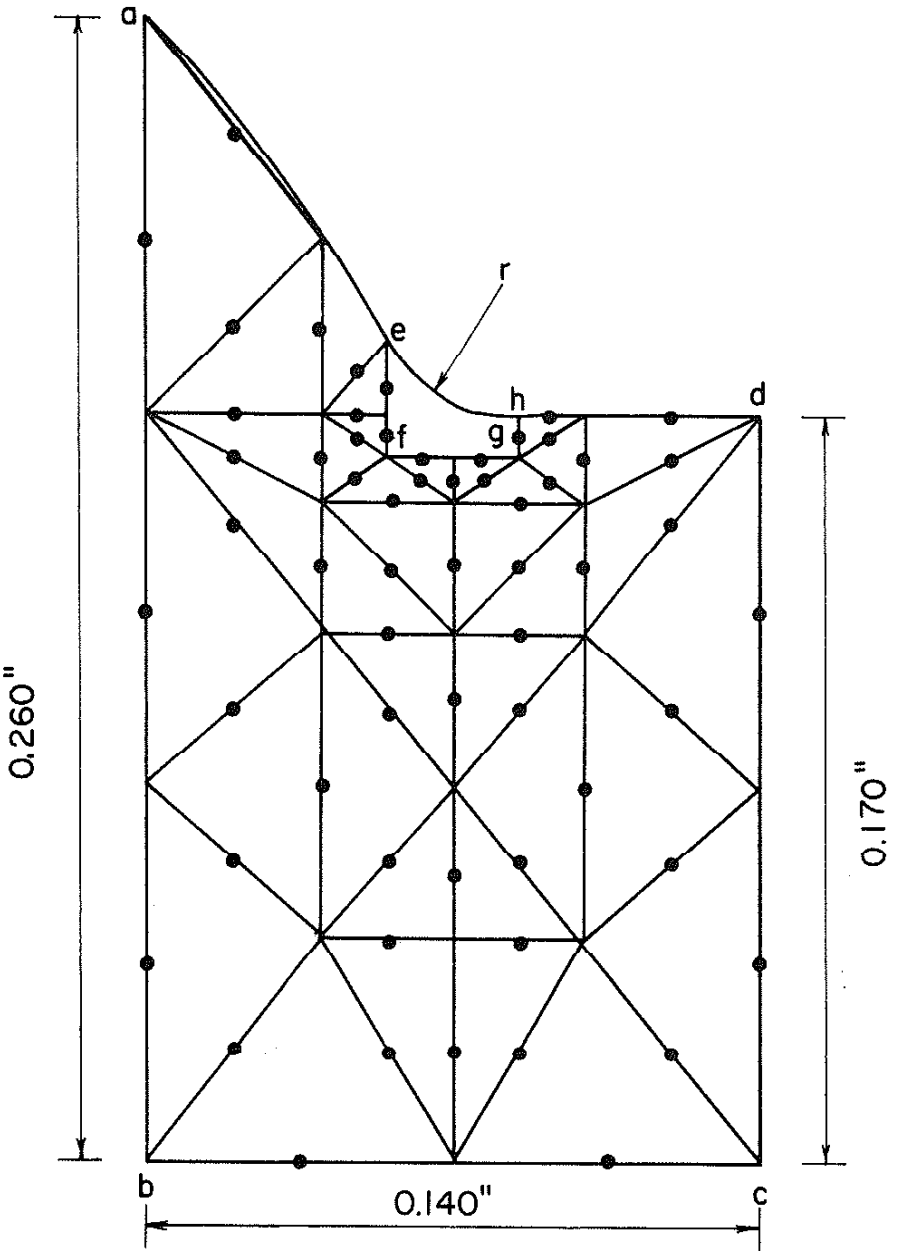

Fig. A-1b Section abcd of Fig. A-1a

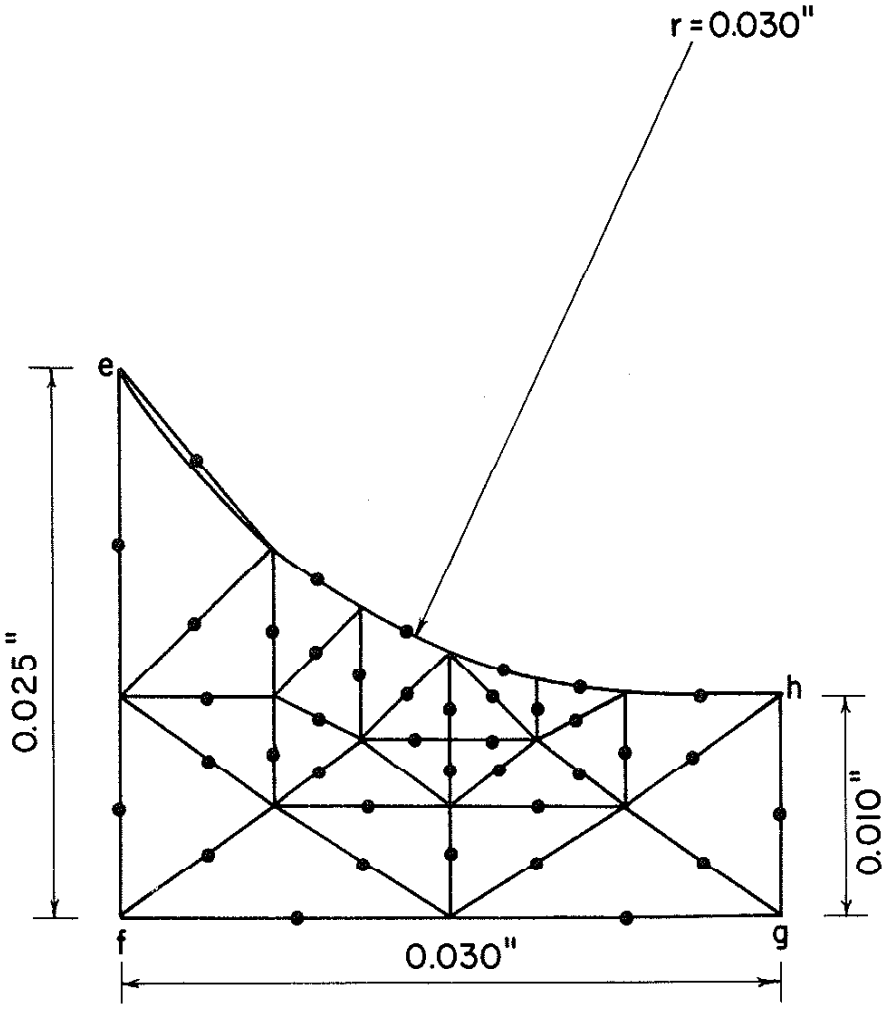

Fig. A-1c Section efgh of Fig. A-1b

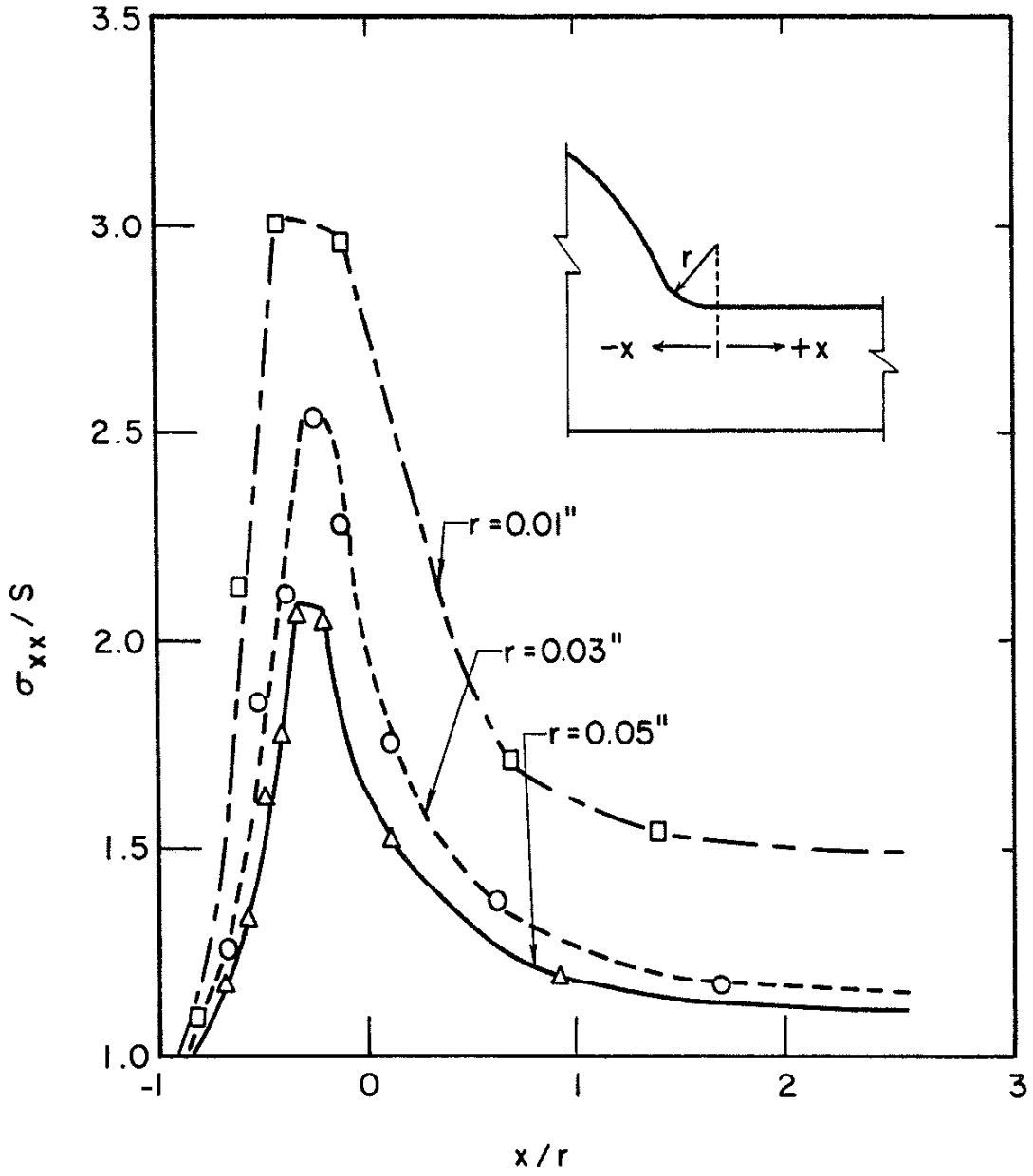

Fig. A-2 Variation of σ_{xx}/S with the Ratio x/r for Simulated Butt Weld Specimens

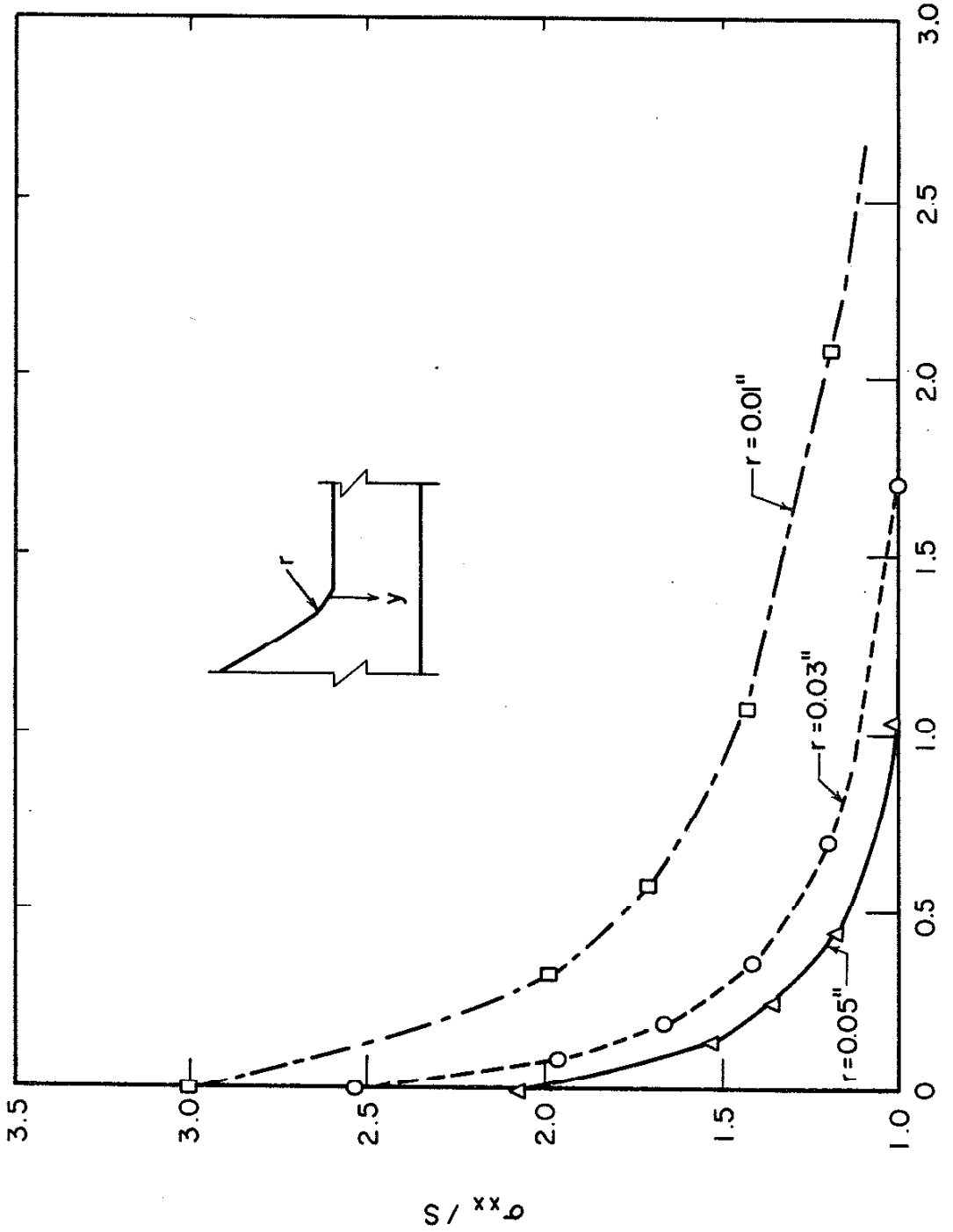

Fig. A-3 Variation of σ_{xx}/S with the Ratio y/r for Simulated Butt Weld Specimens

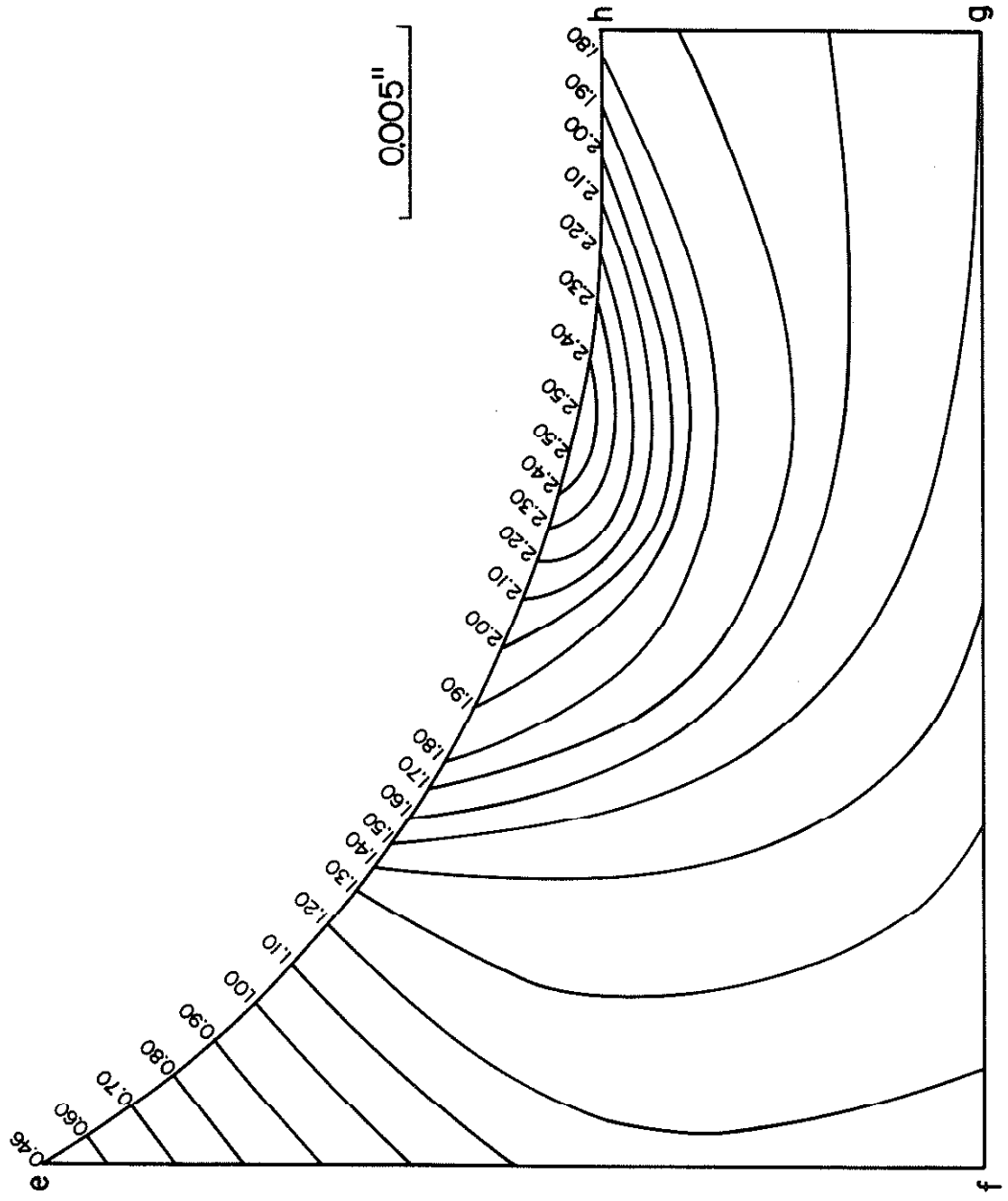

Fig. A-4 Distribution of σ_{xx}/S in the Area Close to the Toe of the Weld for Simulated Butt Weld Specimens

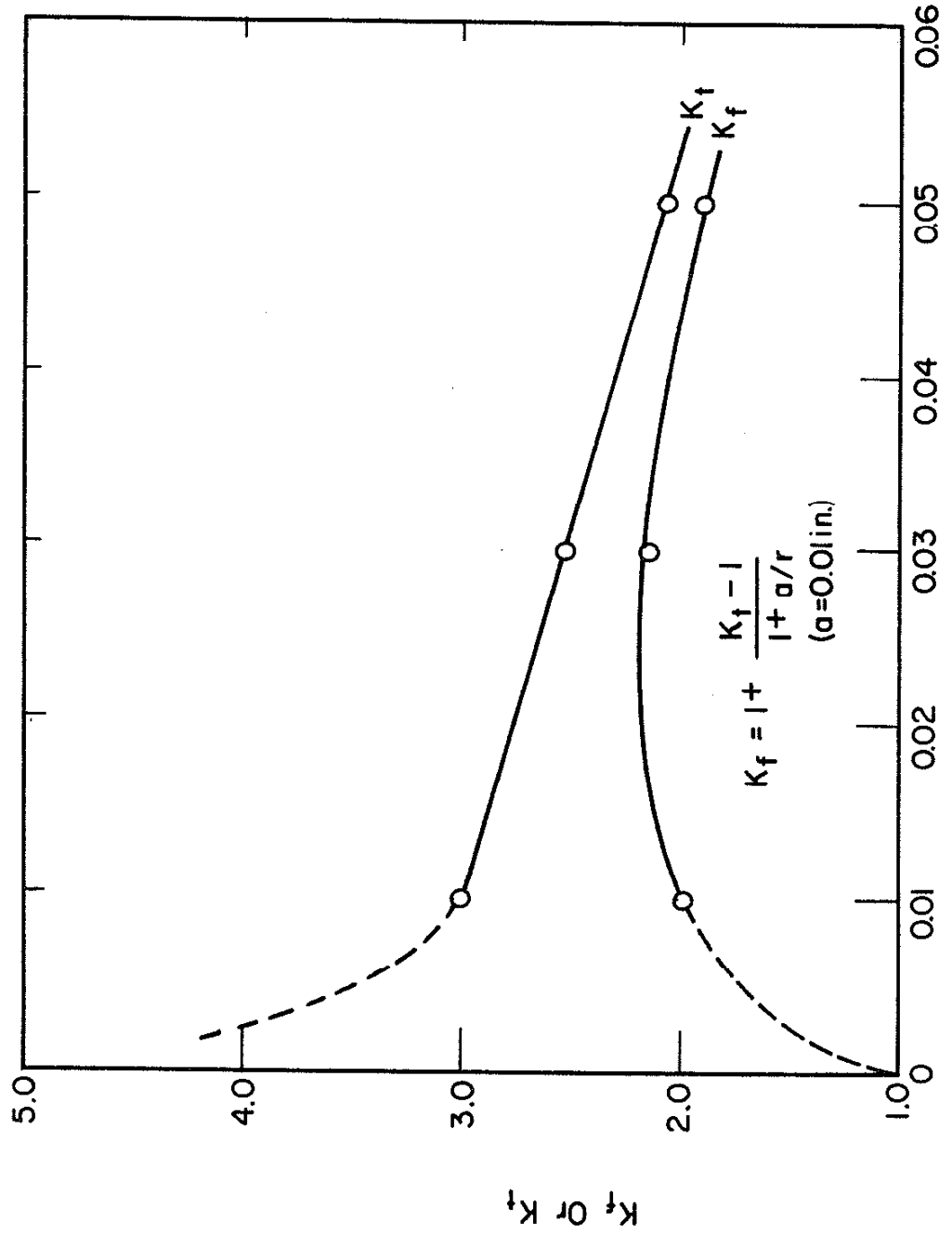

Fig. A-5 Stress Concentration Factor, K_t, and Fatigue Notch Factor, K_f, as a Function of the Radius at the Toe of the Weld for Simulated Butt Weld Specimens

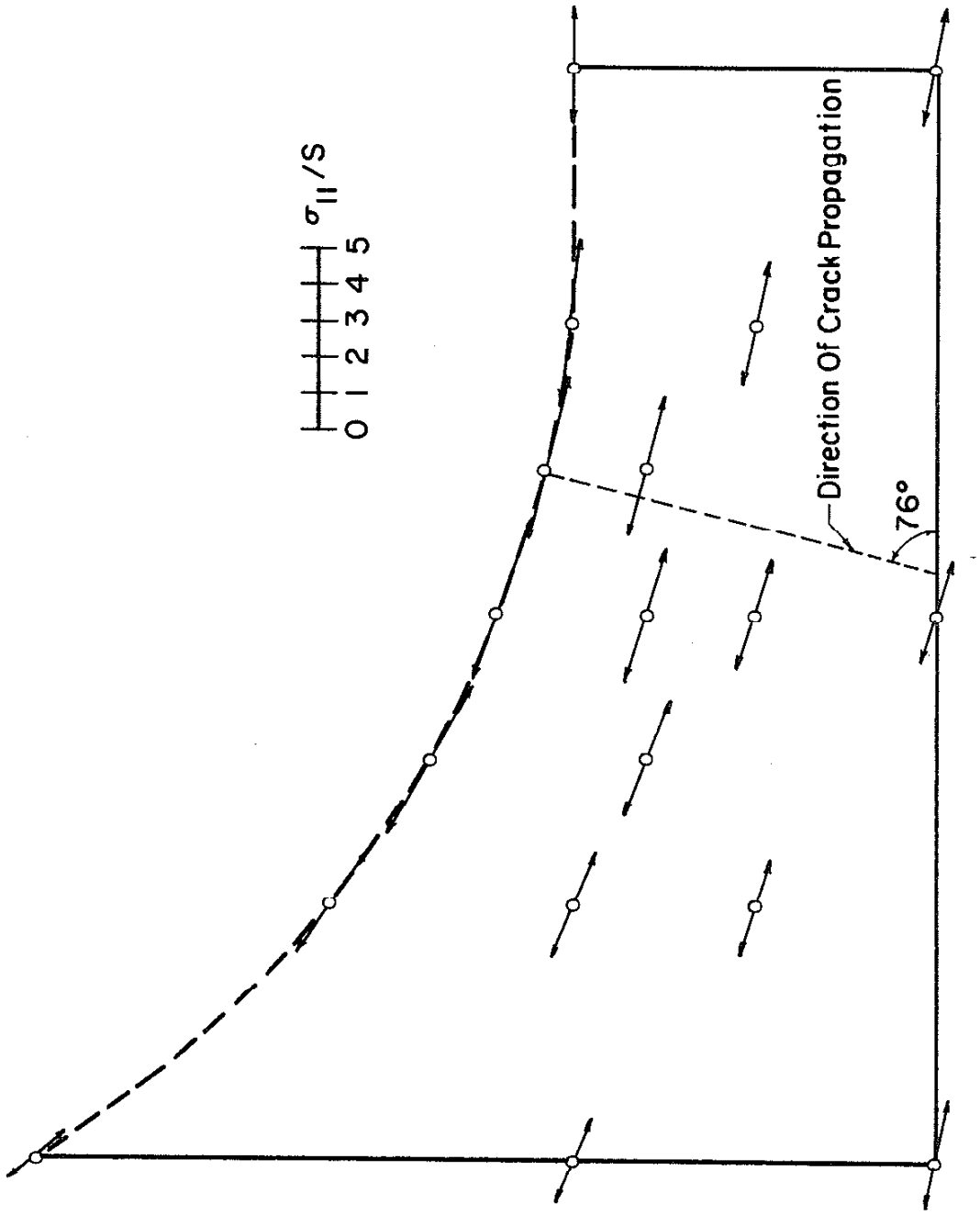

Fig. A-6 Magnitude and Direction of σ_{11}/S and Direction of Crack Propagation for Simulated Butt Weld Specimens

APPENDIX B

COMPUTER PROGRAM TO CALCULATE THE FATIGUE CRACK INITIATION LIFE

The computer program which was used to calculate the crack initiation life of notched members is listed in this appendix. The program was based on the simulation program developed by Martin (49,52) and extended to non-massing materials by Jhansale (54,68) and Plummer (55). The program was developed to model the cyclic stress-strain behavior of A-36 steel under constant amplitude loadings but with minor modifications it could be extended to any other material and/or random loadings. The program is written in FORTRAN IV language and the computation was performed on an IBM 360 computer. A list of the principal variables appearing in the program, the program itself and an output of results for a notch with a fatigue notch factor (K_f) of 2.00 under 0 to 30 ksi fatigue laodings are given below.

List of Principal Variables

Program Symbol	Definition
B	Fatigue strength exponent, b
C	Fatigue ductility exponent, c
DELS	Stress increment, $\delta\sigma$
DELPEP	Increment of plastic strain obtained upon activation of a particular spring-slider element
D1	Damage associated with the elastic strain
DAM	Damage associated with the plastic strain
DM	Damage associated with the mean stress
DAMAGE	Total damage associated to a particular reversal

Program Symbol	Definition
E	Modulus of elasticity, E
EPF	Fatigue ductility coefficient, ε_f'
EPT	Strain obtained after activation of a particular spring-slider element
EDR	Stiffness of the spring-slider element
ERANGE	Strain range, $\Delta\varepsilon$
ESLIDE	Stiffness of the spring-slider element
KS	Monotonic strength coefficient, K
KC	Cyclic strength coefficient needed to model the skeleton curve
K2	Intermediate strength coefficient
KX	Cyclic strength coefficient, K'
KF	Fatigue notch factor, K_f
NS	Number of spring-slider elements needed to model the monotonic curve
NC	Number of spring-slider elements needed to model the cyclic stress-strain curve
N2	Number of spring-slider elements needed to model some intermediate cyclic stress-strain curve
NREV	Number of reversals
NPROB	Number of problems to be solved
PSSUM	Sum of the plastic strain
RC	Relaxation constant
S	Residual stress stored in a spring slider-element
SB	Yield stress of the spring-slider element
ST	Stress obtained after activation of a given spring-slider element

Program Symbol	Definition
STM	Mean Stress, σ_o
STR	Stress range, $\Delta\sigma$
SPF	Fatigue strength coefficient, σ_f'
SADD	Stress amplitude, σ
SANN	Nominal stress range, ΔS
SHES	Monotonic strain hardening exponent, n
SHEC	Cyclic strain hardening exponent needed to model the skeleton curve
SHE2	Intermediate strain hardening exponent
SHEX	Cyclic strain hardening exponent, n'
SOFF	Stress offset, S_{off}
TOTDAM	Summation of the total damage up to a given reversal
YPPS	Yield point plastic strain offset
YIELD1	Yield stress of the skeleton curve

```
C
C++++++++++++++++++++++++++++++++++++++++++++++++++++++++
C+                                                      +
C+     NEUBER CONTROL  A- 36 STEEL  SERIES MODEL        +
C+                                                      +
C++++++++++++++++++++++++++++++++++++++++++++++++++++++++
C
      1 FORMAT('1')
      2 FORMAT (///////)
      5 FORMAT (3E12.4)
      6 FORMAT (6F12.3)
      7 FORMAT (F12.3)
      8 FORMAT (E12.4,I2)
      9 FORMAT (8I10 )
     10 FORMAT (2E12.4)
     19 FORMAT (I10)
     31 FORMAT (T55,' INPUT INFORMATION'///T3,' CONSTANTS FORMING STRESS-S
       1TRAIN RELATION'//T16,' STATIC STRENGTH COEFFICIENT =',F11.1,T76,'
       2STATIC STRAIN HARDENING EXPONENT =',F14.4/T16,' CYCLIC STRENGTH CO
       3EFFICIENT =',F11.1,T77,'CYCLIC STRAIN HARDENING EXPONENT =',F14.4
       4/T11,'INTERMEDIATE STRENGTH COEFFICIENT =',F11.1,
       5 T71,'INTERMEDIATE STRAIN HARDENING EXPONENT =',F14.4
       6/T23,' MODULUS OF ELASTICITY=',F11.1,T82,'FATIGUE STRENGTH COEFFIC
       7IENT=',F14.4/)
     36 FORMAT(T19,' MONOTONIC YIELD STRENGTH=',F11.1,T80,'FATIGUE DUCTILI
       1TY COEFFICIENT=',F12.3/
       2T23,'CYCLIC YIELD STRENGTH=',F11.1,T83,'FATIGUE STRENGTH EXPONENT
       3=',F12.3/
       4T17,'INTERMEDIATE YIELD STRENGTH=',F11.1,T83,'FATIGUE DUCTILITY EX
       5PONENT=',F12.3/
       6T23,'PLASTIC STRAIN OFFSET=',F14.5/)
     32 FORMAT (T3,' RELAXING FUNCTION CONSTANTS'//T26,' RELAXING CONSTANT
       1 =',F14.4///)
     37 FORMAT (T27,'STRESS INCREMENT =',F11.1,
       1 T080,'MONOTONIC NO. OF ELEMENTS =',I9/
       2 T083,'CYCLIC NO. OF ELEMENTS =',I9/
       3 T077,'INTERMEDIATE NO. OF ELEMENTS =',I9/////)
     44 FORMAT(T50, 'FATIGUE STRENTHG RED. FACTOR =', F5.2////)
     58 FORMAT (T5,'STRESS PEAKS:'/T05,'ORDER',T20,'STRESS',
       1 T36,'DIRECTION')
     60 FORMAT (I10,2PE16.6,I10)
        REAL KS,KC,K2,KF,KX
        DIMENSION S(150),SANN( 10),NR( 10),SB(150, 7),ESLIDE(150, 7)
        DIMENSION NPRINT(100)
        READ 9, NPROB
        DO 801 JKLL=1,NPROB
        PRINT 1
C
```

```
C     INPUT DATA
C
  100 READ 5,  DELS,E,YPPS
      READ 5,  SHES,SHEC,SHE2
      READ 5,  KS,KC,K2
      READ 6,  SPF,EPF,B,C,SHEX,KX
      READ 7 , KF
  120 READ 10, RC
      READ 19, NREV
      READ 8,  (SANN(I),NR(I),I = 1,5 )
      READ 19, KK
      READ 9,  (NPRINT(I),I = 1,KK )
      YIELD1 = +10000.
      YPSM = KS*YPPS**SHES
      YPSC = KC*YPPS**SHEC
      YPS2 = K2*YPPS**SHE2
      NS = (KS-YPSM)/DELS + 1
      NC = (KC-YPSC)/DELS + 1
      N2 = (K2-YPS2)/DELS + 1
      PRINT 31,KS,SHES,KX,SHEX,KX,SHEX,E,SPF
      PRINT 36, YPSM,EPF,YPSC,B,YPS2,C,YPPS
      PRINT 37, DELS,NS,NC,N2
      PRINT 44, KF
      PRINT 32, RC
      PRINT 58
      PRINT 60, (J,SANN(J),NR(J),J=1,5)
      PRINT 2
C
C     INITIAL VALUES
C
      DO 200  J=  3,150
  200 S(J) = 0.0
      DO 201 IC=1,7
      DO 201 J= 3,150
      SB(J,IC)=0.0
      ESLIDE(J,IC)=0.0
  201 CONTINUE
      EI = 1.0/E
      PM = 1.0
C
C     MONOTONIC CURVE
C
      A1 = YPPS**SHES
      SHEI = 1.0/SHES
      AK = KS
      N = NS + 4
      IC = 1
      CALL FORMSS(AK,A1,PM,DELS,N,EI,SHEI,SB,ESLIDE,RC,IC,YIELD1)
```

```
C
C     SECOND REVERSAL
C
      A1 = YPPS**SHE2
      SHEI = 1.0/SHE2
      AK = K2
      N = N2 + 4
      IC  =2
      CALL FORMSS(AK,A1,PM,DELS,N,EI,SHEI,SB,ESLIDE,RC,IC,YIELD1)
C
C     SKELETON CURVE FOR CYCLIC BEHAVIOR
C
      A1 = YPPS**SHEC
      SHEI = 1.0/SHEC
      AK = KC
      N = NC + 4
      IC = 3
      CALL FORMSS(AK,A1,PM,DELS,N,EI,SHEI,SB,ESLIDE,RC,IC,YIELD1)
      DLOAD =1.0
      DLOAD = SIGN(DLOAD,SANN(1))
      DL = 1.0E-12
      NH = 0
      STO = 0.0
      EPO = 0.0
      DAMAGX = 0.0
      TOTDAM = 0.0
      STMX = 0.00000
      JP = 1
C
C     START CYCLING
C
      DO 500 M = 1,NREV
      IF(M.EQ.1) GO TO 27
      IF(M.EQ.2) GO TO 28
      IF(M.EQ.3) GO TO 26
      IF(M.EQ.4) GO TO 25
      XZC=0.5*M
      IF(M.EQ.(2*INT(XZC))) GO TO 25
      SAN = SANN(5)
      GO TO 29
   25 SAN = SANN(4)
      GO TO 29
   26 SAN = SANN(3)
      GO TO 29
   28 SAN = SANN(2)
      GO TO 29
   27 SAN = SANN(1)
   29 DAMAGE = 0.000
```

```
      CALL S36(DLOAD,DL,NH,SB,ESLIDE,S,N,STS,SAN,STO,E,EI,EPO,RC,M
     1,NS,N2,NC,DLNEW,KF,EPL ,SPF,EPF,B,C,SHEX,KX,JP,NPRINT,DAMAGE,STM)
      STO = STS
      EPO = EPL
      IF(NR(1).EQ.1) DLOAD = -DLOAD
      TOTDAM = TOTDAM + DAMAGE
      IF(TOTDAM.GE.1.000) GO TO 499
      IF(ABS(STM).LE.100.0) GO TO 498
      IF(ABS(STMX - STM).LE.0.001.AND.NREV.GE.1000) GO TO 498
      IF(M.EQ.NREV) GO TO 498
      STMX = STM
      DAMAGX = DAMAGE
  500 CONTINUE
  499 PRINT 501, M, TOTDAM
  501 FORMAT (///T29,'LIFE OF THE ESPECIMEN =',I10,'  REVERSALS
     1DAMAGE =',1PE16.6)
      GO TO 503
  498 PRINT 502, M, DAMAGE, TOTDAM
  502 FORMAT (//T5,'THE DAMAGE FOR THE REVERSAL ',I8,'  IS ',1PE16.6,'
     1  THE TOTAL DAMAGE UP TO THIS REVERSAL IS ',1PE16.6//)
      LIFE = (1.0000 - TOTDAM )/ DAMAGE + M
      PRINT 504, LIFE
  504 FORMAT (///T29,'LIFE OF THE ESPECIMEN =',I10,'   REVERSALS')
  503 PRINT 1
  801 CONTINUE
      STOP
      END
```

```
      SUBROUTINE S36(DLOAD,DL,NH,SB,ESLIDE,S,N,STS,SAN,STO,E,EI,EPU,
     1RC,H,NS,N2,NC,DLNEW,KF,EPL,SPF,EPF,B,C,SHEX,KX,JP,NPRINT,DAMAGE,
     2STM)
      DIMENSION SB(150, 7),ESLIDE(150, 7),S(150)
      DIMENSION SO(150),EDR(150),ST(150),EPT(150),DELPEP(150)
      DIMENSION X(150),Y(150)
      DIMENSION NPRINT(100)
      REAL KF,KX
      PM = 1.
      PM = SIGN(PM,DLOAD)
      DOLD = 1.
      DOLD = SIGN(DOLD,DL)
      ICHANG = 1
      IF(NH) 10,12,13
   10 IF(DLOAD.NE.DOLD) GO TO 11
      IC = IABS(NH)
      GO TO 15
   11 IC = IABS(NH)-1
      NH = +IC
      GO TO 15
   12 IC = 1
      GO TO 15
   13 IF(DLOAD.NE.DOLD) GO TO 14
      IC = NH
      GO TO 15
   14 IF(IC.GT.6) GO TO 800
      IC = NH + 1
  800 NH = -IC
   15 CONTINUE
      IF(IC.LE.1) N = NS + 4
      IF(IC.EQ.2) N = N2 + 4
      IF(IC.GE.3) N = NC + 4
      IF(NH.LT.0) ERANGE = ABS(DLNEW)
      IF(NH.GT.0) ERANGE = ABS(DL)
      IF(NH.EQ.0) ERANGE = 1.0E-12
      SADD = -PM*SOFF(ERANGE,IC)/2.
      IF(IC.GE.3) GO TO 22
      SO(3) = SB(3,IC)*PM
      EDR(3) = ESLIDE(3,IC)
      DO 20 J = 4,N
      SO(J) = +SB(J,IC)*PM + SADD
      EDR(J) = ESLIDE(J,IC)
   20 CONTINUE
      GO TO 24
   22 CONTINUE
      SO(3) = SB(3,3)*PM
      EDR(3) = ESLIDE(3,3)
      DO 21 J = 4,N
```

```
      SO(J) = +SB(J,3)*PM + SADD
      EDR(J) = ESLIDE(J,3)
   21 CONTINUE
   24 CONTINUE
      IF(ABS(SO(3)).GE.ABS(SO(4))) WRITE (6,603)
  603 FORMAT(//,' WARNING---THE STRESS STRAIN CURVE HAS A NEGATIVE SLOPE
     1',/,' THE INITIAL YIELD STRESS, YIELD1,IS TOO LARGE.',//)
      EPT(1) = EPO
      ST(1) = STO
C
C     FOR FIRST SEGMENT
C
      I = 2
      IF((IC.EQ.1).AND.(ABS(ST(1)).GE.ABS(SO(3)))) S(3)=-ST(1)-SO(3)
      IF((IC.EQ.1).AND.(ABS(ST(1)).LT.ABS(SO(3)))) S(3)=0.0
      ST(2) = -S(3)-SO(3)
      EPT(2) = (ST(2)-ST(1))*EI + EPT(1)
      DELPEP(2) = 0.0
      D1 = (ABS(ST(2) - ST(1)))*(ABS(EPT(2) - EPT(1)))
      D2 = ((SAN*KF)**2)/E
      DD = D1 - D2
      IF( DD )308,343,305
  305 ST(2) = KF*SAN + ST(1)
      EPT(2) = (KF*SAN)/E + EPT(1)
      DELEP = EPT(2) - EPT(1)
      EPL = EPT(I)
      STA = ABS(ST(2) - ST(1))/2.0
      D1 = (STA/SPF)**(-1.0/B)
      DAMAGE = DAMAGE + D1
      GO TO 344
  308 STA = ABS(ST(2) - ST(1))/2.0
      D1 = (STA/SPF)**(-1.0/B)
      DAMAGE = DAMAGE + D1
C
C     FOR REMAINING SEGMENTS
C
  310 I = I + 1
      IF(I.LE.N) GO TO 312
      PRINT 55, N
   55 FORMAT (////' PROGRAM HAS EXCEEDED THE ALLOTTED',I5,' ELEMENTS')
      PRINT 1
    1 FORMAT (1H1)
      GO TO 1000
  312 CONTINUE
      IF((IC.EQ.1).AND.(ABS(ST(1)).GE.ABS(SO(I+1)))) S(I+1) = -ST(1)
     1-SO(I+1)
      IF((IC.EQ.1).AND.(ABS(ST(1)).LT.ABS(SO(I+1)))) S(I+1) = 0.0
      ST(I) = -S(I+1)-SO(I+1)
```

```
      STR = ABS(ST(I-1))
      IF(I.EQ.3) STR = 0.0
      ETDS = EI + EDR(I)/(1.0 - STR/RC)
      EPT(I) = (ST(I) - ST(I-1))*ETDS + EPT(I-1)
      DIFF1 = ST(I)- ST(I-1)
      DIFF2 = EPT(I) - EPT(I-1)
      DELPEP(I) = DIFF2 - DIFF1*EI
      D1 = (ABS(ST(I) - ST(1)))*(ABS(EPT(I) - EPT(1)))
      D2 = ((SAN*KF)**2)/E
      DD = D1 - D2
      IF (DD )310,335,315
  315 A = (1.0/ETDS)*(EPT(I-1) - EPT(1)) - (ST(I-1) + ST(1))
      H = ST(1)*ST(I-1) - ST(1)*(1.0/ETDS)*(EPT(I-1) - EPT(1))
     1 - ((KF*SAN)**2)/(E*ETDS)
      ST(I) = ( -A + PM*SQRT(A*A - 4.0*H))/2.0
      EPT(I) = EPT(1) + ((KF*SAN)**2)/(E*(ST(I) - ST(1)))
      DELEP = EPT(I) - EPT(I-1)
      DIFF1 = ST(I) - ST(I - 1)
      DIFF2 = EPT(I) - EPT(I - 1)
      DELPEP(I) = DIFF2 - DIFF1*EI
  335 EPL = EPT(I)
      EPP = 0.0
      DO 16 K = 2,I
   16 EPP = EPP + DELPEP(K)
      EPPA = ABS(EPP)/2.0
      DAM = (EPPA/EPF)**(-1.0/C)
      DAMAGE = DAMAGE + DAM
C
C     RESET RESIDUAL SRESSES
C
      DO 340 J = 3,I
  340 S(J) = -ST(I)- SO(J)
      GO TO 344
  343 STA = ABS(ST(2) - ST(1))/2.0
      D1 = (STA/SPF)**(-1.0/B)
      DAMAGE = DAMAGE + D1
  344 CONTINUE
      IF(EPPA.LT.(1.0E-07)) GO TO 345
      IF(NH.EQ.0) ICHANG = 2
      IF(NH.LT.0) ICHANG = 3
      NH = IC
      GO TO (53,51,52) ,ICHANG
   51 DLNEW = ABS(EPT(I))
      GO TO 54
   52 DL = DLNEW
      DLNEW = ABS(2.*SB(3,IC)*EI) + ABS(EPT(I) - EPT(2))
      GO TO 54
   53 DLNEW = DLNEW + ABS(EPT(I)- EPT(2))
```

```
   54 CONTINUE
      IF(NH.NE.1) GO TO 345
C
C     CALCULATE FICTITIOUS RESIDUAL STRESSES
C
      X(1) = 0.0
      Y(1) = 0.0
      N = NC + 4
      DO 40 J = 3,N
      S(J) = 0.0
      SO(J) = SB(J,3)*PM
      EDR(J) = ESLIDE(J,3)
   40 CONTINUE
      K = 2
      Y(2) = -SO(3)
      X(2) = (Y(2) - Y(1))*EI + X(1)
      D1 = (ABS(Y(2) - Y(1)))*(ABS(X(2) - X(1)))
      D2 = ((SAN*KF)**2)/E
      DD = D1 - D2
      IF(DD) 42,345,41
   41 Y(2) = KF*SAN + Y(1)
      X(2) = (KF*SAN)/E + X(1)
      DELEP = X(2) - X(1)
      GO TO 345
   42 K = K + 1
      IF(K.LE.N) GO TO 43
      PRINT 55,N
      PRINT 1
      GO TO 1000
   43 Y(K) = -SO(K+1)
      STR = ABS(Y(K-1))
      IF(K.EQ.3) STR=0.0
      ETDS = EI + EDR(K)/(1.0-STR/RC)
      X(K) = (Y(K)-Y(K-1))*ETDS + X(K-1)
      D1 = (ABS(Y(K) - Y(1)))*(ABS(X(K) - X(1)))
      D2 = ((SAN*KF)**2)/E
      DD = D1 - D2
      IF(DD)42,45,44
   44 A = (1.0/ETDS)*(X(K-1) - X(1)) - (Y(K-1) + Y(1))
      H = Y(1)*Y(K-1) - Y(1)*(1.0/ETDS)*(X(K-1) - X(1)) - ((SAN*KF)**2
     1)/(E*ETDS)
      Y(K) = ( -A + PM*SQRT(A*A - 4.0*H))/2.0
      X(K) = X(1) + ((KF*SAN)**2  )/(E*(Y(K) - Y(1)))
      DELEP = X(K) - X(K - 1)
   45 DO 46 J = 3,K
      S(J) = -Y(K)-SO(J)
   46 CONTINUE
  345 CONTINUE
```

```
      STS = ST(I)
      DL = SIGN(DL,PM)
C
C   PRINTOUT
C
      STM = (ST(1) + ST(I))/2.0
      STA = ABS(ST(I) - ST(1))/2.0
      DM = (EPF)**(1.0/C)*((STA/KX)**(-1.0/(SHEX*C)))*(((1.0 - STM/SPF)*
     1*(1.0/(SHEX*C))) - 1.0)
      DAMAGE = DAMAGE + DM
      PSSUM = 0.0
      DELPEP(1) = 0.0
      IF (M.NE.NPRINT(JP)) GO TO 999
      JP = JP + 1
      PRINT 65
   65 FORMAT  (T11,'REV.',T25,'POINT',T39,'STRAIN',T55,'STRESS',
     1 T66,'DEL. P. STRAIN',T84,'P. STRAIN',T098,
     2 'MEAN STRESS',/)
      PRINT 67, M, EPT(1),ST(1),DELPEP(1),PSSUM,STM
   67 FORMAT (I13,T29,'1',1PE16.4,2PE16.4,1P2E16.4,
     1 2PE16.4)
      DO 420 J = 2,I
      PSSUM = PSSUM + DELPEP(J)
      IF(J.EQ.2) PRINT 69,J,EPT(J),ST(J),DELPEP(J),PSSUM
   69 FORMAT (I29,1PE16.4,2PE16.4,1PE16.4,1PE16.4,T098,'RES. STS.')
      IF(J.GE.3) PRINT 70,J,EPT(J),ST(J),DELPEP(J),PSSUM,S(J)
   70 FORMAT (I29,1PE16.4,2PE16.4,1PE16.4,1PE16.4,1PE16.4)
  420 CONTINUE
      PRINT 1001,DAMAGE
 1001 FORMAT(//T55,'DAMAGE = ',1PE16.6,////)
      GO TO 999
 1000 CONTINUE
      STM = (ST(1) + ST(I))/2.0
      STA = ABS(ST(I) - ST(1))/2.0
      DM = (EPF)**(1.0/C)*((STA/KX)**(-1.0/(SHEX*C)))*(((1.0 - STM/SPF)*
     1*(1.0/(SHEX*C))) - 1.0)
      DAMAGE = DAMAGE + DM
      PSSUM = 0.0
      DELPEP(1) = 0.0
      IF (M.NE.NPRINT(JP)) GO TO 999
      JP = JP + 1
      PRINT 65
      PRINT 67, M, EPT(1),ST(1),DELPEP(1),PSSUM,STM
      DO 421 J= 2,I
      PSSUM =PSSUM + DELPEP(J)
      IF(J.EQ.2) PRINT 69,J,EPT(J),ST(J),DELPEP(J),PSSUM
      IF(J.GE.3) PRINT 70,J,EPT(J),ST(J),DELPEP(J),PSSUM,S(J)
  421 CONTINUE
      PRINT 1002,DAMAGE
 1002 FORMAT(//T55,'DAMAGE = ',1PE16.6,////)
      CALL EXIT
  999 RETURN
      END
```

```
      SUBROUTINE FORMSS(AK,A1,PM,DELS,N,EI,SHEI,SB,ESLIDE,RC,IC,YIELD1)
C
C     CALCULATE FRICTIONAL STRESSES AND SPRING STIFFNESSES
C
      DIMENSION SB(150, 7),ESLIDE(150, 7)
      YIELD1 = +10000.
      AKI = 1.0/AK
C
C     SET FRICTION STRESSES
C
      SBI = AK*A1
      SB(3,IC) = -PM*YIELD1
      DELS1 = -PM*DELS
      SY = -PM*SBI
      DO 1 J = 4,N
      SB(J,IC) = SY
      SY = SY + DELS1
    1 CONTINUE
C
C     CALCULATE SPRING MODULI
C
      DSTS = SBI-YIELD1
      IF(DSTS) 4,4,2
    2 DELEP = DSTS*EI + (SBI*AKI)**SHEI
      ETI = DELEP/DSTS
      ESLIDE(3,IC) = ETI-EI
      DO 3 J= 4,N
      DELEP = DELS*EI + ((SBI+DELS)*AKI)**SHEI-(SBI*AKI)**SHEI
      ETI = DELEP/DELS
      ESLIDE(J,IC) = (ETI-EI)*(1.0-SBI/RC)
      SBI = SBI + DELS
    3 CONTINUE
      GO TO 5
    4 WRITE(6,602) DSTS,IC
  602 FORMAT(//,'WARNING---DSTS=',E12.4,'FOR IC=',I5,/
     1,'DECREASE THE INITIAL YIELD STRESS, YIELD1',//)
    5 CONTINUE
      RETURN
      END
```

```
      FUNCTION SOFF(ERANGE,NH)
C
C     DETERMINE THE STRESS OFFSET
C
      IF(ERANGE-.007) 5,1,2
    5 IF(NH.EQ.1) SOFF = 0.0
      IF(NH.EQ.2) SOFF = 0.0
      IF(NH.GE.3) SOFF= 4600000.*ERANGE - 32000.
      GO TO 3
    1 SOFF = 0.
      GO TO 3
    2 CONTINUE
      IF(NH.EQ.1) SOFF = 0.0
      IF(NH.EQ.2) SOFF = 0.0
      IF(NH.EQ.3) SOFF = 666000.*ERANGE - 16000.
      IF(NH.EQ.4) SOFF = 713000.*ERANGE - 14000.
      IF(NH.EQ.5) SOFF = 707000.*ERANGE - 12000.
      IF(NH.EQ.6) SOFF = 693000.*ERANGE - 10000.
      IF(NH.GE.7) SOFF = 700000.*ERANGE -  5000.
    3 CONTINUE
      RETURN
      END
```

```
C
C         INPUT DATA CARDS
C
C234567891234567891234567891234567891234567891234567891234567891234567891234567891234567891234567891
C
C         1
C 1.0000E+03  2.7500E+07  2.0000E-04
C 1.4600E-02  8.0000E-02  8.0000E-02
C 3.5740E+04  6.2000E+04  6.2000E+04
C 147400.000        0.271       -0.132       -0.451        0.249  158750.000
C       2.000
C 2.0000E+07
C       100
C 3.0000E+04 1
C-3.0000E+04 1
C 3.0000E+04 1
C-3.0000E+04 1
C 3.0000E+04 1
C        16
C         1          2          3          4          5          6          7          8
C         9         10         19         20         49         50         99        100
```

INPUT INFORMATION

CONSTANTS FORMING STRESS-STRAIN RELATION

STATIC STRENGTH COEFFICIENT =	35740.0	STATIC STRAIN HARDENING EXPONENT =	0.0146
CYCLIC STRENGTH COEFFICIENT =	158750.0	CYCLIC STRAIN HARDENING EXPONENT =	0.2490
INTERMEDIATE STRENGTH COEFFICIENT =	158750.0	INTERMEDIATE STRAIN HARDENING EXPONENT =	0.2490
MODULUS OF ELASTICITY=	27500000.0	FATIGUE STRENGTH COEFFICIENT=	147400.0000
MONOTONIC YIELD STRENGTH=	31560.9	FATIGUE DUCTILITY COEFFICIENT=	0.271
CYCLIC YIELD STRENGTH=	31367.1	FATIGUE STRENGTH EXPONENT =	-0.132
INTERMEDIATE YIELD STRENGTH=	31367.1	FATIGUE DUCTILITY EXPONENT=	-0.451
PLASTIC STRAIN OFFSET=	0.00020		
STRESS INCREMENT =	1000.0	MONOTONIC NO. OF ELEMENTS =	5
		CYCLIC NO. OF ELEMENTS =	31
		INTERMEDIATE NO. OF ELEMENTS =	31

FATIGUE STRENTHG RED. FACTOR = 2.00

RELAXING FUNCTION CONSTANTS

RELAXING CONSTANT = 20000000.0000

STRESS PEAKS:

ORDER	STRESS	DIRECTION
1	30.000000E 03	1
2	-30.000000E 03	1
3	30.000000E 03	1
4	-30.000000E 03	1
5	30.000000E 03	1

REV.	POINT	STRAIN	STRESS	DEL. P. STRAIN	P. STRAIN	MEAN STRESS
1	1	0.0	0.0	0.0	0.0	16.3284E 03
	2	3.6364E-04	10.0000E 03	0.0	0.0	RES. STS.
	3	1.3477E-03	31.5609E 03	1.9999E-04	1.9999E-04	-2.7804E 04
	4	2.8779E-03	32.5609E 03	1.4939E-03	1.6939E-03	-6.4371E 03
	5	4.0086E-03	32.6568E 03	1.1272E-03	2.8211E-03	-5.4371E 03
			DAMAGE =	8.695743E-06		
REV.	POINT	STRAIN	STRESS	DEL. P. STRAIN	P. STRAIN	MEAN STRESS
2	1	4.0086E-03	32.6568E 03	0.0	0.0	51.3216E 02
	2	3.4685E-03	17.8042E 03	0.0	0.0	RES. STS.
	3	1.6306E-03	-22.3925E 03	-3.7624E-04	-3.7624E-04	1.2392E 04
			DAMAGE =	1.221949E-06		
REV.	POINT	STRAIN	STRESS	DEL. P. STRAIN	P. STRAIN	MEAN STRESS
3	1	1.6306E-03	-22.3925E 03	0.0	0.0	29.7025E 02
	2	2.3579E-03	-23.9248E 02	0.0	0.0	RES. STS.
	3	3.7340E-03	27.7041E 03	2.8171E-04	2.8171E-04	-1.8333E 04
	4	3.7340E-03	27.7041E 03	0.0	2.8171E-04	-7.0659E 03
	5	3.7340E-03	27.7041E 03	0.0	2.8171E-04	-6.0659E 03
	6	3.7340E-03	27.7041E 03	0.0	2.8171E-04	-5.0659E 03
	7	3.7340E-03	27.7041E 03	0.0	2.8171E-04	-4.0659E 03
	8	3.7340E-03	27.7041E 03	0.0	2.8171E-04	-3.0659E 03
	9	3.7340E-03	27.7041E 03	0.0	2.8171E-04	-2.0659E 03
	10	4.1469E-03	28.2671E 03	3.9245E-04	6.7416E-04	-1.0659E 03
	11	4.2113E-03	28.3330E 03	6.2017E-05	7.3017E-04	-6.5918E 01
			DAMAGE =	7.311484E-07		

REV.	POINT	STRAIN	STRESS	DEL. P. STRAIN	P. STRAIN	MEAN STRESS
4	1	4.2113E-03	28.3330E 03	0.0	0.0	42.8330E 02
	2	3.4841E-03	83.3299E 02	0.0	0.0	RES. STS.
	3	2.4521E-03	-14.2369E 03	-2.1126E-04	-2.1126E-04	9.7664E 03
	4	2.1874E-03	-16.2369E 03	-1.9198E-04	-4.0323E-04	-1.5364E 03
	5	1.8408E-03	-18.2369E 03	-2.7382E-04	-6.7705E-04	-2.5364E 03
	6	1.4897E-03	-19.7664E 03	-2.9552E-04	-9.7257E-04	-3.5364E 03

DAMAGE = 1.089529E-06

REV.	POINT	STRAIN	STRESS	DEL. P. STRAIN	P. STRAIN	MEAN STRESS
5	1	1.4897E-03	-19.7664E 03	0.0	0.0	36.9249E 02
	2	2.2170E-03	23.3617E 01	0.0	0.0	RES. STS.
	3	3.1889E-03	21.4905E 03	1.9897E-04	1.9897E-04	-1.7151E 04
	4	3.4537E-03	23.4905E 03	1.9205E-04	3.9101E-04	-7.1972E 03
	5	3.8003E-03	25.4905E 03	2.7392E-04	6.6493E-04	-6.1972E 03
	6	4.1516E-03	27.0200E 03	2.9562E-04	9.6055E-04	-5.1972E 03
	7	4.1516E-03	27.0200E 03	0.0	9.6055E-04	-4.1972E 03
	8	4.1516E-03	27.0200E 03	0.0	9.6055E-04	-3.1972E 03
	9	4.1516E-03	27.0200E 03	0.0	9.6055E-04	-2.1972E 03
	10	4.1516E-03	27.0200E 03	0.0	9.6055E-04	-1.1972E 03
	11	4.2799E-03	27.1514E 03	1.2353E-04	1.0841E-03	-1.9724E 02

DAMAGE = 1.222881E-06

REV.	POINT	STRAIN	STRESS	DEL. P. STRAIN	P. STRAIN	MEAN STRESS
6	1	4.2799E-03	27.1514E 03	0.0	0.0	39.4607E 02
	2	3.5526E-03	71.5136E 02	0.0	0.0	RES. STS.
	3	2.6351E-03	-12.9145E 03	-1.8782E-04	-1.8782E-04	9.2592E 03
	4	2.3704E-03	-14.9145E 03	-1.9196E-04	-3.7978E-04	-8.5255E 02
	5	2.0239E-03	-16.9145E 03	-2.7380E-04	-6.5358E-04	-1.8526E 03
	6	1.5648E-03	-18.9145E 03	-3.8639E-04	-1.0400E-03	-2.8526E 03
	7	1.4592E-03	-19.2592E 03	-9.3040E-05	-1.1330E-03	-3.8526E 03

DAMAGE = 1.325603E-06

REV.	POINT	STRAIN	STRESS	DEL. P. STRAIN	P. STRAIN	MEAN STRESS
7	1	1.4592E-03	-19.2592E 03	0.0	0.0	40.2645E 02
	2	2.1865E-03	74.0777E 01	0.0	0.0	RES. STS.
	3	3.1144E-03	21.0345E 03	1.8995E-04	1.8995E-04	-1.7312E 04
	4	3.3792E-03	23.0345E 03	1.9204E-04	3.8199E-04	-7.1302E 03
	5	3.7258E-03	25.0345E 03	2.7391E-04	6.5590E-04	-6.1302E 03
	6	4.1851E-03	27.0345E 03	3.8655E-04	1.0425E-03	-5.1302E 03
	7	4.2701E-03	27.3121E 03	7.4981E-05	1.1174E-03	-4.1302E 03

DAMAGE = 1.301025E-06

REV.	POINT	STRAIN	STRESS	DEL. P. STRAIN	P. STRAIN	MEAN STRESS
8	1	4.2701E-03	27.3121E 03	0.0	0.0	40.0898E 02
	2	3.5429E-03	73.1213E 02	0.0	0.0	RES. STS.
	3	2.6128E-03	-13.0293E 03	-1.9040E-04	-1.9040E-04	9.2942E 03
	4	2.3481E-03	-15.0293E 03	-1.9197E-04	-3.8236E-04	-8.6535E 02
	5	2.0016E-03	-17.0293E 03	-2.7380E-04	-6.5616E-04	-1.8654E 03
	6	1.5424E-03	-19.0293E 03	-3.8639E-04	-1.0426E-03	-2.8654E 03
	7	1.4613E-03	-19.2942E 03	-7.1497E-05	-1.1141E-03	-3.8654E 03

DAMAGE = 1.293040E-06

REV.	POINT	STRAIN	STRESS	DEL. P. STRAIN	P. STRAIN	MEAN STRESS
9	1	1.4613E-03	-19.2942E 03	0.0	0.0	39.9880E 02
	2	2.1886E-03	70.5844E 01	0.0	0.0	RES. STS.
	3	3.1174E-03	21.0200E 03	1.9014E-04	1.9014E-04	-1.7292E 04

4	3.3822E-03	23.0200E 03	1.9204E-04	3.8219E-04	-7.1371E 03
5	3.7288E-03	25.0200E 03	2.7391E-04	6.5610E-04	-6.1371E 03
6	4.1881E-03	27.0200E 03	3.8655E-04	1.0426E-03	-5.1371E 03
7	4.2714E-03	27.2918E 03	7.3379E-05	1.1160E-03	-4.1371E 03

DAMAGE = 1.296959E-06

REV.	POINT	STRAIN	STRESS	DEL. P. STRAIN	P. STRAIN	MEAN STRESS
10	1	4.2714E-03	27.2918E 03	0.0	0.0	39.9901E 02
	2	3.5441E-03	72.9175E 02	0.0	0.0	RES. STS.
	3	2.6153E-03	-13.0204E 03	-1.9012E-04	-1.9012E-04	9.2937E 03
	4	2.3507E-03	-15.0204E 03	-1.9197E-04	-3.8209E-04	-8.6375E 02
	5	2.0041E-03	-17.0204E 03	-2.7380E-04	-6.5589E-04	-1.8638E 03
	6	1.5450E-03	-19.0204E 03	-3.8639E-04	-1.0423E-03	-2.8638E 03
	7	1.4613E-03	-19.2937E 03	-7.3783E-05	-1.1161E-03	-3.8638E 03

DAMAGE = 1.297057E-06

REV.	POINT	STRAIN	STRESS	DEL. P. STRAIN	P. STRAIN	MEAN STRESS
19	1	1.4615E-03	-19.2977E 03	0.0	0.0	39.9542E 02
	2	2.1888E-03	70.2262E 01	0.0	0.0	RES. STS.
	3	3.1177E-03	21.0170E 03	1.9015E-04	1.9015E-04	-1.7289E 04
	4	3.3824E-03	23.0170E 03	1.9204E-04	3.8219E-04	-7.1313E 03
	5	3.7291E-03	25.0170E 03	2.7391E-04	6.5610E-04	-6.1313E 03
	6	4.1883E-03	27.0170E 03	3.8655E-04	1.0426E-03	-5.1313E 03
	7	4.2715E-03	27.2886E 03	7.3340E-05	1.1160E-03	-4.1313E 03

DAMAGE = 1.296712E-06

REV.	POINT	STRAIN	STRESS	DEL. P. STRAIN	P. STRAIN	MEAN STRESS
20	1	4.2715E-03	27.2886E 03	0.0	0.0	39.9491E 02
	2	3.5443E-03	72.8857E 02	0.0	0.0	RES. STS.
	3	2.6154E-03	-13.0262E 03	-1.9015E-04	-1.9015E-04	9.2987E 03
	4	2.3507E-03	-15.0262E 03	-1.9197E-04	-3.8211E-04	-8.5869E 02
	5	2.0042E-03	-17.0262E 03	-2.7380E-04	-6.5591E-04	-1.8587E 03
	6	1.5451E-03	-19.0262E 03	-3.8639E-04	-1.0423E-03	-2.8587E 03
	7	1.4616E-03	-19.2987E 03	-7.3582E-05	-1.1159E-03	-3.8587E 03

DAMAGE = 1.296509E-06

REV.	POINT	STRAIN	STRESS	DEL. P. STRAIN	P. STRAIN	MEAN STRESS
49	1	1.4624E-03	-19.3128E 03	0.0	0.0	39.8037E 02
	2	2.1897E-03	68.7211E 01	0.0	0.0	RES. STS.
	3	3.1185E-03	21.0019E 03	1.9015E-04	1.9015E-04	-1.7274E 04
	4	3.3833E-03	23.0019E 03	1.9204E-04	3.8219E-04	-7.1162E 03
	5	3.7300E-03	25.0019E 03	2.7391E-04	6.5610E-04	-6.1162E 03
	6	4.1892E-03	27.0019E 03	3.8655E-04	1.0426E-03	-5.1162E 03
	7	4.2724E-03	27.2735E 03	7.3340E-05	1.1160E-03	-4.1162E 03

DAMAGE = 1.295895E-06

REV.	POINT	STRAIN	STRESS	DEL. P. STRAIN	P. STRAIN	MEAN STRESS
50	1	4.2724E-03	27.2735E 03	0.0	0.0	39.7986E 02
	2	3.5452E-03	72.7352E 02	0.0	0.0	RES. STS.
	3	2.6163E-03	-13.0412E 03	-1.9015E-04	-1.9015E-04	9.3138E 03
	4	2.3516E-03	-15.0412E 03	-1.9197E-04	-3.8211E-04	-8.4304E 02
	5	2.0051E-03	-17.0412E 03	-2.7380E-04	-6.5592E-04	-1.8436E 03
	6	1.5460E-03	-19.0412E 03	-3.8639E-04	-1.0423E-03	-2.8436E 03
	7	1.4625E-03	-19.3138E 03	-7.3581E-05	-1.1159E-03	-3.8436E 03

DAMAGE = 1.295693E-06

REV.	POINT	STRAIN	STRESS	DEL. P. STRAIN	P. STRAIN	MEAN STRESS
99	1	1.4639E-03	-19.3377E 03	0.0	0.0	39.5544E 02
	2	2.1912E-03	66.2285E 01	0.0	0.0	RES. STS.
	3	3.1200E-03	20.9770E 03	1.9015E-04	1.9015E-04	-1.7249E 04
	4	3.3848E-03	22.9770E 03	1.9204E-04	3.8219E-04	-7.0913E 03
	5	3.7314E-03	24.9770E 03	2.7391E-04	6.5610E-04	-6.0913E 03
	6	4.1907E-03	26.9770E 03	3.8655E-04	1.0426E-03	-5.0913E 03
	7	4.2739E-03	27.2486E 03	7.3340E-05	1.1160E-03	-4.0913E 03

DAMAGE = 1.294546E-06

REV.	POINT	STRAIN	STRESS	DEL. P. STRAIN	P. STRAIN	MEAN STRESS
100	1	4.2739E-03	27.2486E 03	0.0	0.0	39.5494E 02
	2	3.5467E-03	72.4859E 02	0.0	0.0	RES. STS.
	3	2.6178E-03	-13.0661E 03	-1.9015E-04	-1.9015E-04	9.3387E 03
	4	2.3531E-03	-15.0661E 03	-1.9197E-04	-3.8211E-04	-8.1872E 02
	5	2.0066E-03	-17.0661E 03	-2.7380E-04	-6.5592E-04	-1.8187E 03
	6	1.5474E-03	-19.0661E 03	-3.8640E-04	-1.0423E-03	-2.8187E 03
	7	1.4640E-03	-19.3387E 03	-7.3580E-05	-1.1159E-03	-3.8187E 03

DAMAGE = 1.294346E-06

THE DAMAGE FOR THE REVERSAL 100 IS 1.294346E-06 THE TOTAL DAMAGE UP TO THIS REVERSAL IS 1.360822E-04

LIFE OF THE ESPECIMEN = 772586 REVERSALS

APPENDIX C

ANALYSIS OF THE CYCLIC RELAXATION OF THE RESIDUAL STRESSES

The effect of the residual stresses on the fatigue performance of welded structures is, at the present time, not fully understood. Possible causes of this lack of knowledge have been the limitations of the available methods for their determination, the absence of an analytical model to predict and quantify their influence and their changes throughout the fatigue life of the welded parts, etc.

Most of the studies on the influence of residual stresses on the fatigue life of welds have been concerned only with the initial residual stresses present just before fatigue cycling (81-86). These studies however, do not show the changes of the residual stresses with fatigue cycles so their conclusions are very limited. Few studies have been concerned with periodic determinations of the residual stresses during the fatigue process (87-90), unfortunately they require sophisticated equipment and an enormous amount of time for their determination. For both approaches, the influence of the variables which are known to influence the relaxation of the residual stresses (material properties, stress amplitude, magnitude and sense of the initial residual stress, etc.,) have been controversial, mainly because of the lacking of a unified model to explain the effect of these variables.

The purpose of this appendix is to show that the limitations of the above approaches can be overcome if use is made of the model proposed by Morrow, et al. (91,92). This model is based on the assumption that the

effect of the residual stresses and its cyclic dependent stress relaxation is analogous to that of a mechanically induced mean stress.

A. Cyclic Dependent Stress Relaxation Tests in Smooth Specimens for A-36 Steel Under Constant Strain Amplitude Cycling

For a specific material, the two variables which influence the mean stress relaxation are the mean strain and the strain amplitude. No doubt exists that the strain amplitude is the most important variable influencing this relaxation (49,54,91). Mean strains do not appear to have a significant influence on the relaxation behavior as shown in Fig. 19 and confirmed by Jhansale and Topper (54).

Data from tests in which the mean strains were held constant but in which the strain amplitude was allowed to vary are shown in Figs. 17 and 18. The data presented in Fig. 18 are now replotted in Fig. C-1. Non-dimensional values of the mean stress expressed as ratios of the current mean stress to the initial mean stress (corresponding to the first reversal) are plotted against the number of reversals. A least-squares fit to the data point for each strain amplitude was made assuming that a relationship exists between the ratio $\sigma_{o,2N}/\sigma_{o,i}$ and (2N-1) of the form (54),

$$\frac{\sigma_{o,2N}}{\sigma_{o,i}} = (2N-1)^{k} \qquad (2N>1) \qquad (C-1)$$

where,

$\sigma_{o,2N}$ = Mean stress at reversal 2N

$\sigma_{o,i}$ = Initial mean stress

$$k = k(\Delta\varepsilon/2)$$

The dependence of k with the strain amplitude was investigated assuming that an equation of the form,

$$k = A + B\ (\Delta\varepsilon/2) + C\ (\Delta\varepsilon/2)^2 \qquad (C\text{-}2)$$

where A, B and C are constants, fits the data in the range of strain amplitude under study. Figure C-2 shows that the least squares fit to the data point by Eq. C-2 is,

$$k = 0.139 - 247.6\ (\Delta\varepsilon/2) + 30888.9\ (\Delta\varepsilon/2)^2 \qquad (C\text{-}3)$$

If the expression for k (Eq. C-3) is substituted into Eq. C-1, the dependence of the mean stress with the strain amplitude and with the number of reversals is obtained,

$$\frac{\sigma_{o,2N}}{\sigma_{o,i}} = (2N\text{-}1)^{[0.139 - 247.6\ (\Delta\varepsilon/2) + 30888.9\ (\Delta\varepsilon/2)^2]} \qquad (C\text{-}4)$$

Equation C-4 shows that the relaxation behavior of the mean stress is a strong function of the strain amplitude which is agreement with previous studies (49, 54,91,92). Moreover, Eq. C-4 shows that for any value of (2N-1), the limiting condition for no relaxation of the mean stress is k = 0, i.e., when $\sigma_{o,2N}/\sigma_{o,i} = 1$, which corresponds to $\Delta\varepsilon/2 = 0.00061$ according to Eq. C-3. If this value of the strain amplitude is inserted in the cyclic stress-strain curve (Fig. 12), it can be seen that it corresponds to the cyclic yield strain. Also, if it is assumed that the cyclic yield stress corresponds to the fatigue limit, as confirmed by the constant strain amplitude tests and by Martin (49) and

Mitchell and Wetzel (93), the above result can be interpreted as a criterion which can be used to determine when the mean stress will or will not relax.

From Eq. C-1 the rate of relaxation of the mean stress is,

$$\frac{\partial(\sigma_{o,2N})}{\partial(2N-1)} = \frac{k\,\sigma_{o,i}}{(2N-1)}\,(2N-1)^{k} = \frac{k\,\sigma_{o,2N}}{(2N-1)} \qquad (C-4)$$

from which it can be seen that

1. The rate of relaxation is higher for higher initial mean stresses, $\sigma_{o,i}$.
2. The rate of relaxation diminishes as the number of reversals gets very large.
3. The rate of relaxation is a function of the current mean stress, $\sigma_{o,2N}$.
4. The rate of relaxation depends on the strain amplitude, higher rates of relaxation correspond to larger strain amplitudes, and is nil for strain amplitude of 0.00061 (cyclic yield strain).

The behavior of the mean stress as predicted by Eqs. C-1 and C-4 qualitatively agrees with the results reported by Morrow, et al. (91) for steels with different hardnesses.

B. Cyclic Relaxation of the Mean Stress in Notched Members

The analysis of the cyclic-dependent mean stress relaxation as previously presented can be extended to notched members. To relate local stress and strain to nominal stress, use is made of the modified Neuber's

equation (Eq. 10), and to relate local stress to local strain, the equation proposed by Morrow (31) for the cyclic stress-strain curve (Eq. 14) is used. Eliminating $\Delta\sigma$ from these two equations, Eq. C-5 results:

$$\frac{\Delta\varepsilon}{2} = \frac{(K_f\,\Delta S)^2}{2E(\Delta\varepsilon)} + \left[\frac{(K_f\,\Delta S)^2}{2EK'(\Delta\varepsilon)}\right]^{\frac{1}{n'}} \qquad \text{(C-5)}$$

To know $\Delta\varepsilon/2$, Eq. C-5 has to be solved by trial and error or by graphical methods or by using the low cycle fatigue rheological model. Once $\Delta\varepsilon/2$ is known as a function of the remote applied stress range and of the fatigue notch factor, the mean stress at any given reversal can be calculated using Eq. C-4.

C. Cyclic Relaxation of the Residual Stresses in Welds Under Zero to Tension Loadings

1. Analysis

The results previously presented can be used to study and to predict the cyclic relaxation of the residual stresses in welds for 0-T loading. To do this, the only relationship which is needed is the one relating the values of the residual stresses at any reversal with the local stress amplitude and with the mean stress at any reversal. With reference to Fig. C-3, which represents a notch-root hysteresis loop, the following relationship holds at any reversal;

$$|\sigma_{min,2N}| = |\sigma_{residual,2N}| = \Delta\sigma/2 - \sigma_{o,2N} \qquad \text{(C-6)}$$

where,

$\sigma_{min,2N}$ = Minimum value of the local stress at any reversal, 2N

$\sigma_{o,2N}$ = Mean stress at any reversal, 2N

Combining Eq. C-6 and Eq. C-1, the current value of the residual stress can be expressed as;

$$|\sigma_{residual,2N}| = \Delta\sigma/2 - \sigma_{o,i}\,(2N-1)^{k} \qquad (C\text{-}7)$$

The values of $\Delta\sigma/2$ and $\Delta\epsilon/2$ can be calculated as previously mentioned, and the value of $\sigma_{o,i}$ can be estimated using the low cycle fatigue rheological model after application of one cycle.

If for the sake of simplicity, the equation for the stable cyclic stress-strain curve is represented by

$$\frac{\Delta\epsilon}{2} \approx \left(\frac{\Delta\sigma/2}{K'}\right)^{1/n'} \qquad (C\text{-}8)$$

then, its simultaneous solution with the modified Neuber's equation yields the following expressions for the local strain and stress amplitude as a function of the applied remote stress;

$$\frac{\Delta\epsilon}{2} \approx \left[\frac{(K_f\,\Delta S)^2}{4EK'}\right]^{1/(1+n')} \qquad (C\text{-}9)$$

and

$$\frac{\Delta\sigma}{2} \approx K'\left[\frac{(K_f\,\Delta S)^2}{4EK'}\right]^{n'/(1+n')} \qquad (C\text{-}10)$$

Replacing Eqs. C-9 and C-10 into Eq. C-7, the following expression results:

$$|\sigma_{residual,2N}| = K'\left[\frac{(K_f\Delta S)^2}{4EK'}\right]^{\frac{n'}{1+n'}} - \sigma_{o,i}(2N-1)\left\{A+B\left[\frac{(K_f\Delta S)^2}{4EK'}\right]^{\frac{1}{1+n'}} + C\left[\frac{(K_f\Delta S)^2}{4EK'}\right]^{\frac{2}{1+n'}}\right\} \quad \text{(C-11)}$$

Equation C-11 shows that the residual stress after 2N reversals depends on the local stress amplitude, the remotely applied stress range, the initial mean stress, the fatigue notch factor and on the cyclic strain hardening exponent and cyclic strength coefficient. Moreover, Eq. C-11 shows that in order to calculate the residual stresses at any given reversal, the only parameter, besides material constants, which is needed is the initial mean stress. Although the concepts developed have been based on data from A-36 steel, it is believed that a similar formulation can be carried out for any other material. If this is accepted then, the determination of the residual stresses has to be done only once and the cumbersome experiments used to determine the residual stresses are replaced by the rather easy low cycle fatigue type of experiments for the relaxation of mean stresses.

To illustrate the use of Eq. C-11 for predicting the residual stresses and their relaxation, a hypothetical butt weld with $K_f = 2.20$ and with initial residual stress of +12.5 or -17.5 ksi at the toe of the weld will be discussed. The material properties at the toe of the weld are assumed to be identical to those of A-36 steel and nominal stresses of 24.0 and 36.0 ksi (zero to tension) will be applied.

Using the low cycle fatigue rheological model, tensile residual stress of 12.5 ksi was simulated by precompressing the simulated specimen until upon unloading, the stress was 12.5 ksi ($\varepsilon = 0.00$). From this point, a nominal

stress of 24 or 36 ksi was applied until the product of the local stress and local strain satisfied the Neuber's equation. Figure C-4 shows the simulation of +12.5 residual stress and the local hysteresis loop obtained.* Simulation of -17.5 ksi residual stress was performed using a similar procedure to the one described. Initial mean stresses and stress and strain amplitudes for the two cases considered are summarized below:

S (ksi)	$\Delta\sigma/2$ (ksi)	$\Delta\varepsilon/2$	$\sigma_{residual}$ = 12.5ksi $\sigma_{o,i}$ (ksi)	$\sigma_{residual}$ =-17.5ksi $\sigma_{o,i}$ (ksi)
33.0	26.30	0.00183	5.65	3.56
24.0	21.50	0.00118	5.65	3.25

The predicted residual stresses, as given by Eq. C-11 are shown in Fig. C-5. This figure shows that for A-36 steel under zero-to-tension fatigue loadings, an initial tensile residual stress is "washed out" in the first fatigue cycle and changed to compressive residual stresses which relaxes to a stable value at long life. The initial compressive stress (-17.5 ksi) remains compressive after cycling but also relaxes to a stable value at long life. At long lives and for the same remotely applied stress range, initial tensile or compressive residual stresses converge to a single stable value.

2. Comparison With Actual Data

In order to test the predicted residual stresses in butt welds as a function of fatigue cycles, x-ray residual stress measurements were made on

* The low cycle fatigue rheological model was used for this simulation because it gives a more accurate determination of the initial mean stress than using analytical expressions. It was shown that A-36 steel does not have a truly stable cyclic stress-strain curve as represented by Eq. 14.

an AMR Microfocus unit. Prior to the experimental work, the x-ray machine was aligned and calibrated with a strip of Ferrovac-E (zero check) and with a load ring similar to that described by Ricklefs and Evans (94).

Residual stress measurements were made using the two-exposure x-ray diffractometer technique (95). Vanadium filtered chromium K_α radiation (40 KV, 3ma) diffracted from the {211} crystallographic planes provided the best resolution and peak heights in the high 2θ region between 156 and 157 deg. 2θ.

From the Elasticity Theory (96), the residual stress, $\sigma_{residual}$, can be calculated from,

$$\sigma_{residual} = K\,(2\theta_{\perp} - 2\theta_{\psi}) \qquad \text{(C-12)}$$

where,

$$K = \left(\frac{E}{1+\nu}\right)\left(\frac{1}{\sin^2\psi}\right)\left(\frac{\cot\theta}{2}\right)\left(\frac{\pi}{180}\right)$$

and

K = Stress factor, ksi/deg 2θ

E = Young's modulus, ksi

ν = Poisson's ratio

ψ = Angle of rotation, deg.

θ = Bragg angle, deg.

$2\theta_{\perp}$ = Diffracted angle for $\psi = 0$

$2\theta_{\psi}$ = Diffracted angle for $\psi = \psi$

Calibration of the x-ray machine was performed by elastically straining the load ring at known strains and measuring the corresponding $(2\theta_{\psi=0} - 2\theta_{\psi=45})$ difference. (All the x-ray residual stress measurements

were made with the specimens at normal incidence, ψ = 0 deg. and with the specimens rotated 45 deg. from normal incidence, ψ = 45 deg.). The elastic strains, measured with Micromeasurements EA-06-250BG-120 strain gages mounted on the load ring outer surface, were converted to stress using Hooke's law; the stresses were calculated from the shift of the diffracted peaks and with the help of Eq. C-12 using a stress constant K, equal to 86.3 ksi/deg 2θ (95).

Determination of the 2θ diffraction peak positions was performed using the three-point parabola method of Koistinen and Marburger (97). Intensity data were corrected with the appropriate Lorentz-Polarization factor and absorption correction. A minimum of two 100,000 unit counts was taken as the uncorrected intensity data. Figure C-6 shows the results of the calibration.

Butt welded specimens made from A-36 steel were polished in areas close to the toes of the welds with emery papers up to 4/0 and chemically polished with the solution previously cited. Before fatigue testing, welding residual stresses were determined in areas as close as possible to the toe of the weld. Slits were designed such that the area irradiated on the specimen corresponded to a strip of 1/8 in. wide and 1 in. long. Additional stress measurements were made at intervals. All of these measurements were made by removing the specimen from the fatigue machine and placing it in the diffractometer.

Figures C-7 and C-8 show the results of the residual stress measurements and the relaxation of the residual stresses throughout the life of the specimens. These specimens were tested under zero to tension fatigue loading at stresses of 33.0 and 24.0 ksi respectively. Also included in these

figures are the predicted values of the residual stresses according to Eq. C-11 and previously discussed. Reasonable agreement between the predicted and the experimentally determined residual stresses is noticed for the cases of an initial compressive residual stress and a rather poor agreement between the predicted and experimentally determined residual stresses for the cases of a tensile residual stress. This lack of agreement is believed to be the result of the large area used in the experimental determination of the residual stresses. The results of the finite element method, as discussed in Appendix A, show that the maximum value of the longitudinal stress occurs on a highly localized area at the toe of the weld and that the stress gradient in this area is so steep that the longitudinal stress decreases by 30 percent over a distance of only 0.01 in. away from the point of maximum stress. This means that if residual stresses are to be accurately measured, the width of the area irradiated on the specimen has to be less than 0.01 in.; however, due to the limitations of the available equipment, the width used was 12 times larger than the permissible one.

D. Summary

An analysis of the cyclic relaxation of the mean stress was performed for smooth and notched specimens. From the analysis, the relaxation of the mean stress depends on the cyclic properties (n',K'), on the initial mean stress and on the remotely applied stress for smooth specimens. For notched specimens, the relaxation of the mean stress besides being dependent on the previous parameters also depends on the fatigue notch factor, K_f, and on the range of the remotely applied loading. Implied in the formulation of the

problem is the cyclic yield stress of the material. For "soft" materials, like A-36 steel whose cyclic yield stress is low, cyclic relaxation of the mean stress seems to be very rapid for stresses above the fatigue limit; on the other hand, for "hard" materials, like HY-130 steel, cyclic relaxation of the residual stress may not occur even when fatigue cycled at stresses above their fatigue limit.

Cyclic relaxation of the residual stresses was treated as an extension of the cyclic relaxation of the mean stress. A method was proposed to predict the cyclic relaxation of the welding residual stresses and an attempt was made to check the validity of the method with actual data. However, since the area on which the relaxation of the residual stresses takes place is very small, the use of conventional x-ray techniques proved to be unsatisfactory for the purpose of comparison.

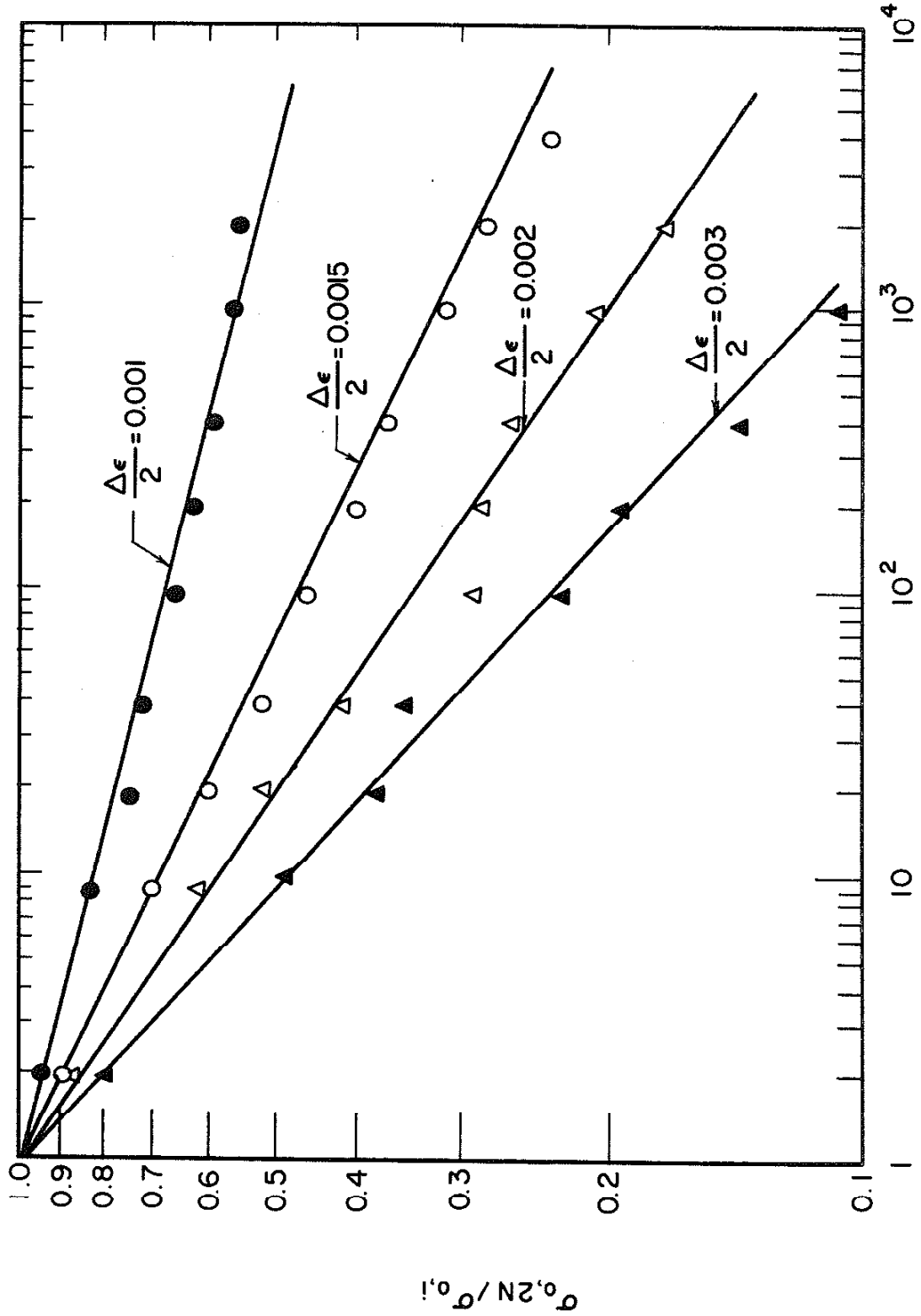

Fig. C-1 Cyclic Relaxation of the Mean Stress for A-36 Steel (Constant Mean Strain of +0.005)

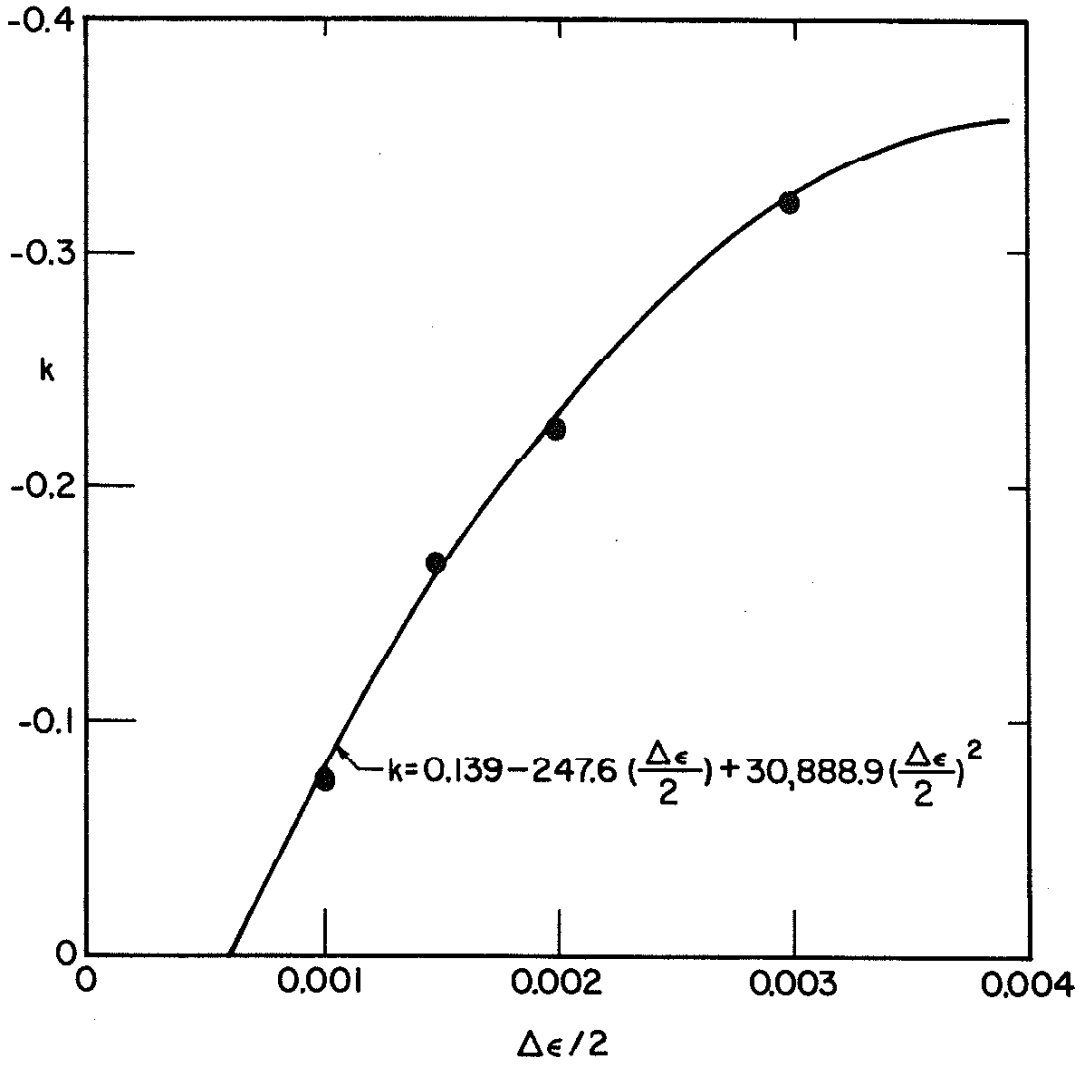

Fig. C-2 Dependence of k with the Strain Amplitude $\frac{\Delta\varepsilon}{2}$ for A-36 Steel

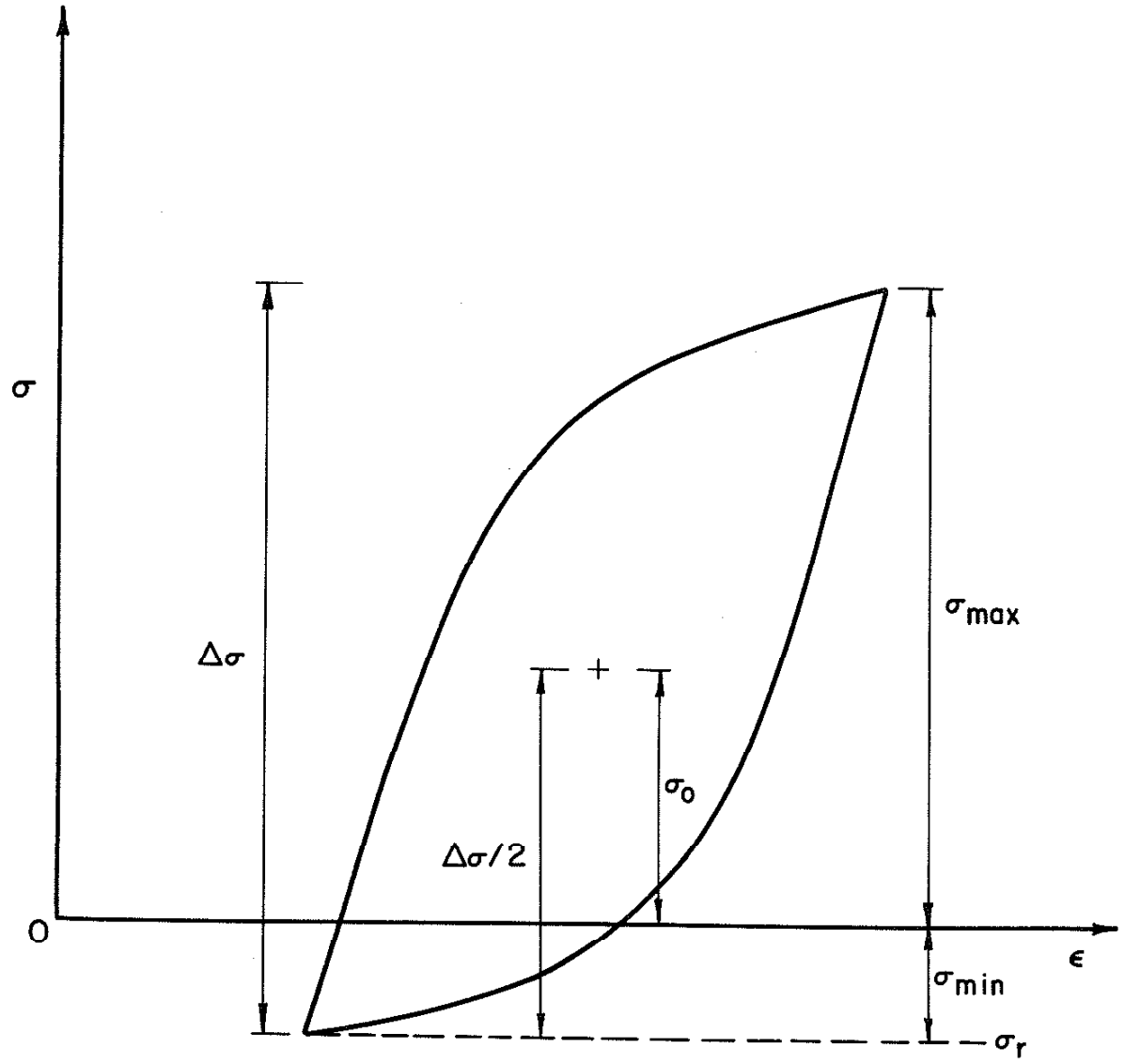

Fig. C-3 Local Hysteresis Loop and Parameters under Zero-to-Tension Fatigue Loading

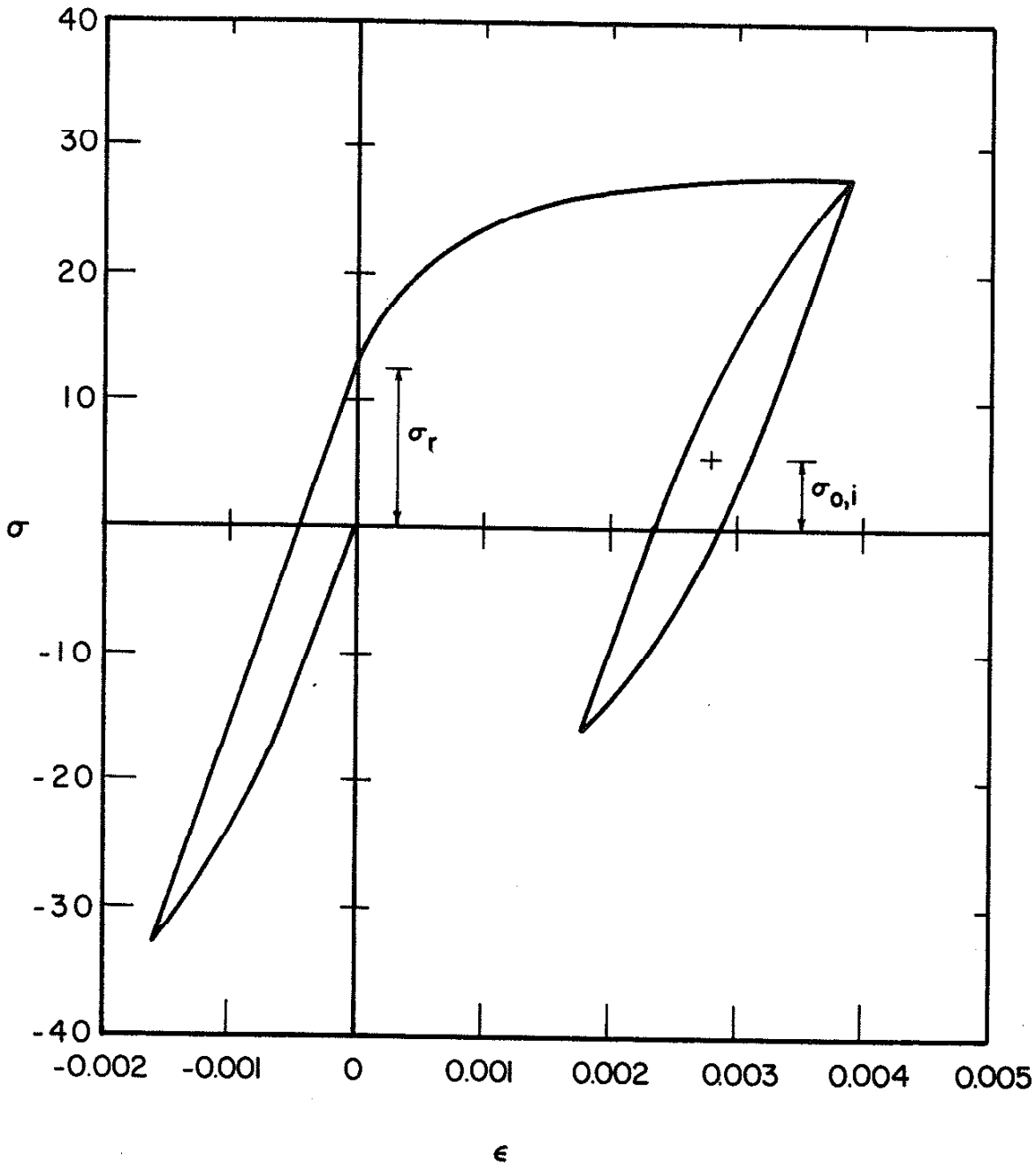

Fig. C-4 Simulation of the Residual Stress, σ_r, and of the Initial Mean Stress, $\sigma_{0,i}$. (A-36 Steel, ΔS = 24 ksi, K_f = 2.20, R = 0)

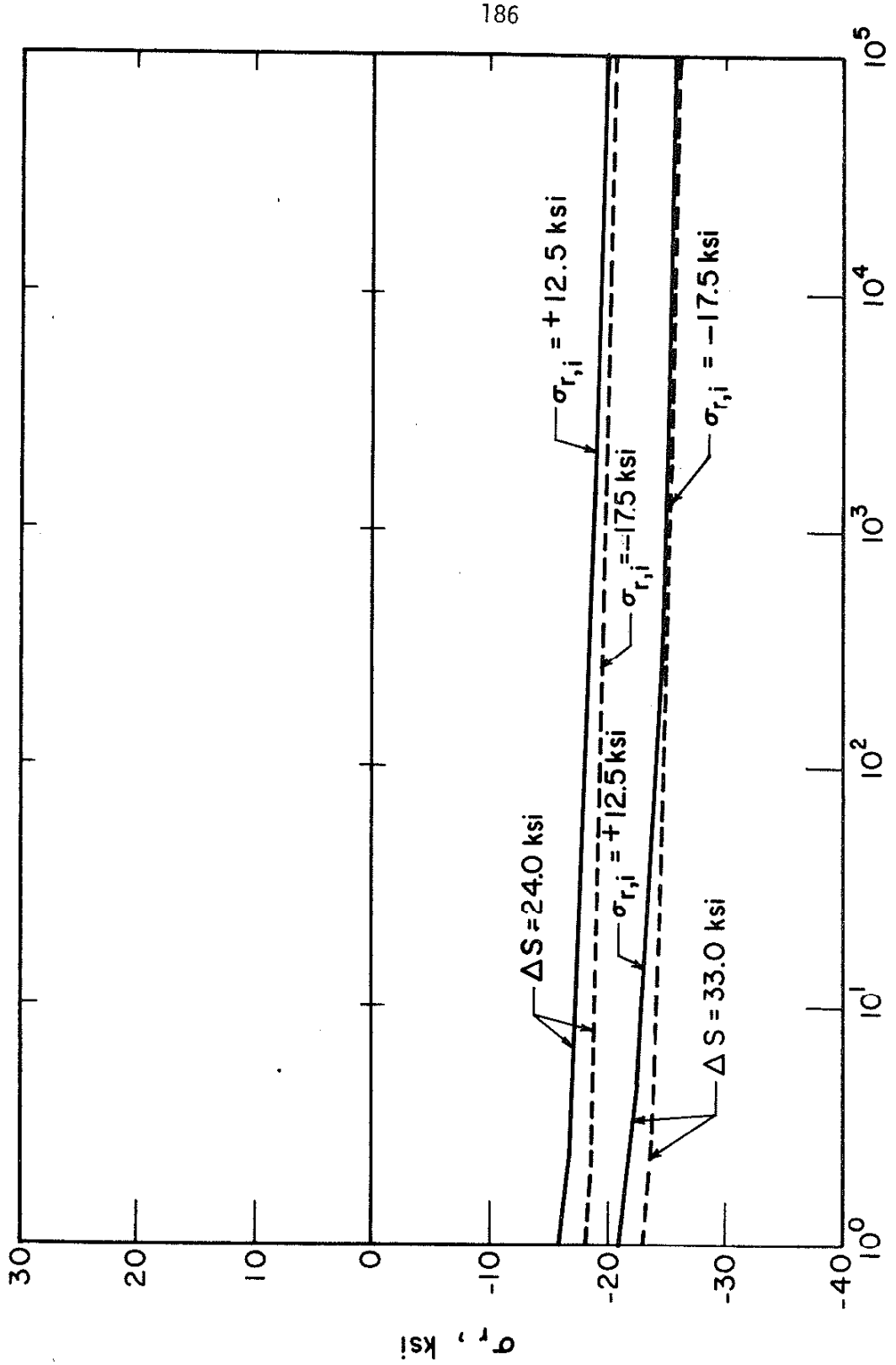

Fig. C-5 Predicted Cyclic Relaxation of Initial Residual Stresses of +12.5 ksi and of -17.5 ksi under Nominal Stress Ranges of 33.0 and 24.0 ksi (A-36 Steel, $K_f = 2.20$, $R = 0$)

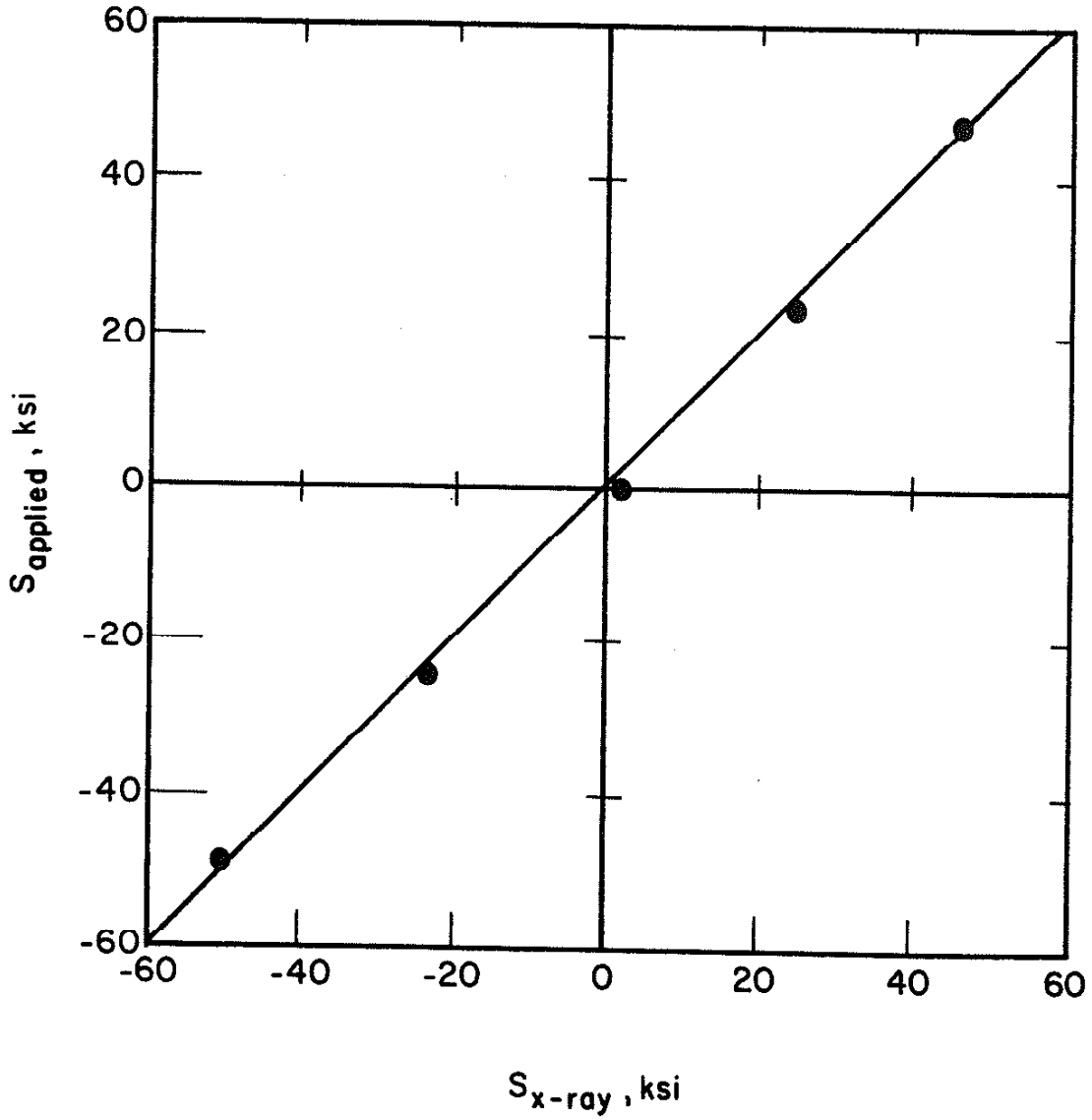

Fig. C-6 Calibration Results of the X-Ray Machine. (Load Ring Made of Quenched and Tempered 1045 Steel)

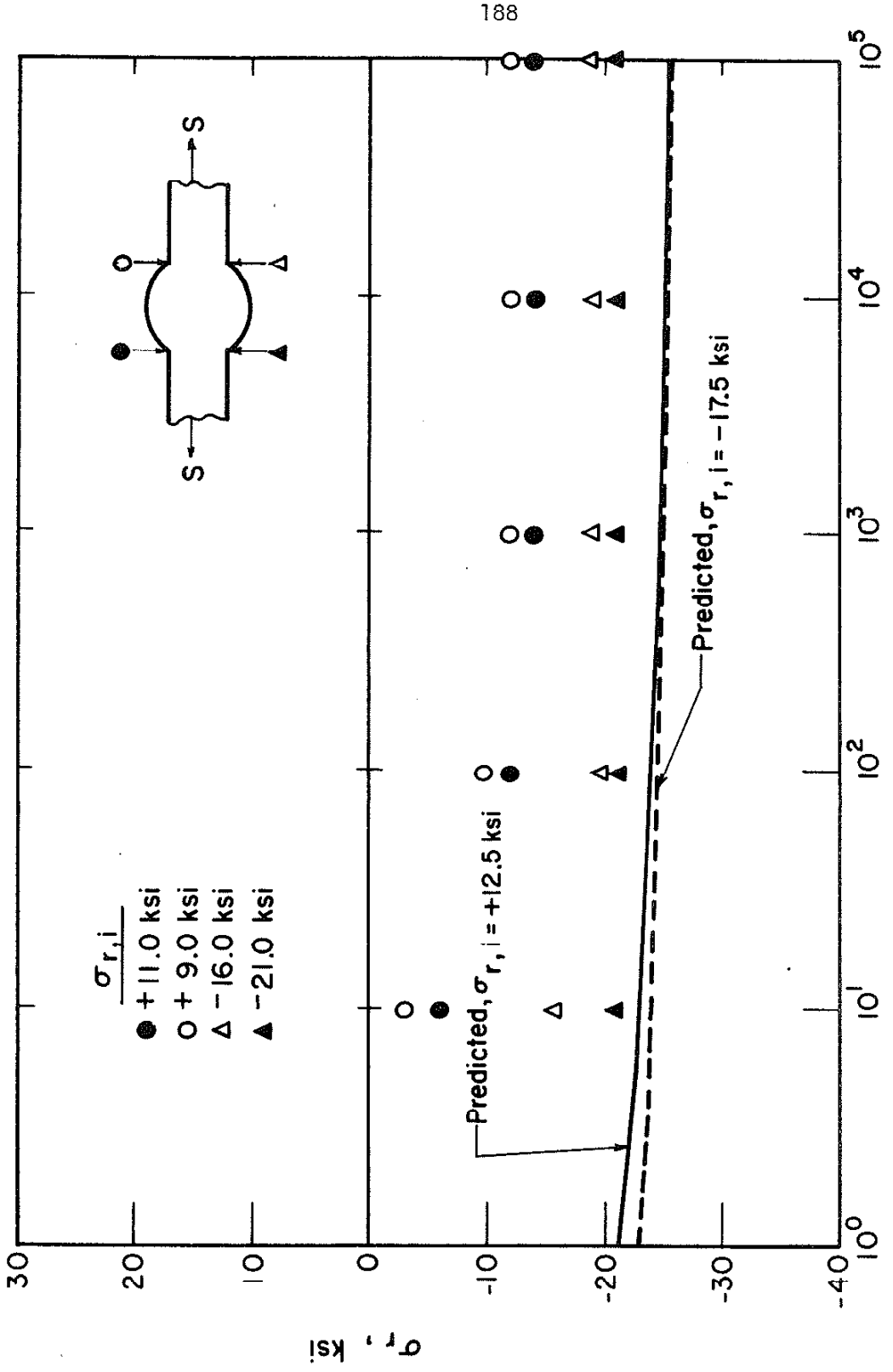

Fig. C-7 Predicted and Actual Cyclic Relaxation of the Residual Stresses for 1020 Steel Butt Welds under 0 to 33.0 ksi Fatigue Loading. The Solid and the Dashed Lines Are the Predicted Residual Stresses for Initial Residual Stresses of 12.5 and -17.5 ksi Respectively; the Symbols Are the Measured Residual Stresses on the Four Weld Toes

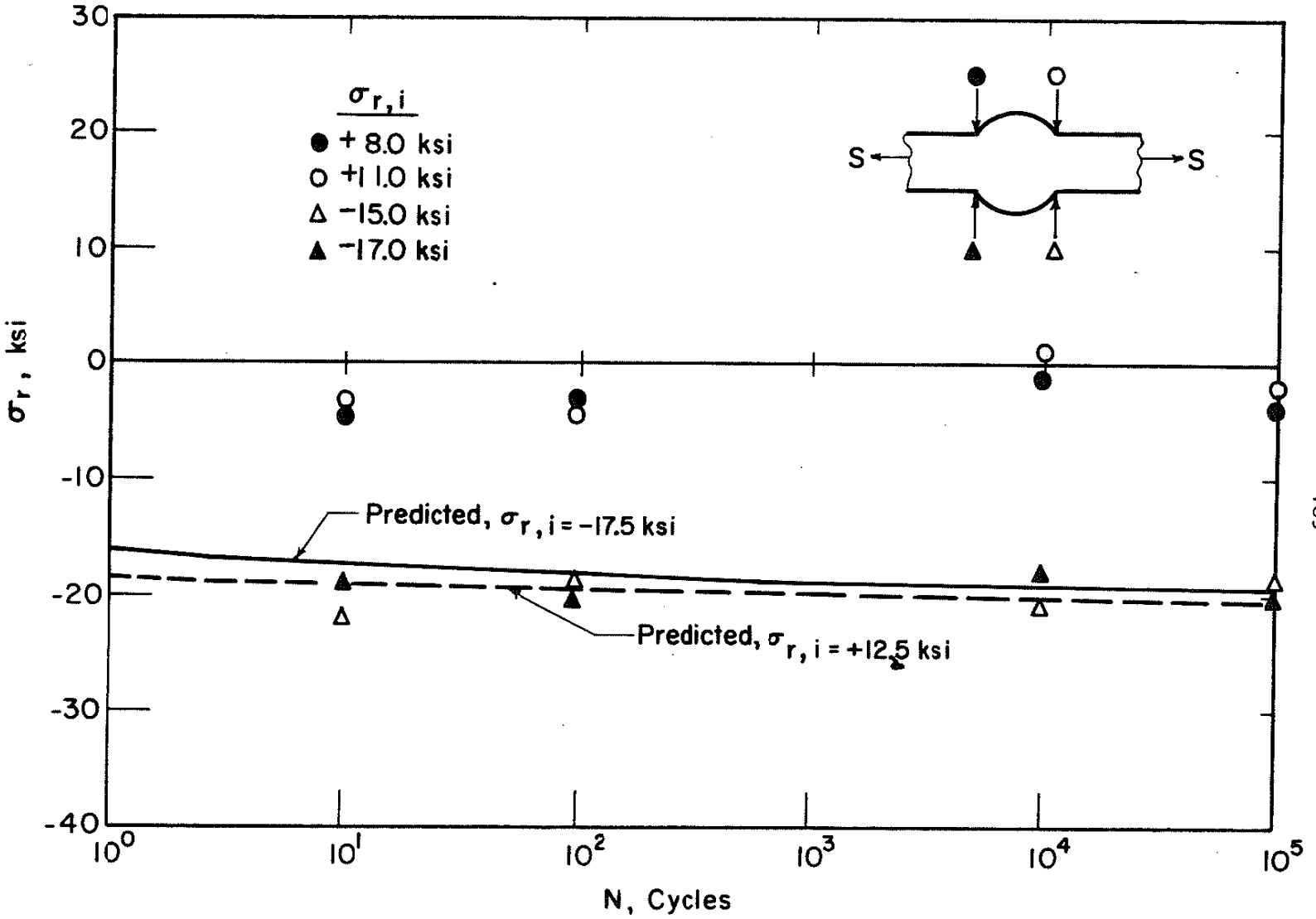

Fig. C-8 Predicted and Actual Cyclic Relaxation of the Residual Stresses for 1020 Steel Butt Welds under 0 to 24.0 ksi Fatigue Loading. The Solid and the Dashed Lines Are the Predicted Residual Stresses for Initial Residual Stresses of -17.5 and +12.5 ksi Respectively; the Symbols Are the Measured Residual Stresses on the Four Weld Toes